PHASE 2 FINAL REPORT

CONTINUOUS FIBER CERAMIC COMPOSITES PROGRAM: GASEOUS NITRIDATION

Authors:

R. Suplinskas G. DiBona, W. Grant
Textron Systems Corporation
2 Industrial Avenue
Lowell, MA 01851

Submitted To:

Robert G. Trimburger
Project Officer
U.S. Department of Energy
Idaho Operations Office
850 Energy Drive
Idaho Falls, ID 83401-1563

Covering the Period:

October, 1993 through 31 July 2001

Cooperative Agreement Number:

DE-FC07-92 CE 41001

TABLE OF CONTENTS

1.0 EXECUTIVE SUMMARY

In the course of this cooperative agreement, Textron has developed a mature process for the fabrication of continuous fiber ceramic composite (CFCC) tubes for application in the aluminum processing and casting industry**.** The major milestones in this project are described below.

System Composition. On the basis of chemical and thermal compatibility with processing and application conditions, the composite system chosen for full development activity was SCS-6 silicon carbide monofilament reinforcing nitride-bonded silicon carbide (NBSiC). Unlike commercially available small diameter ceramic yarns, the SCS-6 fiber does not suffer thermal degradation or adverse chemical interaction either during fabrication or use. The RBSN matrix shows a high degree of stability towards both high temperature oxidation and contact with molten aluminum.

Matrix Formulation. The "green" matrix primarily consists of a mixture of silicon carbide and elemental silicon particulates; the latter are converted to silicon nitride by reaction with nitrogen during a firing step. The green matrix in the form of a slurry is cast around the fibers to form a green body for firing. The slurry formulation developed during the program has the following characteristics: a) high solids loading. Weight percent solids above 80% minimize shrinkage and cracking and permit the fabrication of net-shape parts. b) stability against sedimentation. Stabilizing additives and proper particle size distribution assure interparticle repulsion that produces a stable suspension. c) low viscosity. Water-based suspensions have viscosities in the 150-1000 centipoise range; these are castable and provide infiltration around fibers without residual macroscopic voids. The aqueous base eliminates the need to deal with flammable materials during drying and firing. d) green body porosity. The particle size distribution assures that the green body has a network of open connected porosity for the later gas phase nitridation. The silicon to silicon carbide ratio assures that the volume change upon nitridation fills the porosity, allowing net shape fabrication, and also provides silicon carbide diluent to the exothermic nitridation step, preventing composite damage due to exotherms.

Preform Fabrication. Tooling and winding algorithms were developed for the direct filament winding of closed-end tubes on a 5-axis filament winder. Slurry was added to the mandrel while the fibers were wound dry. Patterns of alternating dome, helical and melt-line band wraps produced uniform wall thickness and fiber dispersion.

Nitridation. A 48 hour nitridation cycle was developed to convert the green slurry to RBSN matrix. Experimental cycles as short as 36 hours were demonstrated.

Material Characterization. An extensive database of physical, thermal and microstructural properties of the SCS-6 RBSN system at both room and elevated temperatures was developed.

Component Evaluation. Testing of sub-scale and representative components in simulated and actual in-service conditions was performed at Doehler-Jarvis, Williams International and General Motors. Gas-fired reheater burner tubes were evaluated at Doehler-Jarvis, combuster cans for stationary gas turbine generators at Williams International, and electrically heated immersion tubes for aluminum casting at General Motors. Performance data was used to further refine the pre-production scale manufacture of components.

2.0 INTRODUCTION

In response to an identified need, the Department of Energy's Office of Industrial Technologies initiated a three-phase, ten-year program designed to develop the processing and supporting technologies necessary to reliably and cost-effectively fabricate continuous fiber ceramic composite (CFCC) components for industrial applications. The program goals were to be accomplished through a long-term coordinated effort involving industry, government and university activity. The Phase 1-Exploratory Development activities were designed to identify and investigate innovative CFCC materials ad processes, industrial applications and benefits. Those CFCC systems which demonstrated the utility and technical performance necessary for viable industrial applications would progress to Phase 2-Process Engineering and Component Development. This phase is directed to the development of process engineering activities that are necessary to fabricate, test and evaluate representative CFCC industrial components with the required properties. The Phase 3-Pilot Scale Process Development activity is intended to result in the development of a pilot-scale facility that demonstrates the operation of a CFCC production line.

Under a Cooperative Agreement with the DOE/OIT, Textron Systems has been leading one of the program teams in an effort to develop and demonstrate the processing methods for the fabrication of low cost continuous fiber ceramic composite (CFCC) tubular components for use in commercial and industrial applications. The Textron team was selected to achieve a balance between OEM, end user, analytical design and materials processing capabilities. The objective of the Textron program is to develop low-cost, simple manufacturing processes that can produce large varieties of CFCC components, with an acceptable range of ceramic fibers and matrices, in essentially "net-shape" fashion.

From the onset of the CFCC Program, Textron's intent was not to develop CFCC processing technology from the "ground up", but rather, to creatively combine specifically-chosen, well-established monolithic ceramic synthesis techniques with automated fabrication methods that are routinely utilized in industries and markets that make use of fiber reinforced composites. We felt that the needs of the CFCC Initiative could best be addressed by drawing upon the collective experience that has been gained in the production of industrial monolithic ceramics and advanced composites, so that overall technical risks would be minimized and that CFCC test components could be fabricated for end user and OEM testing in the most rapid fashion possible. These technical objectives had largely been achieved by the end of the Phase I program.

The CFCC materials systems and fabrication processes developed during the Phase I Program employed gas phase nitridation techniques on mixtures of silicon carbide powders, silicon metal powders and the reinforcement of interest to produce a family of ceramic matrix materials which were colloquially referred to as "nitride bonded SiC" (NB SiC) CFCC'S. The principal technical considerations involved in the selection of this processing route and family of CFCC materials were as follows:

- Inherent possibilities to fabricate CFCC materials with a wide range of technical (i.e. strength) and cost attributes by changing fiber selection, fiber volume fraction and matrix materials composition.

- Potential to fabricate complex CFCC bodies in near-net-shape or totally net-shape fashion.

- Good elevated temperature strength retention and creep resistance to > 1200°C (2192 °F).

- Stability in to oxidizing, reducing or combustion gas environments

- Intrinsically good thermal shock resistance and durability.

By the conclusion of the Phase I Program, Textron had successfully demonstrated a potentially cost-effective, prototype-scale methodology for fabricating planar and tubular CFCC components in near-net or netshape fashion. We were able to show that very high performance CFCC's could be made with ultimate tensile strengths as high as 680 Mpa (100 ksi) and first matrix microcracking stresses up to 272-285 Mpa (40-42 ksi); values that approach or exceed any state-of-the art CFCC materials. A representative-scale CFCC burner component was also successfully fabricated which had a monolithic nitride-bonded silicon carbide flange and nozzle joined to it by gas phase nitridation.

Another important process-related milestone achieved during the Phase I Program was that Textron's Rapid Densification (RDTM) coating and infiltration process was shown to be an effective and rapid means for coating and infiltrating open porosity in porous ceramics with near-stoichiometric silicon carbide. Density measurements and static air oxidation tests also indicated that RD™ processing of nitride bonded SiC CFCC's will have a substantially beneficial effect on long-term oxidation behavior and matrix mechanical properties.

2.1 Program Description

2.1.1 Background

The overall goal of the CFCC Program is to facilitate the introduction of CFCC technology into a wide range of industrial applications. Markets that have specifically been identified as being able to substantially benefit from the availability of suitable continuous fiber ceramic composites include the chemical processing, metals processing and toxic waste incineration industries. Operational and economic benefits to be derived from the use of CFCCs are now fairly well known; increased process yields, reduced energy consumption, higher productivity and reduced environmental emissions are all likely outcomes of incorporating CFCC materials into industrial processes.

Although it is comparatively simple to provide technical motivation for the use of CFCCs in industrial applications, it is more difficult to convince a potential OEM or end user on the merit of employing these new materials in a given component application (especially if there is a significant up-front cost premium) since substantial amounts of time and money have been invested in existing materials technology. CFCCs must be considered as a whole new class of engineering materials, whether they are compared to metals or monolithic ceramics. It is therefore clear that cultural and educational changes in the market place need to accompany materials and fabrication process development activities.

Technical dialogue with Textron's team members during the Phase 1 Program has indicated that for the purposes of our CFCC program, achievement of ultimate technical properties (such as strength and stiffness) is not as important as being able to produce moderately-priced CFCCs that perform "well enough" in their intended operational settings. A recurrent theme that has been encountered is that CFCCs need to survive routine handling and abuse much better than monolithic ceramics if end users are to actively embrace these materials.

Overall chances for successfully introducing one or more classes of CFCC components into commercial service will also be enhanced by pursuing a materials development and testing scheme that balances technical risk, materials property requirements, and commercialization time frame scenarios. Or, in other words, it will be prudent to pursue ranges of CFCC commercialization options that address near-term, less technically-ambitious, goals in addition to longer-term goals that require significant fabrication process development work.

The framework of the CFCC Program is structured in a fashion that allows all of the technical and economic concerns summarized above to be successfully addressed while recognizing that the development of new materials is not a short term proposition. The CFCC Program also provides a mechanism to transition laboratory-scale fabrication processes into prototype manufacturing processes via a multi-phased work effort.

Textron's Phase 1 laboratory-scale fabrication process effort had four specific, major deliverables:

- Starting with the original materials and fabrication concepts presented in the Phase I Proposal, to develop a reproducible and practical lab-scale methodology for producing CFCC materials;

- To conduct technical and economic assessments of applications that would ultimately facilitate introduction of CFCC's in the metals processing, petrochemical processing and energy generation industries;

- To build a strong team of OEM'S, end-users and CFCC materials producers for defining component applications and host sites, along with building mechanisms for feedback on component performance in the field; and, finally,

- To conclude the Phase I CFCC Program with a processing demonstration which clearly demonstrated the utility and technical performance capabilities of Textron's CFCC fabrication processes and materials selections.

During most of the Phase I program, a combination of analysis, application assessment, materials/process development, and definition of performance and economic targets defined the program structure. A routine process for fabricating lab-scale quantities of CFCC's was arrived at early in the program, so that initial mechanical property and environmental stability data could be generated for subsequent material screening purposes. An important milestone was the preliminary component design task (1.3.1), which had a significant influence on choosing specific attributes of CFCC constituent materials and fabrication process routes (i.e. fiber architectures) for test specimens and subscale components fabricated during Phase 1.

On the basis of technical and economic assessments that were conducted to identify specific industrial applications that could potentially make use of CFCC'S, a number of components and systems were identified for further study. The primary candidate CFCC component applications selected for more detailed technical and economic payback analysis studies during the Phase I Program (listed along the relevant team members) were:

- Stationary Turbomachinery Combustor Hardware (Williams International)
- Radiant and Immersion Tube Burners (Hauck Burner and Doehler-Jarvis Die Casting)
- Pyrolysis and Reformer Tubes (Stone and Webster Engineering)

Results of analyses for each of the three types of candidate CFCC components listed above indicated that CFCC immersion tubes probably represented the most technically and economically-desirable near-term commercialization opportunity. Economic payback predictions, however, suggested that CFCC components would need to be priced at no more than two to four times the price of existing metallic hardware for their use in any process industry to become widespread. This implies that significant reductions in reinforcement and manufacturing process costs will need to take place in order for CFCC components to be competitively-priced, and, to this end, Textron chose a fabrication process strategy that should ultimately minimize developmental risks and component costs.

From the onset of the Phase I CFCC Program, Textron's intent was not to develop CFCC processing technology from the "ground up", but rather, to creatively combine specifically-chosen, well-established monolithic ceramic synthesis techniques with automated fabrication methods that are routinely utilized in industries and markets that make use of fiber reinforced composites. We felt that the needs of the CFCC Initiative could best be addressed by drawing upon the collective experience that has been gained in the production of industrial monolithic ceramics and advanced composites, so that overall technical risks would be minimized and that CFCC test components could be fabricated for end user and OEM testing in the most rapid fashion possible. These technical objectives had largely been achieved by the end of the Phase I program.

The CFCC materials systems and fabrication processes developed during the Phase I Program employed gas phase nitridation techniques on mixtures of silicon carbide powders, silicon metal powders and the reinforcement of interest to produce a family of ceramic matrix materials which were colloquially referred to as "nitride bonded SiC" (NB SiC) CFCC'S. The principal technical considerations involved in the selection of this processing route and family of CFCC materials were as follows:

- Inherent possibilities to fabricate CFCC materials with a wide range of technical (i.e, strength) and cost attributes by changing fiber selection, fiber volume fraction and matrix materials composition.
- Potential to fabricate complex CFCC bodies in near-net-shape or totally net-shape fashion.

- Good elevated temperature strength retention and creep resistance to > 1200'C (2192 'F).
- Stability in to oxidizing, reducing or combustion gas environments.
- Intrinsically good thermal shock resistance and durability.

By the conclusion of the Phase 1 Program, Textron had successfully demonstrated a cost-effective, prototype-scale methodology for fabricating planar and tubular CFCC components in near-net or net-shape fashion. We were able to show that very high performance CFCC's could be made with ultimate tensile strengths as high as 680 Mpa (100 ksi) and first matrix microcracking stresses up to 272-285 Mpa (40-42 ksi); values that approach or exceed any state-of-the art CFCC materials. A representative-scale CFCC burner component was also successfully fabricated which had a monolithic nitride-bonded silicon carbide flange and nozzle joined to it by gas phase nitridation.

2.1.2 Phase 2 Program Objectives and Teaming Approach

The overall goal of the Phase 2 CFCC is to demonstrate that the nitride bonding process is a cost effective processing approach that can be scaled for the fabrication of large components, and that the resulting CFCCs have acceptable technical properties.

A successful Phase 2 CFCC Program accomplishes at least three major objectives: (1) demonstrate CFCC processing techniques that can produce representative demonstrator components (at least on the prototype scale); (2) that these representative CFCC components can function acceptably in their intended service environments; and, (3) that an important feedback mechanism is in place to relay component performance data to program team OEMS, end-users and CFCC fabricators. In addition, market assessment and economic studies to be conducted during the Phase 2 Program will identify commercial opportunities where insertion of CFCC technology can offer significant operational and economic benefits to the prospective end user.

Textron's fabrication efforts in this Phase 2 program are primarily directed towards construction of thin-walled tubular structures. Tubular structures are pervasive in applications that span across the chemical process, energy conversion and metals processing industries. Tubes with one closed end present a fabrication challenge; the majority of program efforts was directed towards this end.

The list of candidate CFCC component applications for Phase 2 effort was provisionally identified as:

> *An NB-SIC CFCC Radiant or Immersion Tube Burner for Primary and Secondary Metals Processing* - Both types of burner components are widely used in the primary and secondary metals processing industry. Availability of silicon-carbide based CFCC burner tubes that are thermodynamically stable in molten metal environments could offer major operational and economic benefits to end users in these markets.
>
> *An NB SiC CFCC Combustor Can for a Stationary Gas Turbine Remediator* - Incineration of toxic waste in a high pressure turbine engine, combined with co-generation of electrical power, is an exciting concept that has been put forth by Textron

team member Williams International. A nitride-bonded SiC CFCC combustor can should be nearly ideal for withstanding the high temperature corrosive conditions that will be associated with burning of toxic waste "fuels" in a stationary turbine remediator unit.

A Section of NB-SIC CFCC Reformer or Pyrolysis Tube with an NB SiC Joint - Many thousands of reforming and pyrolysis tubes are used in the petrochemical processing industry. Existing metallic tubes are plagued by coke formation problems that cause costly furnace outages due to tube "burnout". Process efficiency and product yield are also limited by thermal instability of metallic tubes above temperatures of 1000°C. Availability of tough, thermally-stable, nitride-bonded SiC CFCC tubes that are resistant to coke formation could substantially improve many aspects of reforming and pyrolysis applications that affect product quality, furnace maintenance and overall plant output.

The CFCC radiant or immersion tube burner is considered the nearest term application. There are immediate possibilities to simulation test, and possibly field test, CFCC immersion tube burners as soon as technically-acceptable components become available. The CFCC combustor can, is likely a mid-to long-term component application. However, external regulatory factors regarding disposal of toxic wastes could accelerate the commercialization time frame. The CFCC reformer or pyrolysis tube is considered to be a longer-term component application. Operators of chemical processing facilities tend to infuse new technology into their plants in a rather conservative fashion, though here again, chances for near-term commercialization could be promoted by external regulatory or financial factors.

The candidate CFCC component applications summarized above have been selected mainly on the basis of their technical appeal, compatibility with our NB-SIC CFCC processing route, projected economic paybacks and energy/environmental benefits. The three applications were further chosen with the intent of "spreading out." technical, economic and intangible risks that could affect the individual success or delivery timeframe for a given component application.

Textron Specialty Materials has attempted to structure a Phase 2 CFCC team that fills every major link in the connection between CFCC manufacturer, OEM and end-user. A team was chosen that is capable of competently designing, fabricating and eventually commercializing CFCC components. Our principal team members are as follows: (See Figure 1-2)

Doehler-Jarvis Casting Corporation Doehler-Jarvis operates the largest aluminum die casting facility in the United States. They melt over 144 million pounds (65.3 million kg) of recycled aluminum per year at just one of their continuous die casting facilities in Toledo, Ohio. Doehler is widely acknowledged to be capable of fabricating uniquely intricate high quality aluminum castings that have excellent mechanical properties. They have agreed to act as an end-user site for in-service testing of CFCC radiant or immersion burners fabricated in the Phase 2 Program.

F. W. Schaefer Co. - Schaefer Company is a reputable manufacturer of furnaces that are used in a wide variety of metals and materials processing markets. They have an excellent relationship with Doehler-Jarvis, having manufactured virtually all of Doehler's aluminum remelting furnaces. Schaefer was responsible for designing and carrying out furnace modifications that would allow one or more CFCC burner tubes to be installed in

an existing remelting furnace at Doehler. Schaefer also has important links to other die casting and metals processing markets that could present additional CFCC component testing opportunities in the future.

Hauck Manufacturing Corporation Hauck is an OEM of radiant and immersion tube burners that has been involved in combustion applications since 1888. A major market for Hauck burners is the primary and secondary metals processing industries. Hauck has very strong in-house design expertise, and, like Schaefer, has relationships with other potential end-users, such as Alcoa, that have expressed a willingness to support CFCC component testing activities. Hauck's work on the Phase 2 Program involved design and simulation testing of at least one CFCC radiant or immersion tube that would eventually be installed in a Schaefer-designed furnace at a Doehler-Jarvis casting facility.

Williams International - Williams International is an internationally-recognized leader in the design, development and manufacturing of small gas turbine engines. They have manufactured over 10,000 turbines and associated systems for commercial and military markets. Williams is now in the process of designing and planning for production of a stationary gas turbine remediator unit. The remediator unit is a small turbine engine (based on a mature auxiliary power unit design) that is intended to incinerate toxic waste while cogenerating electrical power. Silicon carbide- and/or silicon nitride-based CFCC combustor hardware will be needed to withstand the highly corrosive nature of the burner waste products. Williams activities are to design, simulation (burner rig) test, and if possible, actually field test a nitride-bonded SiC CFCC combustor can fabricated by Textron.

Stone & Webster Engineering Corporation - Stone & Webster is a well-known plant engineer and designer with a wide base of experience in the energy and chemical processing industries. They bring valuable capabilities in processing plant design, component design and economic tradeoff analysis to the TSM/DOE CFCC team. Stone and Webster is responsible for design of an NB-SIC CFCC reformer or pyrolysis tube that could be used in a petrochemical processing facility. Simulation or end user testing of representative CFCC tube components is planned take place within the Phase 2 Program.

Nova Industrial Ceramics - Nova is Textron's primary subcontractor on efforts concerning CFCC materials processing and joining. They provide the team with unequalled expertise in the formulation of reaction-synthesized SiC-based ceramics. Based on their past work involving fabrication of highly-engineered monolithic NB-SIC components, Nova is also be able to generate additional contacts amongst OEMs and end-users that may be interested in evaluating NB-SIC CFCCS.

Material Sciences Corporation - Material Sciences Corporation (MSC) supports efforts concerned with analytical models of CFCC component behavior as they relate to materials constituent properties and reinforcement architectures. More specifically, they address structural modeling, definition of fiber architecture, component reliability and life prediction. Their work forms long-term theoretical underpinnings for empirical materials development and processing activities.

IBIS Associates - IBIS has developed unique capabilities to model manufacturing processes and provides this program with cost models for the fabrication of CFCC components. These models provide Textron the ability to perform economic and processing analysis in support of the commercialization of CFCC's.

2.2 CFCC Process Overview

The ceramic matrices selected for the CFCC program were based on employing gas phase nitridation techniques on mixtures of SiC and Si powders to produce a family of materials which are colloquially referred to as nitride bonded SiC (NBSIC) or nitride bonded silicon nitride (NBSN). NBSN is composed entirely of metallic Si powders prior to nitridation, while NBSic is composed of variable mixtures of silicon and silicon carbide powders prior to nitridation. The technical considerations involved in the selection of this family of ceramic matrices for the CFCC Program were as follows:

- Good elevated temperature strength retention and creep resistance to temperatures greater than 1200°C (2192°F);
- High constituent phase purity and resistance to oxidizing, reducing, combustion, etc. gas exposure;
- Modest cost of starting materials and manufacturing processes combined with rapid (few day turnaround) processing;
- Acceptable thermal conductivity and thermal shock resistance; and,
- Potential to fabricate complex bodies in net or near-net shape fashion with minimal dimensional changes from the "green state" to final firing, along with high degree of commonality for Textron's existing CFCC fabrication process route and baseline materials.

Selection of a continuous fiber reinforcement for the CFCC materials to be evaluated on this program was based on several factors, most of which related to the need to obtain adequate long-term thermodynamic stability, good composite strength and toughness and the highest achievable stresses for the onset of matrix microcracking. In this context, desirable fiber attributes were therefore believed to be as follows:

- Excellent elevated temperature strength retention, creep resistance and microstructural stability to temperatures exceeding 1200°C (2192°F) in oxidizing environments. (Stability in alkali corrosion conditions would also be implied);
- Coefficient of thermal expansion (α) and elastic modulus (E) characteristics appropriately matched to Si-based ceramic matrices (α_f greater than α_m.; E_f greater than E_m.) made via gas phase reaction synthesis (where the subscripts "f" and "m" respectively refer to the fiber and matrix phases).

- Demonstrated thermodynamic compatibility and property retention with regard to Textron's CFCC nitridation processing methods as well as the ceramic matrix phase compositions themselves;

- Ability to tailor surface properties of the fiber for the anticipated operational environment and composite forming processes;

- Robust handleability (from the point of view of automated composite lay-up and fabrication methods); and,

- Commercial availability with reproducible technical properties at reasonable cost.

At the onset of the Phase 1 Program, Textron's SCS-6™ chemically vapor deposited (CVD) SiC monofilament was the only continuous reinforcement which seemed capable of meeting most or all of the criteria mention above. SCS-6™ has excellent thermomechanical properties to temperatures of 1400°C (2552°F) or higher, is technically mature, and is commercially available in reasonable quantity. Projections have also been made to the effect that SCS-6™ could be produced for approximately $2000 /kg (<$1000/pound) at production rates of greater than 2700 kg (6000 pounds) per year.

Textron's 143 μm (5.6×10^{-3} inch) diameter SCS-6™ monofilament is coated with a complex surface treatment that contains a thin layer of turbostratic carbon between two carbon-plus-SiC layers that are ~1.5 μm (6×10^{-5} inch) thick. The presence of this partially graphitic carbon layer has been found to impart good interfacial debonding behavior to many types of SCS-6™ reinforced CFCC materials.[3] The SCS-6™ monofilament can be consistently wrapped around radii of curvatures larger than 50 mm (2 inches) without fracture. Textron also has a prototype production of a 75 μm (3×10^{-3} inch) diameter SiC monofilament that is called SCS-9A™. This fiber has so far shown properties that compare very favorably with the SCS-6™ fiber, and, at half the radius of SCS-6™ this filament., will be more amenable to wrapping around small radii of curvature. (See Figure 2-1 for an optical micrograph of Textron's SCS-6™ CVD SiC monofilament).

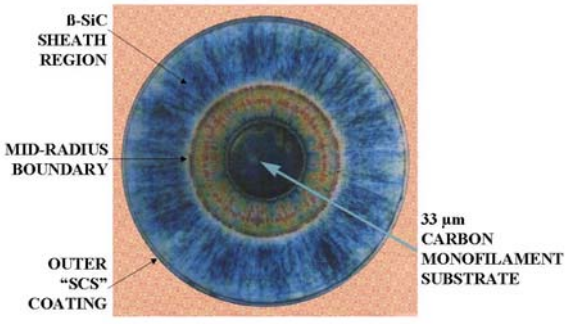

Figure 2-1: Optical Micrograph of Textron SCS-6 ™ CVD SiC Monofilament

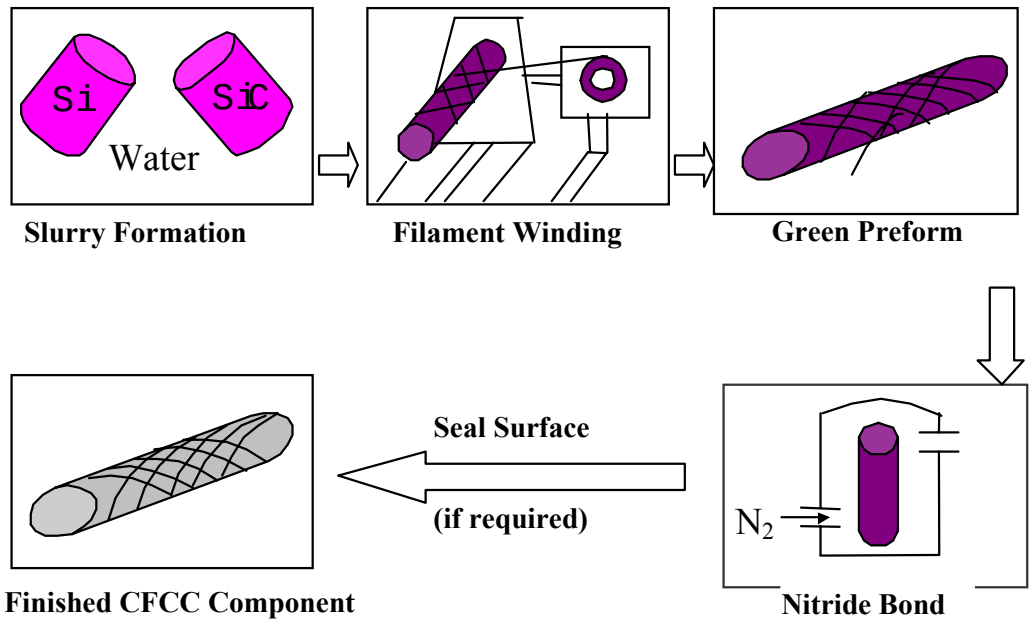

Figure 2-2. Process Schematic for Nitride Bonded SiC CFCC

The key steps in the processing sequence to fabricate nitride bonded silicon carbide CFCC's are outlined below, and are depicted visually in Figure 2.2.

Step 1: Green Body Formation by Filament Winding or Conventional Slip Casting

Appropriate starting powders are first prepared. As previously mentioned, for nitride SiC CFCC materials, the starting constituents are mixtures of SiC + Si powders that have been specially chosen for their particle size and surface chemistry characteristics. This facilitates achievement of optimized slurry density (particle packing behavior) and dispersion stability.

Though aqueous and non-aqueous vehicles can be used to create NBSIC dispersions, water-based vehicles are preferred for environmental reasons and for the superior ability of water to efficiently disperse SiC and Si particulate at high solids loadings.

Binders or resins such as polyvinyl alcohol (PVA) or polyethylene glycol (PEG) can be added to the water-based dispersions in order to modify drying and rheological behavior of the particulate

dispersions and also to increase green body physical strength. This can be advantageous during filament winding processes, which require that the dispersions remain wet and be sedimentation-resistant over a period of hours as the CFCC green body is being wound.

Step 2: Green Body Formation by Filmanet Winding or Conventional Slip Casting

Filament winding of closed-ended or open-ended CFCC tubular shapes was chosen as the baseline composite forming method for this program. Winding of tubular shapes first involves fabrication of a cylindrical, plaster-of-Paris mandrel assembly which forms and controls the inner diameter of the tubular preform. NBSiC slurry is then simultaneously introduced into the mandrel as one or more monofilaments are being wound, as shown in Figure 2-2. When the desired fiber construction is completed, the CFCC green body is allowed to air-dry for a period of up to 24 hours prior to removal from the mandrel.

Monolithic or CFCC green bodies intended for process screening or mechanical and physical property evaluation are produced by slip casting onto flat plaster molds. Monofilament plies consisting of parallel arrays of fiber or spread tows are pre-coated with slurry and placed into the plaster mold during the slip casting process. As in the processing of the tubular shapes, those plates are allowed to air-dry prior to removal from the plaster molds.

Step 3: Gas Phase Reaction Synthesis (Nitridation)

This step of the processing sequence results in densification and ceramic matrix formation in the CFCC part, which may be the final step in the overall fabrication scheme if the component does not require a protective or higher density coating.

Gas phase reaction synthesis of CFCC materials is an attractive route for matrix densification since the process causes essentially no (less than 0.1%) shape change to the overall preform dimensions and requires no mechanical fixturing or restraint tooling during nitridation. Conversion of silicon metal to silicon nitride is carried out in a vacuum furnace or gas-tight box furnace. A nitrogen gas flow is introduced to the furnace load during its heating cycle, which peaks at a temperature of approximately 1400°C (2552°F), converting the silicon metal to a continuous network of silicon nitride which then bonds to the silicon carbide powders and monofilament. Through control of the ceramic slurry formulation, the nitrogen gas flow characteristics and the thermal cycle, nitridation conversion levels of 93-99% can be achieved with temperature exposures that produce only minimal strength loss to the SCS-6™ silicon carbide monofilament selected as the primary reinforcement for this material system. The final matrix density achieved in this process is typically 2.55-2.70 g/cc (80-85% theoretical).

Step 4: Component Coating

A characteristic of Textron's CFCC material system is the presence in the final product of a fine (<μm) dispersion of porosity. For some intended applications where anticipated operational conditions involve exposure to atmospheres in which the fiber or ceramic matrix would be rapidly degraded, or where gas tight through-the-wall conditions must be maintained, it may be desirable to provide an adherent, protective coating to the NBSiC composite.

RD™ utilizes the same principles as contemporary chemical vapor infiltration (CVI). However, by operating essentially at atmospheric pressure, and through utilization of a controlled thermal gradient, deposition rates have been increased by orders of magnitude. The thermal gradient imposed on the preform serves to inhibit deposition until the reactant reaches a surface hot enough to initiate precursor decomposition. Control of this gradient leads to the progression of a deposition front in the porous preform from the inside of the composite to its external surfaces. The major advantage of RD™ over conventional CVI techniques, aside from the dramatically faster deposition rates, is the elimination of the "seal-off" problem that is so common to traditional CVI methods. TSM has been developing this new process for the deposition of carbon in carbon-carbon composite matrices, with expected excellent potential for significantly reducing infiltration/coating costs in silicon carbide matrices.

2.3 Program Plan and Significant Changes

2.3.1 Phase 2 Program Plan

The overall task structure for the CFCC program was established at the beginning of Phase 1, and included four tasks: Task 1-Applications Assessment, Task 2 - Supporting Technologies, Task 3 - Materials & Process Development, Task 4 - Scaleability and Manufacturability. These tasks and their major subtasks tasks, shown in Figure 2.3-1, are intended to carry through all three phases of the program.

Since the primary focus of Phase 1 was the assessment of potential CFCC applications and the feasibility demonstration of a candidate CFCC material/process system, activities in Task 1 and Task 3.1 were essentially completed. In addition, by program design, all Task 2 Supporting Technologies activities are performed at selected universities and national laboratories throughout the country, and are directly managed by DOE.

The task structure for the Phase 2 program being addressed in this report includes Task 3 Materials & Process Development (shown in Figure 2.3-2). Although the primary focus is Tasks 3.2 through 3.5, Process Engineering, Component Fabrication & Testing, Component Evaluation and Joining, respectively, updates and additions to the Phase 1information in Task 3.1 were made as needed.

2.3.2 Significant Program Changes

As might be expected in any research and development activity with the objective of starting from a materials feasibility level and ultimately demonstrating component scaleability and manufacturability, numerous changes have occurred in the Textron Phase 2 program. Although most of the materials and process related changes fall within the broad scope of the definition and intent of the program plan, several of the changes have impacted the makeup of the program team, the fundamental technical approach and the CFCC application assessments. This section is intended to identify and summarize those changes which have significantly altered the direction and/or desired objective of this phase.

Entering this Phase 2 program, the Textron team had selected three candidate CFCC components that met the criteria of technical, economic and DOE-related benefit improvements. These components reflected the team's desire to focus on thin-walled cylindrical components for industrial applications that span near, medium and far-term production opportunities. More specifically these selections were metals processing industry heater tubes (immersion and

radiant), stationary gas turbine engine external combustor components and chemical process industry process tubes (reformer and pyrolysis). Immediately following the initiation of the Phase 2 effort, the Stone & Webster candidate applications for catalytic reformer and pyrolysis tubes were deleted from our program plan due to component design and field testing issues that could not be resolved within the CFCC program scope.

Significant application changes also occurred within the CFCC combustor effort that was being performed with our teammate Williams International (WI). Our Phase 1 selection was an external combustor component for a stationary gas turbine engine, which could be used at remote sites to burn waste fuels while cogenerating electric power. Continuing market studies within Williams during Phase 2 revealed a loss in customer interest in the remediator role for an external combustor gas turbine engine, however, Williams was able to retarget the same engine opportunity to the independent power producer (IPP) market. As this new market opportunity was further defined, however, it became apparent that candidate engine designs with external (therefore cylindrical) combustors would not be continued. Following the completion of CFCC mechanical property test efforts that have been reported in Section 3.2 of this report, further work with Williams was discontinued.

Another significant change to our applications team has been the loss of Doehler-Jarvis as the host aluminum die casting test site for immersion tubes. During a period of process improvement changes to our CFCC fiber winding and tooling procedures after the first two rounds of immersion tube field testing, changes in key management positions and other business considerations at Doehler resulted in the loss of this company as a site for future testing. As we completed our process improvements we also began to look for other partners for this application. As a result of an initial contact made at a DOE OIT trade show booth, we established an agreement with General Motors for testing of aluminum melt furnace immersion heater tubes at their Advanced Development Laboratory and their production casting facility in Bedford, IN. Due to the supplier-end user relationships already in place, Deltamation, a burner manufacturer already working with GM, replaced Hauck Burners and F.W.Schaefer, who supported the team with Doehler-Jarvis. An additional test site opportunity within the automotive industry wss also considered.

In addition to these application team changes, several internal program changes have also occurred during this phase. Primary among these changes has been the transition of Principal Investigator responsibilities from Mr. Steve DiPietro to Mr. Gary DiBona to Dr. Raymond Suplinskas, who also now serves as Program Manager. Steve was primarily responsible for the CFCC material concepts that form the basis of our program, and served the CFCC Program as Principal Investigator from 1992 (Phase 1) until his departure from Textron in 1997. Mr. DiBona served as Principal Investigator and Program Manager until his departure from Textron in 2000. Additional changes include a transition in overall program management responsibility from Mr. Bruce Thompson to Mr. William Grant, Mr. William Darden, Mr. Gary DiBona and now, Dr. Raymond Suplinskas.

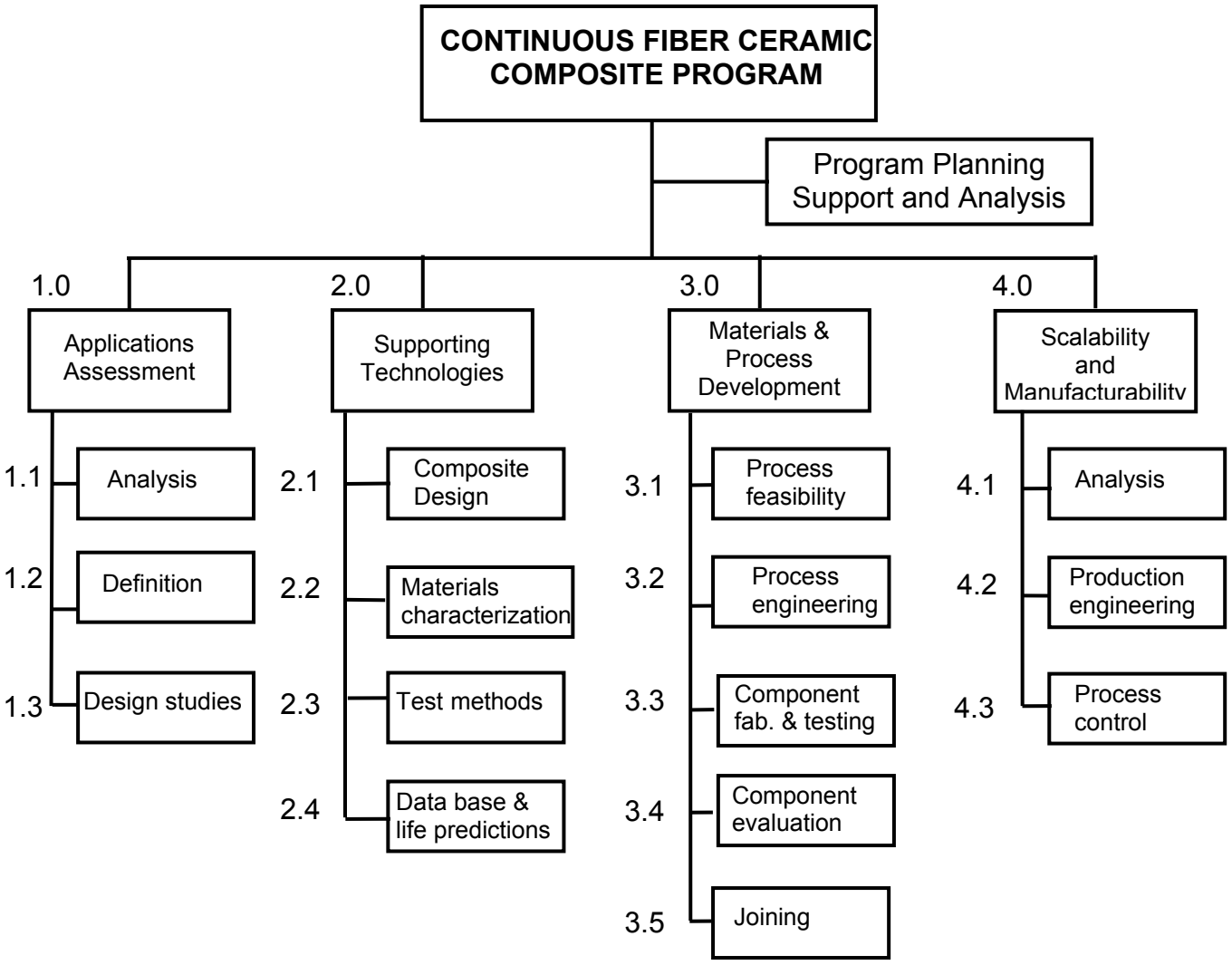

Figure 2.3-1 Continuous Fiber Ceramic Composite Program

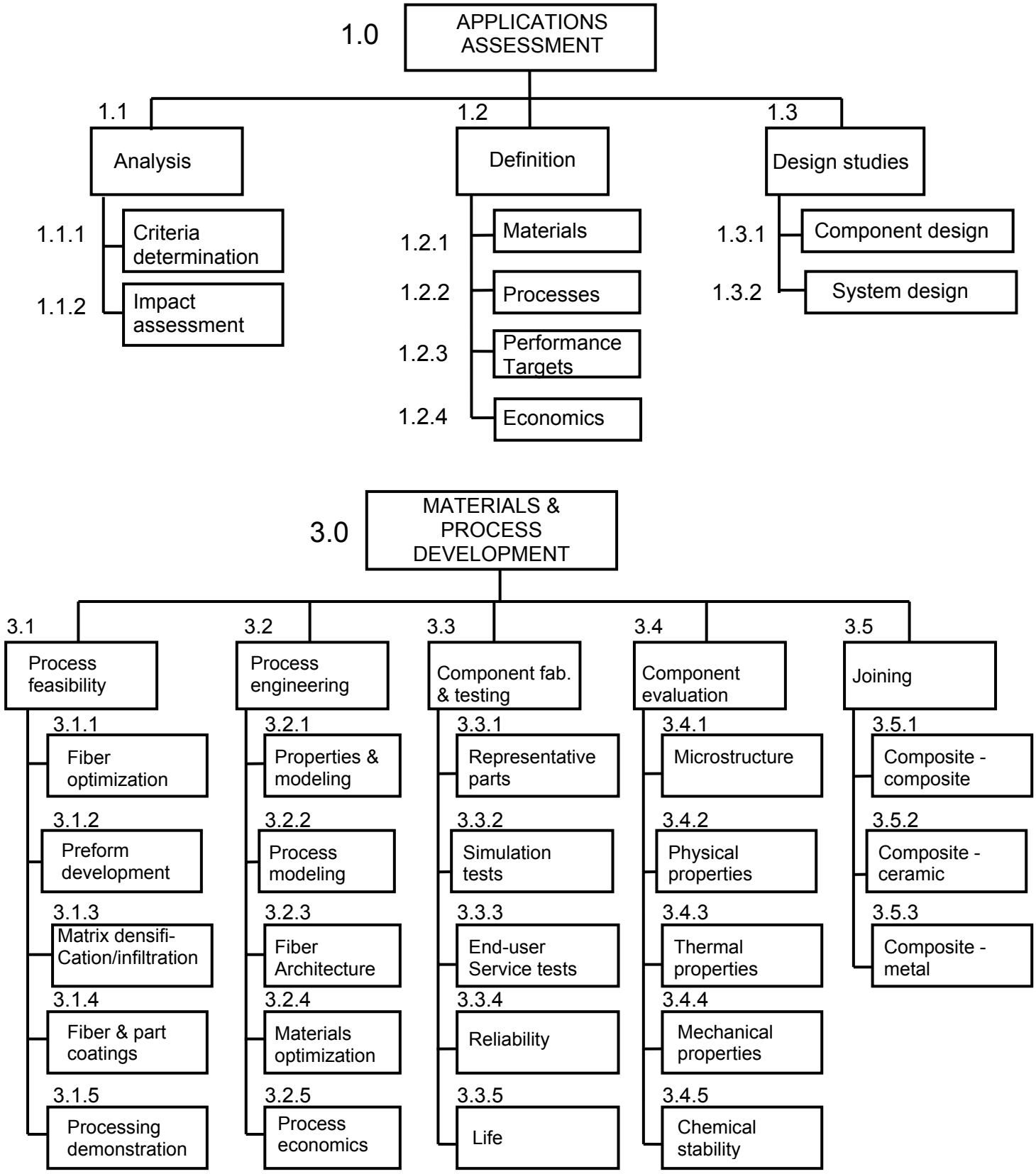

Figure 2.3-2 Textron/DOE CFCC Phase 2 Work Breakdown Structure

3.0 Technical Progress

3.1 Introduction

Technical progress was achieved in the ares of process engineering, component fabrication and testing, component evaluation and non-destructive inspection, and joining.

The major tasks under process engineering were fiber selection, slurry formulation, preform fabrication, nitridation, coatings, process and composite modeling, and low cost alternative fiber.

Component fabrication and testing included in-service prototype testing of gas-fired reheater burner tubes at Doehler-Jarvis, combuster cans for stationary gas turbine generators at Williams International, and electrically heated immersion tubes at General Motors.

Component evaluation and non-destructive inspection studies involved a large number of government, academic and industrial laboratories. These included Textron Systems, the University of Dayton, Oak Ridge National Laboratories, Battelle Pacific Northwest Laboratory, the University of Cincinnati, Argonne National Laboratory, Southern Research Institute, the University of Southern California and Williams International Corporation.

Each of these areas is discussed in detail in the sections that follow.

3.2 Task 3.2 Process Engineering

3.2.1 Status at the End of Phase I

The process engineering task emphasizes the development work necessary to convert laboratory-scale fabrication processes into ones that are suitable for the manufacture of representative CFCC components that exhibit required technical properties and production economies. Phase I of the Textron program demonstrated the feasibility of a nitride-bonded silicon carbide CFCC (NB SiC CFCC) laboratory process for the fabrication of flat plates, simple shapes and tubular structures. Those efforts defined this process within rather broad limits.

- Fiber reinforcements included large diameter silicon carbide monofilaments, SiC-based small diameter multifilament yarns and graphite yarns. Oxide yarn reinforcements were excluded because of serious degradation during nitridation processing.
- Matrix precursors' slurry formulation could be tailored as required by reinforcement type and preform fabrication method. The major constituents are silicon and silicon carbide powders whose weight ratios and size distributions can be varied to affect composition and rheological characteristics. Suspension vehicles can be aqueous or non-aqueous; resin binders can be added to either vehicle if required for preform handling.
- Preform fabrication methods could include drum wrapping, tape forming, filament winding and slip casting. For matrix precursor slurry formulations that include a binder, an additional important step is binder pyrolysis, i.e., the volatilization and removal of the binder without the formation of macroscopic defect voids.

- Nitridation schedules for converting the precursor silicon powders to silicon nitride matrix had been devised. Since the reaction is highly exothermic, runaway exotherms could occur depending on slurry formulation and part geometry. It was recognized that controlling exotherms was an issue requiring further development as part of prototype fabrication.

Phase I also initiated development of processes to provide coatings for CFCC materials either as protection for the underlying structure or to render the structure impervious to gases. The approach investigation employed Textron's Rapid Densification (RD™) process to deposit silicon carbide based coatings from methyl-chlorosilane precursors. The coating technology was demonstrated on subscale graphite-based parts and on a monolithic nitride bonded SiC sample heated indirectly using a graphite susceptor.

Phase I modeling efforts under the Process Engineering task defined both micromechanical and macromechanical composite materials models. Micromechanical models compute effective fiber bundle properties based upon (computed) properties of the reinforcement, matrix and the interface region. Reinforcements may be modeled as discontinuous or continuous, and features such as microcracks and ply disbonds can also be modeled. These models can be used to compute effective properties from the properties and geometrical orientation of fiber bundles within the composite. The composite can consist of laminated plies, fabric plies, multidirectional braids or N-dimensional weaves. Macromechanical models can factor in boundary conditions and structural loads defined by a given CFCC component application for the purpose of calculating contour plots that depict stresses, strains and resultant displacements under mechanical or thermal loads.

The Phase II efforts continued development work in the areas enumerated above but focused those efforts on a process to fabricate those prototype parts identified in the Applications Assessment as combining both substantial benefits to the end user and the opportunity for rapid commercialization.

The prototype component selected for further development is an immersion heater tube used in the metal casting industry. Program efforts focused on a filament winding process utilizing SCS-6 silicon carbide monofilament and a binder-free Si/SiC slurry. The processing developments are described in detail under separate headings below.

3.2.2 Fiber Selection

The four fiber types initially selected for the program were yarns of small diameter oxide fibers, silicon carbide based yarns, graphite yarns and silicon carbide monofilament. Oxide yarns had previously been dropped from consideration because of lack of chemical stability under nitriding conditions. The silicon carbide based yarns, Nicalon and Tyanno, exhibited severe thermal degradation at temperatures corresponding to the nitriding cycle. The graphite fibers are both thermally and chemically stable under processing conditions, but are susceptible to oxidation. The immersion tube application is a highly oxidizing environment; without fiber and/or tube coatings, the reinforcement would be short-lived in this environment. The SCS-6 monofilament had been demonstrated to be thermally and chemically stable under both processing and operating environments. The larger diameter of the monofilaments is not a disadvantage in this application since the tubes are simple shapes without sharp radii. Hence, the work focused on the SCS-6 monofilament, with the understanding that the smaller diameter SCS-9 filament (75μ vs. 140μ) could be used with similar handling and processing methods for structures with tighter bend radii.

3.2.3 Slurry Formulation

A critical aspect of the NB SiC CFCC process is the formulation of the ceramic suspension or slip which is cast around the fibers to form the green body in preparation for nitriding. This slip contains both alpha SiC and silicon particulates in various size distributions along with additives affecting their surface chemistry (i.e., electrical double layer) in the suspension medium. These formulations must satisfy a number of criteria:

a) high solids loading. Weigh percent solids are typically in the range from 60-85%. High solids content minimizes shrinkage and cracking upon later drying.

b) Stability against sedimentation. This is a function of both particle size and surface chemistry. The stabilizing additives assure that particle surfaces are covered with sufficient chemical species that produce interparticle repulsion.

c) low viscosity. The suspensions should have viscosities in the 100-1000 centipoise range to be castable, i.e., to provide infiltration around fibers in the preform without residual macroscopic voids.

d) green body porosity. Since the dried preform will be subject to gas phase nitridation it should have a network of open connected porosity. Ideally, for net shape fabrication, the porosity network should also accommodate the volume expansion as silicon is converted to silicon nitride. This porosity is determined by the particle size distributions.

Textron and Nova Industrial Ceramics had investigated a number of formulations using water, ethanol and methanol as dispersion vehicles. All of these suspensions, when optimized, showed small and homogeneous pore networks. The properties and compositions of these slurries are summarized below:

Table 3.2-1
Representative Physical Data for Aqueous and Non-Aqueous NB SiC Suspensions

Liquid Vehicle	**Liquid Density**	**Viscosity @ 25 rpm on Brookfield viscometer (in centipoise)**	**Suspension Stability (Sedimentation Resistance and Time-Dependent Behavior)**	**Solids Loading (Weight %)**
Methanol	1.5-1.8 g/cc	100-500	fair - volatilization an issue	62-77%
Ethanol	1.6-1.85 g/cc	90-300	good	65-80%
Water	1.8-2.24 g/cc	150-1000	excellent-pH and viscosity very stable over time periods of weeks or more	77-87%

Table 3.2-2
Typical Particle Size Ranges for Aqueous and Non-Aqueous NB SiC Suspensions

Liquid Vehicle	<200 μm SiC (weight %)	<20 μm SiC (weight %)	<5 μm SiC (weight %)	<20 μm Si Metal (weight %)
Ethanol	20-40	10-20	15-30	15-40
Methanol	0-40	20-40	15-30	15-40
Water	45-65	5-15	10-20	15-40

More stable suspensions with higher solids loading could be achieved with water as the suspension vehicle. For these reasons, as well as eliminating the need to deal with flammable materials during fabrication and drying, efforts were focused on water-based slurries.

The addition of resin binders had been investigated. This was an important factor in making handleable preforms via drum wrapping and added to the green body strength of preforms made by other means. The addition of binders adds an additional process step: the binders must be removed by pyrolysis before final processing. Experience with the filament winding preform fabrication process showed that sufficient green-body strength could be achieved without binders. Hence, the slurry formulations considered here were free of binders.

Another variable in the slurry formulation is the silicon to silicon carbide ratio. At one extreme pure silicon nitride matrix can be produced by using silicon powder only; most formulations considered in this program were in the range of 20-60% silicon. In addition to fixing the overall matrix composition, the fraction of silicon in the matrix also has important considerations for nitridation processing. The conversion of silicon to silicon nitride is highly exothermic with the release of 730 kJ per mole of Si_3N_4 produced. Since the rate of reaction increases with increasing temperature, the reaction rate can undergo uncontrolled acceleration unless the heat of reaction can be removed as it is liberated. The result of such an exotherm typically would be the melting of unreacted silicon, at which point it would wick out of the composite. One of the possible approaches that can be used to control against the occurrence of an exotherm is to dilute the reactants. In this case, the silicon carbide powder can be regarded as an inert diluent which can absorb the heat of reaction and conduct it away to the surface of the part. Towards this end slurry formulations were developed with silicon powder contents in the 10-20% by weight range. These formulations, although lower in silicon content than those examined in Phase I, could meet the slurry criteria enumerated above, produced green bodies of handeable strength in the filament process, and could be successfully nitrided to produce parts with mechanical properties consistent with those observed earlier.

The process development tasks described in the sections that follow were performed using this lowered silicon formulation.

3.2.4 Preform Fabrication

A number of preform fabrication methods had been explored successfully in the Phase I program. In the Phase II program, efforts were focused on fabrication methods that would reduce the number of intermediate handling steps, thereby reducing labor requirements and cost.

For the large tubular structures (immersion tubes and combustor liners) under consideration in Phase II, Textron fixed upon direct filament winding as its primary approach.

At the beginning of this phase, Textron had available a McClean-Anderson model W90 filament winder. This winder is a four axis, fully computer-controlled instrument which can be programmed off-line or at the machine console itself. All four axes of motion are independently programmable, providing operator control over inputs such as mandrel rotation, carriage axial travel and pay-out head rotation. Winding angles are unrestricted since carriage travel and mandrel rotation are not coupled. "Canned" functions can be used to calculate winding parameters with limited operator input. Mixed mode programming is also possible using independent axis, point pair, or time-dependent data inputting. Graphic representation of winding parameters can be accomplished via viewing on an off-line personal computer. The winder operates under McClean-Anderson's COMPOSITRAK filament winding control software system.

The preliminary work to adapt the use of this winder to the fabrication of CFCC preforms had been accomplished in Phase I. Areas which required further improvements to develop suitable economical manufacturing procedures were:

- Modifications of NB SiC and/or NBSN suspensions and slurry impregnation procedures to permit direct filament winding of CFCC preforms with no intermediate operator handling steps.
- Generation of winding algorithms and computer programs in addition to the construction of filament winder pay-out head hardware that could wind preform architectures of interest, and which specifically accounted for the handling characteristics of elastically stiff monofilaments like Textron's SCS-6™.
- Selection of tooling materials and design of tooling hardware that could accommodate schemes for processing tubular CFCC preforms. An important long-term goal of this effort was to develop methodologies for fabricating both closed-ended and open-ended CFCC tubes.

These areas are discussed below:

Slurry Impregnation

Modifications to slurry formulation have been described in Section 3.2.3 above. The winding development was accomplished using a high-solids water based slurry with no organic binder.

The pay-out head of the W90 filament winder is vertically above the rotating work piece. This made possible three different schemes for combining fiber and slurry in the preform. In the first, the fibers pass through a bath of slurry placed between the pay-out spool and take-up mandrel. The fibers are wet by the slurry and carry it to the preform as it builds up on the mandrel. However, because of surface tension, liquid films coating fibers are unstable and break up into a periodic array of droplets. (The "Rayleigh instability" is discussed in Science, vol. 249, pp. 1256-1260 (1990). This string-of-beads configuration provides poor preform structure with numerous voids and irregular thickness build up, especially at fiber crossover points. The second approach is to dispense slurry onto the mandrel from a vessel traversing independently from the fiber pay-out head. This approach introduces a great deal of flexibility into the process in terms of controlling reinforcement volume fraction. In practice, however, the results were very

sensitive to the drying rate of the slurry which could be significantly different between a fresh mandrel at the start of a run vs. a nearly complete wet preform. The third approach, which was also the simplest, is to add slurry periodically to the mandrel while winding the fibers dry. The particle size distribution in the slurry gives good infiltration into the fiber array; few voids are formed and preform densities are high. This is the procedure used for most of the composites made in this phase of the program.

Filament Winding

Filament winding procedures evolved continuously during the Phase II activities in response to both hardware upgrades and feedback from the evaluation of tubes that had been in service at end user sites. The overall objective was to develop winding algorithms for both open and closed-ended tubes which accommodate the high modulus fibers being wound. These winding patterns were required to have a "good" fiber distribution which dispersed the reinforcement uniformly (on a microscopic scale) throughout the matrix. Preform thickness had to be controlled to achieve thermal conductance appropriate to the application, while at the same time fiber volume fraction had to be controlled to achieve cost targets. Finally, fiber distribution over the preform was adjusted to maximize fiber at areas of high stress while reducing fiber content at low stress areas.

Open-ended tubes present the least complex winding situation. The optimum winding pattern to provide both radial and axial reinforcement is a helical wrap. The angle of the helix with respect to the tube axis can specified in the COMPOSITRAK software which is used to generate the machine motion control codes. For a given helix angle, a variable remaining to be determined is the repeat pattern, i.e., the axial spacing between one fiber and the fiber that was laid down on the previous pass of the pay-out head. Normally, if one were winding with fiber tows, this distance would be the width of the tow. With the small diameter SCS-6 fibers, attempting to wind using the fiber diameter or some length close to it to determine this spacing gives unacceptable results in that the composite shows small areas of high fiber density separated by large areas of unreinforced matrix. The values used were on the order of 10-100 times the fiber diameter.

For shapes other than simple tubes, e.g., a change in diameter as a function of axial position, one can enter the mandrel geometry into the software to calculate a modified machine motion which accommodates the change in diameter.

Figure 3.2-1 illustrates an open-ended combustor liner tube with a helical angle of 45°. This tube was wound using the COMPOSITRAK software on the W90 filament winder. Although the fibers appear to be clustered in a window frame pattern, this is only a surface appearance effect; fibers buried in the matrix have a relatively uniform distribution. This is still not a fully optimized winding however since the clusters of fiber crossover points increase tube thickness beyond the desired value.

As can be seen in the photo, there are three rows of holes in the composite arranged around the circumference beginning at about half height. These holes were machined in the tube after processing. Attempts to produce a preform with holes by filament winding around pins placed in the mandrel were not successful since fibers bunched up at the pins.

The winding of closed end tubes presented considerably more problems. The type of part required is shown in Figure 3.2-2. The tube is slightly tapered; one end is open to full diameter

with an integral flange, while the other end has a completely closed dome. The BOTTLEMASTER subprogram of COMPOSITRAK provides some assistance in generating machine winding codes but does not describe this particular geometry. The BOTTLEMASTER winding specifications are shown in Figure 3.2-3.

The procedure employed was to use BOTTLEMASTER to generate machine code for an approximation to the desired shape and then make "on-the-fly" adjustments to that machine code. The greatest difficulty was encountered in preventing fibers from rolling off the dome end of the preform at the turnaround of the carriage motion. As noted above, the usual application of filament winding techniques involves the winding of multifilament tows which lay down on the mandrel in a ribbon configuration. The small diameter, round and smooth SCS-6 fibers have a much greater tendency to slip; this requires that the fiber path be very nearly geodesic. The high modulus of the fibers also tends to lift them off the curved dome surface exacerbating slippage. To counter this effect, the winding motion has to be smooth at the turnaround so as not to introduce bouncing resulting in momentary lack of tension.

These problems were overcome, resulting in the winding shown in Figure 3.2-2. Although the preform was "passable" in that an intact immersion tube could be fabricated, it was still deficient in several respects:a) As in the combuster tube, fiber clusters at filament crossover points produced a thicker than desired part at a given fiber volume fraction; b) Fiber concentration at the dome end produced a further thickening in this region; and c) Fiber slippage became worse at higher winding speeds; maximum usable sped was 4-8% of the machine capability.

Figure 3.2-1

Figure 3.2-2

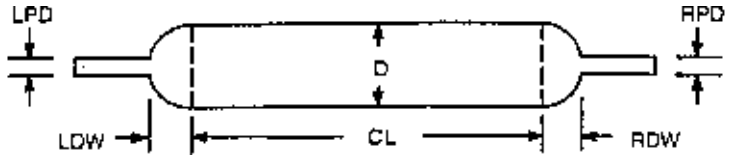

Diameter	*Diameter of cylindrical section in inches.* D in Illustration 12.
Cylinder Length	*Length of cylindrical section in inches.* CL in Illustration 12.
Left Dome Width	*Width of the left dome in inches*. LDW in Illustration 12.
Right Dome Width	*Width of the right dome in inches*. RDW in Illustration 12.
Left Polar Diameter	*Diameter of the left polar opening in inches.* LPD in Illustration 12.
Right Polar Diameter	*Diameter of the right polar opening in inches.* RPD in Illustration 12.

Figure 3.2-3

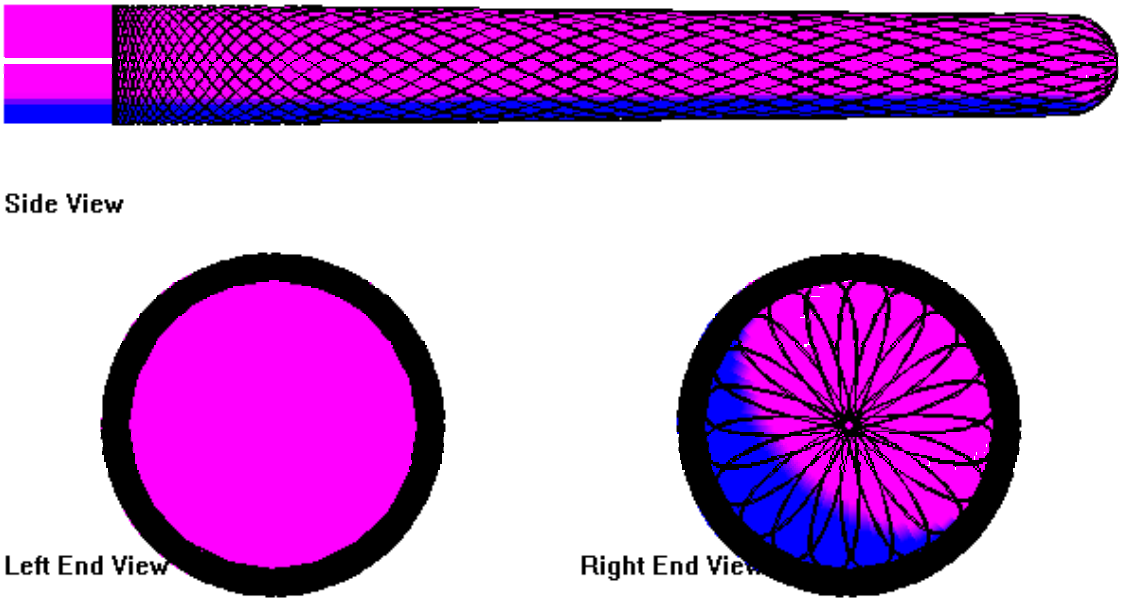

Figure 3.2-4

These issues were resolved when during the course of Phase II Textron acquired a new 5 axis filament winder from McClean Anderson. In addition to mandrel, carriage, cross-feed and eye rotation, the new winder also had independent control over pay-out eye yaw, i.e. the orientation angle of the pay-out eye relative to the mandrel axis. On the 4 axis winder, this was fixed such that the direction of fiber pay-out was normal to the mandrel axis. This added axis allowed much more flexibility in defining a stable winding path over the dome end of the tube and allowed winding speeds to be increased 4-fold.

The five axis winder is under the control of an enhanced computer system (486 vs. Z80 based) and could be programmed using Composite Designer software running under Windows NT. Adjustments to winding programs could be made quickly on the winder console and tested immediately. With the 4 axis machine, winding code adjustments had to be made offline on another computer and downloaded to the winder in a laborious two-step process. This enhancement provided far greater opportunity to achieve improved winding patterns. Figure 3.2-4 illustrates the dome winding pattern used for the immersion tubes tested at the General Motors development facility. The smaller mesh size in this pattern as compared to that in Figure 3.2-2 produced a thinner tube with a smoother surface. To eliminate the diameter enlargement at the dome end seen in earlier tubes, this dome winding was alternated with a similar helical wrap which covered only the cylindrical portion of the tube. A typical overall wrap could include 6 pairs of dome/helix wraps and then end with a dome overwrap. This overall sequence, including smooth transitions between segments, was readily programmed using the Composite Designer winding software.

Modeling results from MSC and experience at GM Saginaw indicated that the area around the melt line of the tube when submerged in molten aluminum was subject to the greatest stresses. The dome end of the tube, on the other hand, was not highly stressed. The winding pattern was

again modified for the most recent tubes being produced for the General Motors production facility in Bedford, Indiana. In the most recent modifications, the mesh pattern for the dome winding was made still finer while decreasing fiber content at the end of the dome. The helical winding was extended to slightly overlap the domed section of the mandrel; it was found that this type of wrap allows removal of the preform from the mandrel with less chance of damage. Finally a shortened helical wrap sequence was added which allows adding a band of fiber concentrated near the melt line region of the tube. The angle of these wraps is approximately 30° with respect to the tube axis except in the transition region near the turnaround point.

The discussion of winding above is all in the context of winding a single SCS-6 monofilament. Some experiments were performed where three fibers were wound simultaneously. The payout carriage on the five-axis winder has provision for six payout spools with individual tension controls. It is clear that the rate of fiber addition to the preform can be substantially increased by multiple spool winding but those winding experiments and other process experience show that there are pitfalls in this approach that are associated with fiber distribution. A great deal of the programming efforts described above were aimed at separating fibers at controlled spacing. Multiple fiber windings had the opposite effect of bundling fibers together. Further, the practical rate at which fibers can be added to the preform is controlled by the slurry drying rate. The matrix has to dry to the point of stably maintaining fiber distribution before too many further fibers are overwrapped. Neither of these considerations presents an insurmountable barrier to multiple filament winding but would have seriously delayed making test and evaluation parts available to the end users. The decision was made to proceed with single filament winding and defer multifilament winding development.

Preform Tooling Development

Early winding trials to establish winding procedures were performed on graphite or steel mandrels. This approach was not acceptable for the fabrication of large closed ended tubes required for field evaluation. The next design consisted of a two part plaster mandrel which was split axially for the length of the tube. The two half-cylinder shells fit over a removable central core. After winding, the central core was removed. This allowed the two half shells to move sufficiently toward the axis to be removed from the preform. The plaster, which was coated with a water-permeable release agent, assisted in the drying of the slurry by absorbing water. During slurry development, some formulations dried too rapidly. This could be retarded by pre-wetting the mandrel.

The immersion tubes provided to Doheler-Jarvis for field testing were wound on this type of mandrel. Examination of returned failed tubes from Doehler-Jarvis revealed a flaw with this design. The composite tubes had two axial lines on the inner surface corresponding to the mating surfaces of the mandrel. Cracks in the tubes that appeared during service propagated to these lines and then along them. Hence, the mandrel was introducing flaws into the composite.

A modified mandrel design is illustrated in Figure 3.2-5. The main body of the tube has a minimum taper to assist in removal of the preform. The separate nosepiece forming the domed

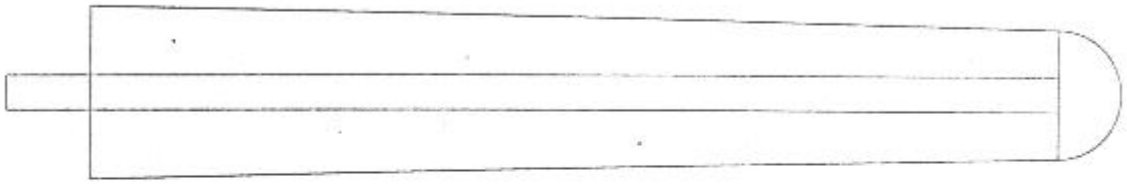

Figure 3.2-5 New Mandrel Design

end is attached to a jackscrew on the axis of the mandrel. The nosepiece fits smoothly onto the main body so as not to introduce a flaw-causing seam. As in the earlier mandrel design, the body and nosepiece are cast of plaster to absorb water from the slurry. After winding the dried green body is released from the mandrel by turning the jackscrew.

This design has worked well and was used for all immersion tubes supplied to General Motors.

3.2.5 Nitridation

As was noted previously, the reaction converting silicon powder in the slurry to silicon nitride matrix is extremely exothermic. Reaction rates become appreciable at about 1000°; hence, temperature control must be precise in order to prevent runaway exotherms. As noted, the possibility of exotherming increases with increasing silicon content. Early development work on the nitridation cycle was performed in the small laboratory chamber. It provided a cycle which performed complete nitridation for a range of slurry compositions without a damaging exotherm. This cycle was a conservative one, requiring two days for the ramp up to 1150°C, and an additional two days for processing up to 1400°C.

The laboratory chamber was too small for the processing of the immersion tubes. A larger chamber with controls similar to the laboratory chamber was ordered and installed.

Prior to the completion of the installation of the new chamber, the set of immersion tubes sent to Doehler-Jarvis was nitrited in a chamber normally used for carbon products graphitization. Although the chamber was reprogrammed for the nitridation cycle, several tubes apparently underwent an exotherm leading to some loss of silicon. The reasons for this occurrence are not clear.

When the new larger nitridation chamber became operational, experiments were performed to reduce the time required for the slurry composition and part geometry of interest. The results are shown in Figure 3.2-6. The original schedule required approximately 100 hours. The schedule currently in use (solid line) cut this time in half. One experimental run (dotted line) cut this further to about 36 hours. For processing of program parts, the more conservative 48-hour schedule was adopted.

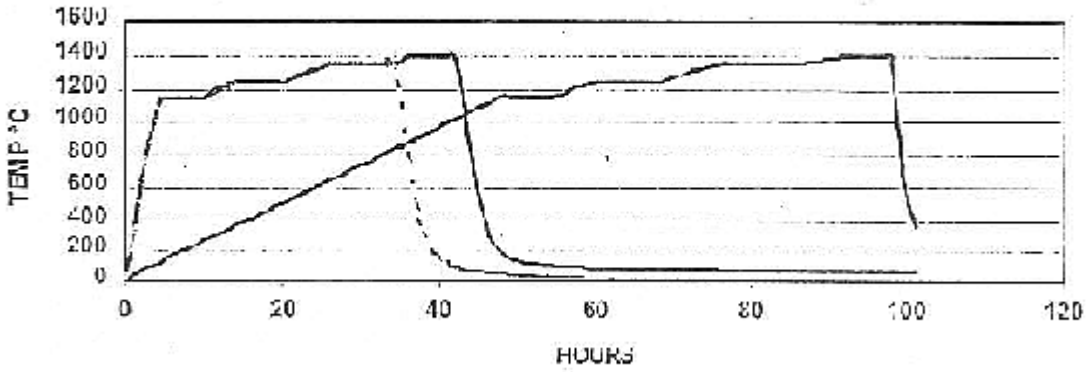

Figure 3.2-6 Nitridation Cycle

3.2.6 Coatings

3.2.6.1 Rapid Densification Coating Process

The objective of this task is to explore processes for coating CFCC components with materials to provide oxidation resistance and to decrease gas permeability. The Phase 1 program examined the applicability of Textron's Rapid Densification (RD™) process for the deposition of silicon carbide based coatings on CFCC materials. The results of those efforts were:

a) Thermodynamic analysis and laboratory-scale trials demonstrated that dimethyl dichlorosilane and methyl dichlorosilane are the precursors of choice for deposition of stoichiometric silicon carbide using the RD™ process.

b) Subscale open-ended graphite fiber based tubes, heated by induction, were coated with silicon carbide by the RD™ process.

c) Monolithic nitride bonded silicon carbide, heated by contact with a graphite susceptor, was coated and infiltrated with silicon carbide. The density of the monolithic material increased from 2.7to 2.9g/cc and the oxidation rate was decreased by an order of magnitude.

The RD™ coating approach continued to be examined in the Phase II program.

One issue to be addressed relative to the coating or densification of CFCC tubes by the RD™ process is the ability to inductively heat the tubes. The tubes' electrical characteristics, and hence, induction coupling efficiencies, are determined by fiber volume fraction and orientation. The problem was explored with a theoretical modeling approach using the MagNet

electomagnetic software package. The objectives of the modeling effort were: a) establish limits on composite construction that can be heated effectively; b) explore the effects of composite architecture variations on heating characteristics; and c) establish preliminary design requirements on the induction heating hardware that will be required.

A. Model Description

1. Materials Properties

The materials under consideration consist in general of up to 10% by volume of SCS-6 fibers in a non-conducting matrix with fiber orientation varying from parallel to the tube axis (0°) to circumferential (90°). Because of the insulating matrix, the composite on a micro-scale consists of a large number of discrete, small conducting wires. However, except for highly conducting or magnetic materials and very high frequencies, the penetration depth of the field into the composite is much larger than fiber or interfiber dimensions. In this case we approximate the bulk properties of the composite by the volume-averaged constituent properties, adjusted for fiber orientation relative to the field.

The measured resistance of SCS-6 fiber at RD™ process temperatures is approximately 175 ohms/inch. For a nominal 140 micron diameter fiber, this corresponds to a resistivity value of $1x10^{-4}$ ohm meters. Fiber radial resistivity is not considered since the fibers are insulated from one another. A composite with 10 vol% fibers all oriented optimally in the electric field would have a resistivity Of $1x10^{-3}$ ohm meters. or, equivalently, a conductivity of 10^3 S. This material was designated COMI in the model calculations. At the same volume fraction, but with the fibers at 45° to the field, the equivalent bulk conductivity would fall to $0.707x10^3$ S (COM2); a 5 vol % composite with 45° fibers would have a conductivity of $0.35x10^3$ S (COM3). To examine the effects of adding unidirectional plies to the structure, a material COM4 was defined with a conductivity of $2x10^3$ S; this would correspond to a ply 10 mils thick with 80 fibers/inch. Any ply with fibers oriented perpendicular to the induced voltage would exhibit a conductivity of zero. The defined material properties are summarized below:

Material	Fiber Volume	Orientation	Conductivity	Relative Permeability
COM1	10	0°	$1x10^3$	1
COM2	10	45°	$0.7x10^3$	1
COM3	5	45°	$0.35x10^3$	1
COM4	20	0°	$2x10^3$	1

2. Model Geometry

A possible scenario for the application of RD™ technology to CFCC would be the coating or densification of a 6" diameter x 36" long tube by translating it through a circumferential solenoid coil. A typical coil would have 2 - 3 turns of 0.5" copper tubing

for the conductor with the coil axis coincident with the CFCC tube axis. For modeling purposes, we examine a 5" high segment of the tube; the tube is taken to have an inner diameter of 6" and a wall thickness of 0.25" ' The coil has a diameter of 8 " and a turn spacing of 1" (both measurements relative to the centers of the conductors). Since the problem is axisymmetric, it can be completely specified in the r, z plane, i.e., a vertical plane containing the tube and coil axis. Figure 3.2-7 shows the basic problem definition illustrating a 3 turn solenoid coil and the CFCC tube wall in cross section; the tube and coil axes are coincident with the left hand edge of the figure. The tube wall is shown as segmented solely for convenience in calculating power density vs. height.

The computational mesh used to solve the electromagnetic problem is shown in Figure 3.2-8; it contains approximately 1200 elements. The regions labeled F are assigned the electrical properties of air (non-magnetic, non-conducting). The mesh is much finer in the vicinity of the coil conductors. This is illustrated in Figure 3.2-9 which shows the region near the lowest coil segment.

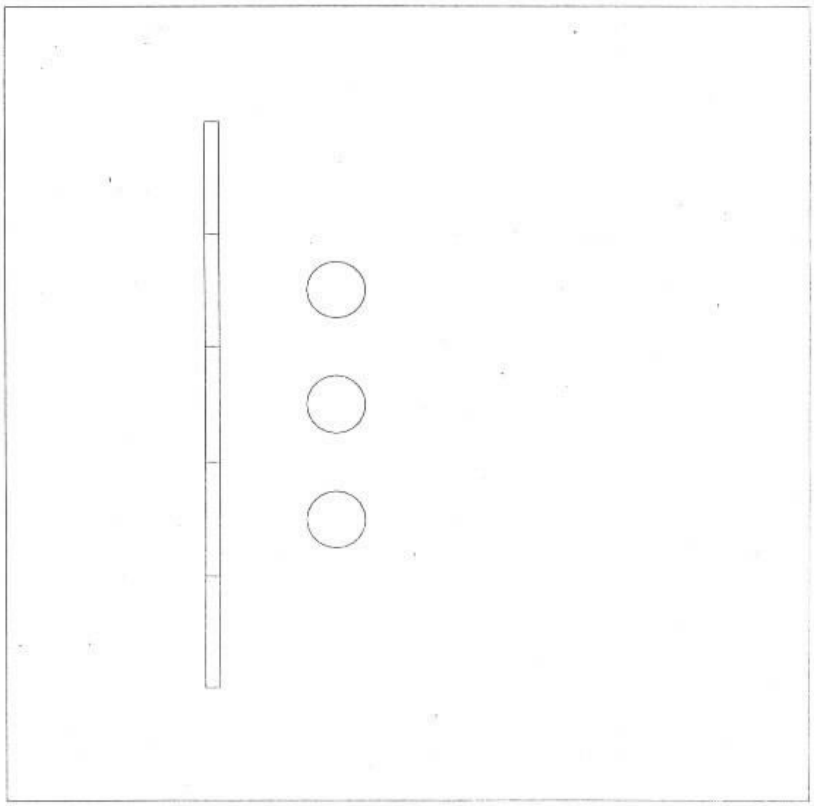

Figure 3.2-7 Electromagnetic Model Definition

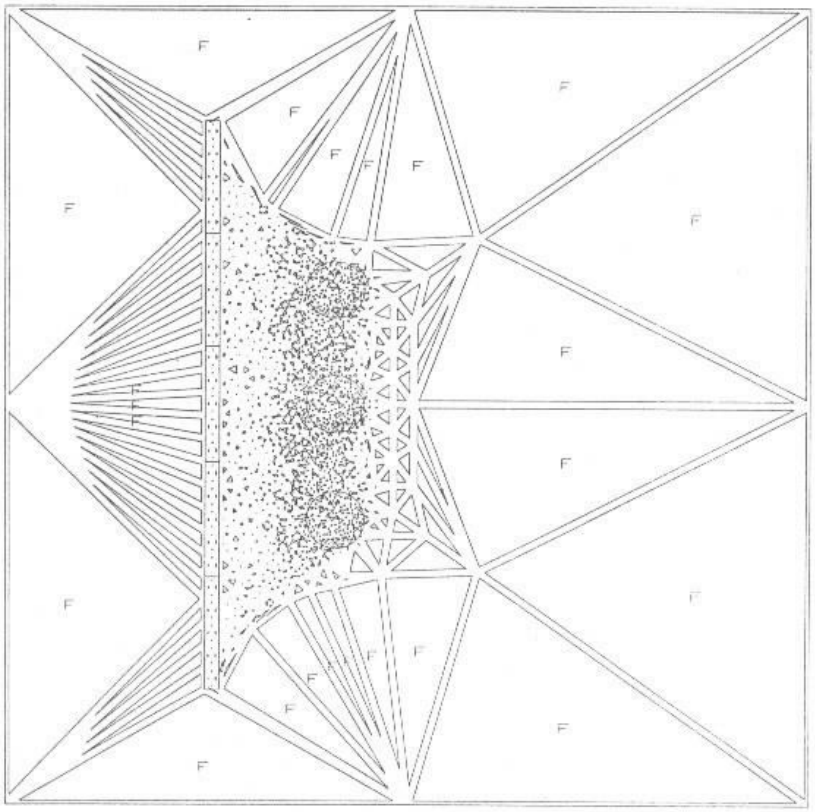

Figure 3.2-8 Mesh for Modeling Power Loss in CFCC Tube

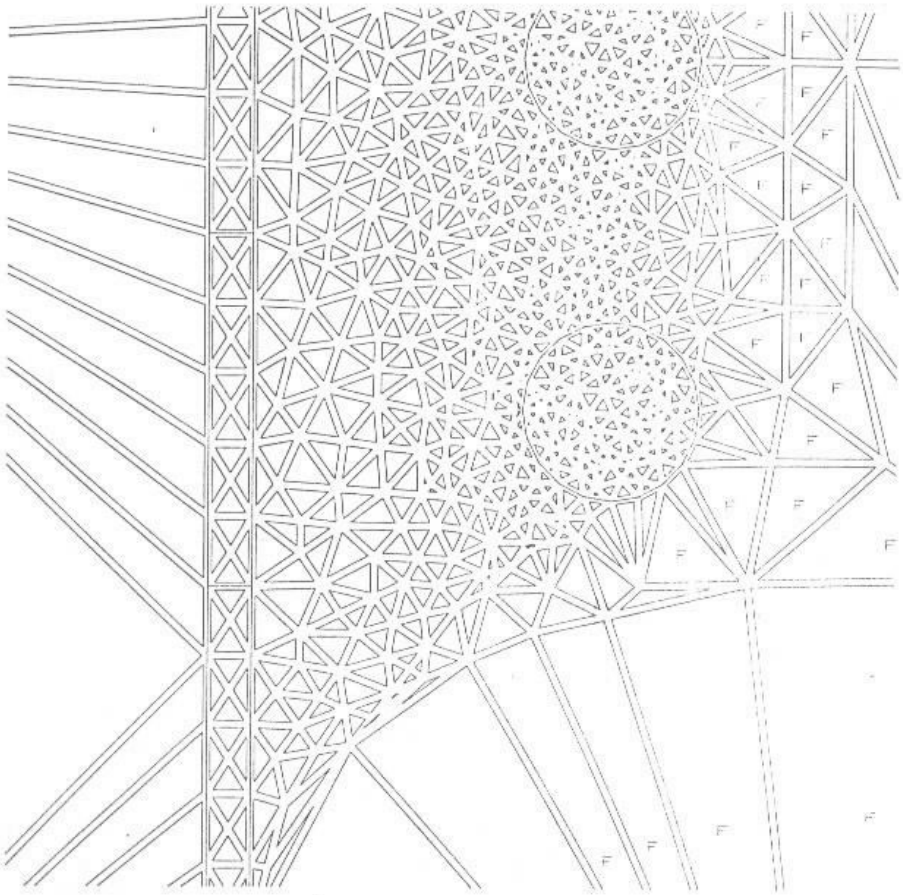

Figure 3.2-9 Detail of Computational Mesh

3. Problem Definition

Two geometries were examined: the tube and 3-turn coil illustrated in the figures and an analogous 2-turn coil arrangement. The inputs required for the electromagnetic problem are coil current and frequency. These were chosen to be within the range of a 50–300 khz

variable frequency 100kW power supply which is part of the RD™ facility. For this set of calculations, the coil current was fixed at 600 amps, a typical operating value.

The problem was solved using the MagNet software (version 5.la) from lnfolytica Corporation. This provides the full solution of Maxwell's equations for the problem. Attributes extracted from the solution were induced current density and induced power in the preform. For convenience of examining the output, the power dissipation was calculated for five 1" high zones in the tube.

B. Results

1. Frequency and Conductivity

The relationship between total power induced in the tube and material conductivity is shown in Figure 3.2-10. For this range of frequencies and conductivities, field penetration depth into the preform is not an important factor; in this case, the relationship is linear. The calculations below were performed for the 'worst case", i.e., 5 vol% fibers oriented at 45° to the tube axis.

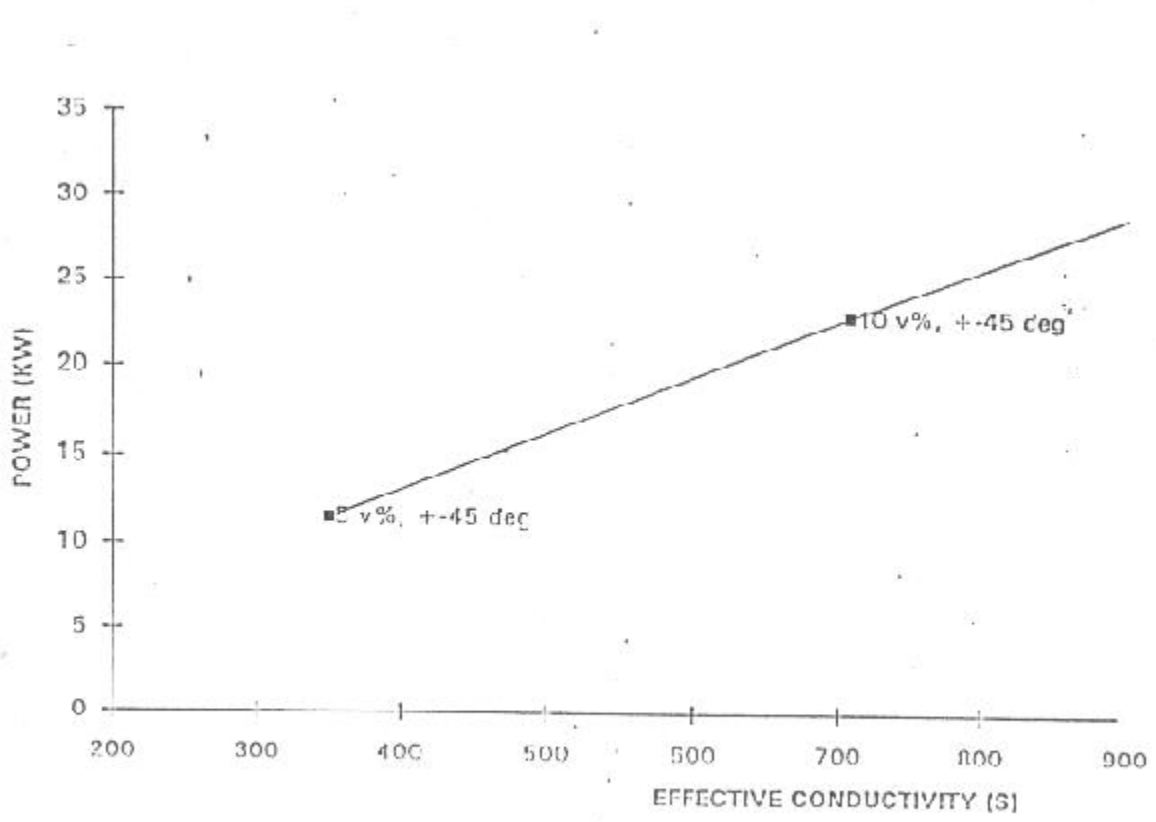

Figure 3.2-10 Induced Power (3 turn coil, 150 kHz)

Figure 3.2-11 shows the relationship between total induced power and the frequency. The coupling increases as the square of the frequency. For both the 2-turn and 3-turn coils considered, the heating efficiency (power in the tube vs. supply output power) also increases from approximately 40% at 50 khz to above 90% at 300 khz.

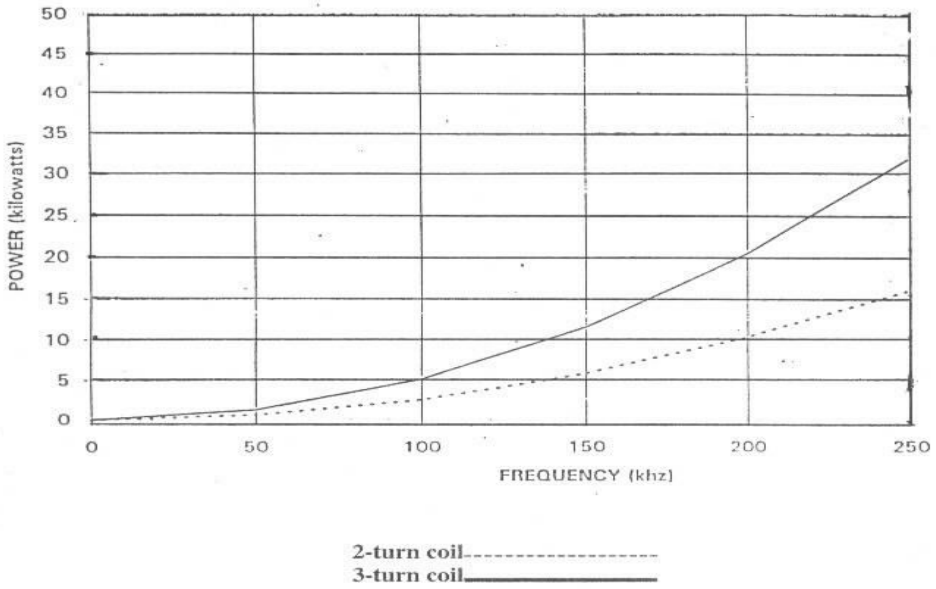

Figure 3.2-11 Total Induced Power vs. Frequency

While the total power in the preform demonstrates the basic characteristics of the problem, further refinement is necessary to evaluate the possibility of applying RD™ to this system. Figure 3.2-12 illustrates the computed current distribution in the tube. The power dissipation was calculated for 1 " high segments of the tube; those results are shown in Figure 3.2-13. The quantity of most interest is the power in the "hot zone" which is situated symmetrically with respect to the coil elements.

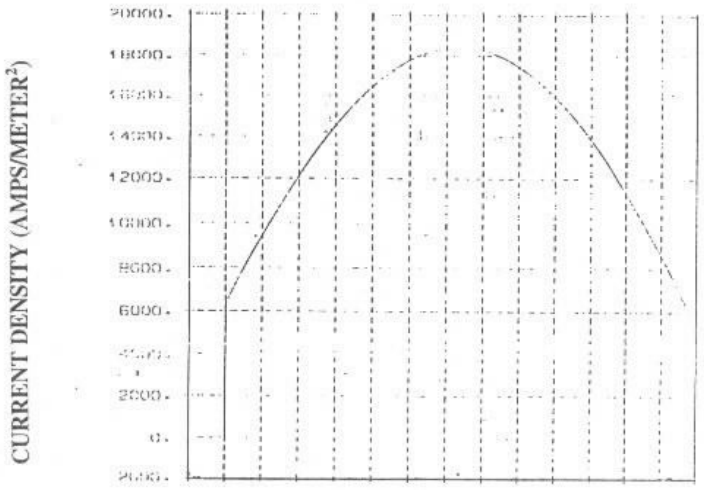

Figure 3.2-12 Induced Current: 250 kHz, 3-turn coil

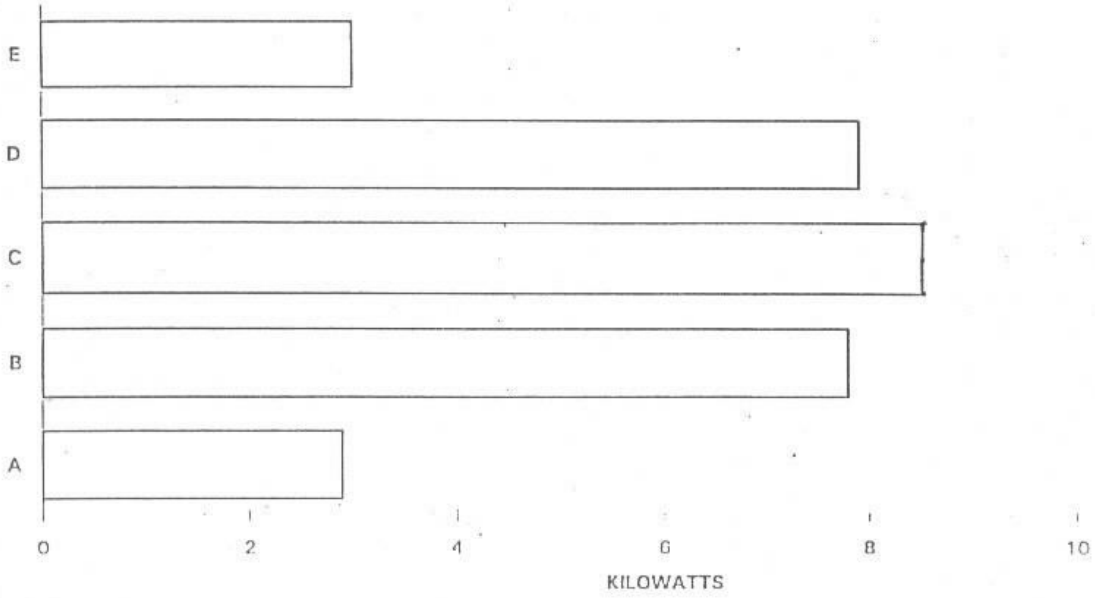

Figure 3.2-13 Induced power vs. Height – 3-turn coil,250 kHz

An important element of the RD™ process is the extreme heat transfer which occurs between the preform and the surrounding boiling precursor. The most useful parameter for characterizing this is the power flux, i.e., induced power divided by preform surface area. The power flux vs. frequency for the central region of the tube is plotted in Figure 3.2-14 for the two coils under consideration. The flux was calculated using both the

inner and outer surfaces of the tube. This is appropriate for the open-ended tube being considered here, since both surfaces would be in contact with the precursor liquid. For the closed-end tube, however, the net heat loss from the inner surface would be small. Energy loss would be forced to occur from the outer surface and flux levels would roughly double.

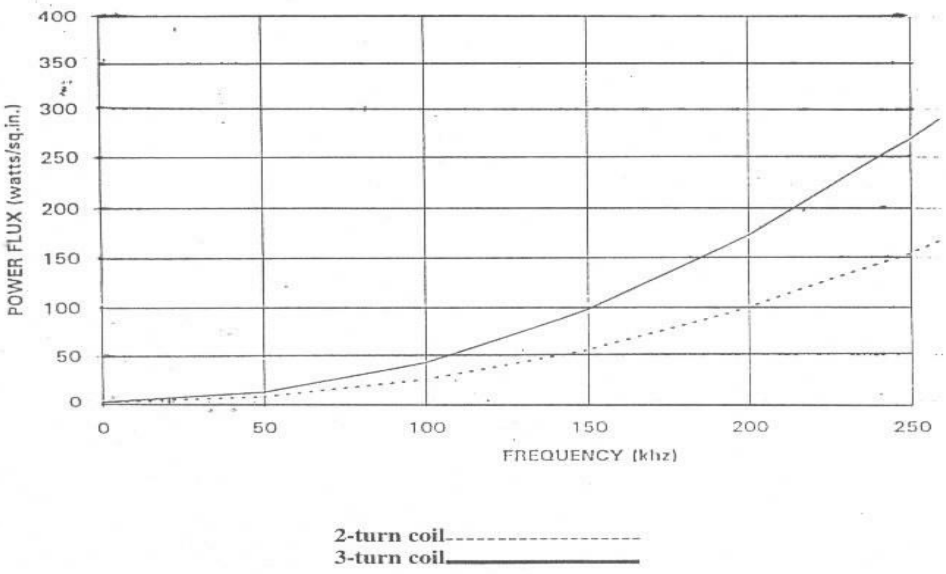

Figure 3.2-14 Power Flux at Tube Mid-point

The deposition of SiC under RD™ conditions is not yet well characterized. The case of carbon deposition is well characterized, however: energy fluxes in the range of 100 - 400W/in^2 are required depending on the preform thickness and thermal conductivity and on whether interior densification or surface coating is desired. At this stage, the carbon deposition results provide the only quantifiable guidelines.

With regard to the 100 - 400W/in^2 guideline, Figure 3.2-14 shows that the 5 vol% fiber, +/- 45° orientation case is marginal for heating purposes. Even assuming that all net energy flux is through the outer surface only, the required energy levels are reached at the highest frequency only for the 3-turn coil case. Hence, this tube architecture should be

considered a limiting case. Higher fiber volume fractions or an increase in the circumferential component of fiber orientation will make the tube easier to heat adequately.

2. Tube Architecture Variations

   In light of the results of the preceding section, a preliminary investigation was initiated on the effects of a tube architecture variation. The basic problem is the same as treated above (5 vol% fiber, +/ 45° orientation), except that one circumferential ply was added to the filament winding. The ply was assumed to have 80 fibers per inch, have an overall thickness of 10 mils and be positioned 0.04" below the outer surface of the tube. The finite element mesh in this case consisted of 1900 elements. The solution showed that the addition of this ply increased energy accumulation in the preform by 20%. The result indicates that in a marginal heating situation, relatively small changes in tube architecture could cause significant changes in heating.

3. Hardware Requirements

   In addition to coupling effectively to a preform, the induction coil being used must also couple to the power supply. A large mismatch between power supply and load impedances would prevent power from reaching the coil. For the power supply in question, this requires that the inductance of the coil circuit be on the order of 0.5 microhenry or less. The coils considered above were analyzed with the LCD (Litz Coil Design) software from MIT. The simplest case of a continuous 2 or 3 turn spiral coil gives inductance values 2 - 4 times higher than the optimum. Experience has shown that the values can be brought into the desired range through series-parallel circuit variations using discrete coil turns.

The application of coatings using the RD™ process was re-examined in light of the requirements posed by the immersion tube component. As the program progressed, the design that evolved was a closed-ended tube with 2-5 volume percent fibers arranged primarily ± 30° relative to the tube axis. This design presents severe technical problems for RD™ processing.

The modeling results showed that a 5v% composite with ± 45° fiber orientation is a marginal case for induction heating. The ± 30° fiber orientation would decrease induced power by 28% relative to the ± 45° case, and the lower fiber volume fraction would decrease heating even further.

The closed end tube configuration presents another problem, especially for infiltrating and coating the inside of the tube. An essential feature of the RD™ process is the severe and controllable thermal gradient through the part caused by the heat loss to the boiling liquid precursor. With a closed end, the inside wall is not exposed to natural convection. At best, the process would require redesign to provide the necessary cooling.

There are also environmental and cost impacts associated with RD™ of CFCC tubes. The RD™ process is suited to carbon deposition (for carbon parts) using cyclohexane as the precursor. Deposition of SiC requires using organochlorosilanes as the precursor which require far more stringent control procedures. The capital requirements for the silane control are much larger than for Carbon RD™.

Given the aforementioned technical, environmental and cost issues it was decided that the RD™ process would no longer be considered for the CFCC program.

3.2.6.2 CVC SiC Coatings

Thermotrex Corporation has developed a silicon carbide coating process in which chemical vapor deposition onto a substrate is enhanced by the simultaneous addition of SiC particulate and chopped SiC fibers. The fibers and particulates provide nucleation sites for the CVD, greatly increasing the rate of deposition.

Textron initiated a subcontracted program with Thermotrex to apply CVC coatings. The objective of this program was to investigate-the potential synergistic benefits of Thermotrex Corporation's (TTC) CVC fiber reinforced ceramic composite process to Textron's CFCC material system. Enhancements to CFCC product density and complex shape fabricapability were evaluated.

TTC used the CVC process to fabricate a composite of SiC reinforced with 1/8" to 1/4" long Textron fibers and 30μ SiC powders. Two types of materials were fabricated, A. CVC SiC deposited on nitrited SiC material supplied by Textron; and B. CVC SiC deposit was bonded to a fiber/slurry and exposed to the gas nitridation process by Textron. These materials were deposited in a vertical CVC reactor in the shape of 6" diameter disks. The CVC SiC deposited with chopped 1/8" to 1/4" fiber and 30μ SiC powder was evaluated to determine strength, toughness and microstructure.

TTC also used the CVC process to fabricate freestanding SiC tubes 4" in diameter reinforced with chopped 1/8" to 1/4" fibers and 30μ SiC powder to deposit SiC reinforced with 1/8" to 1/4" fibers and 30μ SiC powder on CFCC cylindrical section supplied by Textron.

TTC conducted 20 CVC experiments to deposit SiC reinforced with Textron fibers. Three 6" diameter disks of CVC SiC were delivered for gas nitridation processing by Textron. The bond between the CVC material and the CFCC material was excellent. TTC deposited 3 disks 6" in diameter of CVC SiC reinforced with Textron fibers on CFCC material supplied by Textron. The bond between these two materials was also excellent. TTC also deposited four CVC SiC 4" diameter tubes 4" to 12" long. These tubes were delivered to Textron. Finally, TTC deposited CVC SiC on the inside and outside surfaces of two CFCC nitrided tubes. These experiments are described in detail below.

Textron fabricated three flat CFCC disk substrates for CVC SiC deposition. These disks were coated on one side in the 30 kW vertical CVC reactor. The diameter of the CVC SiC deposit on the graphite disk was 7". A drawing of the vertical reactor is shown in Figure 3.2-15. The reactor could use dual or single injectors for particulate and gas reactants. The position of the injectors from the center line of the rotated graphite disk controls the particulate distribution in the matrix and the thickness profile of the deposited SiC.

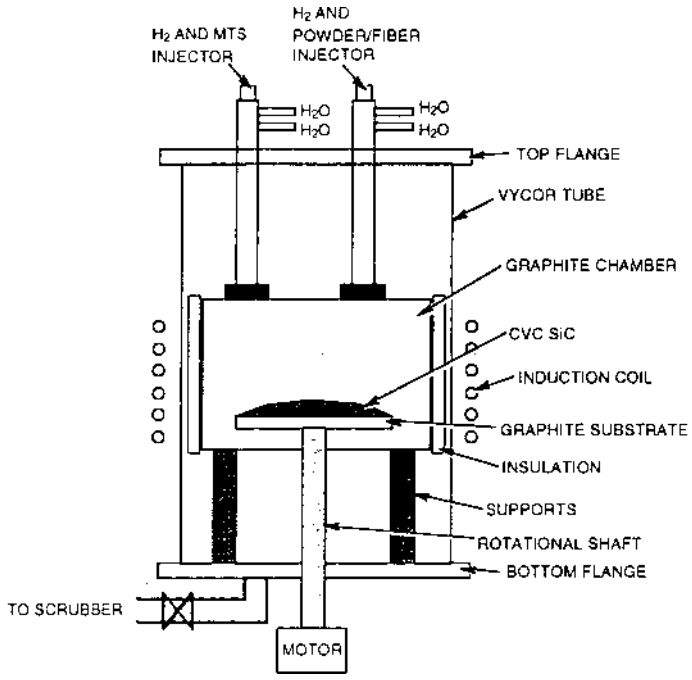

Figure 3.2-15 Dual Injector Vertical Reactor

Table 3.2-3, Test 7, 8 and 9 summarize the CVC process parameters used to coat the CFCC disks. The bonds between the CVC SiC coating and the CFCC substrate appeared excellent. The SiC coatings had five transitional layers and are summarized as follows: 1.) Start with pure CVD SiC, 2.) CVC SiC with 30μ SiC powder, 3.) CVC SiC with Textron fiber and 30μ SiC powder, 4.) CVC SiC with 30μ SiC powder, and 5.) End with pure CVC SiC. The majority of the coating time was conducted in the third layer with fibers and powder. Layers 1, 2, 4 and 5 were approximately 10 minutes in duration.

Table 3.2-3, Tests 3, 4, 5, 6, 10, 11 and 12 summarize the CVC process parameters used to fabricate SiC disks. CVC SiC Runs No. 4001 and 4002 were used for material characterization which is summarized in Section 3.4. The CVC SiC deposit from runs 4001 and 4002 was sectioned for bend bars and microstructure evaluation. Three CVC SiC disks were sent to Textron for gas nitridation processing. The bond between the CFCC material and the CVC SiC was excellent.

Table 3.2-3, Tests 15 and 16 summarize the CVC SiC parameters used to coat the inside and outside diameter of the CFCC tubes in a single stop. All tube deposit experiments were conducted in the 20 kW horizontal CVC reactor. Powder and gas reactants were mixed in a single half inch diameter manifold inlet. A water cooled molybdenum inlet manifold was utilized. Material was deposited on the inside, graphite tube substrate 4.5 inches in diameter by 24 inches long. A drawing of this reactor is shown in Figure 3.2-16. The graphite tube was heated by a 20 kW inductive power supply. The reactor's hot zone produced uniform CVC SiC material 4"-6" long. Materials from the flat plates were subjected to microstructural examination (optical microscopy), flexural strength and fracture toughness testing.

Table 3.2-3 CVC SiC Runs: Summary of Process Parameters

Test No.	Run No.	Temp (Deg C)	MTS Feed (Lb/hr)	H2 Feed (LPM)	H2-MTS Feed LPM	H2-MTS Molar Ratio	Powder Feed (g/hr)	Fiber Feed (g/hr)	Growth (mil/hr)	Reactor H-Hor V-Ver	Substrate	Deposit Thickness (mil)	Comments
1	3972	1370	1.50	17.0	6.0	10.0	4.0	10.00	8.00	H	Graphite Tube	50	Horizontal Thickness Uniformity Calibration
2	3973	1370	1.50	17.0	6.0	10.0	4.	20.00	10.0	H	Graphite Tube	100	Increase Fiber Volume %
3	3977	1360	1.40	11.0	6.0	6.9	5.0	8.00	35.5	V	Graphite Disk	150	Vertical Thickness Calibration
4	3978	1370	1.40	11.0	6.0	6.9	5.0	8.00	35.5	V	Graphite Disk	230	CVC SiC Disk (6")
5	3985	1370	1.40	11.0	6.0	6.9	5.0	15.00	35.5	V	Graphite Disk	230	CVC SiC Disk (6")
6	3986	1360	1.40	12.0	6.0	7.5	5.0	10.17	32.0	V	Graphite Disk	40	Test Auto Temp Control
7	3987	1370	1.40	12.0	6.0	7.5	5.0	11.37	36.0	V	Graphite Disk	180	Abort Run MTS Pressure Textron Disk
8	3991	1370	1.40	1.4	12.0	6.0	5.0	10.00	35.7	V	Nitrited Disk	180	CVC SiC on Textron Disk
9	3992	1365	1.40	1.4	12.0	6.0	5.0	7.65	30.0	V	Nitrited Disk	120	CVC SiC on Textron Disk
10	4001	1360	1.40	12.0	6.0	7.5	5.0	6.75	34.0	V	Graphite Disk	230	CVC SiC For Bend Bars
11	4002	1360	1.40	12.0	6.0	7.5	5.0	12.00	34.0	V	Graphite Disk	240	CVC SiC For Bend Bars
12	4006	1360	1.40	12.0	6.0	7.5	5.0	12.00		V	Graphite Disk	300	CVC SiC For Bend Bars
13	4013	1360	1.60	12.0	6.0	6.6	5.0	16.00	10.0	H	Graphite Tube	30	Shack Down Run
14	4014	1360	1.60	12.0	6.0	6.6	5.0	8.	8.0	H	Graphite Tube	30	CVC SiC Tube
15	4062	1370	1.60	12.0	6.0	6.6	3.0	4.0	15.7	H	Textron Tube	110	CVC SiC on Textron Tube
16	4067	1370	1.60	12.0	6.0	6.6	3.0	4.0	15.0	H	Textron Tube	120	CVC SiC on Textron Tube
17	4069	Run	Aborted	Due	To	MTS	Problem				Graphite Tube		CVC SiC Tube
18	4070	1370	1.80	12.0	6.0	7.0	3.0	4.0	16.0	H	Graphite Tube	150	CVC SiC Tube
19	4075	1370	1.8	12.0	6.0	7.0	3.0	4.0	16.0	H	Graphite Tube	100	CVC SiC Tube

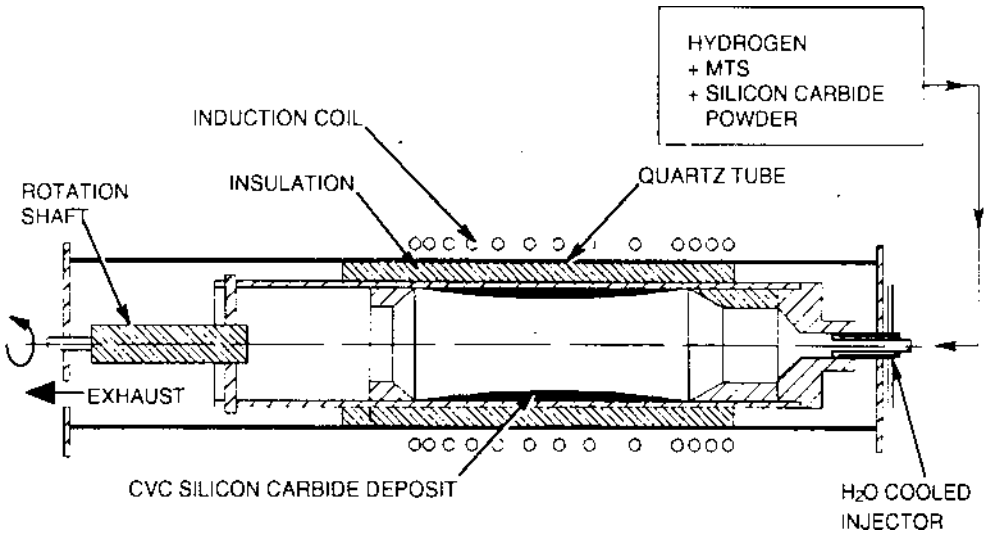

Figure 3.2-16

Microstructure

The #4001 material shows uniformly distributed fibers and particles in a CVD SiC matrix. The matrix has a layered structure, which is similar to those observed in the previous runs (2-4). The porosity of the #4001 material is approximately 3%. The volume percentages of the dispersed fibers and particles are 7% and 4% respectively. High-magnification views of the microstructure reveal satisfactory bond between the particles and the matrix. It appears that the particle-matrix-bond is stronger than the fiber-matrix bond, presumably due to the fact that the particle has a rough and irregular surface while the fiber has smooth surface.

The nucleation of CVD apparently occurred on the surfaces of the solid objects (graphite, SIC particles, and SiC fibers), probably due to reduced formation energy. The orientation of the CVD SiC layers was therefore controlled by the curvature of the nucleation surface. With continuous additions of SiC particles and SiC fibers during CVD processing, the near spherical SiC particle surfaces and the tubular SiC fiber surfaces became the nucleation sites of CVD SIC. Therefore, the growth of CVD SiC resulted in a layered structure with either an onion-like shape or a tubular shape.

Similar to the #4001 material, the #4002 material also shows uniformly distributed fibers and particles in a CVD SiC matrix. On the other hand, the porosity and particle/fiber fractions in the #4002 is substantially higher than the #4001 material. The porosity of the #4002 material is approximately 6% , while the volume percentages of the dispersed fibers and particles are approximately 11% to 7% respectively. The relatively high porosity level in the #4002 material is believed to result from the large amounts of the fibers and particles.

Flexural Strength

A total of 30 beam bar specimens (15 specimens from each run number) were used in the present study. The specimen geometry is in accordance with ASTM C1161, "B" configuration, with a length of 45 mm, a width of 4.0 mm, and a height of 3.0 mm. The four-point flexural tests were conducted at room temperature on a computerized MTS machine.

Five specimens from each run number were fractured during initial loading or broken at locations beyond the top span, probably due to internal flaws in the specimens. The results from these specimens are not reliable and are therefore disregarded. 20 specimens fractured at the beam bar middle, within the top span (inner span). The CVC SiC specimens exhibit limited deflection and very little ductility, which is typical of a brittle material.

Fracture Toughness

A total of 20 notched beam bar specimens (10 specimens from each run number) were used in the present study. The specimen geometry is in accordance with ASTM C1161, "B" configuration, with a length of 45 mm, a width of 3.0 mm, and a height of 4.0 mm. A pre-cracked notch, with a penetration depth of 1 mm, was made at the middle point of the specimen. The four-point flexural tests were conducted at room temperature on a computerized MTS machine, per ASTM C1161 (1).

Two specimens from #4002 material were broken at locations beyond the top (inner) span during testing, probably due to internal flaws in the specimens. The results from these two specimens are not reliable and are therefore disregarded. The other 18 specimens fractured at the beam bar middle, at the notch. Most of the CVD SiC specimens exhibit slow load drop after the peak load is reached, suggesting a good fracture toughness.

The results obtained from the present study are summarized in Table 3.2-4. Layered and fine-grain structures are observed in the subject materials. The presence of voids (pores) in the matrix are believed to be mainly responsible for the relatively low flexural strength and fracture toughness of the subject materials. CVC SiC with reduced porosity is expected to show improved mechanical properties.

The free-standing tubes and coated composites shipped to Textron have not been evaluated. ThermoTrex is unable to provide coatings for full scale immersion tubes with its present capabilities. Further coating and evaluation efforts in this area are on hold.

Table 3.2-4
SUMMARY OF THE RESULTS FROM THE #4001 AND #4002 CVC SiC MATERIALS

Run No.	#4001	#4002
H_2/MTS Ratio (-Ratio)	7.56	7.56
Microstructure	Layered	Fine Grain and Layered
Porosity	3°	6°
Fiber Content	7 Vol. °	11 Vol. °
Particle Content	4 Vol. °	7 Vol. °
Flexural Strength	168 MPa (24.4 ksi)	174 MPa (25.2 ksi)
Fracture Toughness	0 MPa $\sqrt{m}$ (2.90 ksi $\sqrt{in}$)	3.59 MPA $\sqrt{m}$ or 3.26 ksi $\sqrt{in}$
Fracture Surface	Rough	Rough
Fiber Rupture	Yes	Yes
Fracture Path	Transgranular	Transgranular

3.2.6.3 CVD SiC Coatings

Introduction

The objective of this effort was to determine the technical feasibility and economic viability of ultimately coating full-scale Textron CFCC immersion tubes (approximately 8" ID x 43" long close-ended tubes). The coating material was silicon carbide (trade name PerformanceSiC™) applied by a low pressure chemical vapor deposition (LPCVD) process developed by Performance Materials, Inc. (PMI). The purpose of applying a CVD SiC coating to the Textron CFCC material was to improve its high temperature oxidation resistance, and thus extend the performance life of the Textron composite material. The approach of this effort was to determine the materials compatibility of the Textron CFCC material with PerformanceSiC™ CVD silicon carbide, as well as the Performance Materials LPCVD process. This report covers the coating feasibility study as laid out in Phase One of Performance Materials, Inc., original proposed effort. Included in this report are the results of three test CVD deposits in the PMI R&D scale LPCVD apparatus, as well as one test deposit in the PMI large manufacturing LPCVD system. In addition, a brief assessment of the economic feasibility of this approach is presented.

CVD Coating Deposits and Characterization Results

Substrate samples of Textron reaction bonded silicon carbide/silicon nitride composite material were provided by Textron Systems for the application of PerformanceSiC™ CVD silicon carbide coating. Photos of typical sample substrates are shown in Figures 3.2-17 and 3.2-18. Substrate geometries included both flat and curved surfaces. An additional larger composite substrate was provided for a test coating in PMI's large manufacturing scale LPCVD system. The following sections show the results of three coating runs in the R&D system as well as one coating run in the manufacturing system.

The R&D system consisted of a three zone furnace rated to 1600°C with a hot zone of 5 inches diameter by 14 inches. The internal chamber was graphite with custom fixturing for the substrate materials. Process gases, metered through microprocessor-controlled mass flow controllers, were admitted through a water-cooled high temperature alloy gas injector. The system was connected to a 32 cfm dry vacuum pump, with pressure controlled by a microprocessor-controlled throttling valve. Pump effluent was scrubbed. Process control, data logging and database storage was accomplished through Windows-based software with graphical interface.

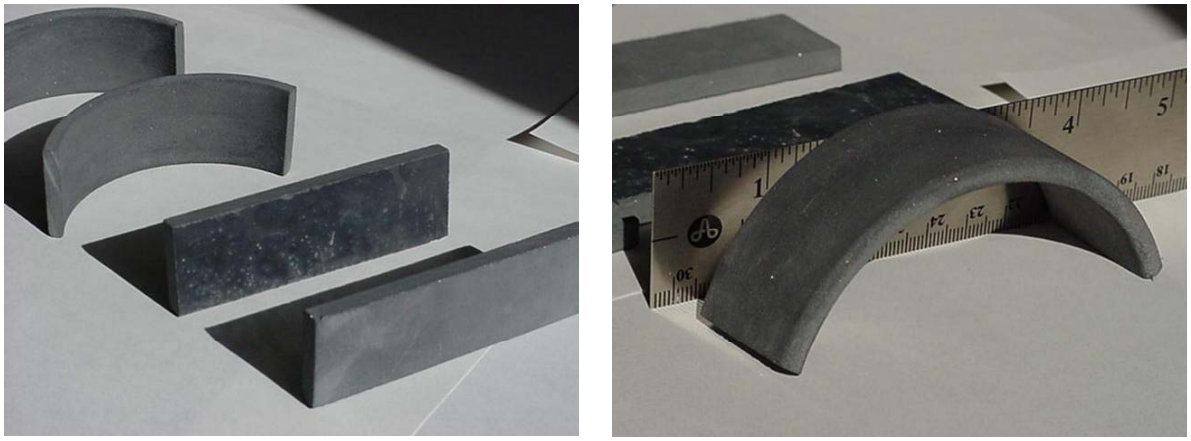

Figure 3.2-17 Samples of Textron's silicon carbide/silicon nitride composite material to be used as substrates in this coating feasibility study. Samples with both flat and curved geometry were coated.

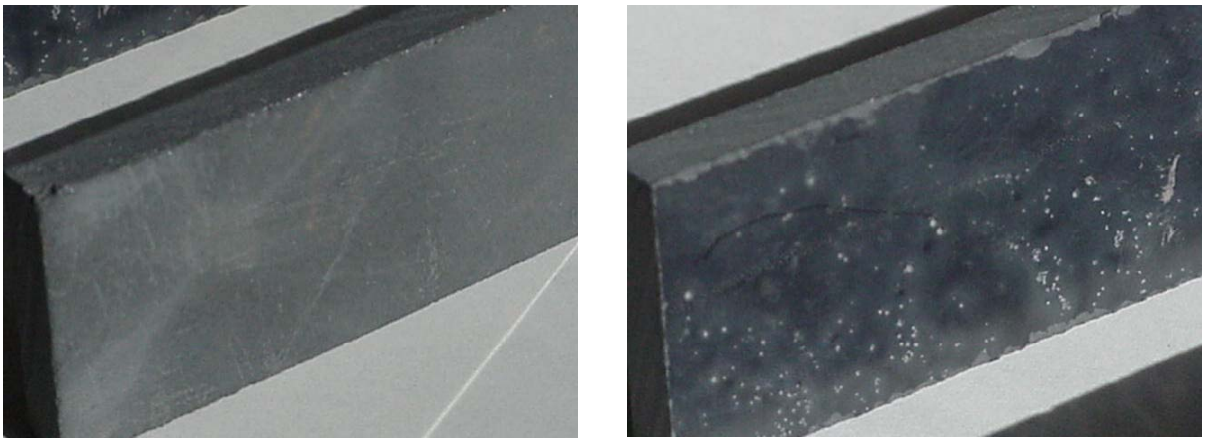

Figure 3.2-18 Close-up of surface textures of Textron SiC/Si_3N_4 composite samples. The photo on the left shows the dull grainy texture typical of the inside of a Textron-manufactured CFCC tube. The photo on the right shows the smooth, shiny texture typical of the outside the CFCC tube.

R&D CVD Scale Test Deposit No. 1

The first LPCVD deposit of SiC was carried out in the PMI R&D scale apparatus. A flat composite substrate was used as shown in Figures 3.2-17 and 3.2-18. The deposit was carried out at a control temperature of 1385°C for 4.5 hours. The characteristics of the coating are summarized in the following series of micrographs. The coating was approximately 250 μm in thickness. The surface of the coating was highly nodular. This is attributed to the CVD reactive gas initiation procedure as well as the temperature of the deposit. The CVD SiC coating was very well bonded to the SiC/Si_3N_4 substrate. While there was no appreciable porosity or delamination observed at the substrate/coating interface, there was a band of porosity observed in the coating approximately 20-80 μm from the interface. One possible explanation for this phenomenon is a reorganization of porosity during the deposition by a mechanism analogous to the Kirkendall Effect (JOM, 49(6), 1997, pp. 15-19). It should be noted that the porosity disappeared as the deposit proceeded, and that approximately the outer

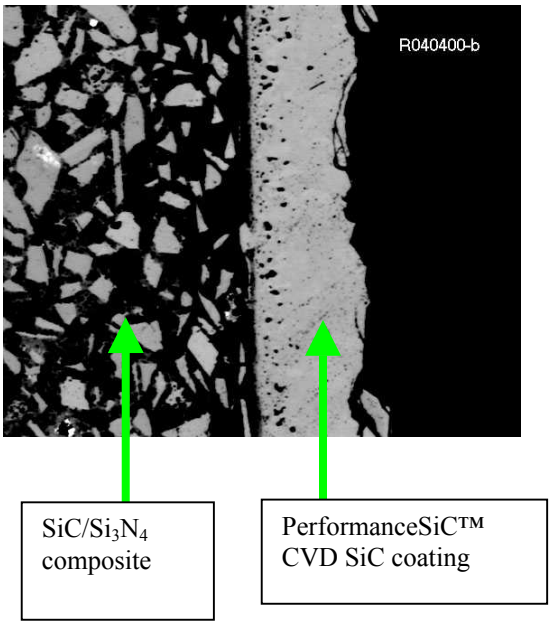

Figure 3.2-19 Optical micrograph (Mag = 50X) of a polished cross-section of test deposit #1. Notice the band of porosity in the coating close to but not at the interface.

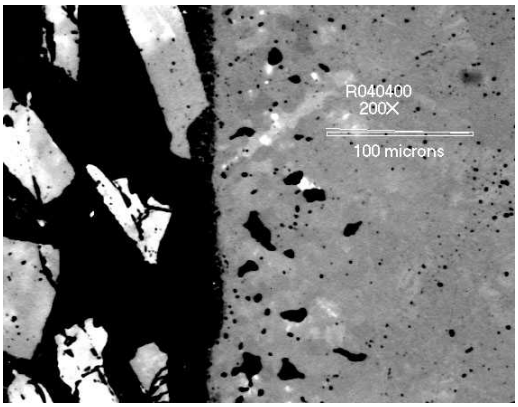

Figure 3.2-20 Optical micrograph (Mag = 200X) of a polished cross-section of test deposit #1. Again, notice the band of porosity resembling a series of black ink spots in the coating close to but not at the interface.

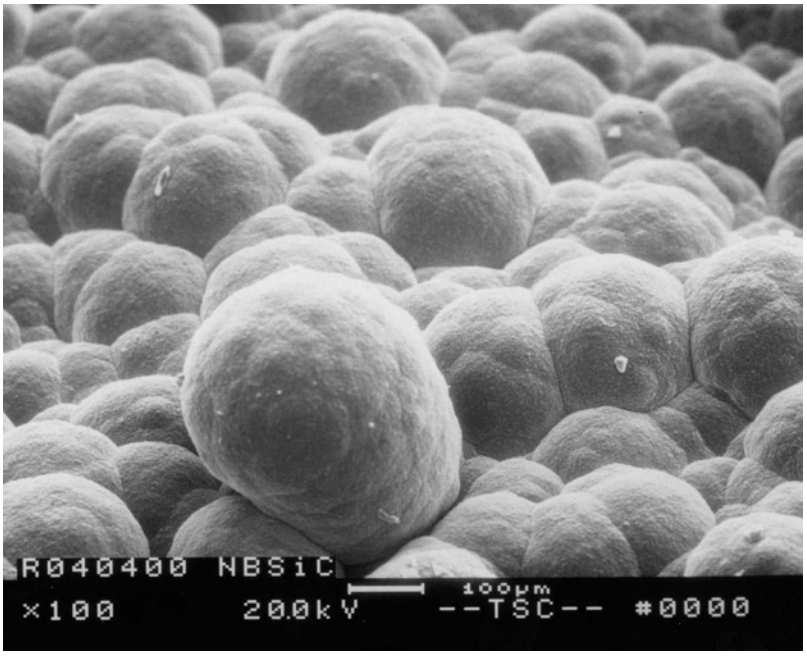

Figure 3.2-21 Scanning electron micrograph (SEM) of the surface of test deposit #1. The nodular surface is attributed to the CVD reactive gas initiation procedure and the temperature of the deposit.

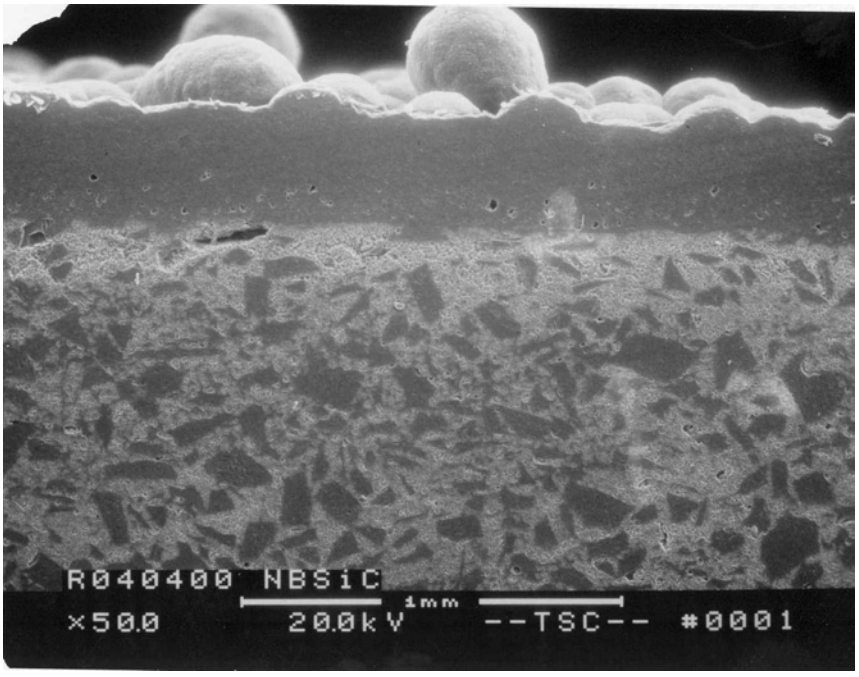

Figure 3.2-22 SEM micrograph of a cut cross-section of test deposit #1. From this view, the nodular surface, the well-bonded interface, and some porosity in the coating are all evident. Notice that in the latter half of the deposited coating that the material appears fully dense.

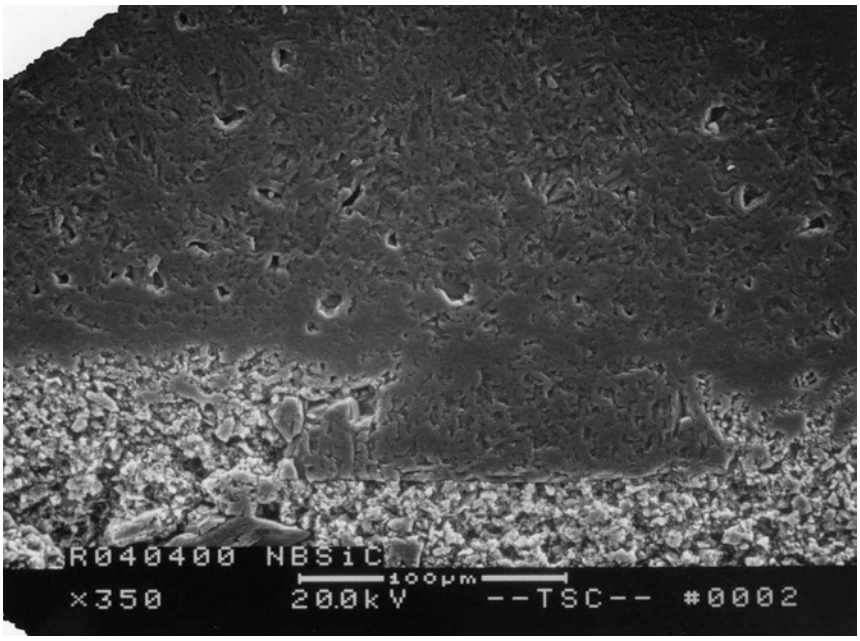

Figure 3.2-23 SEM micrograph of a cut cross-section of test deposit #1. Notice the continuity between the SiC grain in the substrate and the CVD SiC coating.

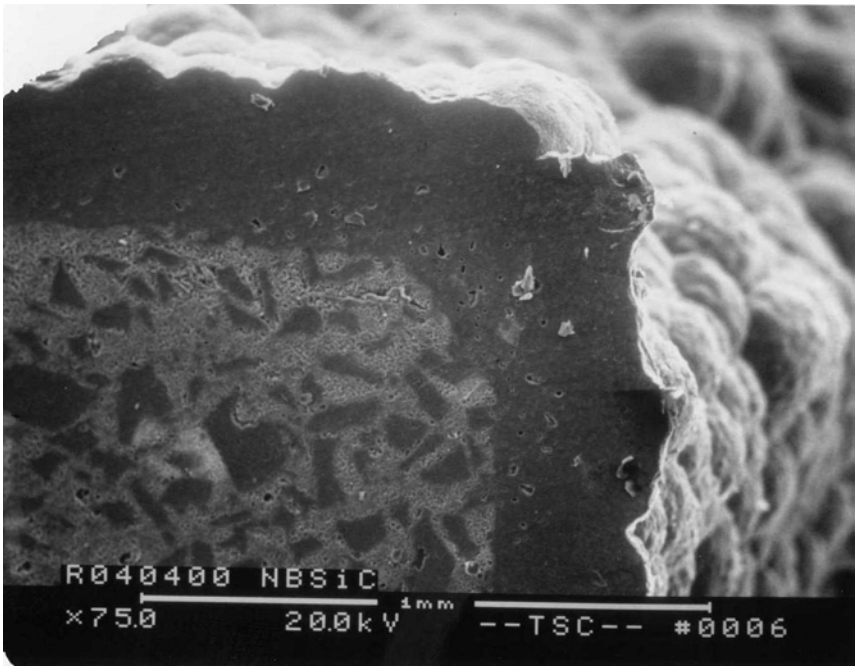

Figure 3.2-24 SEM micrograph of a cut cross-section of test deposit #1. Notice the continuity of the coating around a tight radius in the substrate. There is no evidence of cracking or delamination in the coating.

half of the coating appeared fully dense. So the porosity observed in test deposit number 1 can be characterized as closed rather than open porosity. In such a case, the integrity of the coating as an oxidative or diffusion barrier should be preserved. Further evidence of the intimate bond formed between coating and substrate may be seen in Figure 3.2-23, in which a SiC grain of the substrate appears to be continuous with the CVD SiC coating. Furthermore, the coating was able to be deposited over a tight radius in the substrate without evidence of cracking or delamination (see Figure 3.2-24).

R&D CVD Scale Test Deposit No. 2

The second LPCVD deposit of SiC was carried out in the PMI R&D scale apparatus. A curved composite substrate was used as shown in Figures 3.2-17 and 3.2-18. The deposit was carried out at a control temperature of 1375°C for 8 hours. The characteristics of the coating are summarized in the following series of micrographs. The coating was approximately 250 μm in thickness. The surface of the coating was less nodular than that of test deposit #1. This is attributed to an adjustment in the CVD reactive gas initiation procedure and a lowering of the temperature of the deposit. The CVD SiC coating was very well bonded to the SiC/Si_3N_4 substrate. As in test deposit #1, there was no appreciable porosity or delamination observed at the substrate/coating interface, but there was a band of porosity observed in the coating approximately 20-80 μm from the interface. Again, the porosity disappeared as the deposit proceeded, and the outer half of the coating appeared fully dense. Thus the porosity observed in test deposit number 2 can be characterized as closed rather than open porosity, and the integrity of the coating as an oxidative or diffusion barrier should be preserved. As was observed in test deposit #1, the intimate bond formed between coating and substrate may be seen in Figure 3.2-27 and 3.2-28, in which a SiC grain of the substrate appears to be continuous with the CVD SiC coating. Furthermore, the coating was able to be deposited over a tight radius in the substrate without evidence of cracking or delamination (see Figure 3.2-29).

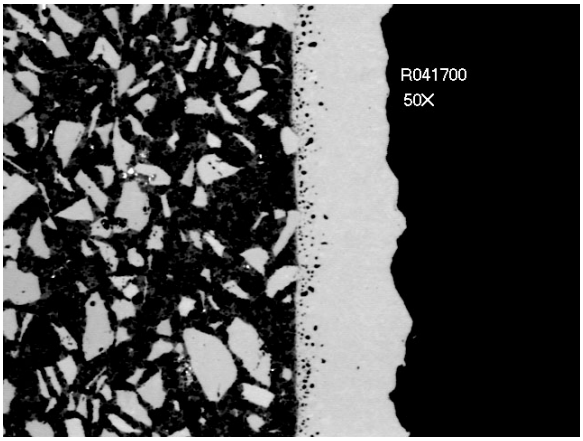

Figure 3.2-25 Optical micrograph (Mag = 50X) of a polished cross-section of test deposit #2. Notice the band of porosity in the coating close to but not at the interface. Also notice that the latter part of the coating appears fully dense.

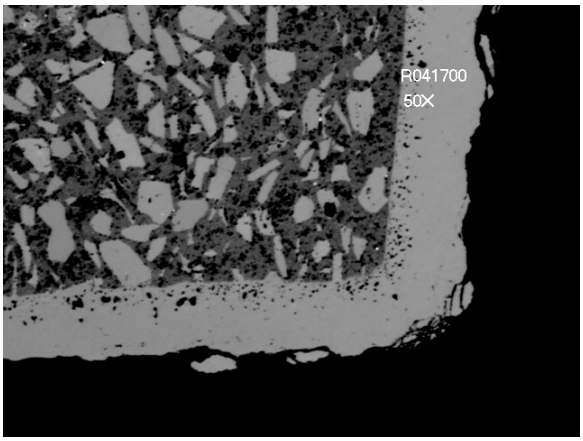

Figure 3.2-26 Optical micrograph (Mag = 50X) of a polished cross-section of test deposit #2. Notice the continuity of the coating around a tight radius in the substrate. There is no evidence of stress cracking or delamination in the coating.

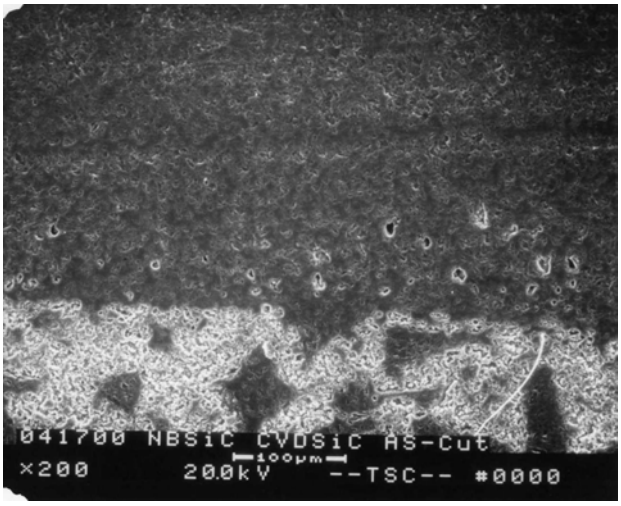

Figure 3.2-27 SEM micrograph of a cut cross-section of test deposit #2. Notice the continuity between the SiC grain in the substrate and the CVD SiC coating.

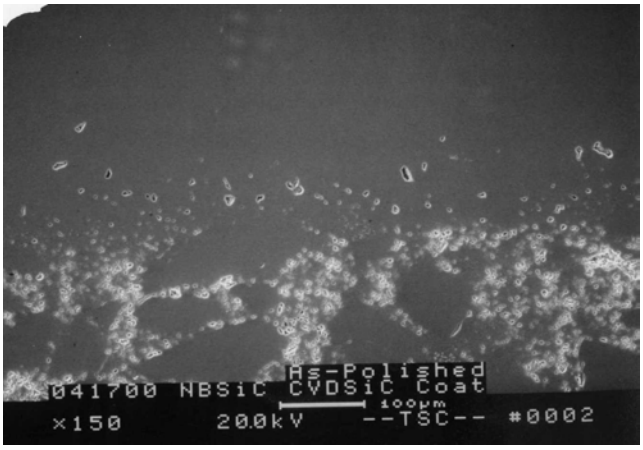

Figure 3.2-28 SEM micrograph of a polished cross-section of test deposit #2. Notice the continuity between the SiC grain in the substrate and the CVD SiC coating.

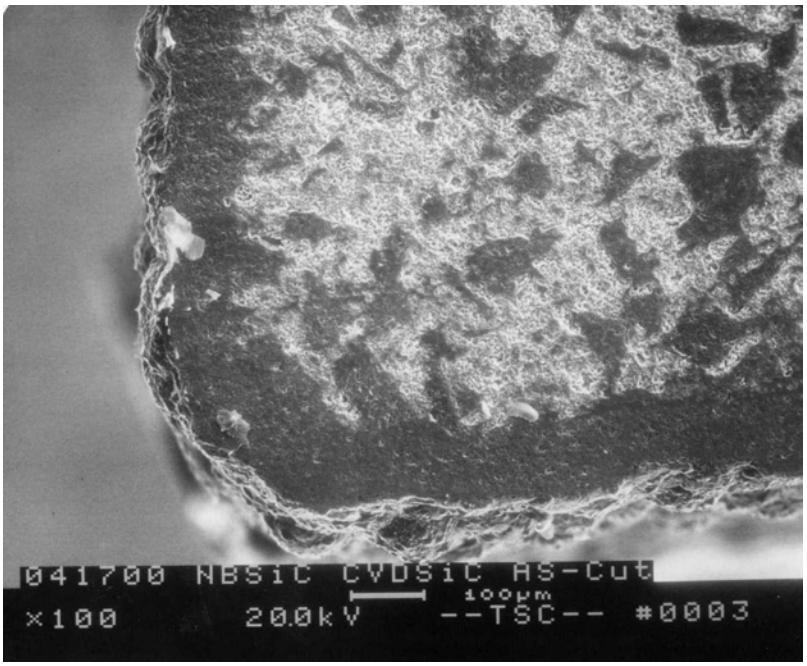

Figure 3.2-29 SEM micrograph of a cut cross-section of test deposit #2. Notice the continuity of the coating around a tight radius in the substrate. There is no evidence of cracking or delamination in the coating.

R&D CVD Scale Test Deposit No. 3

The third LPCVD deposit of SiC was carried out in the PMI R&D scale apparatus. A curved composite substrate was used as shown in Figures 3.2-17 and 3.2-18. The deposit was carried out at a control temperature of 1365°C for 9 hours. The characteristics of the coating are summarized in the following series of micrographs. The coating was approximately 250 μm in thickness. The surface of the coating was less nodular than that of test deposit #2. This is attributed to an adjustment in the CVD process and a lowering of the temperature of the deposit. The CVD SiC coating was very well bonded to the SiC/Si_3N_4 substrate. As in test deposits #1-2, there was no appreciable porosity or delamination observed at the substrate/coating interface. In certain locations of deposit #3, there was a band of porosity observed in the coating approximately 20-80 μm from the interface. However, unlike test deposits #1 and #2, there were also areas where the coating appeared fully dense from the start to the end of the deposit. As in the first two test deposits, there was very little evidence of porosity in the latter half of the deposit. Thus the porosity observed in test deposit number 3 can be characterized as closed rather than open porosity, and the integrity of the coating as an oxidative or diffusion barrier should be preserved. All microscopic evidence indicated that an intimate bond formed between coating and substrate. Furthermore, the coating was able to be deposited over a tight radius in the substrate without evidence of cracking or delamination (see Figure 3.2-33).

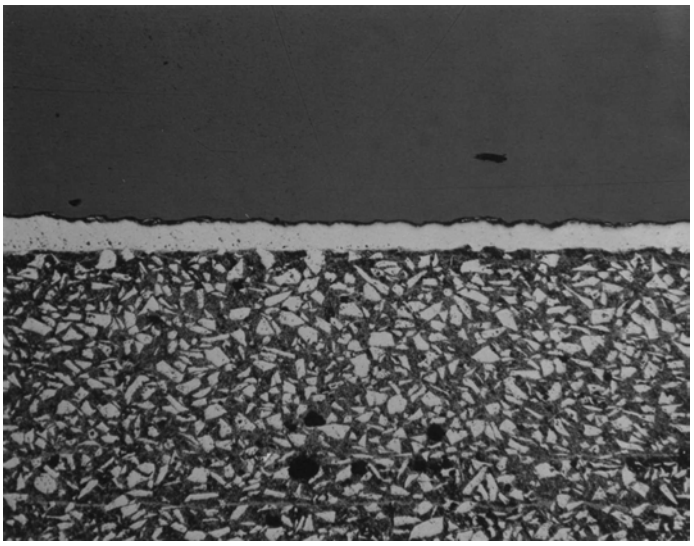

Figure 3.2-30 Optical micrograph (Mag = 20X) of a polished cross-section of test deposit #3. Notice that there is no observed band of porosity in the coating (contrast with test deposits #1 and #2).

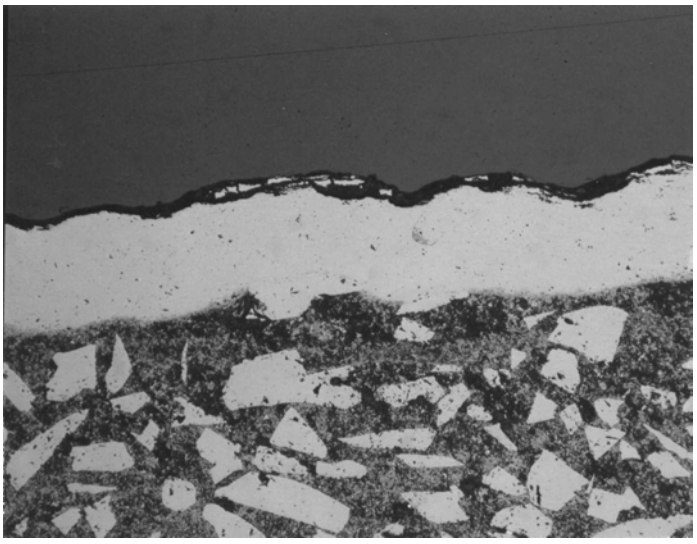

Figure 3.2-31 Optical micrograph (Mag = 80X) of a polished cross-section of test deposit #3. Notice that there is no observed band of porosity in the coating (contrast with test deposits #1 and #2).

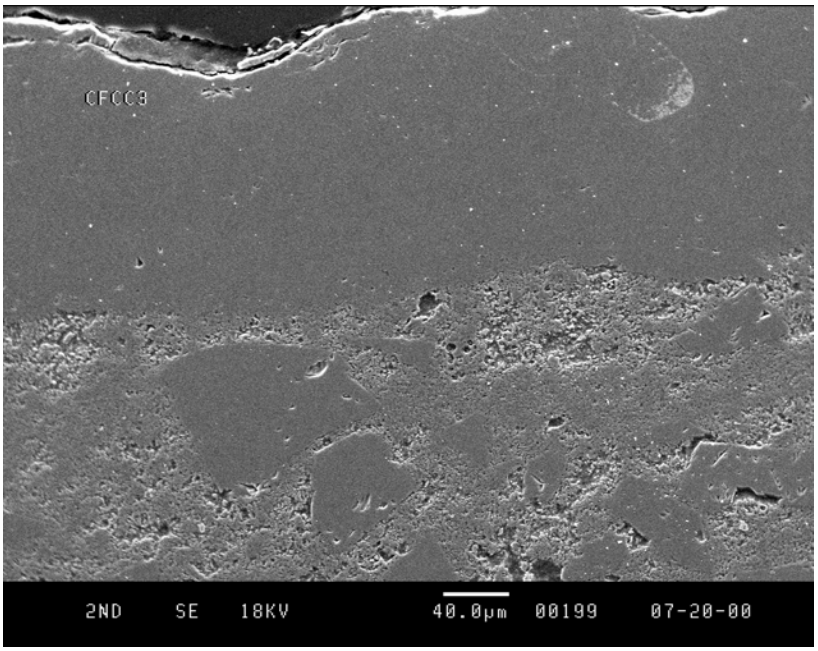

Figure 3.2-32 SEM micrograph of a polished cross-section of test deposit #3. Notice that there is no observed band of porosity in the coating (contrast with test deposits #1 and #2).

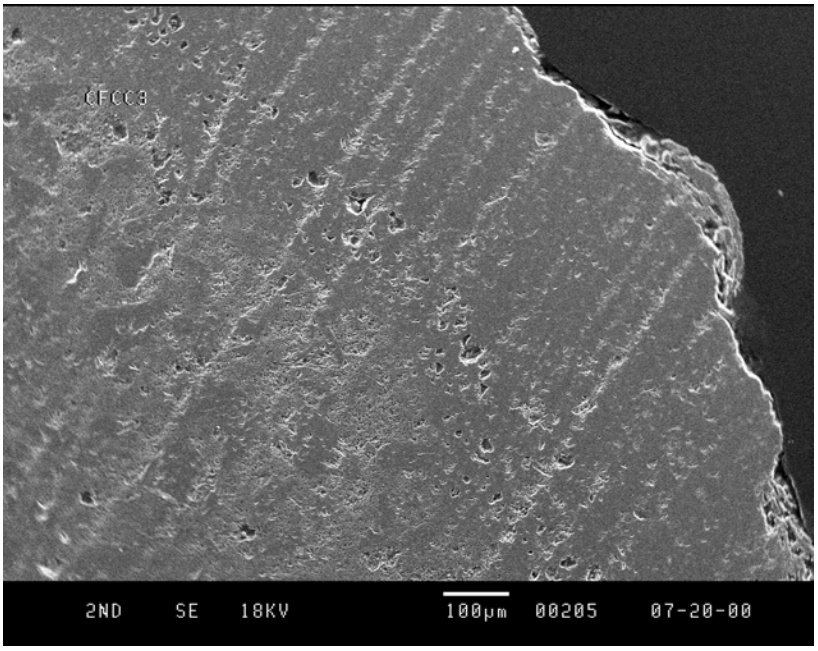

Figure 3.2-33 SEM micrograph of a polished cross-section of test deposit #3. Notice the continuity of the coating around a tight radius in the substrate. There is no evidence of cracking or delamination in the coating. There is some evidence of porosity in a band located 20-80 µm from the interface.

Manufacturing Scale Test Deposit No. 4

The fourth LPCVD deposit of SiC was carried out in the PMI large scale manufacturing system. A large, flat composite substrate affixed to a graphite cylinder as shown in Figure 3.2-34. The cylinder pedestal set-up was used for the purpose of trapping any products of out-gassing of the Textron composite material during the LPCVD process. There was, in fact, a white powdery

substance deposited on the inner surface of the graphite cylinder (see Figure 3.2-35). This is probably due to the differences in processing pressures in the Textron reaction bonding composting process (1 atm) versus the PMI LPCVD process (0.25 atm). The characteristics of the coating are summarized in the following series of micrographs. The coating considerably thicker than test coatings 1-3 due to the deposit lengths of products being manufactured in parallel with test deposit #4. The surface of the coating was much smoother than that of test deposits 1-3. The CVD SiC coating was very well bonded to the SiC/Si_3N_4 substrate. As in test deposit #1-3, there was no appreciable porosity or delamination observed at the substrate/coating interface. Unlike test coatings 1-3, there was no visible band of porosity observed in the coating approximately 20-80 μm from the interface. The coating appeared fully dense from the start to the end of the deposit. It is expected that the integrity of the coating as an oxidative or diffusion barrier should be preserved. All microscopic evidence indicated that an intimate bond formed between coating and substrate. Furthermore, the coating was able to be deposited over a tight radius in the substrate without evidence of cracking or delamination (see Figure 3.2-38).

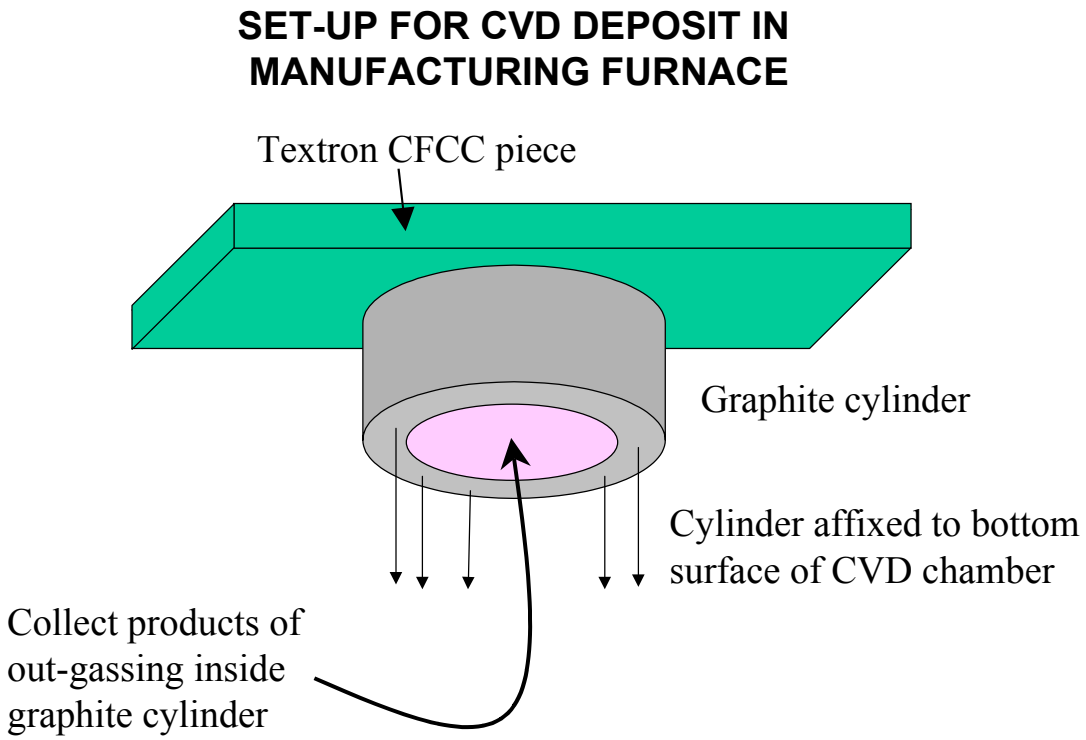

Figure 3.2-34

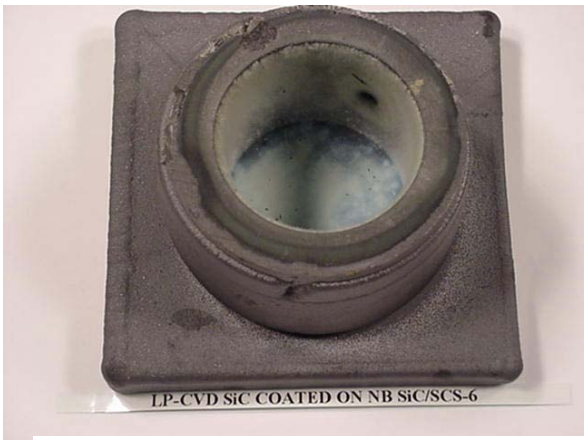

Figure 3.2-35 Photographs of coated Textron substrate (test coating #4) as viewed from the bottom of the graphite cylinder pedestal. Notice the white powdery substance deposited on the inside walls of the cylinder. This is attributed to out-gassing of the Textron SiC/Si_3N_4 composite material.

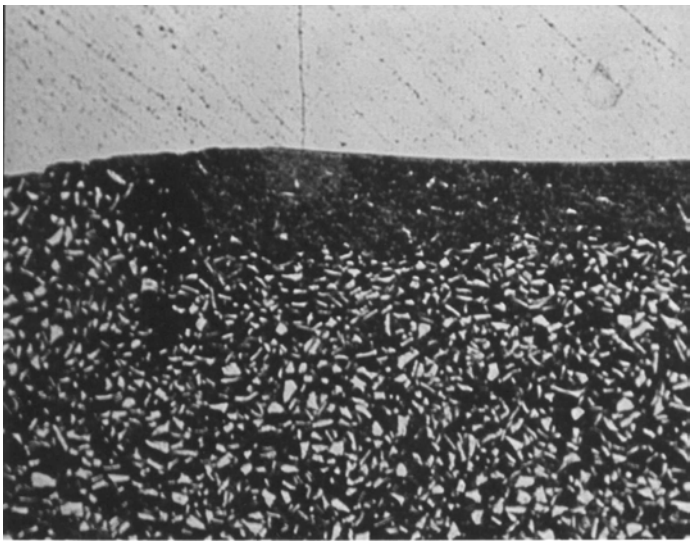

Figure 3.2-36 Optical micrograph (Mag = 20X) of a polished cross-section of test deposit #4. Notice that there is no observed band of porosity in the coating.

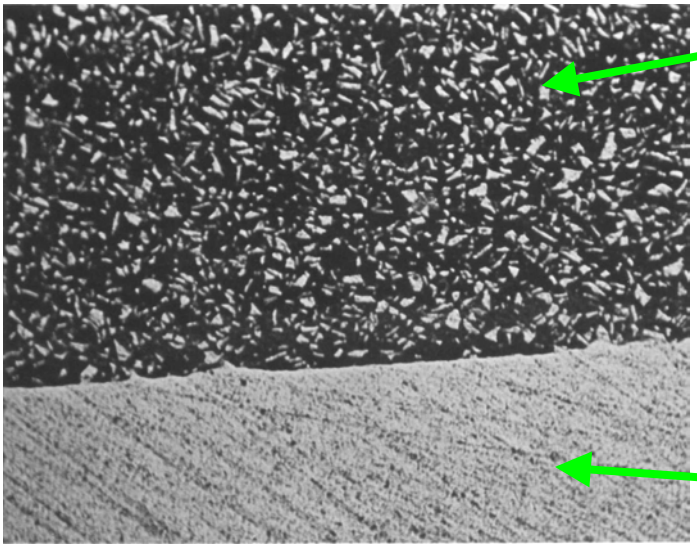

Textron SiC/Si_3N_4 composite

PerformanceSiC™ CVD SiC

Figure 3.2-37 Optical micrograph (Mag = 20X) of a polished cross-section of test deposit #4. Notice that there is no observed band of porosity in the coating.

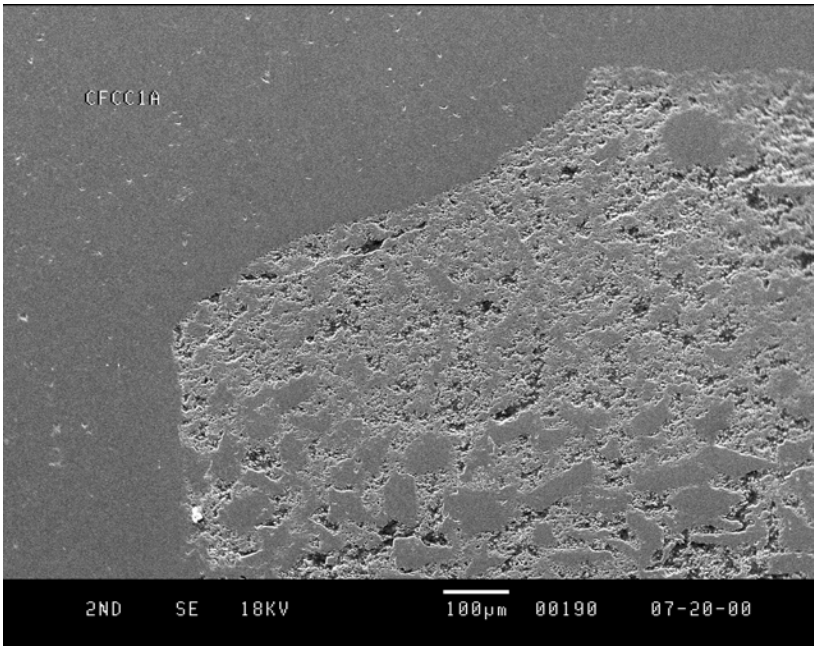

Figure 3.2-38 SEM micrograph of a polished cross-section of test deposit #4. Notice the continuity of the coating around a tight radius in the substrate. There is no evidence of cracking or delamination in the coating. In contrast with test deposits 1-3, there is no evidence of porosity in a band located 20-80 µm from the interface. There was some observed grain pullout, which appears to be an artifact of the polishing process.

Summary of CVD Coating Deposits and Characterization Results

This program demonstrated the feasibility of using PMI's LPCVD process for depositing CVD silicon carbide onto Textron's reaction bonded SiC/Si_3N_4 composite material. All coatings were very well bonded to the substrate. Bands of porosity that were observed in the initial stages of

this program were reduced or virtually eliminated by systematic process changes. When bands of porosity were observed, they were not near the coating-substrate interface, nor was porosity observed in the outer half of the coating. Thus, all coatings produced under this program were arguably sufficient barriers to oxidation and diffusion.

Brief Economic Assessment of Coating Process – Recommendation for a Scaled-Up Manufacturing Method

The following is a simplified assessment based on what would be a manufacturing scale coating process of a full-scale immersion tube (approximately 8" ID x 43" long close-ended tubes). This assessment also takes into account that the target price for the application of a CVD coating is approximately $500-1000 per tube. All cost estimates are engineering estimates.

Assumptions

- Tube size: approximately 8" ID x 43" long close-ended tubes
- Coating thickness: 100-500 μm
- Number tubes/year: 100-500
- Target cost: $500-1000 per tube

Recommendations

- Dedicated CVD system with RF furnace sized for a single tube
  - Cost: $100K
- Rapid (~2 hr) heat up and cool down
- Interchangeable internal furnace fixturing for rapid turnaround
  - Cost: $30K
- Custom engineered gas injection system for coating inside and outside of tube
  - Cost: $50K materials and development

With the system recommended above, the target coating price should be achievable. The payback on capital equipment investments depends on many variables and is not estimated here.

PMI has concluded that, using its present in-house manufacturing LPCVD facilities, the full-scale coating manufacturing process cannot be economically carried out. The PMI LPCVD systems are designed for thick standalone deposits of silicon carbide. The heat-up and cool-down times, and well as furnace turnaround times are not compatible with the economic manufacture of a coated immersion tube as described above. A dedicated system specially designed for the tube coating process would be needed to accomplish this.

3.2.6.4 Application of Glaze Coatings

Experiments were performed to determine if oxidation-resistant coatings could be applied as glazes to the RBSN CFCC material. The substrates were 4-ply flat panels fabricated from drum-wrapped fiber mats molded with program slurry. The panels were processed through the standard nitriding cycle. After nitridation, the panels were cut into 2" x 2" squares for further processing.

The first coating applied was ZYP SC-1400 oxidation protection coating from ZYP Coatings, Inc. Three coupons were coated with one layer of the paint and three were coated with two layers. Coupons were then fired at 350, 1395, and 1450°C. The matrix is shown in the table below.

COUPON NUMBER	NUMBER OF COATS	FIRING TEMPERATURE °C
1-1	2	350
1-2	2	1395
1-3	2	1450
1-4	1	350
1-5	1	1395
1-6	1	1450
1-7	NONE	-
1-8	NONE	-
1-9	NONE	-

Coupons 1-1 through 1-8 were then placed in an oven in air and exposed to 900°C for 1000 hours. After oxidation exposure, the coupons were sent to H.T. Lin at Oak Ridge National Laboratories for evaluation.

Figure 3.2-39 shows an SEM photomicrograph of a polished section of an uncoated oxidized coupon.

SEM of As-Received Textron CFCC Coupons

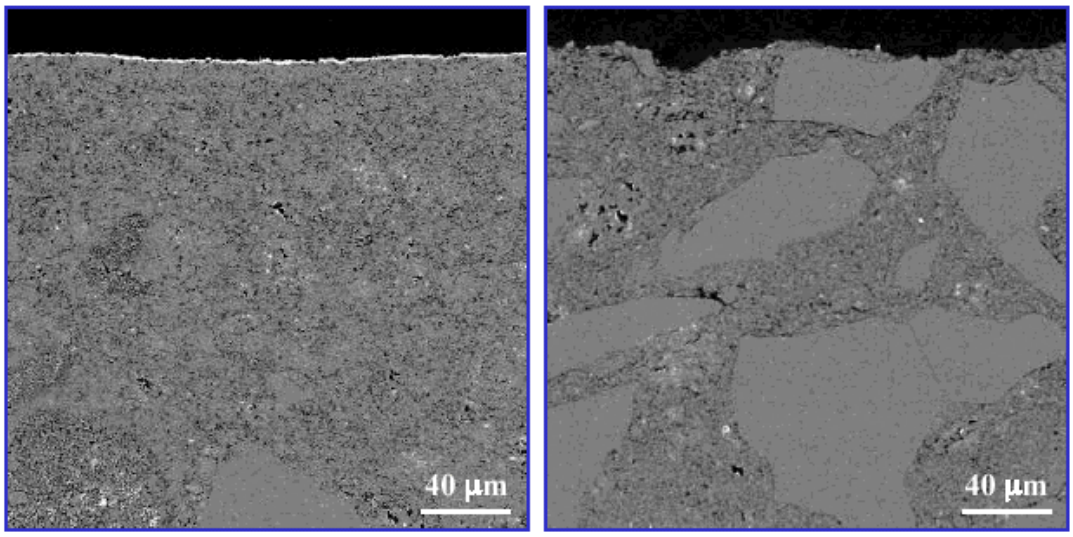

Figure 3.2-39 SEM of Polished Uncoated Coupons

Examination of the oxidized ZYP-coated samples show that the coating, in general is very porous, which may not be an effective barrier to application environments. The porous microstructure of the ZYP coating is independent of the coating thickness and firing temperature up to 1395°C. No Zyp coating was observed after 1000 hours exposure for those coupons fired at 1450°C. Photomicrographs of the samples fired at the three temperatures and then exposed to air at 900°C for 1000 hours are shown in Figures3.2-40 through 3.2-42.

The flexural strengths (averages of 7 tests each) of oxidized coated and uncoated samples are shown in Figue 3.2-43. The flexural strengths exhibit little degradation.

Figure 3.2-40

Textron CFCC Coupons With ZYP Oxide Coating
Fired @ 350°C, Exposed to 900°C in air for 1000h

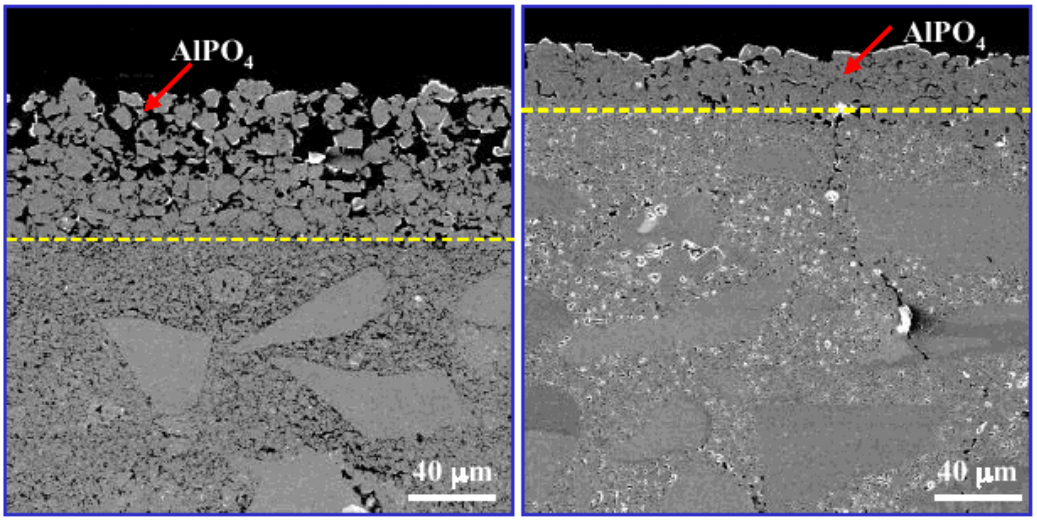

2-coats (# 1-1) **1-coat (# 1-4)**

$AlPO_4$ (Aluminum Phosphate) is identified by X-ray analysis

Figure 3.2-41

Textron CFCC Coupons With ZYP Oxide Coating
Fired @ 1395°C, Exposed to 900°C in air for 1000h

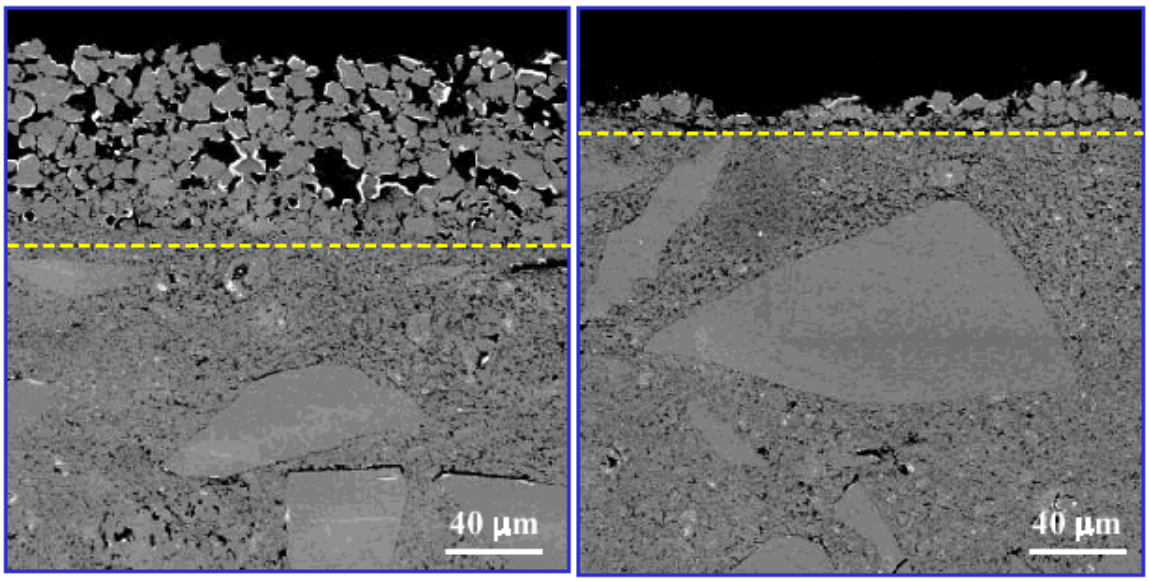

2-coats (# 1-2) 1-coat (# 1-5)

Figure 3.2-42

Textron CFCC Coupons With ZYP Oxide Coating Fired @ 1450°C, Exposed to 900°C in air for 1000h

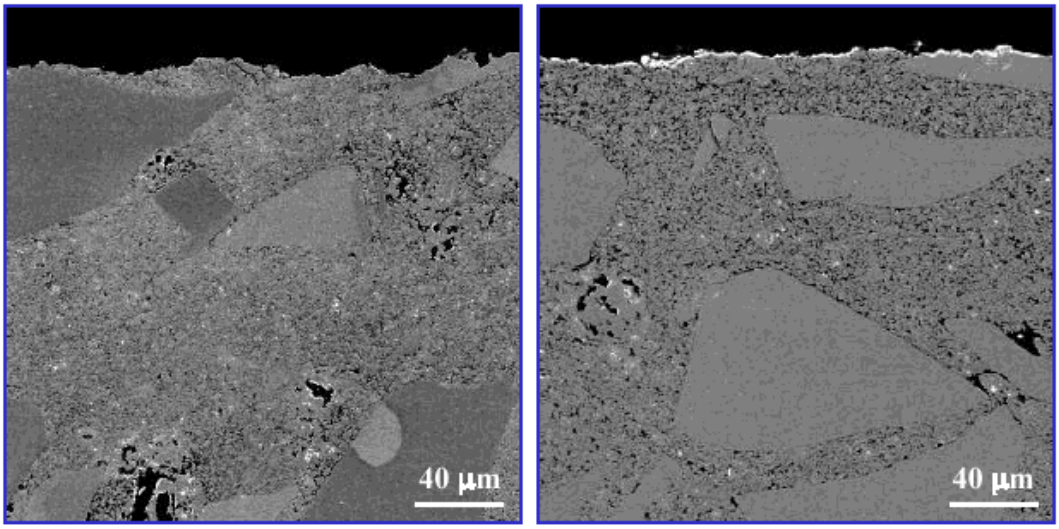

2-coats (# 1-3) 1-coat (# 1-6)

Figure 3.2-43

Flexural Strength of Textron CFCC Coupons With ZYP Oxide Coating After Exposed to 900°C in air for 1000h

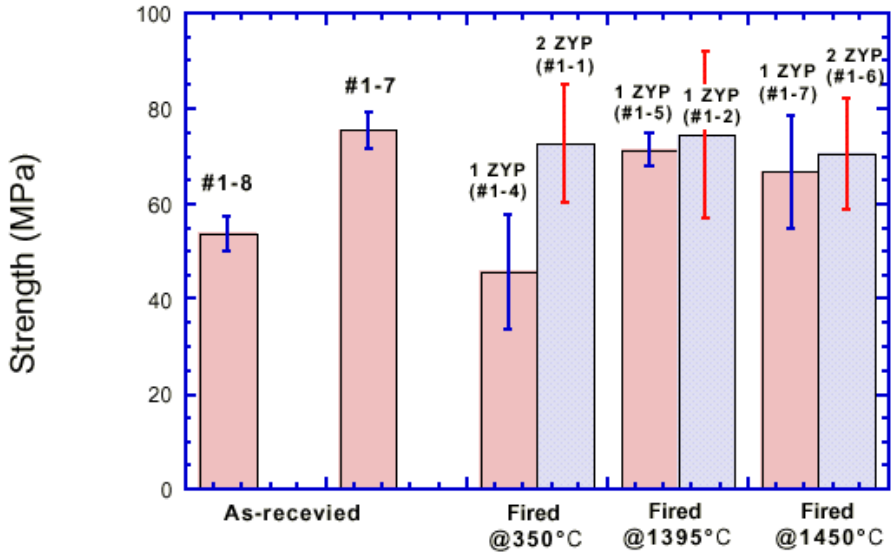

Strength results are the average of seven MOR bars per coupon via the ASTM standard

Another coating system applied to the CFCC material was a Ca-Al oxide . The coupons were painted with an aqueous mixture of calcium and aluminum formates (20 weight%) and then fired at 1300°C in nitrogen. Samples with 1, 2, 3, and 4 coats were exposed to air at 900°C for 1000 hours and supplied to ORNL for evaluation. SEM photomicrographs of the samples are shown in Figures 3.2-44 and 3.2-45. In contrast to the ZYP coatings, the Ca-Al oxide coating was dense and adherent, which could be an effective barrier. However, the coatings exhibited numerous macro cracks perpendicular to the surface after the 1000 hour exposure. In addition, the coating thickness results were inconsistent. The flexural strength of the materials after exposure is shown in Figure 3.2-46. Samples with 3 and 4 coats of the glaze show no degradation after exposure.

Figure 3.2-44

Textron CFCC Coupons With Ca-Al Oxide Coating Fired @ 1300°C, Exposed to 900°C in air for 1000h

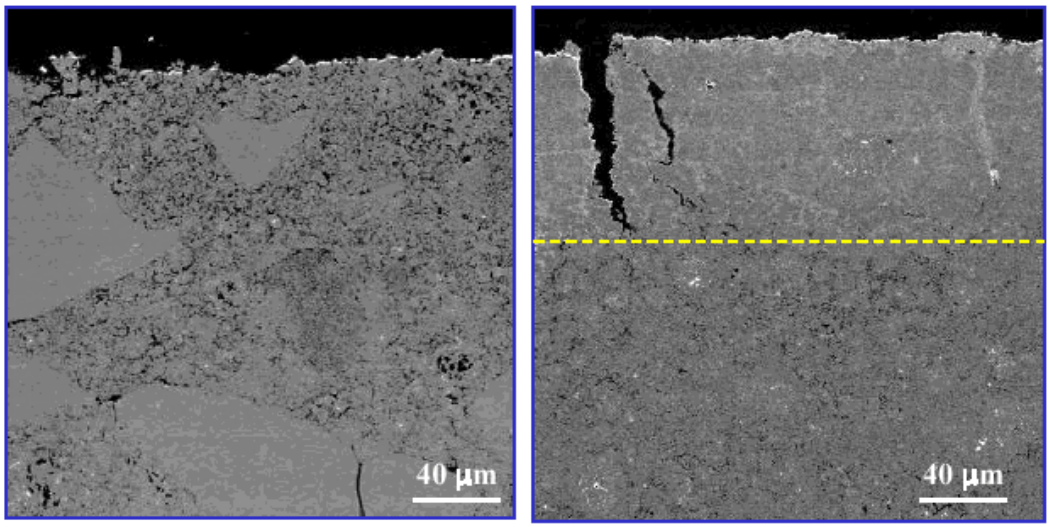

1-coat (#4-1) 2-coats (#4-2)

Figure 3.2-45

Textron CFCC Coupons With Ca-Al Oxide Coating Fired @ 1300°C, Exposed to 900°C in air for 1000h

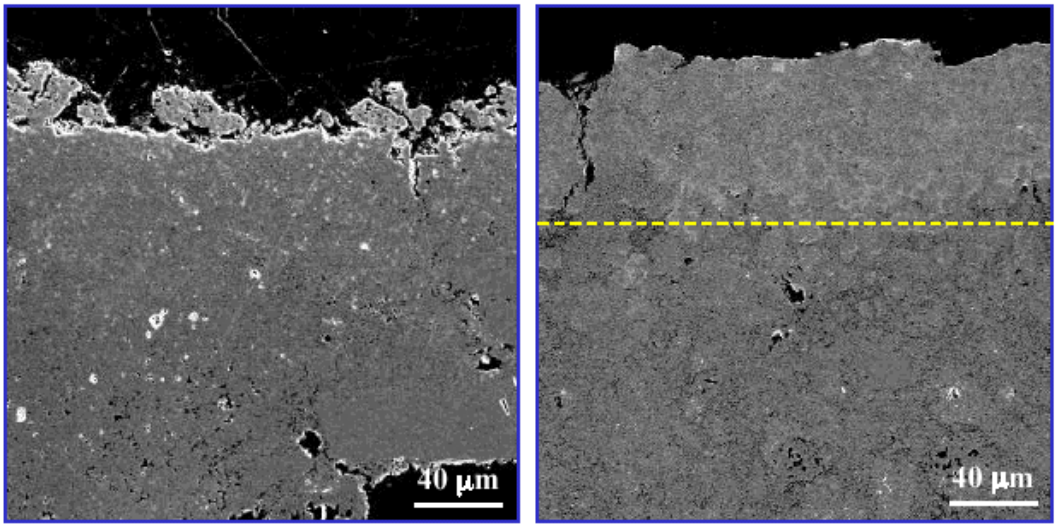

3-coats (#4-3) 4-coats (#4-4)

Figure 3.2-46

Flexural Strength of Textron CFCC Coupons With Ca-Al Oxide Coating After Exposed to 900°C in air for 1000h

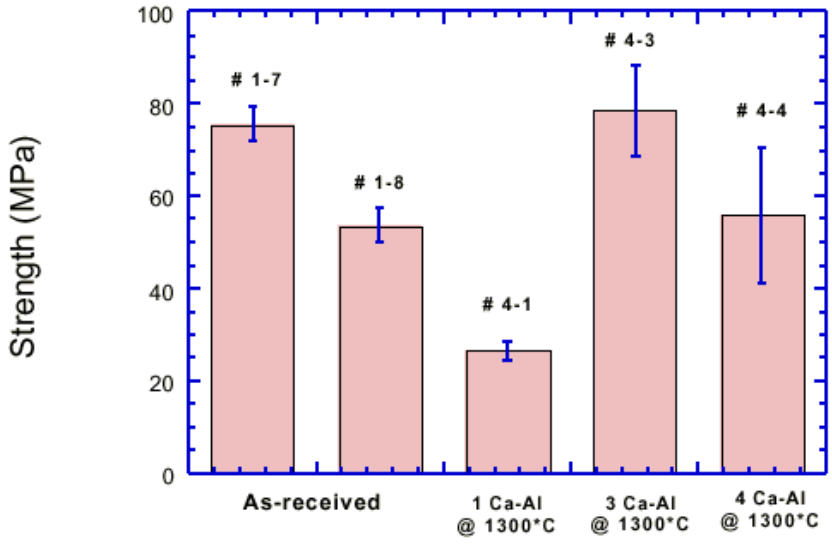

Strength results are the average of seven MOR bars per coupon via the ASTM standard

A third material used as a glaze was sol-gel cordierite: $2MgO2Al_2O_35SiO_2$. Stoichiometric amounts of aluminum nitrate and magnesium acetate were dissolved in ethlyene glycol; the appropriate amount of tetraethylorthosilicate was added and the solution was gelled with ammonia. The gel was painted onto the surface of the RBSN coupons and fired to 1300°C. After firing, the coatings spalled off; no further work with the cordierite was attempted.

3.2.7 Process Modeling

Materials Sciences Corporation as part of the Textron/CFCC team performed analytical modeling of the composites and their behavior under mechanical and thermal stresses. A major objective of this program was to assist Textron in defining an optimum material configuration. The micromechanical model describing the composites was defined in the Phase I program.

The activities in Phase II were in four major areas:

- Fiber/Matrix Sensitivity Analysis
- Thermal Conductivity Data Correlation
- Material Property Parametrics
- Heater Tube Analysis

These are described below.

Sensitivity Analysis

As noted above the micromechanical computer model for the CFCC composite material had been developed in Phase I. The validity of the model in describing the properties of the composites has been demonstrated. Table 3.2-5 lists the material constituent properties used in the calculations. A comparison predicted and measured strength and modulus for two fiber volume fractions is shown in Table 3.2-6 The comparison of predicted and measured stress-strain curves is shown in Figure 3.2-47.

Table 3.2-5 - Constituent Properties Utilized in Model Calculations

Constituent	E_{11} (Msi)	ν_{xy}	G_{xy} (Msi)	UTS_x (ksi)	α_x (10^{-6}/F)	K_x (W/m-K)
SCS-6 Fiber	37.0	0.14	16.2	264*	2.44	190
Nitrided SiC Matrix	35.4	0.19	10.6	20	1.98	13

* Properties reduced to match test data.

Process conditions DO NOT substantiate process influencing fiber properties

Low volume fractions and testing conditions may have influenced results

Using this model, the sensitivity of the behavior of the composite to the following factors was investigated: fiber-matrix interfacial strength, fiber-matrix sliding friction, initial matrix cracking stress, matrix crack saturation stress, fiber volume fraction and matrix modulus. For each parameter, a set of stress-strain curves was calculated. The results are shown in Figures 3.2-48 thru 3.2-52. The results are summarized in Table 3.2-7.

Table 3.2-6 Predicted vs. Measured Properties

	Fiber Volume Fraction (%)	Measured Properties	Predicted Properties
E_{xx}, (Msi)	6	18-22	26
E_{xx}, (Msi)	18	25-30	27.5
UTS_x, (ksi)	6	23-36	35
UTS_x, (ksi)	18	60-65	64

Fig 3.2-47 PREDICTED AND MEASURED UNIAXIAL RESPONSE

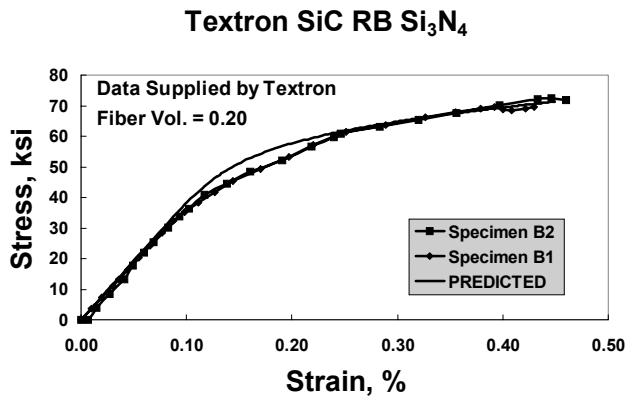

Fig 3.2-48 INFLUENCE OF INTERFACE FRICTION

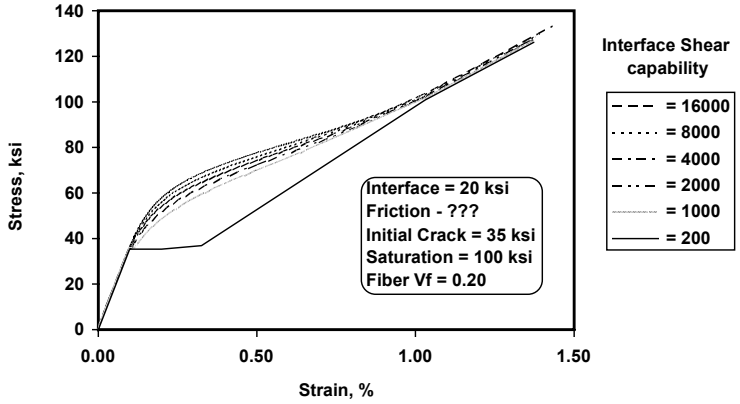

Fig 3.2-49 INFLUENCE OF INTERFACE STRENGTH

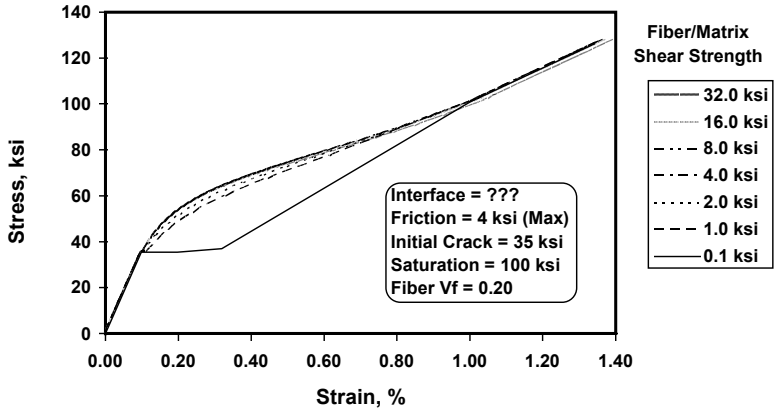

Fig 3.2-50 INFLUENCE OF INITIAL MATRIX CRACKING STRESS

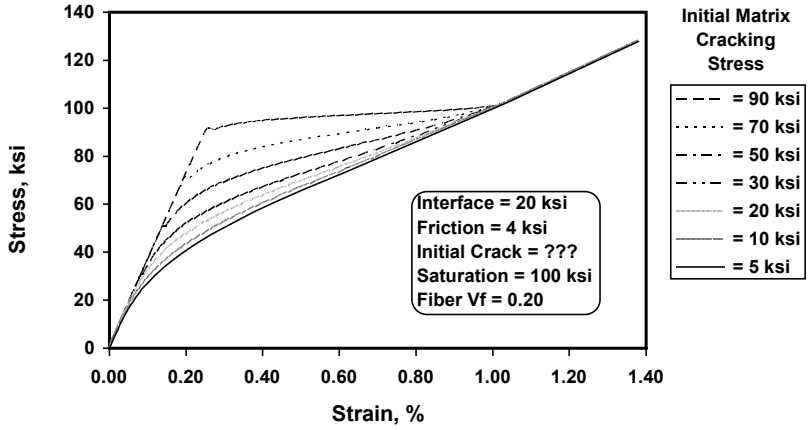

Fig 3.2-51 INFLUENCE OF FINAL MATRIX CRACKING STRESS

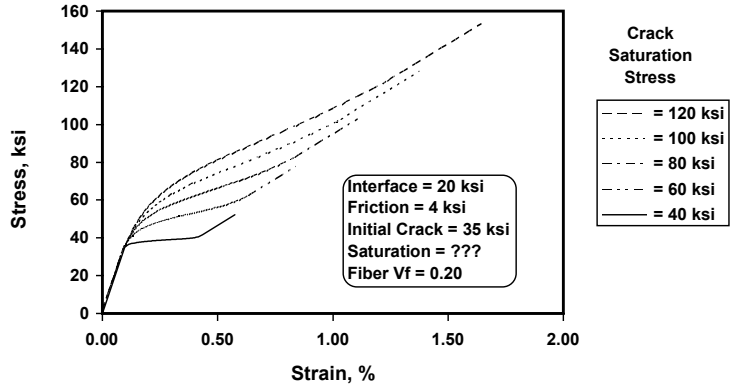

Fig 3.2-52 INFLUENCE OF FIBER VOLUME FRACTION

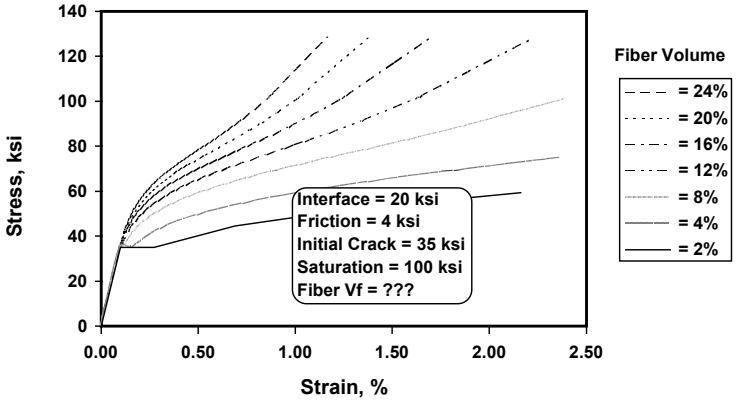

TABLE 3.2-7 SENSITIVITY RESULTS

Property	Effect
Interface Strength	Below 1000 psi poor, above beneficial, but not significantly
Interface Friction	Below 1000 psi poor, above beneficial, but not significantly
Initial Matrix Cracking Stress	Higher is better, but at some point, behavior becomes brittle
Matrix Crack Saturation Stress	Higher is better for ultimate strength, but linear region is not sensitive
Fiber Volume Fraction	Below 8% start seeing initial jump in curves, higher values straighten stress/strain curve
Matrix Modulus	Lower modulus gives lower composite modulus, but more linear behavior

Thermal Conductivity Data Correlation

The objective of this activity was to deduce thermal conductivity values for the SCS-6 and reaction bonded matrix constituents from observed thermal diffusivity measurements on a uniaxial SCS-6/RBSN composite. The composite consists of thin layers of RBSN. The composite was modeled as a sandwich construction consisting of a thick RBSN core with face sheets of 92 vol% fibers. The thicknesses of the core and face sheets were adjusted to yield the appropriate fiber volume fraction. The resulting values are

CONSTITUENT	K_{11} W/M°K	K_{22} W/M°K
SCS-6 FIBER	192	192
RBSN MATRIX	13.4	13.4

Using these derived constituent properties to predict composite properties provides good agreement with experimental data:

	K_{XX} W/M°K	K_{YY} W/M°K	K_{ZZ} W/M°K
MEASURED	42.1	36.2	13.3
PREDICTED	42.0	36.3	15.9

Material Property Parametrics

The previously defined micromechanical model was used to investigate the effective properties of CFCC materials as a function of the following parameters:

– Consider Effects Of Fiber Orientation $[90_2/\pm\theta]_s$ & $[\pm\theta]_s$ Laminates

– Influence Of Fiber Volume Fraction
- 3% vs. 12%

– Influence Of Fiber Type
- SCS-6 vs. SCS-9

The constituent properties used in the calculation are given in Table 3.2-8

The results can be summarized as follows:

For both $[90_2/\pm\theta]_s$ and $[\pm\theta]_s$ composites, Young's modulus and coefficient of thermal expansion were not affected by fiber orientation while there was a slight decrease in axial thermal conductivity and a slight increase in hoop thermal conductivity with an increase in θ.

With respect to composite strength the $[90_2/\pm\theta]_s$ results show

- Axial Tensile & Compressive Strengths Are Maximum For $[90_2/\pm\theta]_s$ Materials
- Hoop Strengths Are Maximum At θ=90° And Slightly Less For θ=0°
- Hoop Strengths Are Much Lower For Other θ Orientations
  - Shear Failure Occurs In Off Axis Layers Prior To Hoop Layer Failure Resulting In Decreased Strength
- Shear Strength Is Maximum For $[90_2/\pm 45]_s$ Configuration

The corresponding results for $[\pm\theta]_s$ laminates are:

- Axial Tensile & Compressive Strengths Are Maximum For $[0_2]_s$ Materials
- Hoop Strengths Are Maximum For $[90_2]_s$
- Shear Strength Is Maximum For $[\pm 45]_s$ Configuration
- At Other Orientations Composite Strength Is Unaffected

The effects of increased fiber volume are:

- Slight Increases In Youngs Moduli And C.T.E.
- Substantial Increases In Thermal Conductivity
- Slight Increase in Compressive Strengths
- Significant Increase In Axial Tensile Strengths Only When θ=0°
- Significant Increase In Hoop Tensile Strength Only When θ=90° for the $[\pm\theta]_s$ case.
- Significant Increase In Hoop Tensile Strength Only When θ=0° and 90° for the $[90_2/\pm\theta]_s$ case
- Significant Increase In Shear Strength For θ= 45°

The comparison between SCS-6 and SCS-9 fibers indicates only minimal change in effective composite properties. SCS-9 fibers have slightly lower strength and modulus than SCS-6 fibers, but the low fiber content of the composites under consideration dilutes these differences even more.

The estimated properties of some representative laminate constructions are shown in Table 3.2-9.

Heater Tube Analysis

The immersion heater tube which was of major interest during the Phase II activities is subjected to a severe thermal environment and accompanying induced stresses at steady state. There are steep thermal gradients through the wall and axially since there is a heater inside the tube and a meltline on the outside with air above and molten aluminum below. Thermal stresses during cold-start heat-up, extraction from the melt and cooldown must also be considered.

The immersion tube/aluminum system was modeled with the ABAQUS finite element software which provides a coupled temperature-displacement transient analysis.

The details of this analysis and the results are discussed in the section of this report describing the evaluation of the immersion tubes at the end user.

TABLE 3.2-8

Materials Constituent Properties for Full Model Calculations

CONSTITUENT	E_A Msi	E_T Msi	ν_A -	ν_τ -	G_A Msi	α_A $x10^{-6}$in/in/°F	σ_T $x10^{-6}$in/in/°F	K_A W/M°K	K_T W/M°K	σ_A^{TENS} ksi	σ_τ^{TENS} ksi	σ_A^{COMP} ksi	σ_T^{COMP} ksi	τ_A ksi
SCS-6 FIBER	59.00	59.00	0.14	0.14	25.88	2.77	2.77	192	192	550	550	400	400	55.0
SCS-9 FIBER	48.00	48.00	0.14	0.14	21.05	2.77	2.77	192	192	475	475	350	350	45.0
RBSN MATRIX	20.00	20.00	0.20	0.20	8.33	1.67	1.67	13.4	13.4	35.0	35.0	35.0	35.0	10.0

Table 3.2-9
ESTIMATED PROPERTIES FOR SCS-9 REINFORCED RBSN COMPOSITES

MATERIAL	V_1 %	E_{11} Msi	E_{22} Msi	ν_{12} -	G_{12} Msi	α_{11} x10^{-6}in/in/°F	σ_{22} x10^{-6}in/in/°F	K_{11} W/M°K	K_{22} W/M°K	σ_{11}^{TENS} ksi	σ_{22}^{TENS} ksi	σ_{11}^{COMP} ksi	σ_{22}^{COMP} ksi	τ_{12} ksi
$[90_2/\pm 45]_s$	3	20.80	20.82	0.20	8.70	1.73	1.74	17.96	18.50	36.7	36.42	36.37	36.42	10.44
$[\pm 45]_s$	3	20.80	20.80	0.20	8.70	1.74	1.74	18.23	18.23	36.38	36.38	36.38	36.38	10.51
$[90_2/\pm 45]_s$	12	23.18	23.29	0.19	9.79	1.91	1.92	31.63	33.76	40.45	40.65	40.45	40.65	20.87
$[\pm 45]_s$	12	23.21	0.19	9.81	1.91	1.91	32.69	32.69	40.51	40.51	40.51	40.51	40.51	41.58

ESTIMATED PROPERTIES FOR SCS-6 REINFORCED RBSN COMPOSITES

MATERIAL	V_1 %	E_{11} Msi	E_{22} Msi	ν_{12} -	G_{12} Msi	α_{11} x10^{-6}in/in/°F	σ_{22} x10^{-6}in/in/°F	K_{11} W/M°K	K_{22} W/M°K	σ_{11}^{TENS} ksi	σ_{22}^{TENS} ksi	σ_{11}^{COMP} ksi	σ_{22}^{COMP} ksi	τ_{12} ksi
$[90_2/\pm 45]_s$	3	21.09	21.14	0.20	8.83	1.75	1.75	17.96	18.50	36.87	36.96	36.87	36.96	10.59
$[\pm 45]_s$	3	21.10	21.10	0.20	8.84	1.75	1.75	18.23	18.23	36.89	36.89	36.89	36.89	11.53
$[90_2/\pm 45]_s$	12	24.34	24.54	0.18	10.31	1.95	1.96	31.63	33.76	42.45	42.81	42.45	42.81	23.50
$[\pm 45]_s$	12	24.38	24.38	0.19	10.35	1.95	1.95	32.69	32.69	42.50	42.50	42.50	42.50	46.90

3.2.8 Low Cost Fiber Alternative

As noted in Section 3.2.2, the fiber chosen for the final program efforts was SCS-6, since it had demonstrated thermal and chemical stability under both processing and application environments. Further, the thick (~ 3 micron) surface layer of the fiber provided an appropriate level of fiber-matrix bonding that gave both reinforcement and toughening of the composite in the RBSN system. A disadvantage of SCS-6 is that the thick surface layer requires an extra step in the production process, thereby increasing the cost. Textron's SCS-2 fiber is identical to the SCS-6 fiber in both structure and properties except for the surface layer which is approximately 0.5 microns thick. This thinner layer does not withstand processing in reactive environments such as compositing in titanium, but should not be adversely affected by the nitridation cycle used to form RBSN composites. Since the thinner layer does not require an extra processing step during manufacturing, SCS-2 is inherently lower in cost than SCS-6. Preliminary experiments were performed to assess the feasibility of using SCS-2 in RBSN composites.

SCS-2 – RBSN panels were produced as described in the Section 3.2.6 by cast drum-wrapped plies of fibers in program slurry and processing in the usual nitridation cycle. These were provided to H.T.Lin at Oak Rigde National Laboratories for mechanical characterization. The results of a comparison of SCS-2 and SCS-6 RBSN composites is shown in Figure 3.2-53. These tests were conducted at room temperature. The material reinforced with SCS-2 exhibited similar strength and Weibull modulus to that reinforced with SCS-6. For the SCS-2 samples, the weibull modulus was lower, reflecting a larger scatter of strength data.

Samples were also tested at 900°C in air at two different stressing rates, 30 and 0.003 Mpa/s. The purpose of the 0.003 stress rate was to see if the composite exhibited any susceptibility to slow crack growth (SCG) at temperature. The results are shown in Figure 3.2-54. The composite did not exhibit any slow crack growth in air at 900°C. Further, the mechanical properties were not strongly dependent upon temperatue or stressing rates.

This preliminary study indicates that further characterization would be warranted to qualify lower cost SCS-2 as the reinforcement for CFCC RBSN composites.

Figure 3.2-53

Textron CFCCs Reinforced With SCS2 Fibers Exhibited Similar Mechanical Properties to Those With SCS6 Fibers

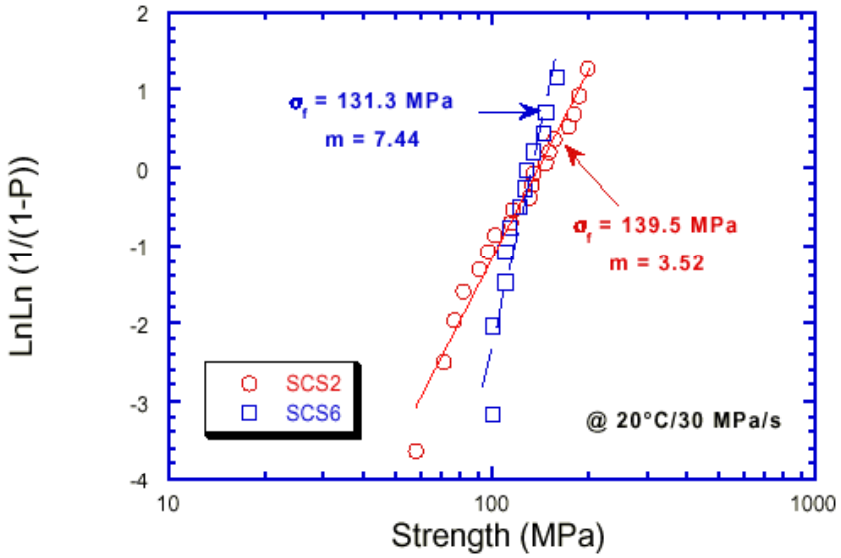

Figure 3.2-54

Mechanical Properties of Textron CFCC-SCS2 Fiber Are Not Strongly Dependent Upon Test Temperature and Stressing Rates

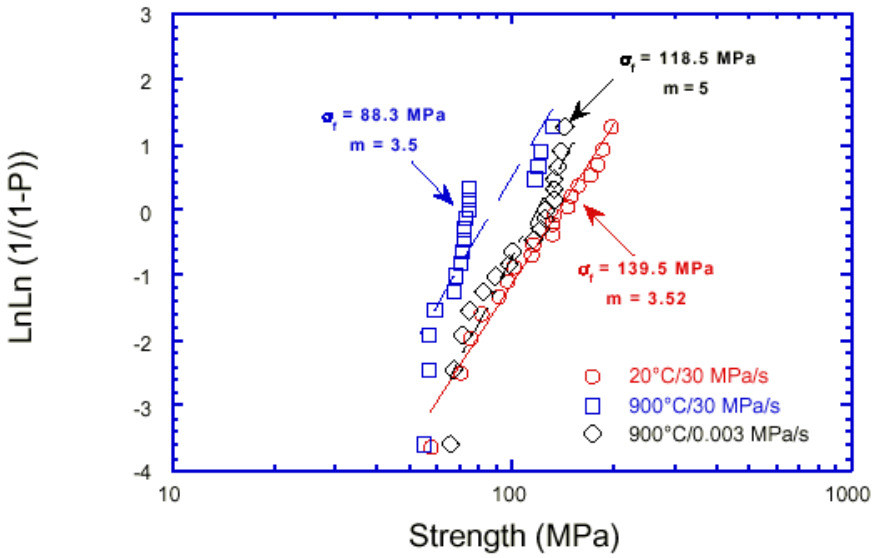

3.3 Task 3.3 Component Fabrication and Testing

Fabrication of representative CFCC components for testing in simulated and actual in-service conditions was performed. Process and CFCC component performance data that was generated in this task was used to further refine and improve those specific aspects of CFCC processing and materials optimization that need further refinement before pre-production scale manufacture of components. Fabrication of these components was accomplished in net-shape geometries that demonstrated Textron Systems NB SiC processing approaches can accommodate complex CFCC shapes.

Testing of sub-scale and representative components in simulated and actual in-service conditions have been performed at Doehler-Jarvis, Williams International, and General Motors.

Representative Parts

CFCC components for testing in simulated and actual process environments were concentrated initially in two primary application areas, metal processing and turbomachinery industries. The three principal CFCC demonstrator components that were selected for Task 3.3.1 fabrication efforts are as follows:

(1) NB-SiC CFCC Gas Fired Re-Heater Burner Tubes - These CFCC components were fabricated with design inputs by Hauck Manufacturing and Material Sciences Corporation. The length of these immersion heater tubes was about 30” (77 cm) and the diameter was 6” (15.6 cm). Wall thickness was 0.32" (8 mm) range. The NB-SiC matrix contained 20% Si3N4 and 80% SiC. Filament winding was performed on Textron Systems McClean-Anderson four axis winder using SCS-6™ fiber.

(2) NB SiC CFCC Combustor Can for a Stationary Gas Turbine Generator - These CFCC components were fabricated with design inputs by Williams International. The length of these liner tubes was about 10” (25 cm) and the diameter was 3.5” (8 cm) on the exhaust end and necked down to 1.5” (4 cm) at the throat. Wall thickness was 0.15" (3.8 mm). The NB-SiC matrix contained 20-25% Si3N4 and 80-75% SiC. Filament winding was performed on Textron Systems McClean-Anderson four axis winder using SCS-9A ™ fiber.

(3) NB-SiC CFCC Electric Heated Immersion Tubes - These CFCC components were fabricated with design inputs by Deltamation. The length of these immersion heater tubes ranged from 36” to 43” (91-109 cm) and the diameter for the shorter tube was 6” (15.6 cm) and for the longer tube 8.5” (21.6 cm). Wall thickness was 0.3 to 0.4" (8 - 10mm) range. The NB-SiC matrix contained 20% Si3N4 and 80% SiC. Filament winding was performed on Textron Systems McClean-Anderson five axis winder using SCS-6 ™ fiber.

Other CFCC components being considered for applications in the chemical industry are CFCC thermocouple tubes for gasifier applications and sensor sheaths for spectrographic analysis of molten metal constituents.

3.3.1 Representative Parts: NB-SiC CFCC Gas Fired Re-Heater Burner Tubes

The first series of immersion tubes fabricated for burner testing at Doehler-Jarvis consisted of an inner monolithic NB SiC tube fabricated by Nova Industries. The inner tube is not exposed to accidental impact or molten aluminum after installation, therefore no strong technical reason existed to use a CFCC inner tube. The outer burner tube was a NB SiC/SCS-6 closed end tube manufactured by Textron Systems. A total of six tubes were manufactured and shipped to Doehler-Jarvis for installation in a Schaefer multi-zoned re-melt furnace.

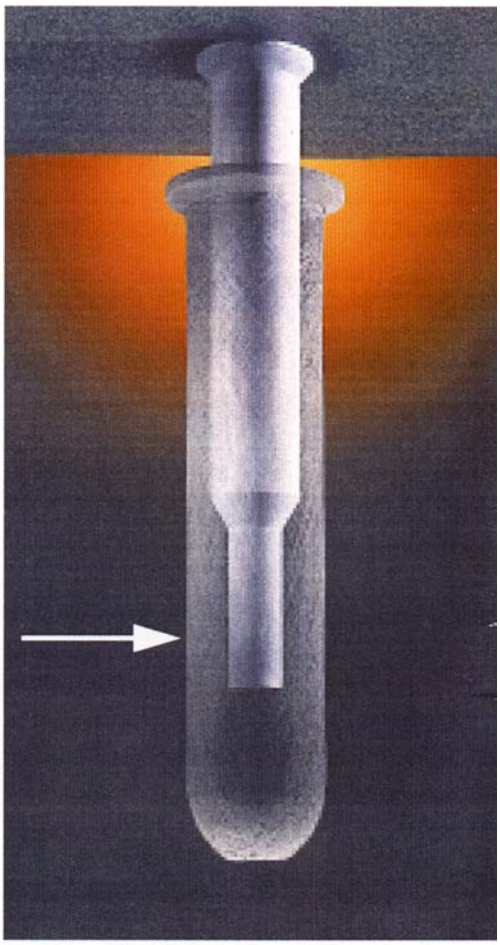

30 " long 6 " diameter immersion tube reinforced with continuous SiC fiber
(Superimposed over a monolithic ceramic inner tube)

Simulation Tests: NB SiC CFCC Re-Heater Burner tube

Hauck Manufacturing tested ring samples cut from a fully nitrided NB-SiC/SCS-6 tube for thermal shock performance. These rings were exposed to an oxyacetylene torch on the outer side and cold compressed air on the opposite side. Hauck reported the CFCC rings survived this rather aggressive exposure and did not show visually detectable indication of gross oxidation or damage.

CFCC tubes were fabricated and shipped to Hauck manufacturing for testing in air. The burner operated with the maximum outer temperature maintained at 1800°F. After two weeks of firing on a single shift basis cracks and delamination on the closed end developed. This behavior was not totally unexpected since this tube was fabricated with the early mandrel designs which employed a through spindle on the closed end. This opening was closed with monolithic material. A replacement tube was fabricated with filament reinforcement on the closed end. The open air burner test was restarted and this tube lasted six weeks before cracks developed. The location of the cracks was at the interface between the exit of the inner burner tube nozzle and the outer immersion tube. The cracks were circumferential about this interface and the tube remained in one piece held together by the SCS fibers.

End User Field Tests: NB SiC CFCC Re-Heater Burner tube

The Schaefer multi-zoned aluminum holding furnace with six CFCC burner tubes became operational in July of 1995 at Doehler-Jarvis. Although the furnace was designed to accommodate six immersion tube burners, only five were operated during furnace heat up prior to introduction of molten aluminum. The sixth burner was removed when it was observed to have surface cracks on the outer tube. After the introduction of molten aluminum, it was necessary to shutdown one additional burner and to operate only four burners to keep from overheating the molten aluminum. The burner test continued for a month before shutdown was necessary due to failure of two of the four tubes. All four tubes had significant corundum buildup located at the meltline, and cracked and broken tubes at two of the four test positions. These tubes were removed from the furnace and shipped to Textron Systems for evaluation.

Figure 3.3-1 shows the position of the burners in the furnace. Photographs of the burners prior to diassembly are shown in Figures 3.3-2 through 3.3-4.

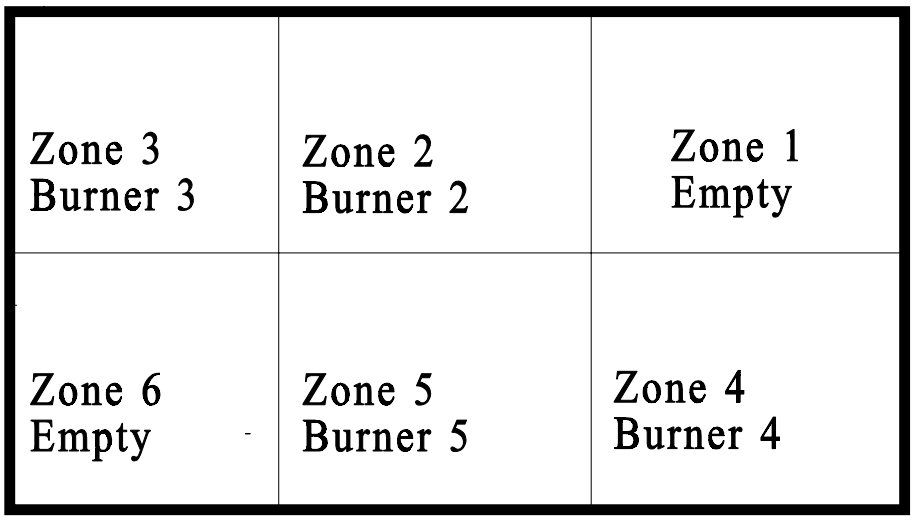

Figure 3.3-1 Burner locations in the test furnace

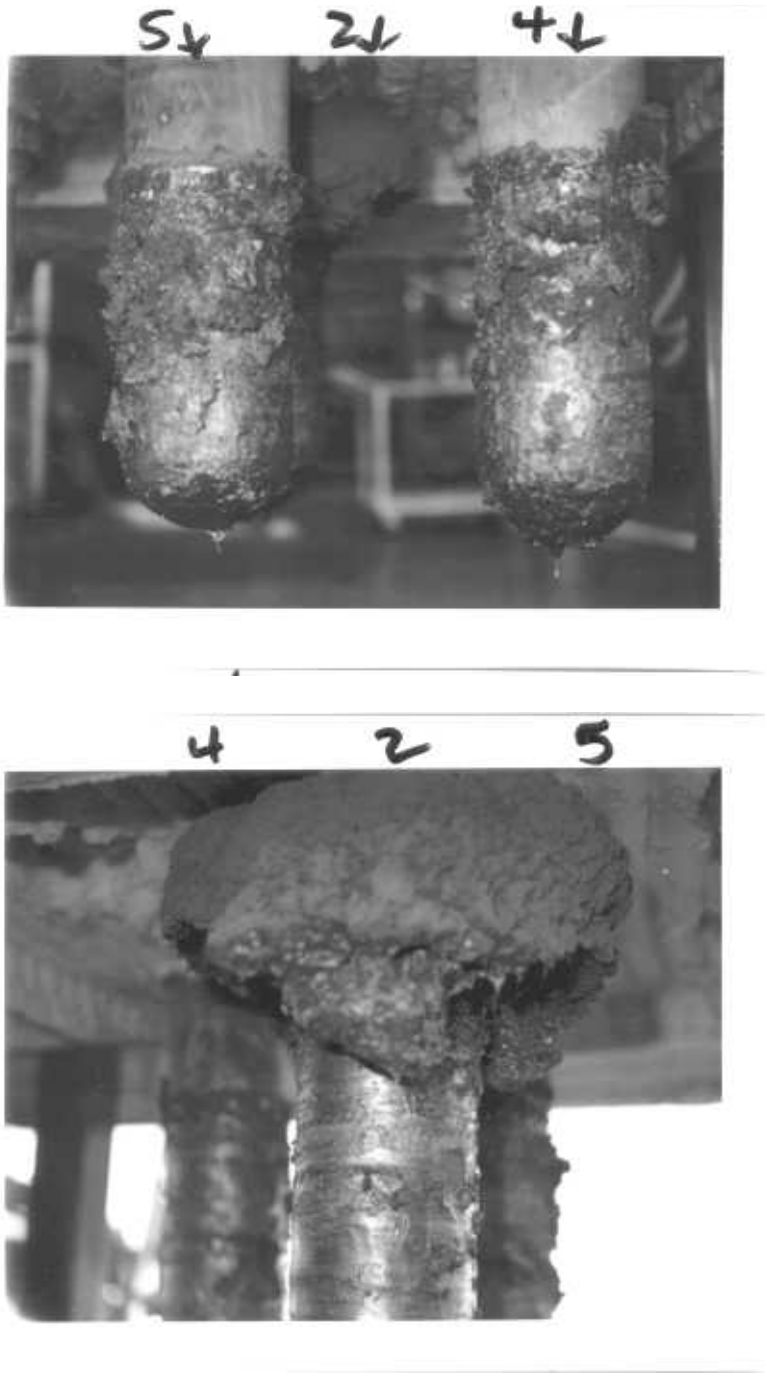

Figure 3.3-2 Burners 4 and 5 showed no significant corundum buildup, but contained surface cracks.

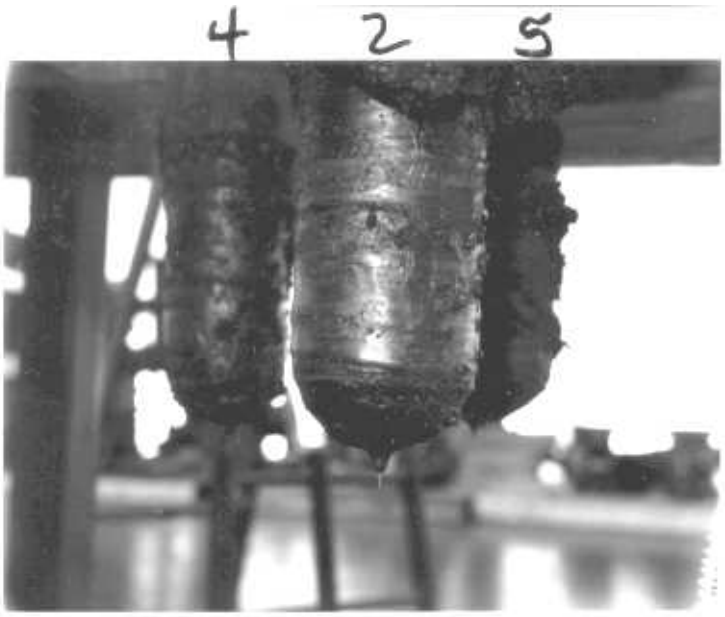

Figures 3.3-3 Shows significant corundum buildup on burner 2.

Figure 3.3-4 Shows complete fracture of burner 3 at the meltline. A significant corundum bloom existed on the missing half of the tube.

It is interesting to note that both tubes with significant corundum buildup were located on the same side of the furnace. As can be seen in the photographs, the inner burner tube nozzle transition, the meltline and the outer CFCC tube fracture location all coincided. This is the highest thermal gradient location in the assembly. All four inner burner tubes exhibited cracking or fracture at a location just above the diameter transition point, which also coincides with the internal burner flame cup.

Of the two "best" surviving CFCC tubes, one was an original (~20 week intermittent firing) installation, and the other had been in service for about 6 weeks. These tubes had been fired in previous immersion tube trials at Doehler-Jarvis prior to the multi-zoned furnace burner test.

Post-test Component Evaluation

Microstructure: NB SiC CFCC Re-Heater Burner tube

The CFCC outer burner and monolithic inner burner tubes which was tested in air at Hauck for approximately a six week period were inspected. Based on this inspection it is believed the cracks developed as a result of incomplete conversion of silicon to silicon nitride during nitridation. A change was made to the nitriding cycle to increase conversion of the silicon.

The CFCC immersion burner tubes returned from the Schaefer multi-zoned aluminum holding furnace tested at Doehler-Jarvis underwent visual inspection. One of the four tubes suffered complete ftacture at the meltline. The three remaining tubes were intact, though all experienced some degree of cracking. The fractured tube and one other tube experienced significant corundum buildup. Much smaller amounts of buildup were observed on the remaining two tubes. The cracking observed in these two tubes with the smaller buildup does not appear to penetrate the wall thickness. The monolithic inner burner tubes appear to have experienced extensive deterioration during the testing. The smaller diameter extension at the exit end of two of these tubes, which corresponds to the end of the internal flame section of the actual burner, had completely fractured. Additionally, the inner tubes removed from the outer assemblies revealed side wall bulging and cracking. These conditions could have resulted in localized impingement on the I.D. of the outer tubes, promoting thermal cracking and internal oxidation. Record keeping during disassembly of the burners at Doehler-Jarvis indicate these assemblies of tube #2 and #5 were not plumb in the mounting base, and the bolting was loose. The other two tubes did appear to be plumb and level, but the mounting bolts were found loose.

Sections of the returned immersion heater tube tested at Doehler-Jarvis have been taken from several locations for comparison to baseline and control specimens. Initial visual examination revealed that fracture paths followed existing I.D. surface circumferential cracks to major axial surface marks created by the segmented plaster tool used for filaments winding. The major fractures then followed these axial tool marks.

Microscopic examination of several sections revealed very low fiber vol.% in localized regions of the tube. Also of significance was a much larger size and distribution of ceramic matrix porosity (Figures 3.3-5 and 3.3-6).

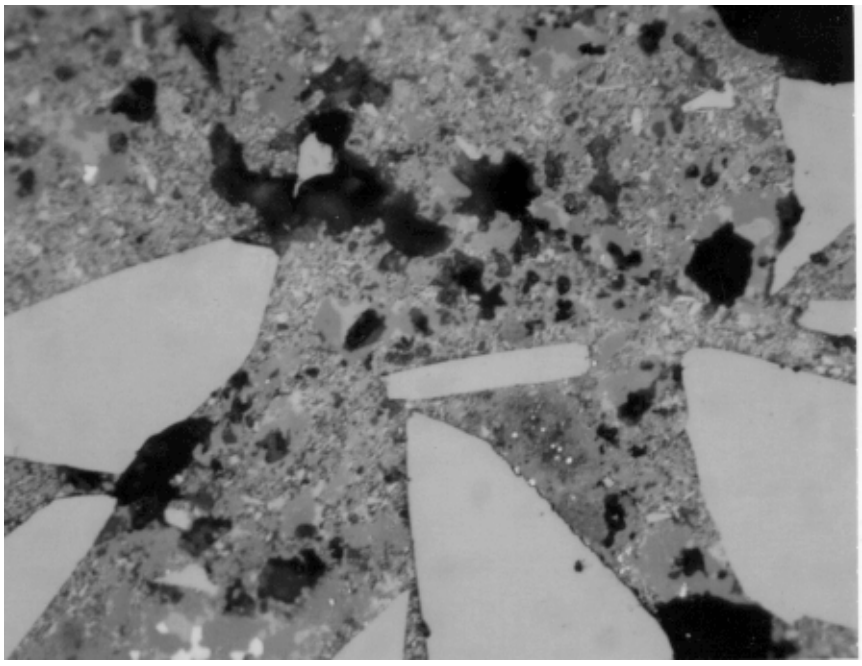

Figure 3.3-5 Section of returned CFCC immersion tube (~800X)

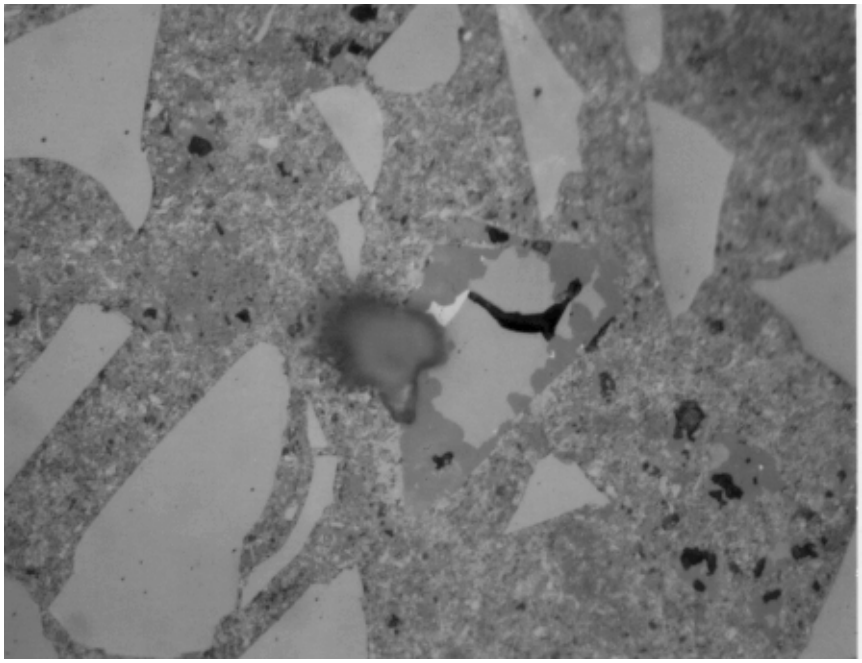

Figure 3.3-6 Section of monolithic NBSiC control material (~800X)

Also observed in these specimens was evidence of larger-than-anticipated amounts of free Si. These examinations, as well as confirming chemistries, were contined and augmented with the results of the other tubes returned from service. Microstructural examination of some immersion tubes returned from service testing at Doehler-Jarvis have revealed clear evidence of exotherming, especially in thicker sections like flange areas. Locally violent exotherms in the matrix can cause complete loss of the silicon nitride bond-phase, resulting in internal oxidation and decreased molten aluminum wetting resistance. Non-exothermed areas of the microstructure look quite good, even when in contact with molten aluminum for prolonged periods.

Based upon previous concerns with the Williams combustor can fabrication, and the initial indications observed in the failed immersion tube from service at Doehler-Jarvis, the segmented manifold tool design was modified to a one piece construction that eliminated seams. These seams on the mandrel are believed to have caused marked off condition observed on the ID surfaces of the failed tubes, apparently providing a fracture site for premature failure.

Analysis of CFCC immersion tube field test results have indicated that a burner/tube redesign is desirable if the longer lives are to be achieved. CFCC tube failures have initiated primarily at the location corresponding to the aluminum bath meltline, which is the region of highest thermal gradient on the tube OD surface. In addition, the current burner design has the flame holder located at the diameter transition point of the internal monolithic combustor tube. This transition also corresponds with the position of the meltline on the OD tube. Review of the field test failures has revealed that the internal ceramic tubes have failed at the transition, which exposes the burner flame to the ID of the CFCC outer tube, at the location of highest thermal gradient in the aluminum bath.

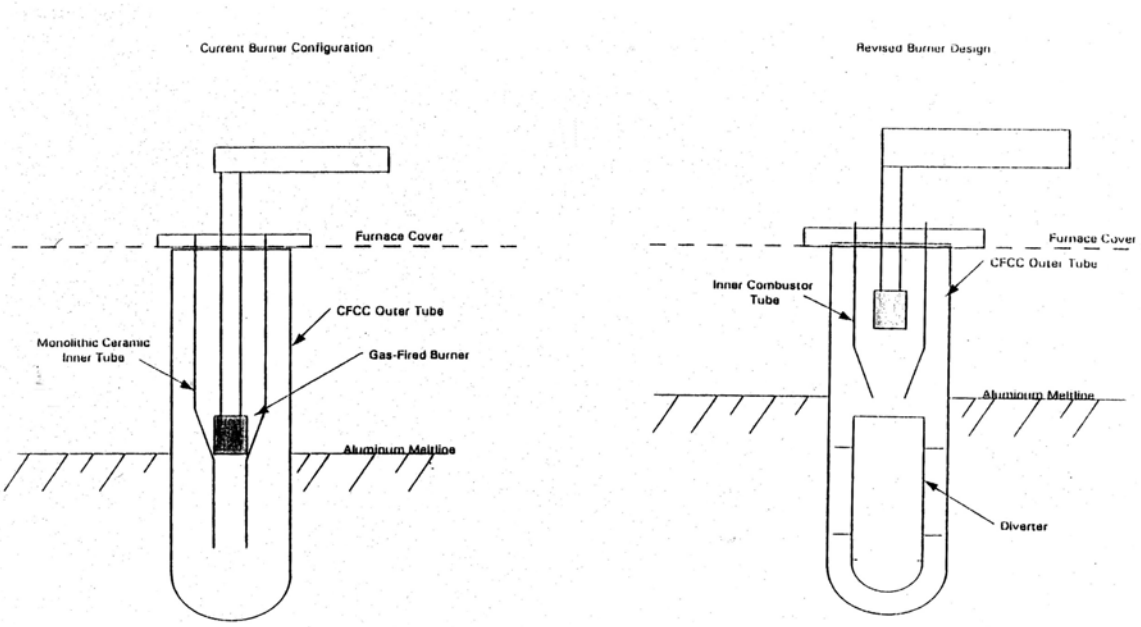

Initial immersion tube trials conducted at Hauck and Doehler-Jarvis have revealed that component reliability can be affected by the resulting microstructure from nitridation, fiber distribution within the component, and by damage due to processing effects (tooling and drying rates). Further work with Doehler-Jarvis was suspended once notification was received that they were no longer in business.

3.3.2 NBSiC CFCC Combustor Can

The Phase 1 program identified stationary turbomachinery as an area in which the potential advantages of CFCC components could be utilized. Textron contracted with Williams International to identify a particular application, provide component design, material testing, rig testing and evaluation support.

The application chosen was the combustor can of a remediator engine. The remediator engine burns hazardous waste materials and uses the power produced to generate electricity. The combustor can serves as a containment zone for the combustion of the fuel/air mixture. The cross section of the burner rig is shown in Figure 3.3-7. The detailed combustor design is shown in Figure 3.3-8.

Fig 3.3-7 Cross Section of the Williams International Burner Rig

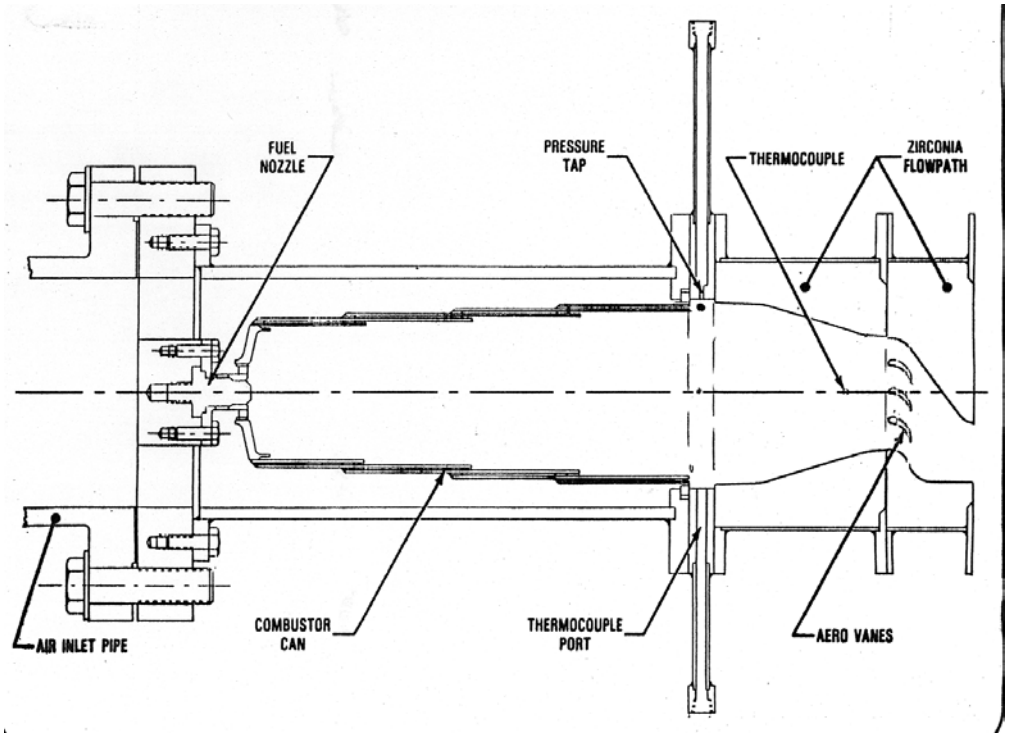

Fig 3.3-8 Textron Ceramic Combustor Design for the Burner Rig

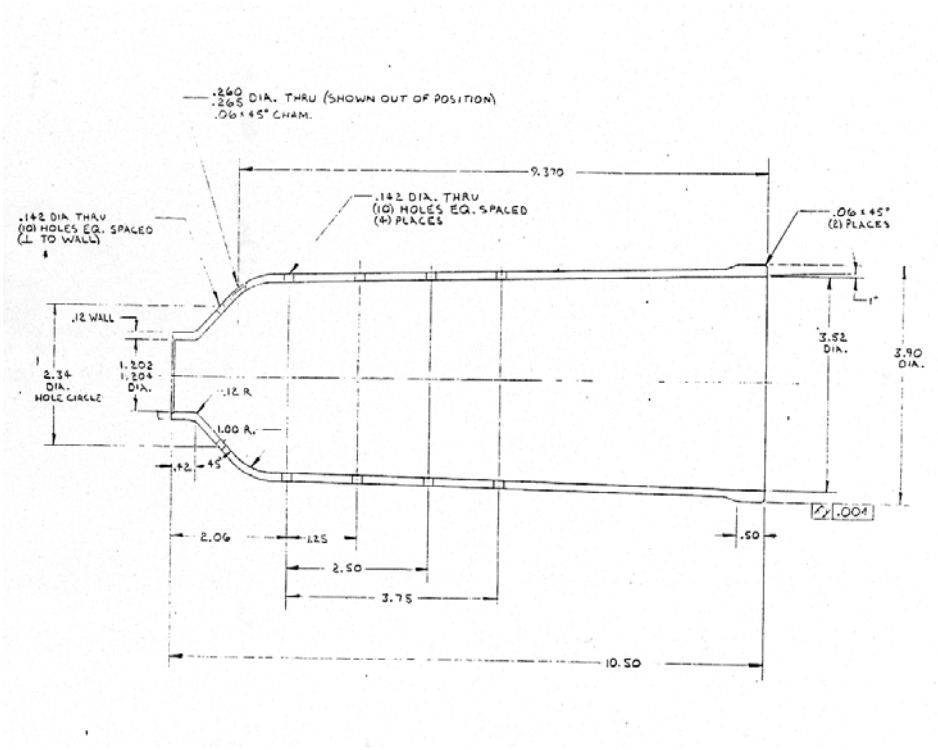

The current nickel-based liner materials have limitations particularly in the area of hot corrosion. The potential advantages of a CFCC liner are higher temperature capability, environmental stability and lower lifecycle cost.

Williams provided Textron with design details and Textron produced a tube for preliminary testing. The tube consisted of 3 mil diameter SCS-9 fibers filament wound in a matrix slurry which gave 30% Si_3N_4. Efforts were made to filament wind over pins in the mandrel to give a net shape part with the air inlet holes already in place. This was not successful in that fibers bunched up around the holes. The final part shipped to Williams had holes drilled after nitridation.

In the preliminary round of evaluation, this combustor was rig tested for 22 hours of exposure up to 2500°F. Other than some slight cracking observed around the air inlet holes, the combustor was intact after testing. Heavy carbon build up was also observed. At this point Williams modified the design of the air inlet hole pattern to improve combustion and reduce carbon build-up.

During the same time frame, significant processing improvements had been accomplished at Textron. Fiber manufacturing process conditions had been modified to produce a 50% increase in the strength of the 3 mil SiC fiber. This improved fiber, denoted SCS-9A, was used for the rest of the Williams program. Filament winding procedures had been modified to place fibers in the matrix more uniformly. This minimized the fiber piling up at crossover points and led to reduced wall thickness at equivalent fiber volume fraction. Slurry modification had been made that yielded a silicon nitride fraction in the matrix closer to 20% compared to earlier values close to 30%.

Three improved CFCC combustor liners were fabricated. Two of these were finish machined for burn rig testing at Williams. The test plan included computed tomography and thermal imaging of the tubes at Argonne National Laboratory both before and after rig testing. In addition, a number of flat plates of both unidirectional and ±45° fiber orientation were provided to Williams for material property determination. This testing included tensile testing at room and elevated temperature, stress rupture testing at 2200, 2400 and 2500°F, and stress oxidation testing at 2200 and 2400°F.

The results of these tests are presented below.

Burner Rig Testing

The burner rig is operated with JP5 or JET A jet fuels that is sprayed through a simplex fuel nozzle. The mass flow of air through the rig is approximately 0.244 lbm/s with a fuel flow of about 30 pounds per hour. These values are approximate and vary according to the desired run conditions. Both the fuel and air are independently adjustable to the required test conditions.

Instrumentation

The burner rig was installed into test cell A8 and setup for semi-automated testing. The combustor can was instrumented with K type thermocouples on both the outside and inside surfaces of the combustor. Stainless steel lock wire was used to hold the thermocouples near the surface of the combustor. Alumina cement was used on the ends of the thermocouples on the inside diameter, however it spalled off during installation into the burner rig. The thermocouples were positioned as close to the surface of the combustor as possible before the testing was initiated.

Platinum type B thermocouples were used at the burner rig exit and the exit of the ceramic combustor can. Fuel pressure into the fuel nozzle was monitored by a pressure transducer and fuel flow was monitored with a Cox turbine flow meter. Fuel pump pressure, nozzle pressure and flow were also monitored on separate gauges in the test cell.

A strip chart recorder was used to monitor critical parameters of the combustor and rig operation. A fuel shutoff valve was used in conjunction with a high and low temperature limit monitor. If the temperature of the rig was outside of the limits the fuel shutoff valve was activated to stop the test.

All of the gauges and sensors were calibrated before the testing was initiated.

Combustor Liner #1 Testing

The test plan for the first liner was to run 8 to 12 hours at a material temperature of 2200°F to 2300°F then visually inspecting the liner. The next segment of testing would be the same as the first, 8 to 12 hours at 2200°F to 2300°F. The last test segment was to be a 24 hour test at 2300°F to 2400°F for a total test time of approximately 50 hours.

During the testing of the combustor a number of cycles were accumulated. Some of the shut downs were due to manpower constraints and others either due to equipment upgrades and interference due to testing in other test cells.

After 50 hours of testing the ceramic combustor was in excellent shape. The appearance of the outside is unchanged with no evidence of cracking, delaminations or any other problems. Inside of the combustor is also in excellent condition. The end near the small diameter is darker from carbon buildup due to the combustion of the fuel. There is no evidence of cracking or delaminations. Slight erosion can be seen in some areas of the surface near the end of the combustor. These are slight indications with a depth of approximately 0.010”.

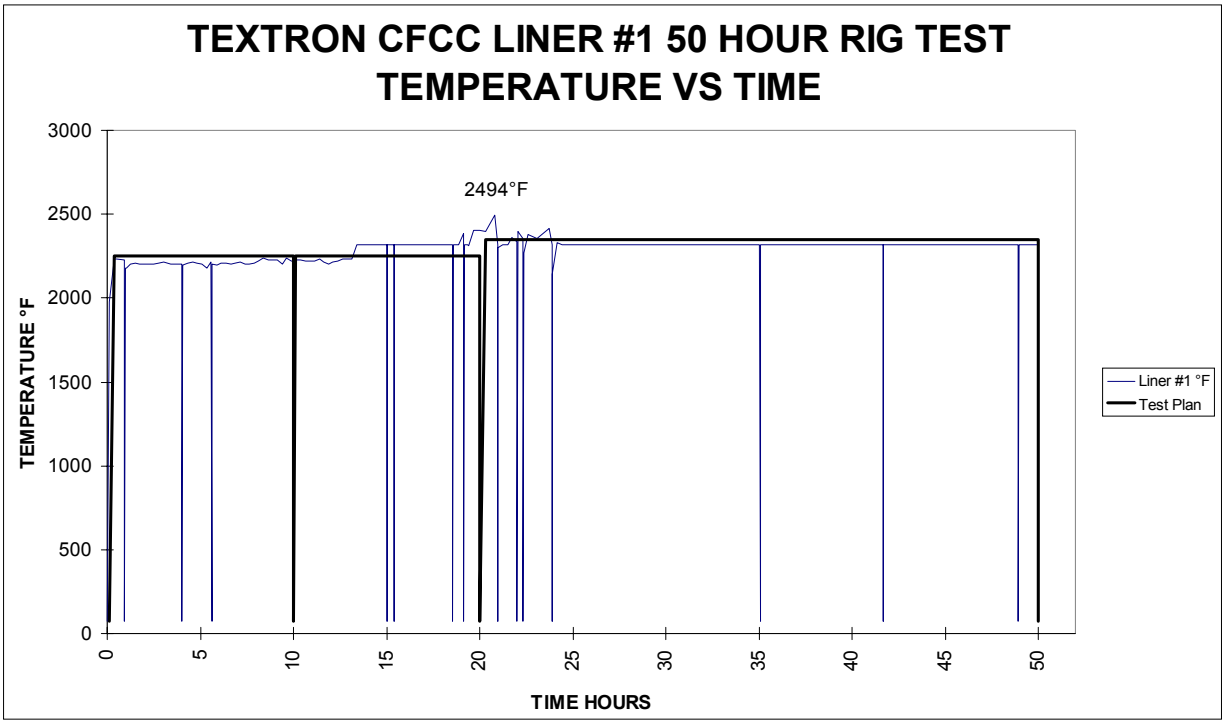

Figure 3.3-9 Liner #1 Time versus Temperature Plot

Time versus temperature plot was made for combustor liner #1 in 3.3-9. This plot does not account for down time which is not included. The maximum temperature excursion measured during the test is recorded on the plot.

Combustor Liner #2 Testing

Testing for the second liner was planned for 50 hours with a material temperature of 2300°F to 2400°F. The second phase of testing this liner was 50 hours at 2400°F to 2500°F for a total of 100 hours of exposure. During the testing of this combustor there were a total of 10 cycles accumulated. A summary of the shut down descriptions is given in Table 3.3-1.

Table 3.3-1 100 Hour Burner Rig Test Liner #2

CYCLE	SHUT DOWN DESCRIPTION
1	Instrumentation check
2	Vibration/buzzing sound
3	Remove carbon buildup
4	Remove carbon buildup and add smaller flow path exit
5	Remove carbon buildup and setup of equipment for other test cell
6	Equipment setup for other test cell
7	Weekend with removal of carbon buildup
8	Automatic shut down, shop air pressure drop
9	Automatic shut down, shop air pressure drop
10	End of test

Combustor liner #2 before testing was in excellent condition. There were no apparent voids, delamination or cracks. Tempil thermal paints were painted on both the inside and outside surfaces of the combustor. Thermocouples were placed at the outside and inside surfaces of the combustor.

The combustor was visually inspected before every restart of the test rig. Notes were taken on the condition of the rig and any anomalies were noted. A summary of the test temperature and time is shown in Figure 3.3-10. Near the end of the test the temperature spiked during the test.

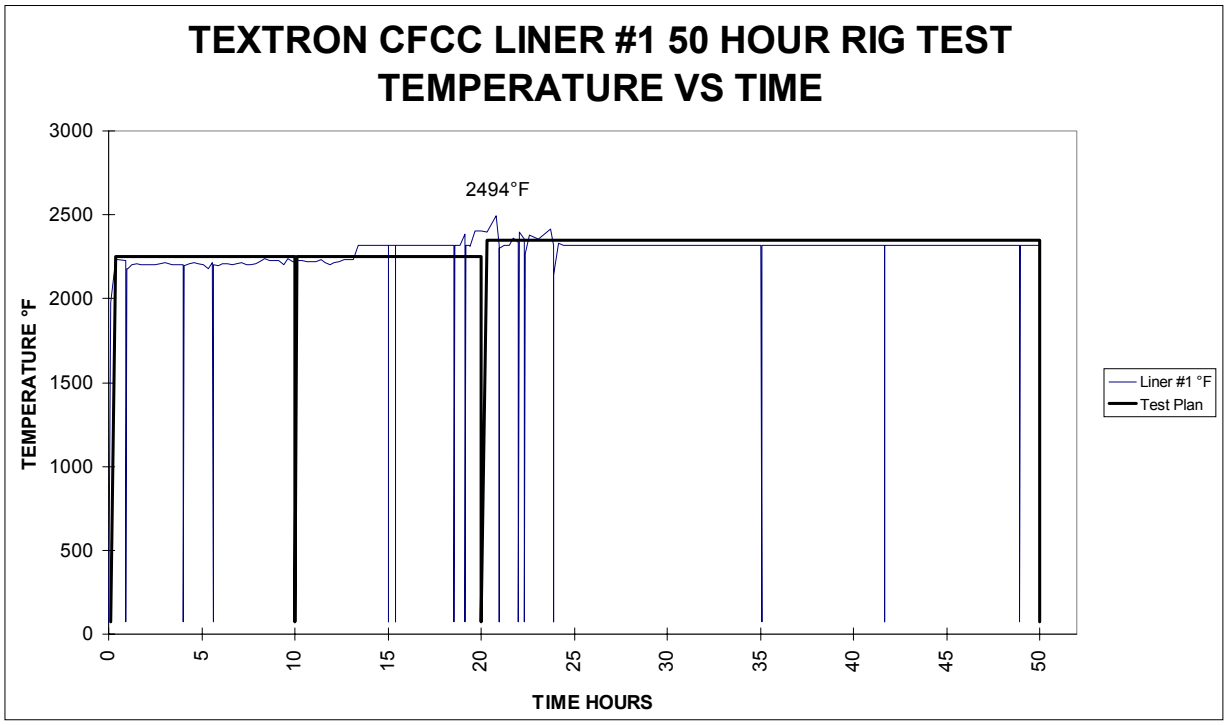

Figure 3.3-10 Liner #2 Time Versus Temperature Plot

Since the processing of the ceramic material was approximately 2552°F, changes in the material probably occurred which may have caused the cracks in the combustor component.

Summary of Combustor Testing

Although one of the combustors was run over temperature there were no catastrophic failures. At the end of the testing of each component the combustor was functioning.

Combustors that were tested below 2400°F were in excellent condition after testing with no visual cracking, delamination or spalling. The color of the material appeared unchanged on the outside and only a little darkening on the inside due to carbon in the combustor.

The material was subjected to many start/stop cycles which produces real engine start thermal transients. No evidence of thermal fatigue cracks were observed in the combustor components during the second phase of testing.

Non-Destructive Inspection (NDI)

Inspection of the ceramic combustors was conducted by Argonne National Laboratory using computed tomography (CT) and thermal imaging. Argonne National Laboratory inspected the combustor components both before and after rig testing.

Figures 3.3-11 and 3.3-12 show the CT images of combustor liner #1 while Figures 3.3-13 and 3.3-14 show the images for #2 before rig testing. The CT data show some pores near the top of the liners, but show no major structural flaws. The pores are in the size range of 0.5-1.0 mm. One such pore is shown in detail in Figure 3.3-15.

Fig 3.3-11 CT Images of Textron Liner # 1

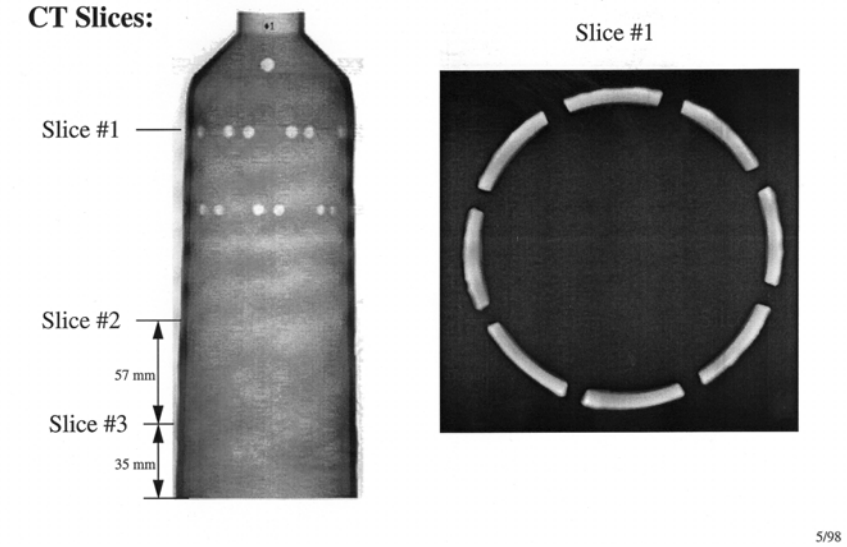

The pre-test thermal diffusivity results are shown in Figures 3.3-16 and 3.3-17.

The diffusivity data are shown as gray-scale images, with a darker gray-scale corresponding to low diffusivity and a brighter gray-scale to high diffusivity. A low diffusivity at a certain region usually indicates some type of "defect", -e.g., delamination, voids, cracks, or high porosity. However, thickness variation may also contribute to the diffusivity data.

The thermal diffusivity image of the whole liner consists of section images in four rows in the axial direction and eight columns in the circumferential direction. Small rectangle tapes were attached at the comers of these sections on the liner surface, as can be seen in the images. The holes were sealed to block the flash light from reaching the IR camera; they are seen as black

Fig 3.3-12 CT Images of Textron Liner # 1

Slice # 2

Slice # 3

5/98

Fig 3.3-13 CT Images of Textron Liner # 2

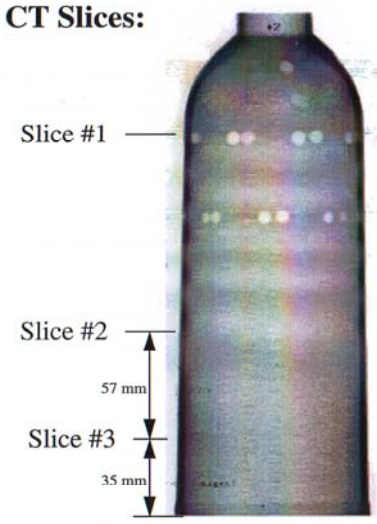

Slice #1

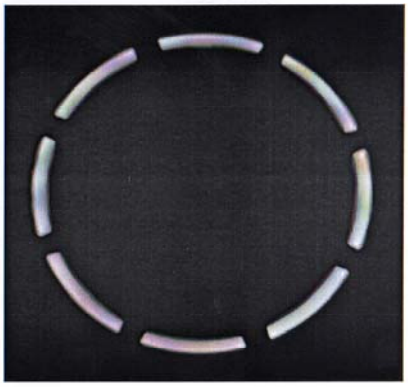

5/98

Fig 3.3-14 CT Images of Textron Liner # 2

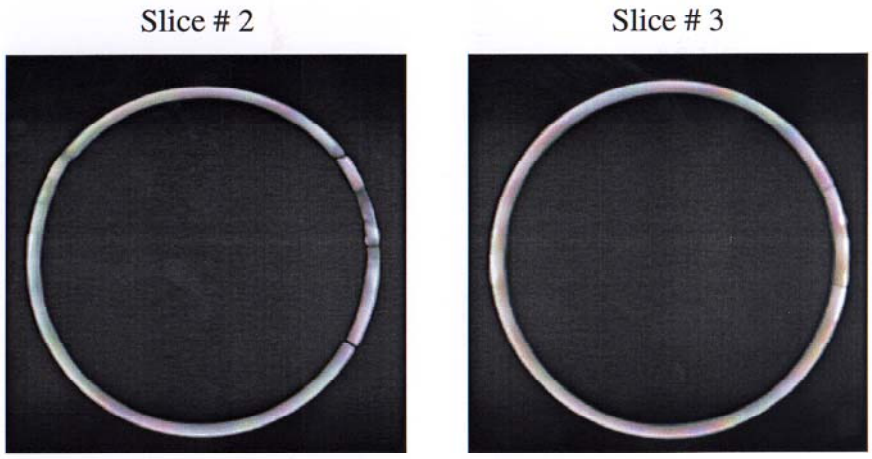

5/98

Fig 3.3-15 CT Slice 2 for Liner # 1

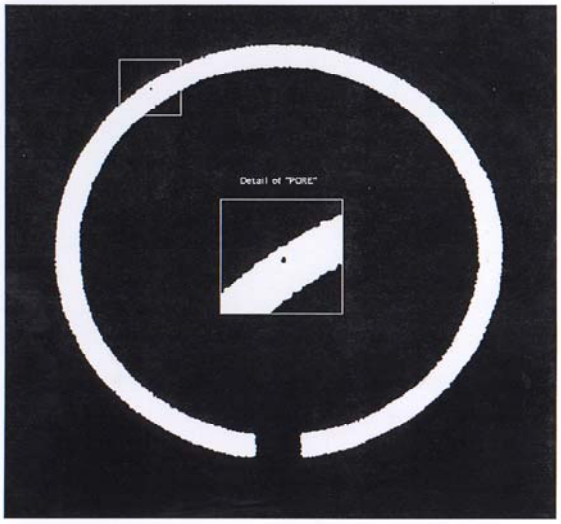

Fig 3.3-16 Thermal Diffusivity Image of Textron Liner # 1

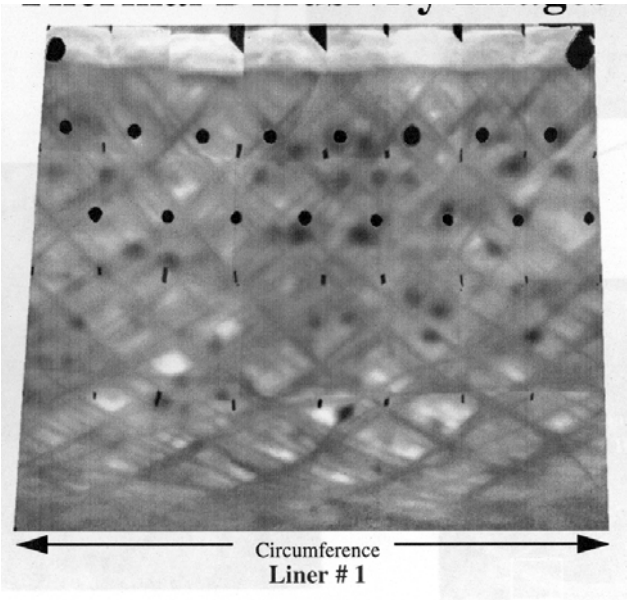

Fig 3.3-17 Thermal Diffusivity Image of Textron Liner # 2

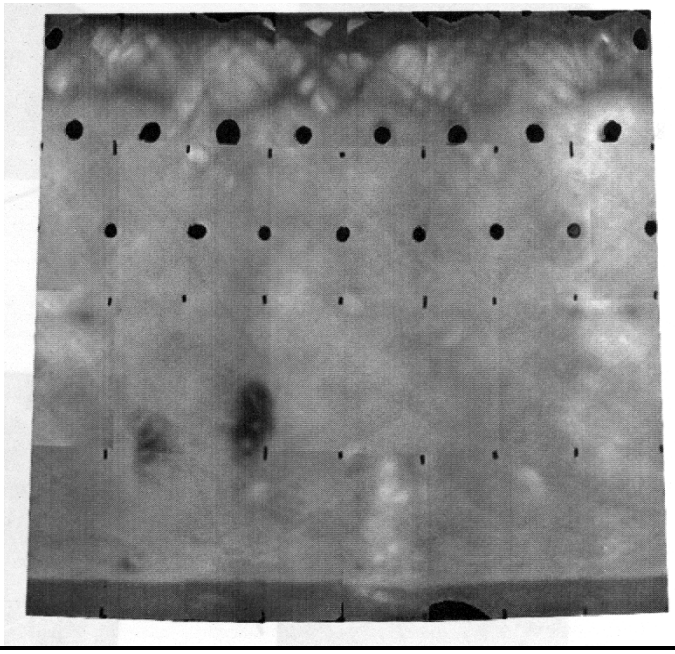

circular spots in the images. Because of the curvature effect, the size of the holes are different, depending on the distance from the camera. For the same reason, the single hole at the top of the liner (smaller diameter section) appears twice in the thermal diffusivity images of the liners. Thermal diffusivity image of Liner # 1 shows clearly the thickness effect. Fibers are shown as darker lines (low diffusivity) because the wall is thicker where the fibers were wound. Many darker spots are seen in the image which may due to the wall thickness variation or local defects. Further analysis by correlating the thermal diffusivity data with the CT data may identify a low diffusivity region (darker region) is due to. defect or wall thickness, as described below; however, a complete analysis was not performed here. For Liner # 2, its surface was machined so a uniform wall thickness is expected. The thermal diffusivity image is more uniform. The apparent two darker regions in the image indicate defects (see discussion below), possibly high porosities.

Some of the regions with low diffusivities for Liner #l are due to the increase of wall thickness (similarly, a region with high diffusivity maybe due to reduced wall thickness). A low thermal diffusivity region in the diffusivity image is correlated with the wall thickness variation data from the CT images. Regions with low diffusivities that are not correlated with increased wall thickness can be identified as having some defect, since the wall thickness is the only parameter used to determine the thermal diffusivity for a "good" material (specimen).
The post-test data are shown in Figures 3.3-18 through 3.3-21.

Fig 3.3-18 Thermal Diffusivity Image of Textron Liner # 1 (After Rig Test)

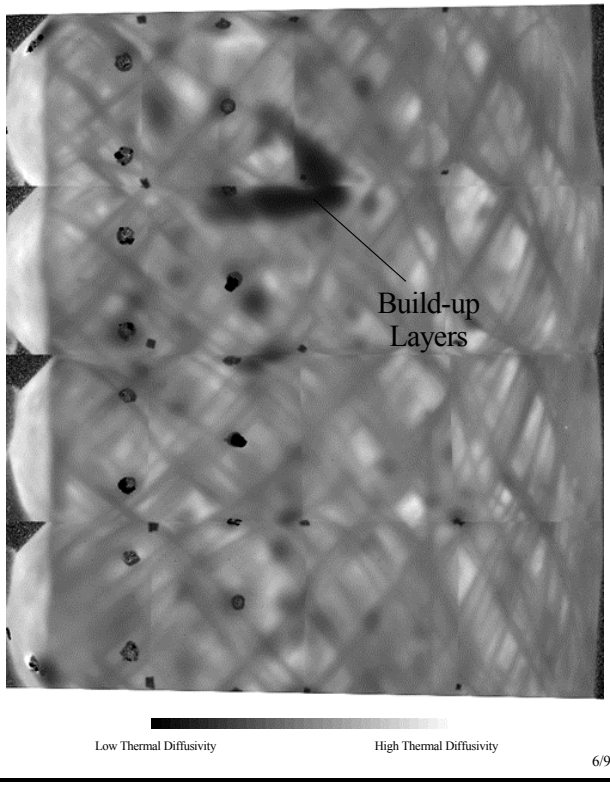

Fig 3.3-19 Thermal Diffusivity Image of Textron Liner # 2 (After Rig Test)

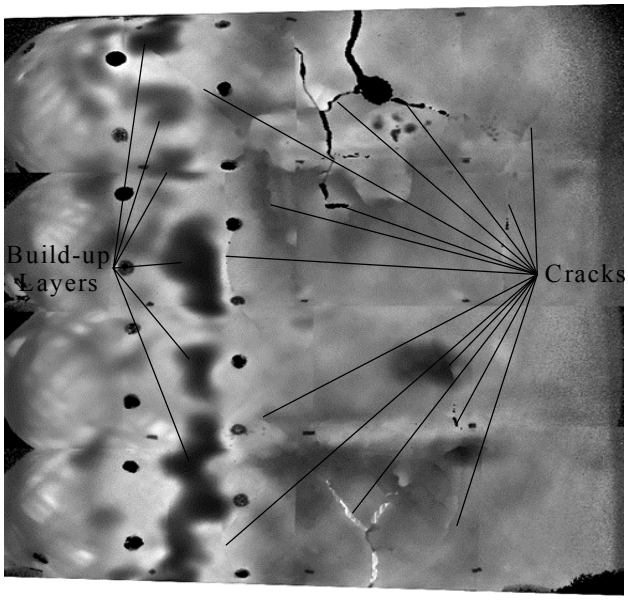

Fig 3.3-20 Textron Liner # 1

Comparison of a Section of Thermal Diffusivity Images

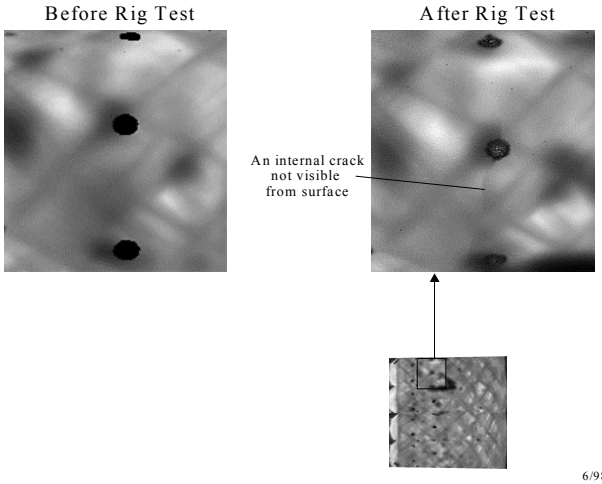

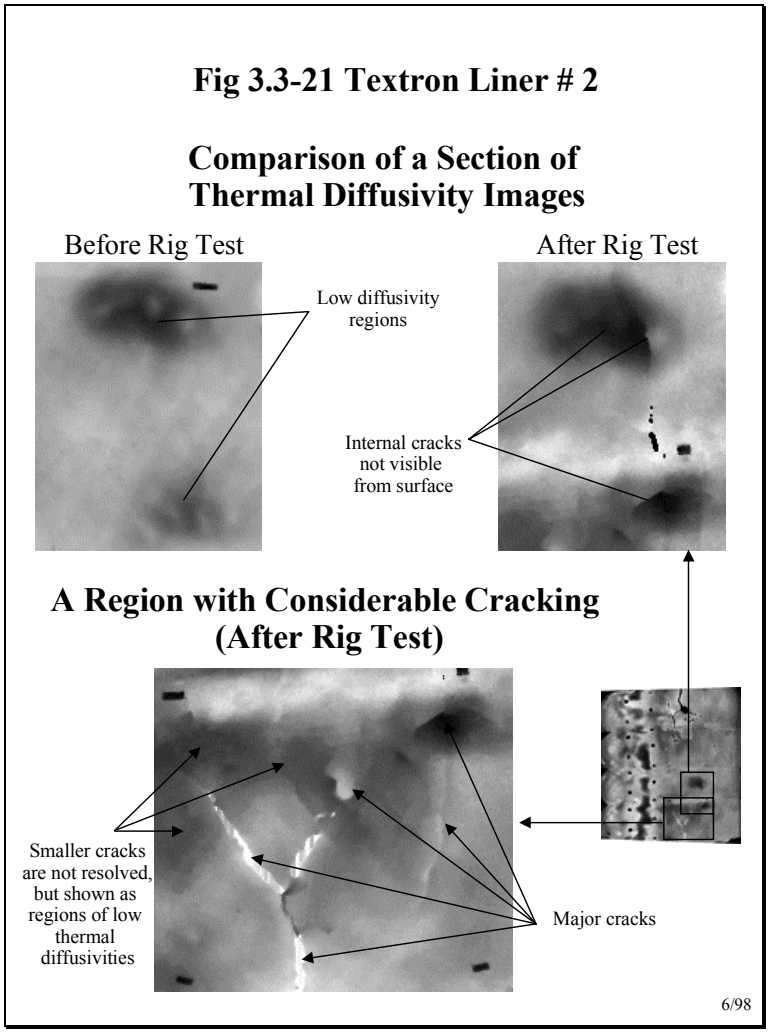

The compiled images of Liners # 1 and 2 are shown in approximately the same orientation as the ones taken before the rig test. Note that the curvature effect is more prominent in these data compared with the earlier ones because we took only four sectional images in the circumferential direction this time as compared with 8 before.

There are some materials attached on the inside surface of the liners. They are shown as regions of low diffusivities (dark) and are marked as "build-up layers" in the images.

The new thermal diffusivity image for Liner # 1 is very close to the image data taken before the rig test. However, in one location (between two holes) the new image shows presumably a crack developed due to the rig test. It is, however, not visible from the liner surface. The ends of the "crack" are located near two low-diffusivity regions. As discussed before, low diffusivity obtained from thermal imaging test could be due to defects or thicker material.

Liner # 2 contains many cracks which are detected by the thermal imaging and by CT. A region with intensive cracking is separately shown. While major cracks can be identified directly from

the thermal diffusivity (or CT) images, as marked in the data, groups of small cracks will be shown as low material thermal diffusivities.

The diffusivity data in a section on Liner #2 is compared with that before the rig test. This section is of interest because it has been previously identified to contain two low-diffusivity (or high porosity) regions. The thermal diffusivity data seen indicates that internal cracks developed within the regions which are undetectable from surface.

Except for the apparent effects of the over-temperature spike during the rig testing of liner #2, the performance of the two liners appeared to be satisfactory. At this point, however, a market assessment at Williams indicated that there was no market pull at this time to justify development of remediator engines in lieu of existing incinerators. There was no further program activity in this area.

3.3.3 Representative Parts: NB-SiC CFCC Electric Heated Immersion Tube No. 6

Textron Systems attended the North American Die Casting Association Conference & Exposition in Minneapolis, MN on November 4-5, 1997. General Motors was identified as a potential site to test immersion tubes in their Advanced (Casting) Development Laboratory in Saginaw, MI. A meeting was held at the Advanced Development Laboratory on December 2nd, 1997. Representatives from GM, Deltamation (furnace manufacturer and consultant to GM), and Textron were in attendance. There was much interest in trying a CFCC immersion tube (or several tubes) in the Saginaw facility. There was a small casting furnace using a monolithic ceramic immersion tube that was ideally suited to accept, in substitution, Textron's immersion tube. The monolithic tube is 0.75 inches thick, whereas Textron's tube would be closer to 0.25" thick. The potential for quicker heating cycles was projected for Textron Systems immersion tubes, which was very important to General Motors. A drawing of the immersion tube design used at ADL has been sent to Textron from Deltamation. Textron Systems CFCC components were fabricated with design inputs by Deltamation. The length of these immersion heater tubes ranged from 36" to 43" (91-109 cm) and the diameter for the shorter tube was 6" (15.6 cm) and for the longer tube 8.5" (21.6 cm). Wall thickness were in the 0.3 to 0.4" (8 - 10mm) range. The NB-SiC matrix contained 20% Si3N4 and 80% SiC. Filament winding was performed on Textron Systems McClean-Anderson five axis winder using approximately 2.3 Vol. % SCS-6 ™ fiber. A total of three immersion tubes was tested at GM in Saginaw, MI between July, 1998 and April, 1999. One larger scale tube was tested at GM in Bedford, IN in May of 1999.

Simulation Tests: NB-SiC CFCC Electric Heated Immersion Tube No. 6
Materials Sciences Corporation (MSC) visited Textron to present a review of the design studies on the immersion tube application that have been completed to date and to obtain feedback on what additional work should be performed with the remaining available funds. It was decided that (with the remaining funds) MSC will further exercise the existing process model to look at boundary conditions which more accurately reflect the actual conditions expected in service at General Motors Advanced Development Laboratory in Saginaw, MI.

A draft report was received from Materials Sciences Corporation (MSC) who exercised their existing immersion tube model, revising the models boundary conditions to better simulate the actual conditions at General Motors casting facility. The conclusion of the report was that the immersion tube's thinner cross section would be viable under the conditions used at GM, i.e., cold start-up with an "air" gap between the aluminum and the tube. The stresses modeled indicate that the tube should function well; actual experience to date has confirmed MSC's findings.

End User Field Tests: NB-SiC CFCC Electric Heated Immersion Tube No. 6
Fabrication, including NDE at Argonne National Laboratory, of several immersion tubes for implementation into an aluminum die casting furnace at the Advanced Development Laboratory for General Motors in Saginaw, MI was conducted. Immersion tube #6 was delivered to GM on July 23, 1998 and installed and fired up during the week of July 27, 1998.
Figure 3.3-22 shows the immersion tube just before it is lowered into the crucible.

Figure 3.3-22 Textron CFCC Immersion Tube held over the melting crucible

Figure 3.3-23 shows the tube lowered into the crucible with aluminum ingots carefully placed around it. The electric heating element inside the immersion tube is gradually heated up and the aluminum is melted; the following day additional ingots are added to the melt. This process is referred to as a "cold start" and is probably the most aggressive conditions that the tube has to endure (see Figure 3.3-24). Once the crucible is full of molten aluminum and casting begins, the crucible is replenished with molten aluminum from another holding furnace.

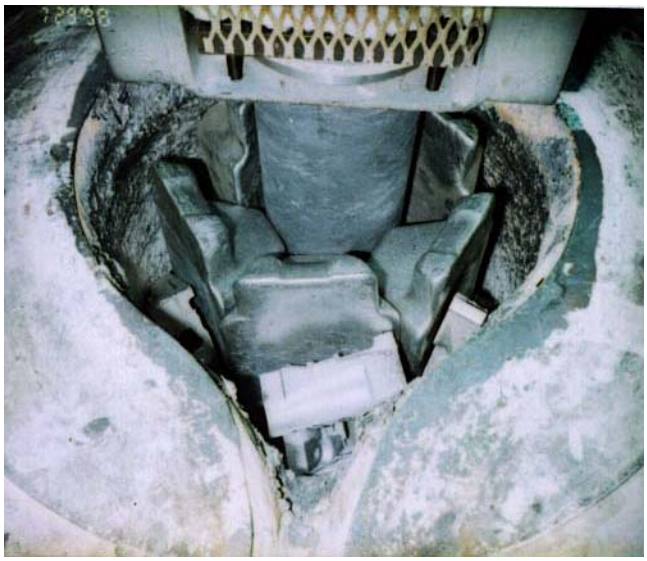

Figure 3.3-23 Textron CFCC Immersion Tube surrounded by aluminum ingots

Figure 3.3-24 Cold Start up – Ingots partially melted

This immersion tube had performed extremely well in service at GM's facility. Early indications were that the tube is more energy efficient than the thicker unreinforced tubes previously used. Warm-up periods during a "cold start" were reduced by 1/3 and (non-transient) static hold heating conditions required a lower heater temperature to maintain the melted aluminum at temperature. Figure 3.3-25 shows the 12 kW Kanthal heating element assembly used inside the immerstion tube.

Figure 3.3-25 The electric heating element being used in immersion tube #6 at GM Advanced Development Center in Saginaw, MI

A report that immersion tube No. 6 had failed in August turned out to be a false alarm; the thermocouple had degraded and malfunctioned causing the heating element to shutdown. At that time the tube had run continuously for over 1,011 hours and had melted 28 heats of aluminum. The thermocouple was replaced and the tube was placed back in service. GM-Saginaw was running the immersion tube at temperatures to maintain the aluminum at 1350°F. Prior to the thermocouple failure they had increased the heater temperature and aluminum temperature to 1521°F. This is when the thermocouple first failed. After this tube was placed back in service a "cold start" was performed at these higher temperatures. An additional two casting cycles were performed at the higher temperatures before the tube fractured outside the crucible. At the time of failure a technician was wiping down the outside wall of the immersion tube with a piano wire to remove any mobile aluminum from its surface. Tube #6 provided approximately 1100 hours of service.

During the investigation of this 2nd failure Textron learned that this tube was exposed to a series of adverse conditions before and after the initial thermocouple failure. When the first failure occurred the tube was removed from the crucible of aluminum and cooled with a large fan. The technician observed a crackling noise and immediately turned off the fan. When the thermocouple was replaced an electrical check of the heater element and temperature control system was performed. During this check the tube was allowed to heat in open air for three hours. During the final hour of testing the tube was running above 1700°F. After testing, the tube was exposed to an abrupt cooldown by shutting off the heater element power supply for the weekend. Normally, if the tube is going to be taken out of service it will cool down at a controlled rate. The following week this tube went through another "cold start" at elevated temperatures (1840°F). During a "cold start" ingots of aluminum are placed around the immersion tube to be melted. Once they melt additional ingots are added to top off the crucible. During this cold start the immersion tube was left partially immersed for a long period because the operation was left unattended overnight. The following morning additional ingots were added to complete the "cold start".

After tube #6 went through its second "cold start" it was used in three more casting cycles at higher temperature settings than what was used for the first 28 cycles. A casting cycle will require the immersion tube heater to preheat and hold aluminum at 1350°F to 1520°F. When the aluminum is ready for casting the immersion tube is removed, with the heater element power still on, and left in ambient air for fifteen minutes. When the crucible is returned it is already filled with molten aluminum taken from a melt furnace. The immersion tube is placed in the molten aluminum to start the cycle again. After the 31st casting cycle, while the crucible was being poured, the immersion tube fractured while it was being cleaned.

The second tube (#8) delivered to GM was placed in service the week of October 5th. It was outfitted with the same heating element used in tube #6. The thermocouple sheath used inside tube #6's heating element was found melted. It was made of Inconel 601 which melts at 2374 to 2494 °F. Since this implies the heating environment inside tube #6 got much hotter than expected it was decided to perform routine checks on the thermocouple assembly used inside tube #8. Tube #6 was returned to Textron Systems and is undergoing failure analyses.

Component Evaluation Immersion Tube No. 6

Immersion tube No. 6 was the first prototype immersion tube shipped to GM in Saginaw, MI. This tube represented improvements in filament winding and slip casting that allowed a thin walled tube to be fabricated. This tube was X-rayed and shipped to Argonne National Laboratory for NDE.

Immersion tube #6 was nondestructively evaluated at Argonne National Laboratory prior to being delivered to GM's Advanced Development Lab in Saginaw, MI. Thermal imaging of the tube indicated no areas of concern. The image is shown in Figure 3.3-26.

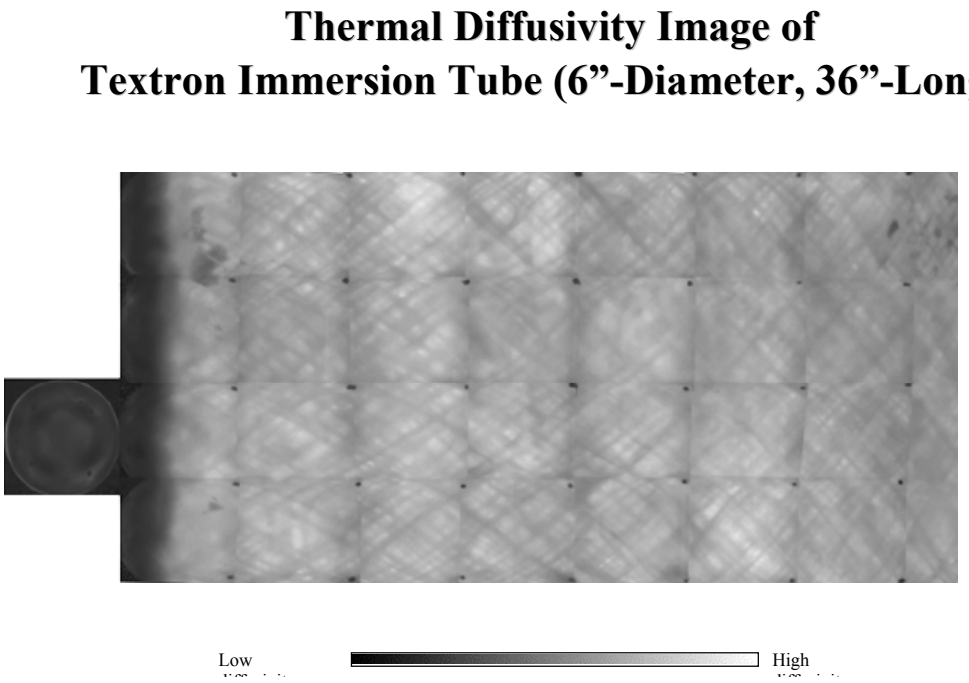

Figure 3.3-26 Thermal diffusivity image of Textron's CFCC immersion tube No. 6

Pictures of the failed tube No. 6 along with radiographic inspections are show in figures 3.3-27 thru 3.3-32. In general, it appears that the major fractures are consistent with the region of the immersion tube that is sometimes not fully immersed in molten aluminum, but is exposed to direct radiation from the heating element. A failure analysis effort has begun to look at fracture sites and regions along the axis of the tube in order to better understand the failure mechanisms.

Figure 3.3-27 Immersion Tube No. 6 Fracture

Figure 3.3-28 Upper region of fractured tube No. 6 toward flange end

Figure 3.3-29 Lower Section of Tube No. 6

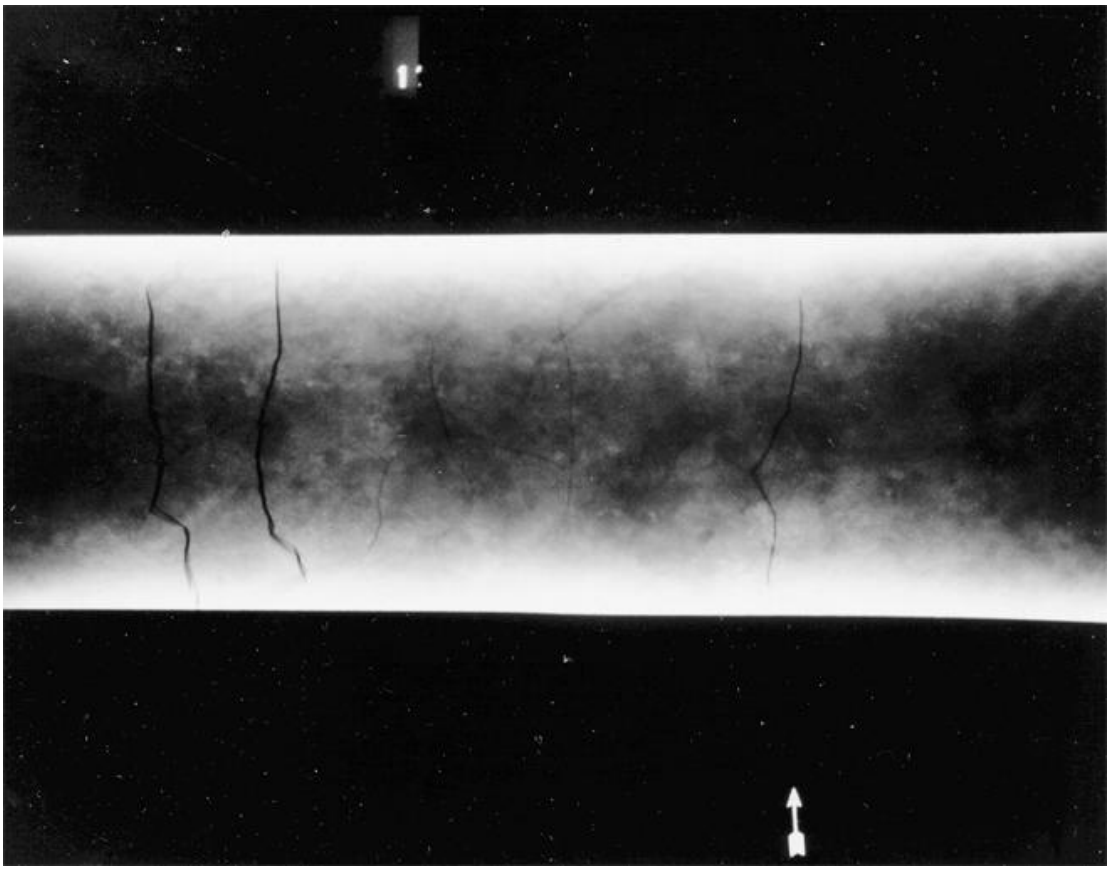

Figure 3.3-30 X-ray of upper section - tube No. 6

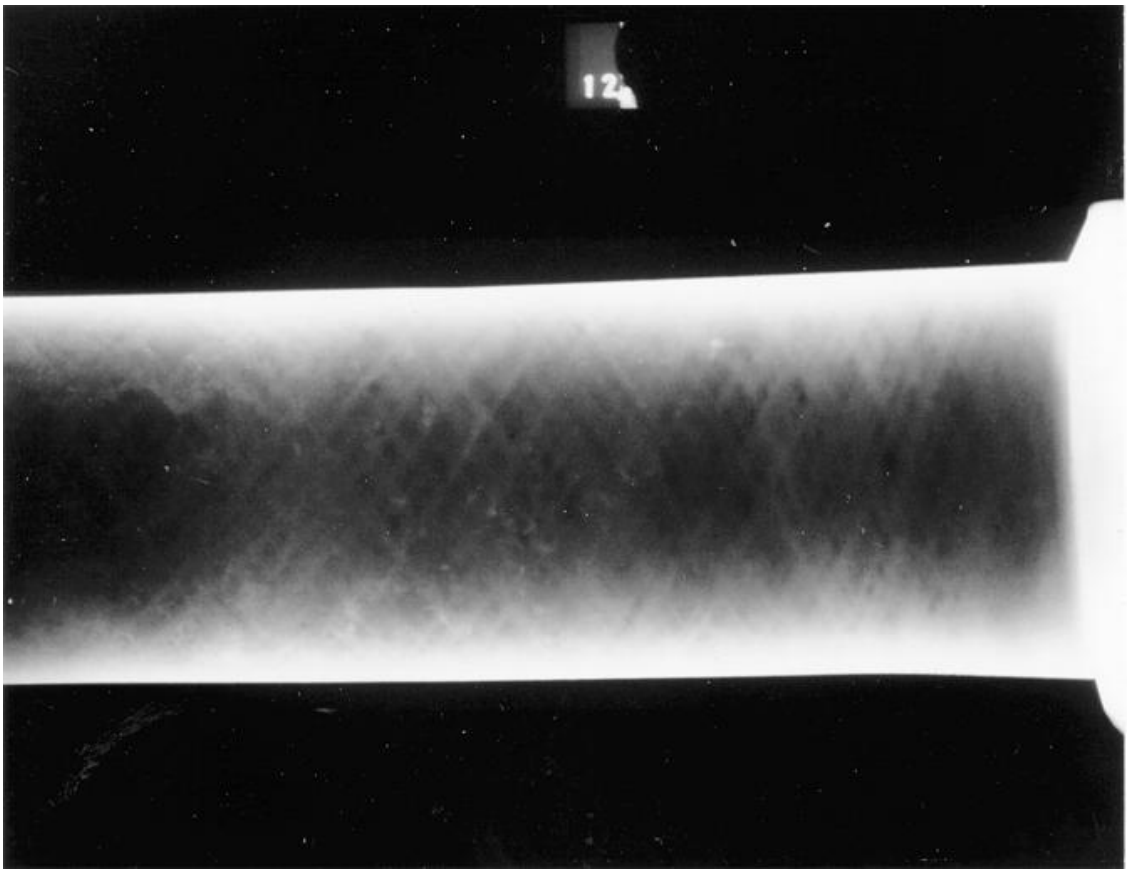

Figure 3.3-31 X-ray of tube No. 6 - section above heating element

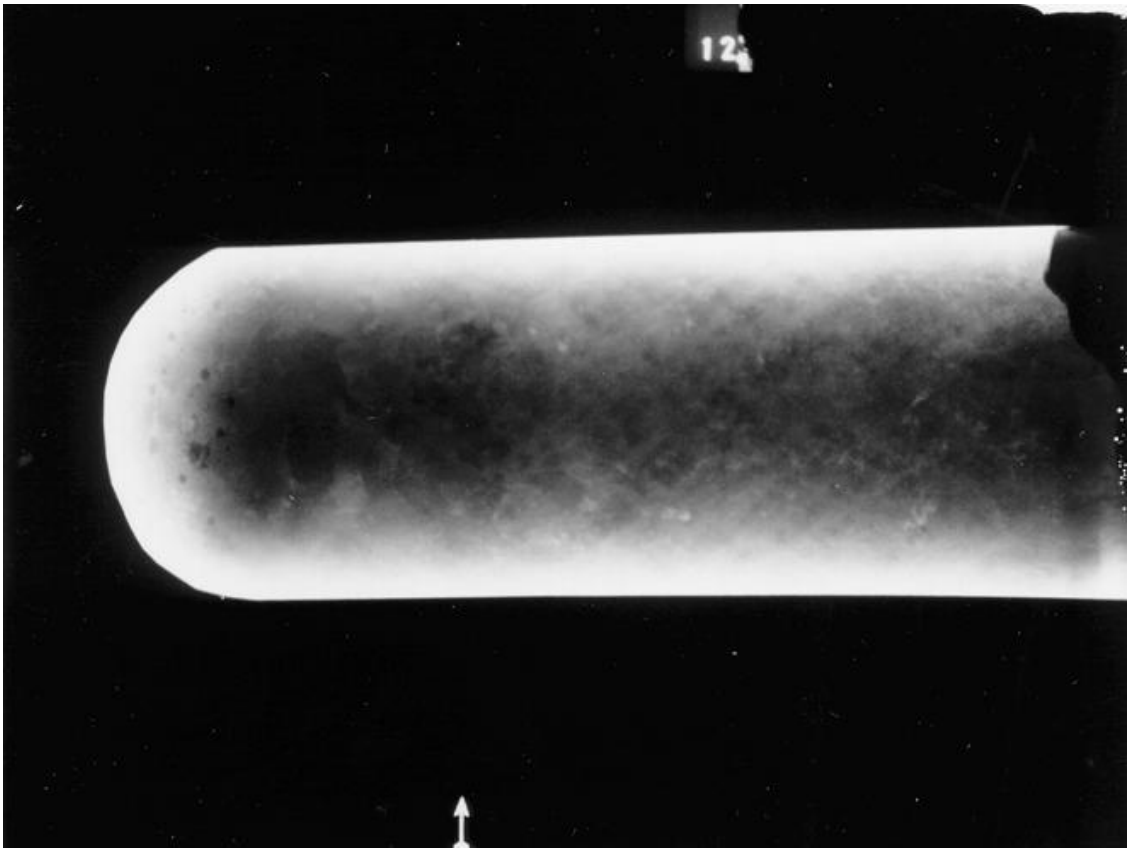

Figure 3.3-32 X-ray of lower section - tube No. 6

Immersion Tube No. 6, which performed 1100 hours of service at GM's Advanced Development facility before failing, was sent to Oak Ridge National Laboratory for material characterization studies. Textron Systems retained sections of this fractured immersion tube. These sections were cut into specimens used in a test matrix similar to the one conducted by SoRI on a virgin immersion tube. The original test matrix included hoop tension, axial flexure at RT and 1600°F, circumferential and axial coefficients of thermal expansion.

Edgar Lara-Curzio at Oak Ridge National Laboratory completed the hoop stress testing for immersion tubes No.'s 5&6. The hoop strength of the baseline material (tube No. 5) was 23 MPa. This result is similar to that obtained by SoRI (21.9 MPa). For immersion tube No. 6, which was field tested at GM in Saginaw, MI the hoop strength for the non-immersed region was 32.5 MPa. Areas of this tube that were exposed to excessive overheating (> 2200°F) could not be tested due to the high population of cracks. For the bottom section of this tube which was also exposed to excessive overheating, but remained immersed during this period, the hoop strength was degraded. This section did have radial cracking which contributed to a 55 – 85% strength degradation. The following charts depict the origin of these samples and their stress test results (see Figures 3.3-33 thru 3.3-36).

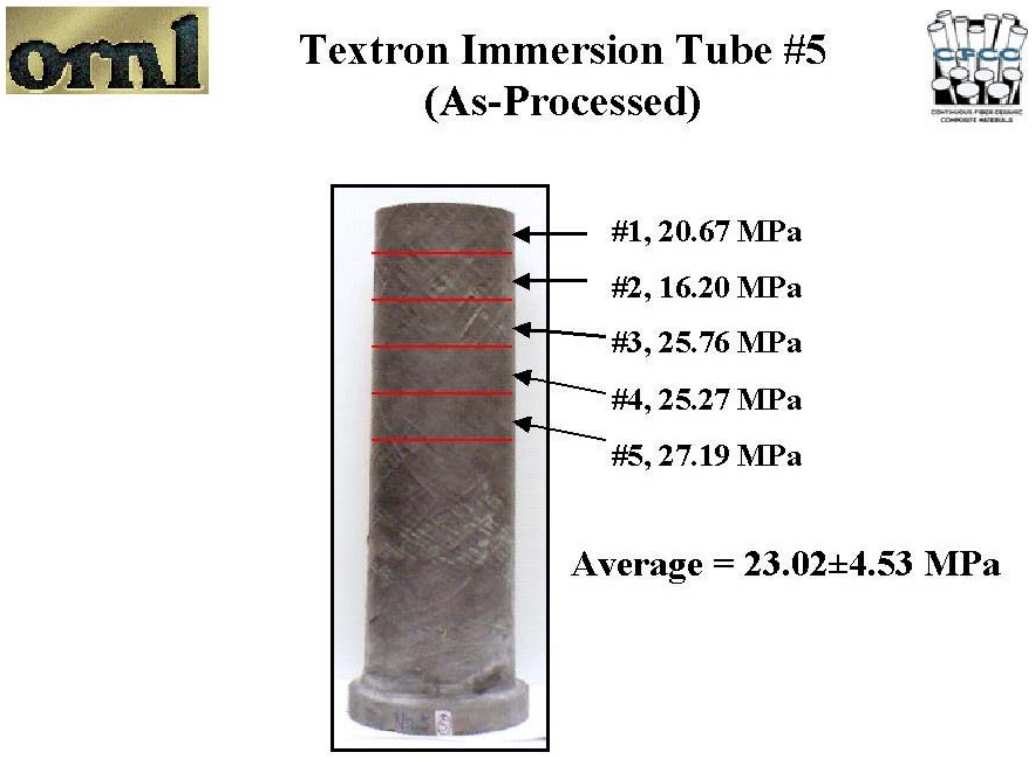

Figure 3.3-33 Baseline Tube No. 5 Hoop Strength Results

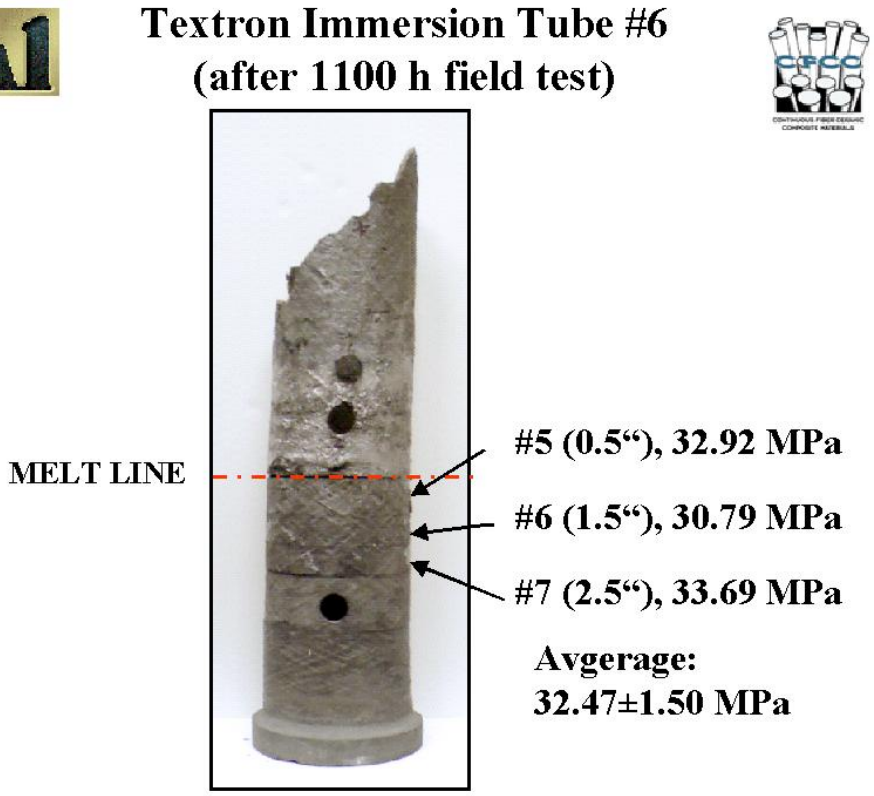

Figure 3.3-34 Immersion Tube No. 6 Non-immersed Region Hoop Strength

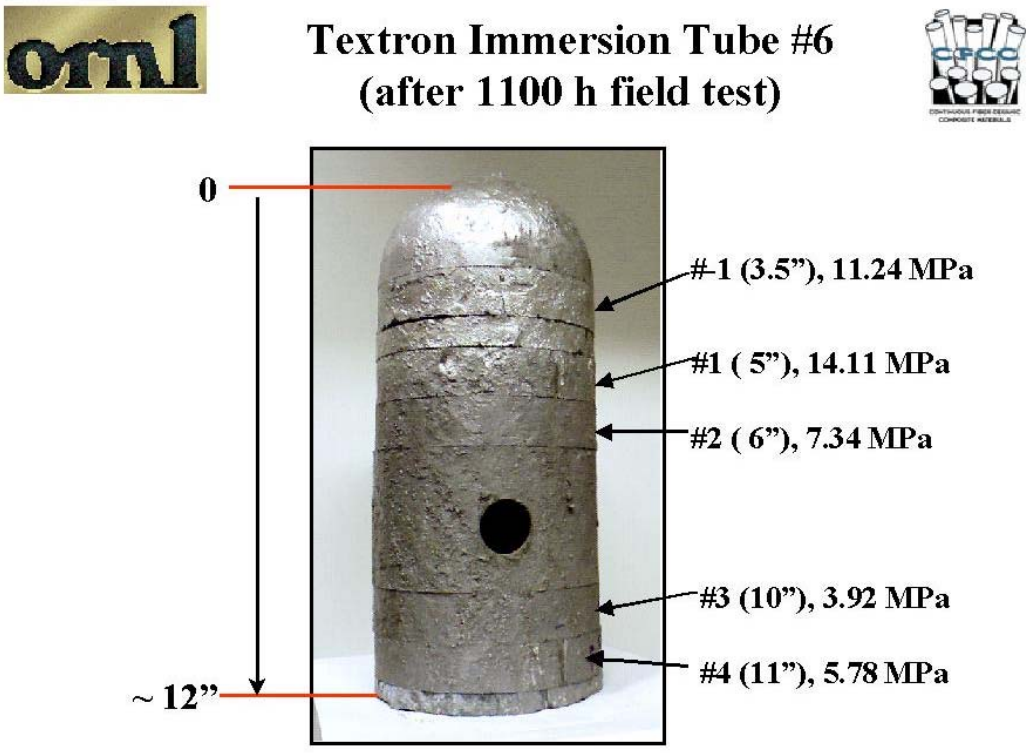

Figure 3.3-35 Immersion Tube No. 6 Immersed Region Hoop Strength

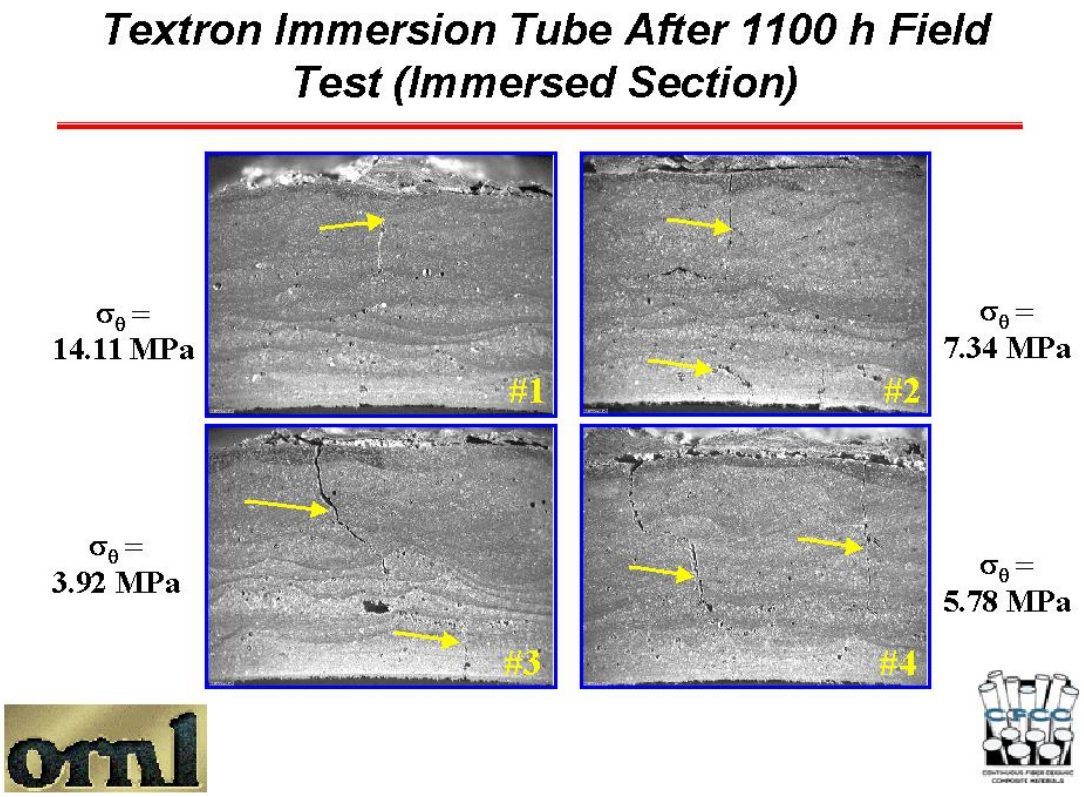

Figure 3.3-36 Immersion Tube No. 6 Immersed Region Radial Cracking

Thermal models have been developed to simulate the immersion tube in its field test environment. The simplified model constructed consisted of 37 nodes representing the immersion tube in three regions. The immersion tube was analyzed for the region above the heating element, the region directly aligned with the heating element while not immersed in aluminum, and the region inline with the heating element and immersed. The thermal network analyzer program was used to estimate the heat inputs to these regions and the transfer of heat through the tube wall and into the aluminum or the ambient above the aluminum. This model accounted for the refractory materials and the crucible as well as radiant losses from the aluminum to the non-immersed tube walls and insulating materials. The results of this thermal model were used to identify boundary conditions for the finite element stress model developed for CFCC materials by Material Sciences Corporation. Mr. Tom Cassin ran this model with updated material properties generated at SoRI for Textron Systems immersion tubes and predicted the stresses for our worst condition.

The worst case scenario is when the control thermocouple has failed and the power supply to the heater stays on at near full power. In this condition, the non-immersed tube wall aligned with the internal heating coil gets very hot and potentially reaches the melting point of Inconel 601, which is one of the hypothesis for how the t/c probe oxidized. This hot tube region is surrounded by cooler tube walls that are either immersed in the aluminum or are above the heating element region.

To validate the thermal model, Normal immersion tube transient warm up conditions were modeled and compared to observations made in Saginaw, MI. The results of this model did replicate the conditions seen at GM for a fully immersed tube heating up 500 pounds of aluminum (Fig. 3.3-37).

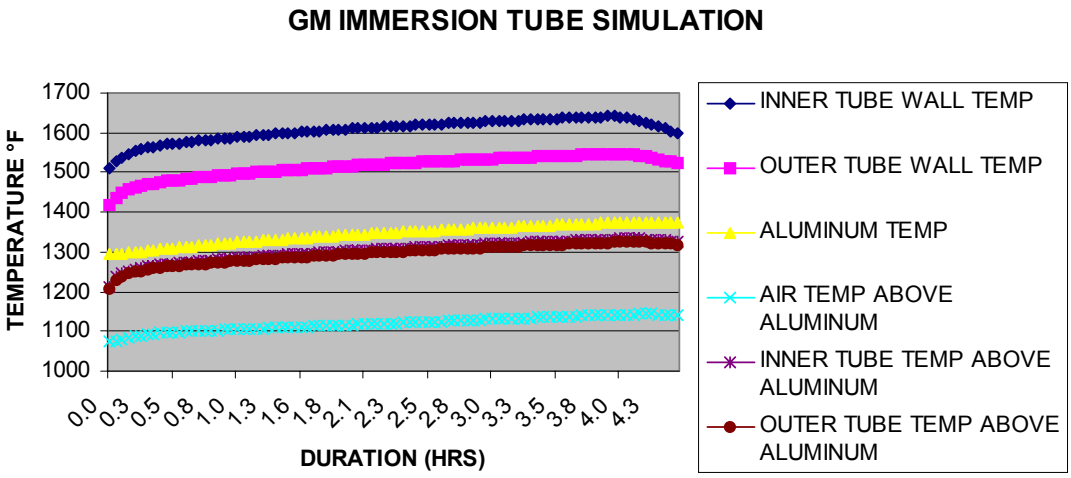

Figure 3.3-37 Thermal model projection for a fully immersed tube

The results of the thermal model for an immersion tube having one half of its heating element zone immersed, combined with lost temperature control due to a failed thermocouple probe, show it is plausible to hypothesize that extreme heating conditions were reached, resulting in thermal stresses that exceeded the mechanical properties for the immersion tube. This model did show the non-immersed region capable of reaching temperatures that would melt Inconel 601 (Fig 3.3-38). It also projected that the immersed region of the tube would not be under as much thermal stress due to the heat transfer into the aluminum. Because the heating element design is resistive, the heat build-up inside the tube is variable along the axis due to the varying heat removal efficiencies at constant power.

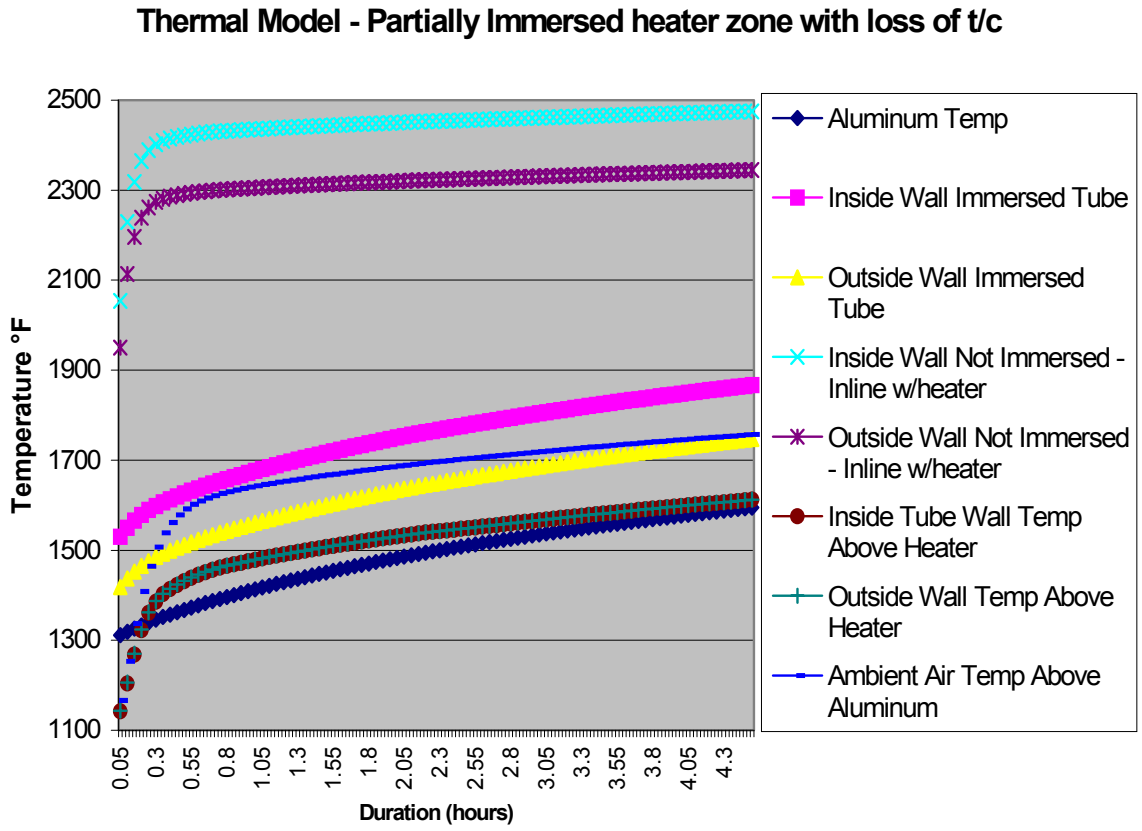

Figure 3.3-38 Thermal model of partially immersed heating element zone with loss of temperature control

The temperature boundary conditions predicted by the thermal model were used in the finite element model. The results of this model is summarized in the following contour plot for a partially immersed tube (Figures 3.3-39 to 3.3-41).

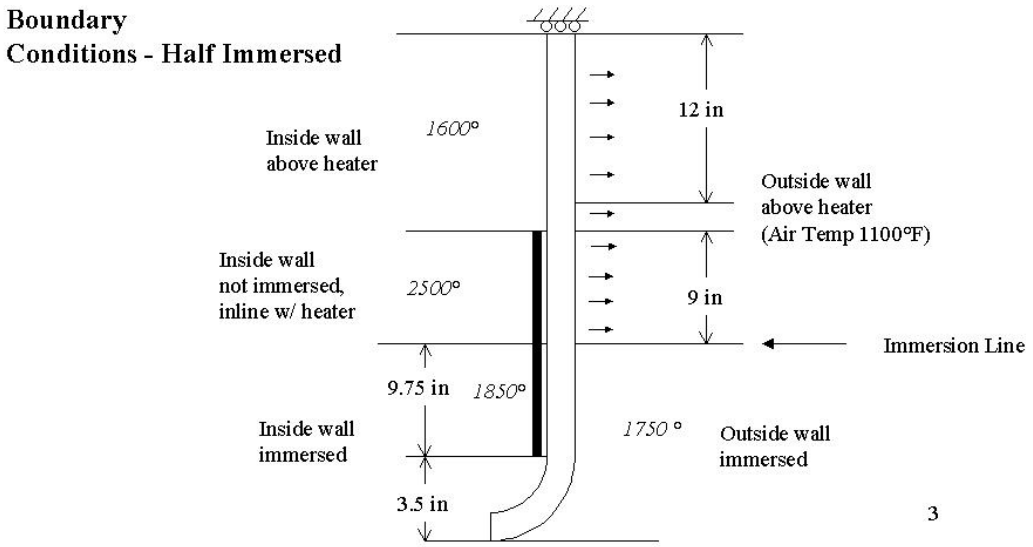

Figure 3.3-39 Temperature Boundary Conditions for a Partially Immersed Tube

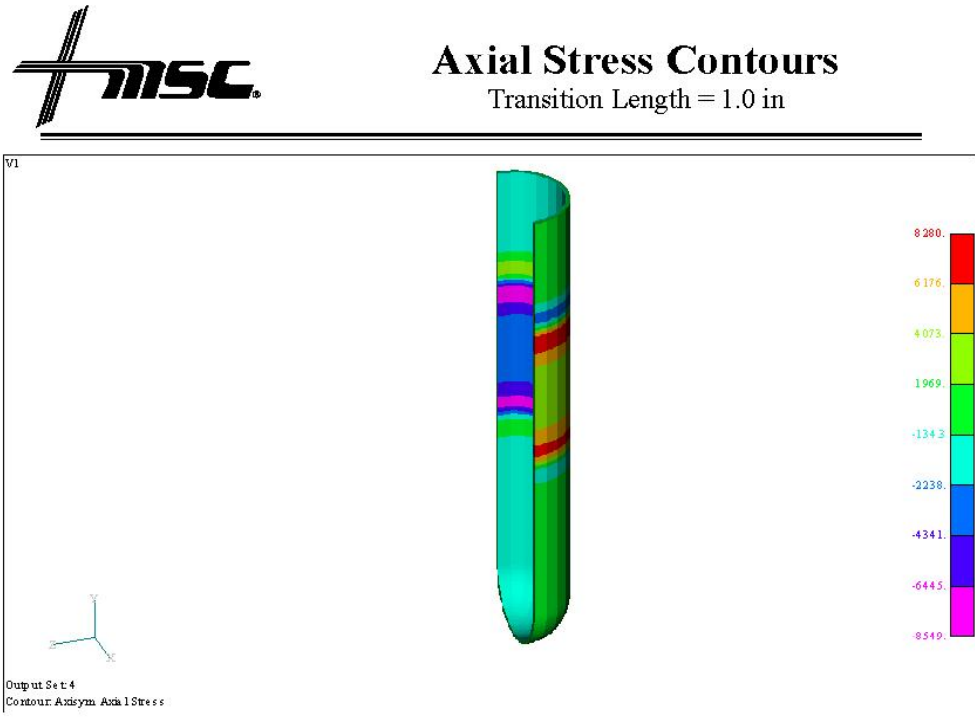

Figure 3.3-40 Axial Stress Contour Plot (-8.5 to +8.3 ksi)

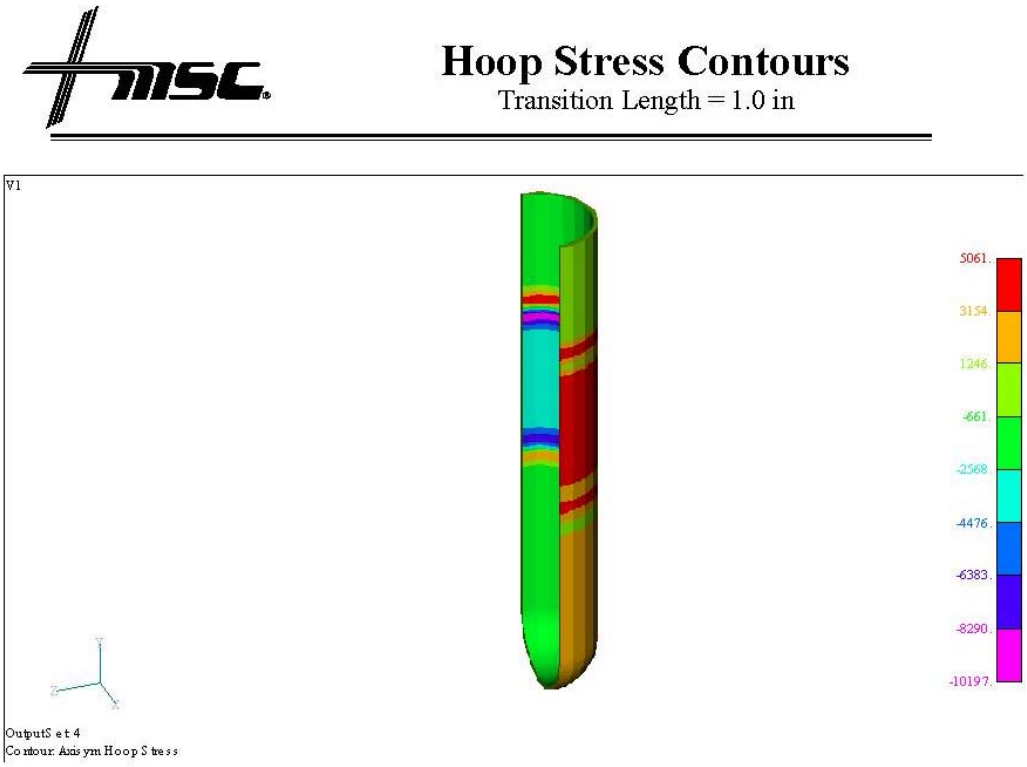

Figure 3.3-41 Hoop Stress Contour Plot (-10 to + 5 ksi)

3.3.3 Microstructure: NB-SiC CFCC Electric Heated Immersion Tube No. 6

Immersion tube #6 was evaluated along its fracture face to better understand what mechanisms may have lead to the tube matrix weakening and eventual failure. It is known that the initial investigation of a reported tube failure, after 29 heat cycles, resulted in the replacement of a failed thermocouple. During this investigation a dark circumferential stain was observed on the inside surface of the tube (Fig 3.3-42). It was decided to continue field testing this tube because the primary reason for shutdown was the faulty thermocouple. After three more heat cycles the tube did fracture at the same position as was observed for the stained region.

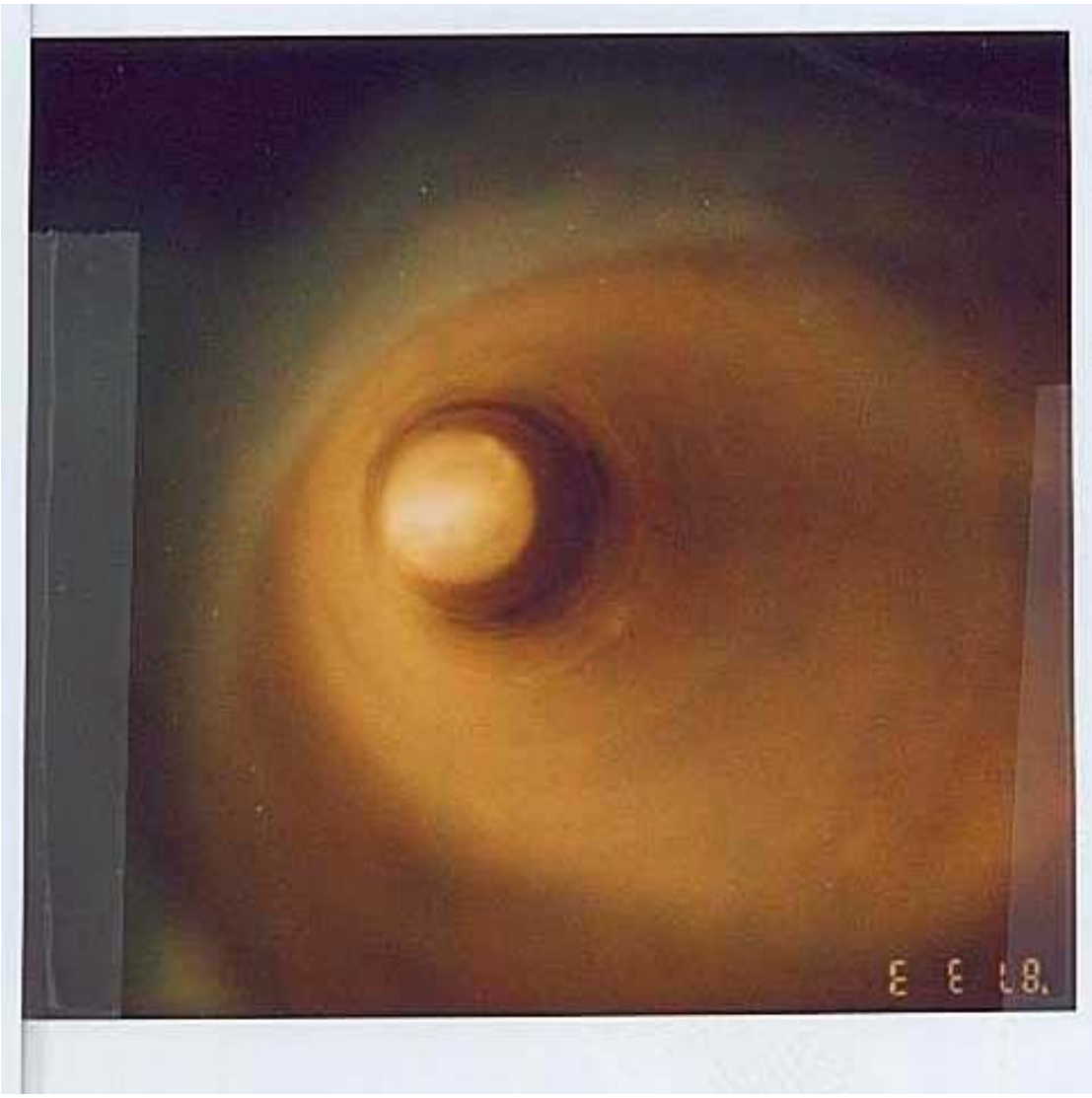

Figure 3.3-42 Polaroid picture of the inside of tube #6 showing the dark stain located 22 inches down from the top flange end

Immersion tube No. 6 was exposed to several thermal stress cycles caused by the "cold start-ups", routine heat and pouring cycles, and overheated conditions caused by two thermocouple failures. The series of events just prior to this tubes failure describe extreme thermal shock conditions that occurred prior to or as a result of a second thermal couple failure. At some point the failing thermocouple interfaced to the temperature controller allowed part of the immersion tube to see temperatures hot enough to melt Inconel 601. There was also an observation that the immersion tube was left partially immersed with the heater still on. This combined with a thermocouple failure, could have more than doubled the thermal gradients this tube was normally exposed to. The immersed region of the tube had the aluminum as a heat sink, preventing this region of the tube from becoming severely overheated. The portion of the tube directly aligned with the heating element, but not immersed didn't have this benefit, resulting in an overheated zone that reached internal temperatures of 2400 to 2500 °F.

Failure analyses were conducted on microscopic evaluations at the primary fracture site and on specimens taken at five different positions along the axis of the tube. As was pointed out, radiomicrographs of the failed tube showed most of the cracking was located in the upper region of the tube. This is the section that saw extremely high temperatures and thermal gradients at the interfaces between the immersed and non-immersed sections of the tube and between the interface in the upper section that was exposed and not exposed to direct radiation from the heating element. The cracks and inside wall of this upper region of the immersion tube showed a glassy phase shiny deposit (Fig. 3.3-43). Energy dispersive X-ray spectroscopy (EDS) analysis identified this phase to be enriched with sodium. Other parts of the inside wall had yellow and rust colored deposits. The yellow material was identified as sulfur and calcium. These components were also identified in the fused silica refractory used inside the heating element winding. The rust was identified as iron oxide and chromium. The iron and chromium are components of the kanthal heating element.

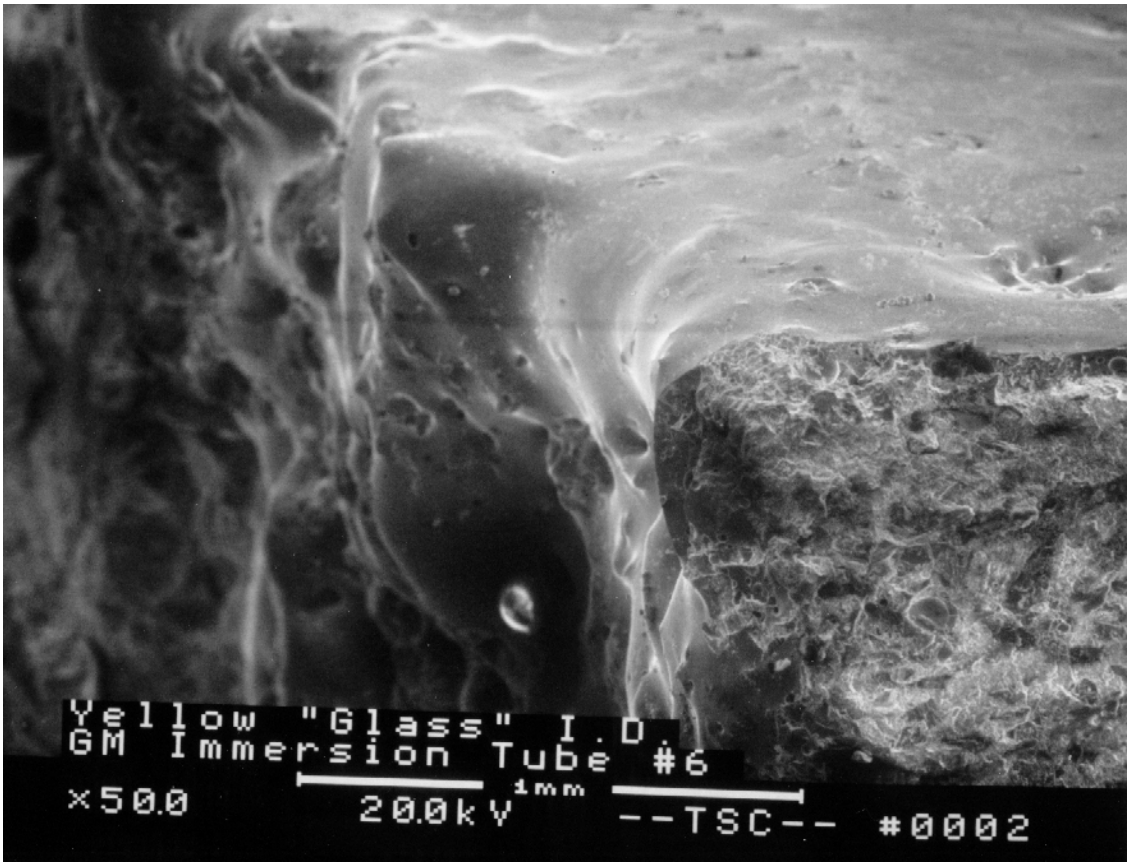

Figure 3.3-43 Glassy phase deposit along the inside wall (x-direction) and through the wall along the fracture face (y-direction).

Failure analyses conducted by electron spectroscopy have identified increased levels of oxygen in the NB-SiC matrix. Both energy dispersive element dot mapping and wavelength dispersive methods have indicated some trends that indicate higher amounts of oxygen within the matrix closer to the inside wall of the tube. These methods have not been quantitative, therefore we are interested in finding out what is the retained properties of the field tested immersion tube.

Core samples were taken along the axis (Z-direction) of the fractured tube (Fig. 3.3-44). Two samples were taken from the potentially non-immersed and immersed heated regions of the tube that were exposed to direct radiation from the heating element inside the immersion tube (cores 4 & 5). Other core samples were taken from less severely heated region. These include the interface between the directly radiated and non-directly radiated section of the upper immersed portion of the tube (core 3), a sample taken from the immersed region of the tube not exposed to direct radiation from the heater element (core2), and a section taken above the melt line (never immersed region– core 1).

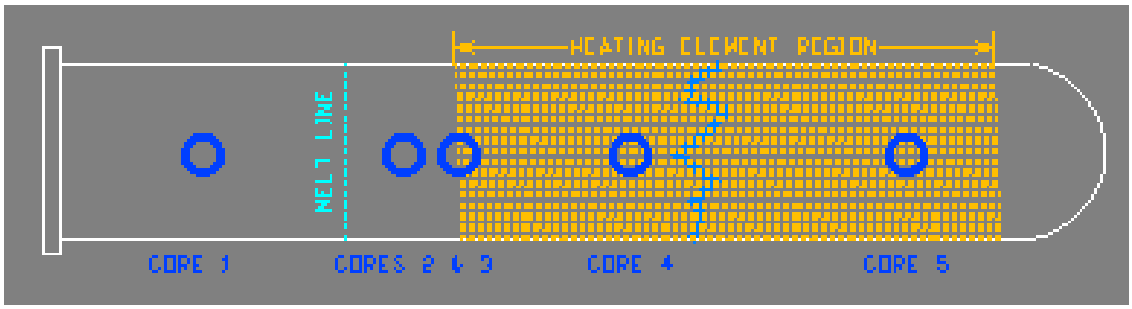

Figure 3.3-44 Core Sampling from Immersion Tube No. 6

Core sample No. 1 is taken from the part of the immersion tube which is never exposed to direct radiation from the heater element. It is also a region of the tube which is never submerged into the molten aluminum, therefore, the maximum temperature this section of the tube normally sees is estimated to be between 1250 and 1350 °F. After 1100 hours of service this region of the immersion tube showed no difference when compared to a specimen taken from a virgin immersion tube No. 7 (Fig. 3.3-45).

Microscopy - Polished Core Samples from Immersion Tubes 6 and 7

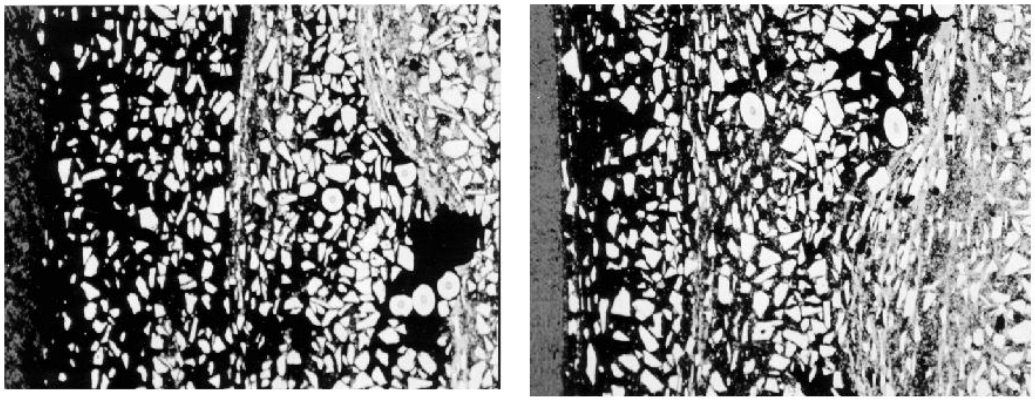

GM Tube 6 - Core 1 Inner Wall **GM Tube 7 - Inner Wall**

Figure 3.3-45 Microscopy of immersion tube showing no degradation to the matrix for the upper tube region.

Core sample No. 2 is taken from a region of immersion tube No. 6 below the melt line of the molten aluminum, but not directly exposed to radiation from the heating element. This specimen didn't show any degradation to the matrix. Core sample No's 3 and 4 were exposed to direct heater element radiation and toward the end of tube No. 6's service period, overheating consistent with being not immersed in the molten aluminum. Our thermal model estimates this region may have had peak operating temperatures around 2450 °F. Core No. 5 was taken from a region of the immersion tube believed to be immersed during the thermocouple failure and overheating conditions occurring in the upper section of the tube. Its maximum temperature was estimated to be between 1550 and 1600 °F. Microscopic evaluation of these specimens show thermal degradation on the inside wall for core samples 3 and 4 (Fig. 3.3-46).

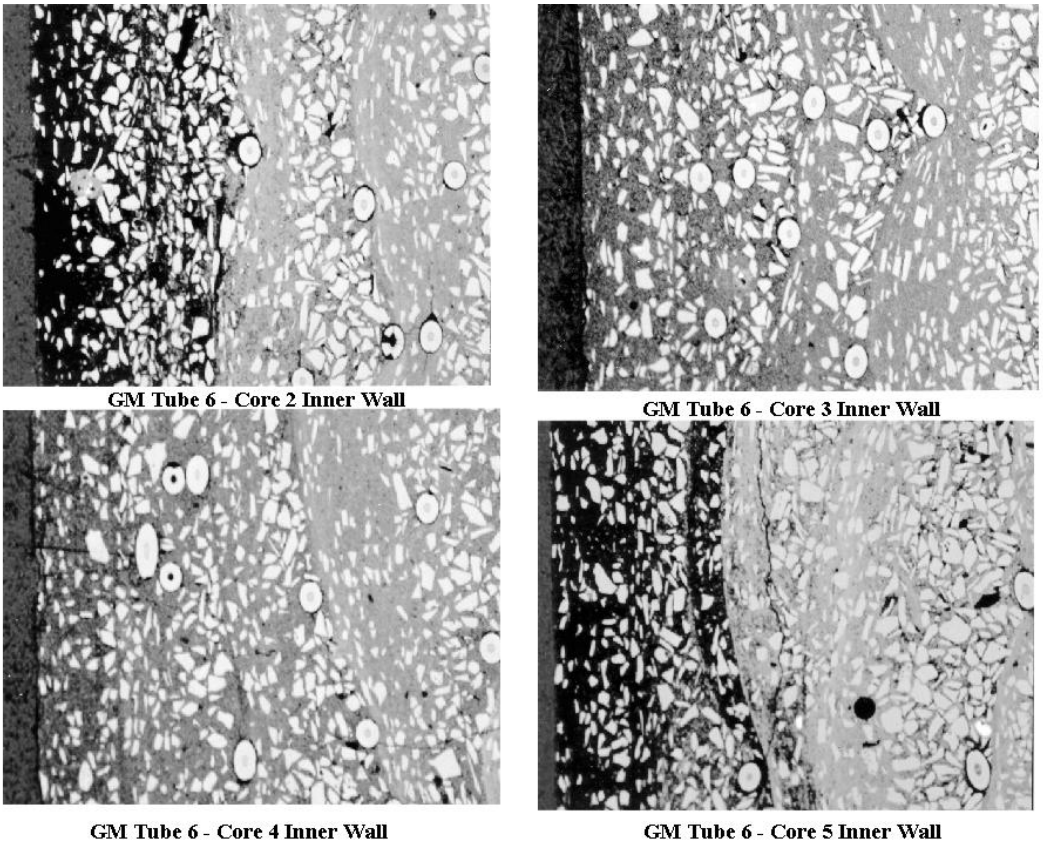

Figure 3.3-46 Core samples 3 & 4 show a change in the matrix associated with the regions of the immersion tube exposed to the highest temperatures.

Wavelength dispersive analyses for these specimens were taken at 200 micron intervals looking at a 20 micron spot through the tube wall. Again the information is not quantitative, but there appears to be more consistent oxygen counts through the wall for the immersion tube sections that are exposed to direct radiation from the heating element (Fig. 3.3-47). We still don't know if the level of oxidation is tenths of a percent or percents, or whether it impacts the performance of the immersion tube. Figures 3.3-48 through 3.3-50 show element mapping for the first 200 microns starting on the inside wall of immersion tube No. 6.

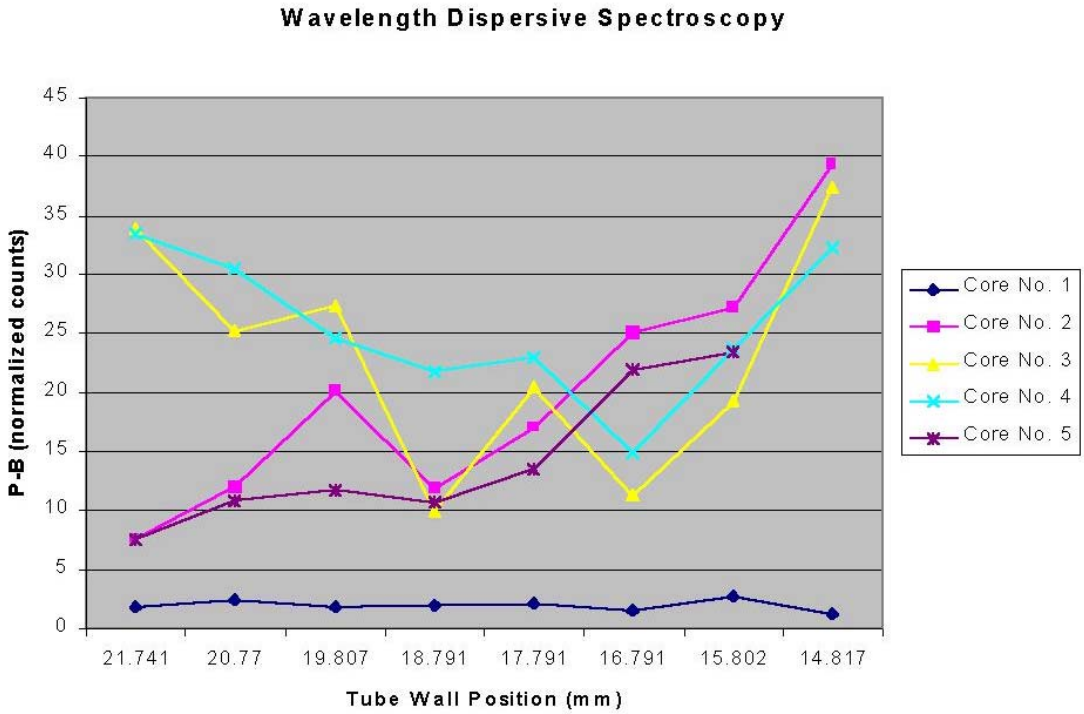

Figure 3.3-47 Wavelength Dispersive X-ray analysis showing oxygen counts through the tube wall (21.7 mm is inside wall, 14.8 mm is outside wall)

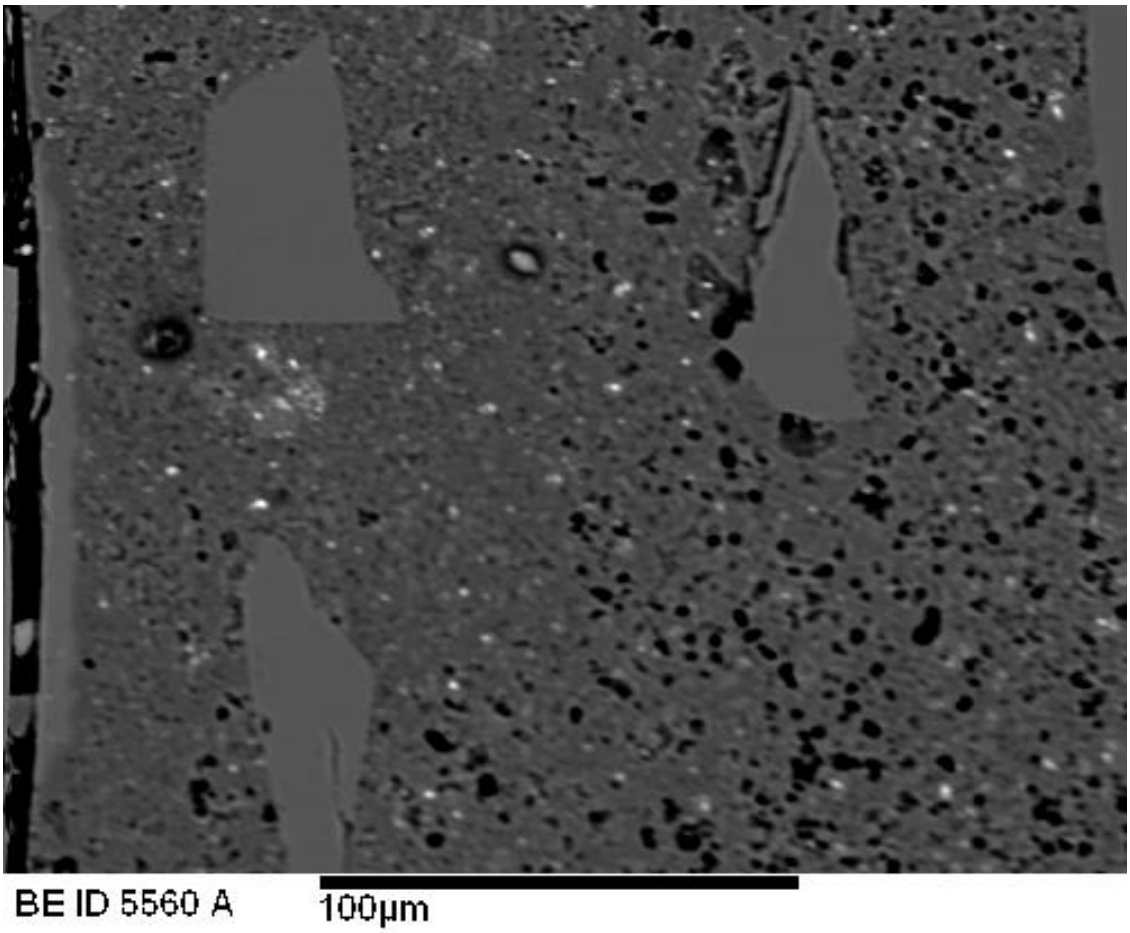

Figure 3.3-48 Baseline photograph of inside tube wall near fracture face.

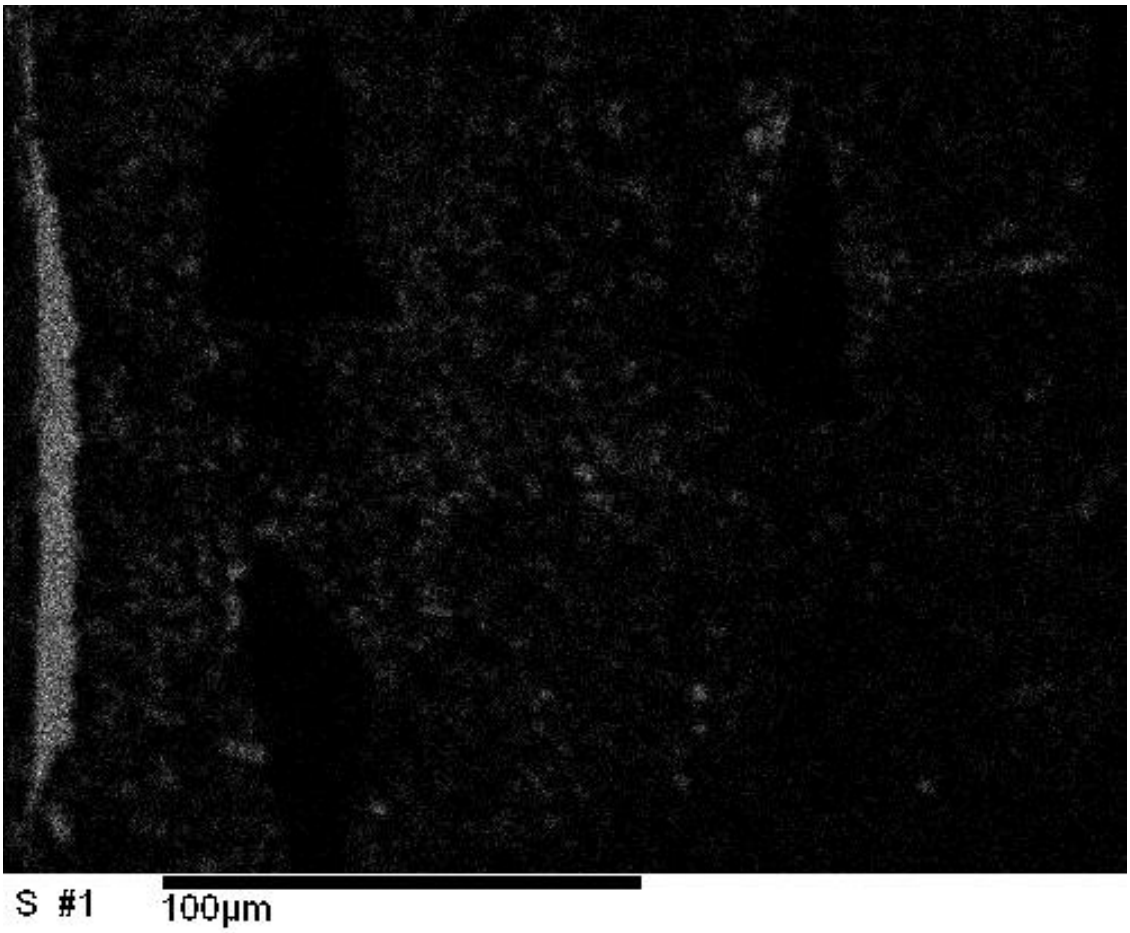

Figure 3.3-49 Wavelength Dispersive Dot Map for Sodium (Na). Vertical sliver of glass is along inside wall of tube.

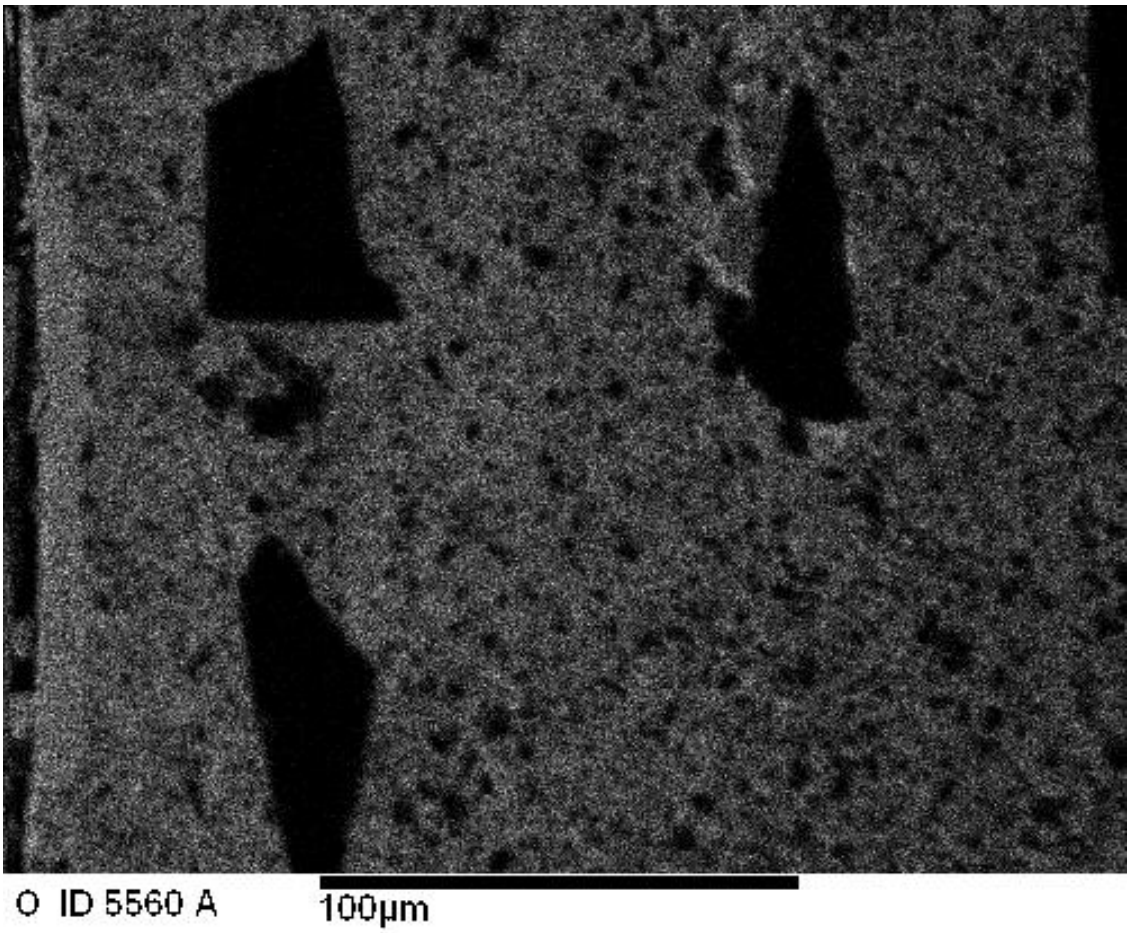

Figure 3.3-50 Wavelength Dispersive Dot Map for Oxygen (O).

Electron Spectroscopy for Chemical Analysis (ESCA) techniques were initiated on specimens taken from the fractured tube and virgin material. These initial attempts at using photoelectron spectroscopy were found to be inconsistent in quantifying the types of oxides present and whether there is any free silicon in the virgin material.

Two tube furnaces running at 1800 and 2150°F were loaded with immersion tube specimens. These specimens were withdrawn at approximately 125 hour intervals for an oxidation study. The two tube furnaces, which were loaded with virgin immersion tube specimens were shutdown after 1000 hours of testing. The furnace run at 2150 °F had a heating element failure and had to be shutdown. Two specimens were taken from this furnace; one after 125 hours of exposure and another after 250 hours. Samples were taken at 125, 250, 500, and 1000 hours exposure from the furnace running at 1800 °F. None of these samples showed signs of oxidation and no glassy phases developed. This implied that heating conditions at GM were much more severe that static isothermal heating in an oxygen atmosphere.

3.3.3 Representative Parts: NB-SiC CFCC Electric Heated Immersion Tube No. 8

End User Field Tests: NB-SiC CFCC Electric Heated Immersion Tube No. 8

The second tube (#8) delivered to GM was placed in service the week of October 5th, 1998. It was outfitted with the same heating element used in tube #6. Immersion tube #8 was removed from service in November during the Thanksgiving holiday. At that time it had logged 1200 hours of service and 28 heat cycles. GM disassembled the immersion tube to inspect the thermocouple (t/c), heating element, and tube internals. The t/c and heating element looked good. GM did observed circumferential cracking about the top of the heating element region and at the melt line. These location of these cracks were sketched by GM before the tube and heating system was reassembled and placed back in service (Fig 3.3-51,52). GM also did observe glassy phase deposits inside the tube aligned with the heating element region (Fig 3.3-53). This glassy phase appears as a darkened region and gives the tube a stained appearance

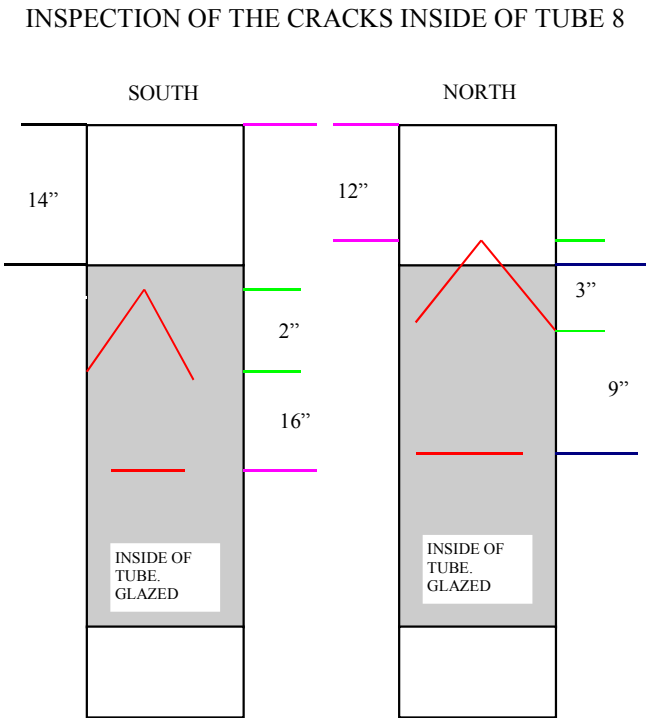

Figure 3.3-51

INSPECTION OF THE CRACKS INSIDE OF TUBE 8

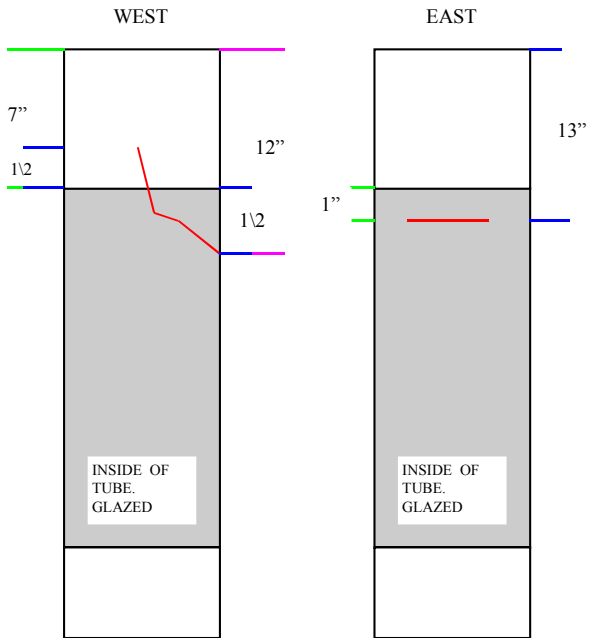

Figure 3.3-52

Figure 3.3-53 Photograph taken during the inspection of the inside of Tube No. 8

Tube #8 was placed back in service for the month of December. On December 23 it was removed from service for the Christmas Holiday. This tube was removed from service on January 4th after inspection of the heating element assembly and tube structure. GM didn't want to continue use of this tube due to visible cracks and heavy deposits on the inside wall of the

tube. Tube No. 8 was exposed to one cold start, two modified start-ups (less severe than cold starts) and 47 heating cycles. It performed 1752 hours of service without failure or infiltration of the tube with molten aluminum (Fig 3.3-54).

Fracture Analyses have started for the 2nd field-tested immersion tube No. 8 used at General Motors Advanced Development Laboratory. What was very impressive is the fact that many of the cracks were observed and documented in November at the 1200 hour point of service. This tube continued to perform without failure for an additional 550 hours and 20 thermal cycles.

Figure 3.3-54 Tube No. 8 – 1750 Hours of Service – 49 Thermal Cycles

Similar to observations made for tube No. 6, tube No. 8 developed circumferential cracks primarily about the melt line region (see x-rays Figures 3.3-55,56,57). This region extends a few inches above the top of the heating element to a few inches below the highest immersion line.

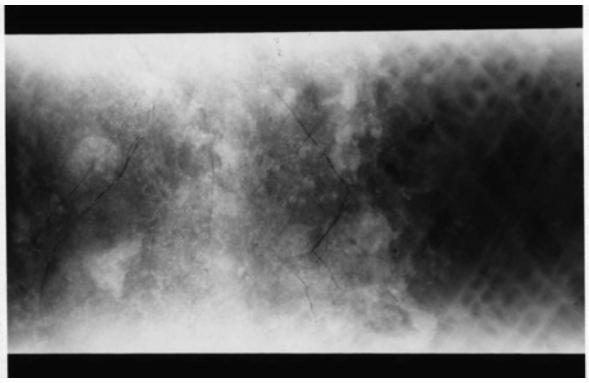

Figure 3.3-55 Radiograph Tube #8 Cracks - 0°

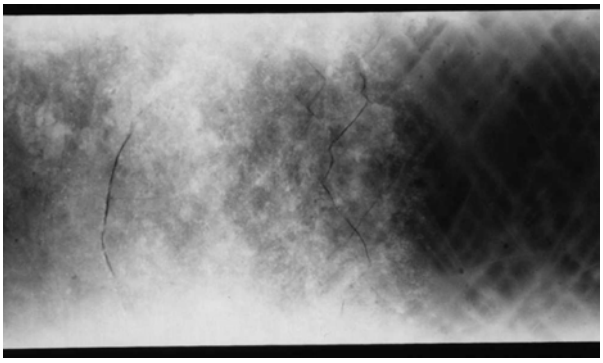

Figure 3.3-56 Radiograph Tube #8 Cracks - 120°

Figure 3.3-57 Radiograph Tube #8 Cracks - 240°

Portions of the inside wall were coated with a glassy phase deposit. Looking down inside tube No. 8 one could observe an unaffected region, from the top flange down to the interface where the aluminum melt line was maintained (Fig 3.3-58). Then there was a transition to a heavily deposited glassy phase which extends down to the base of the heating element region. After the heating element region the inside of the tube cleared up and looked similar to the top section of the tube. There appeared to be no relationship to the glassy phase region and the cracked upper band beneath the melt line (Fig 3.3-59). Similar to tube No. 6 an unknown source of sodium is present and is a major constituent of the glass deposit (Fig 3.3-60).

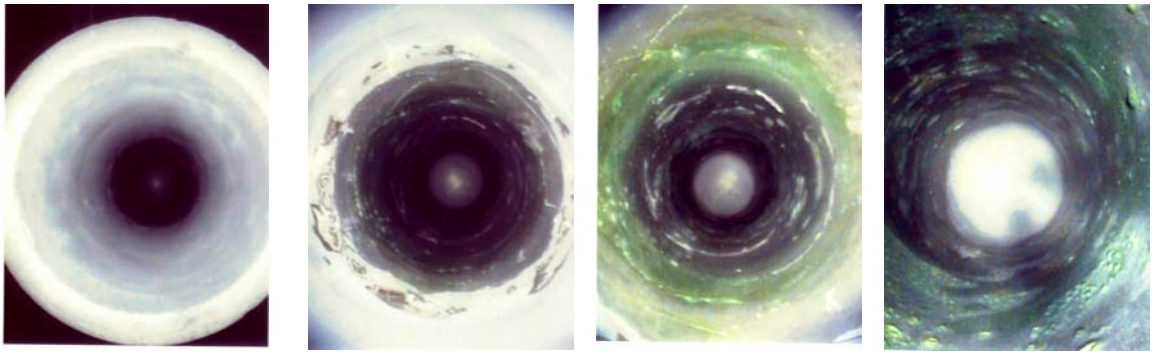

Figure 3.3-58 Looking Down into Tube #8. Transition at melt line. Glassy phase deposit throughout the heating element region.

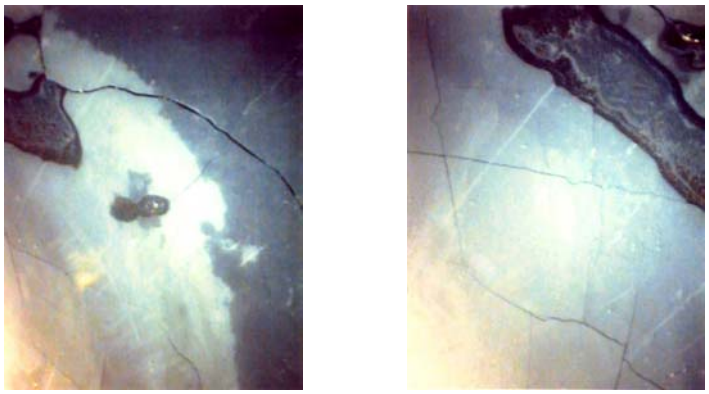

Figure 3.3-59 Cracks as seen from the inside of the Tube No. 8 about the melt line region.

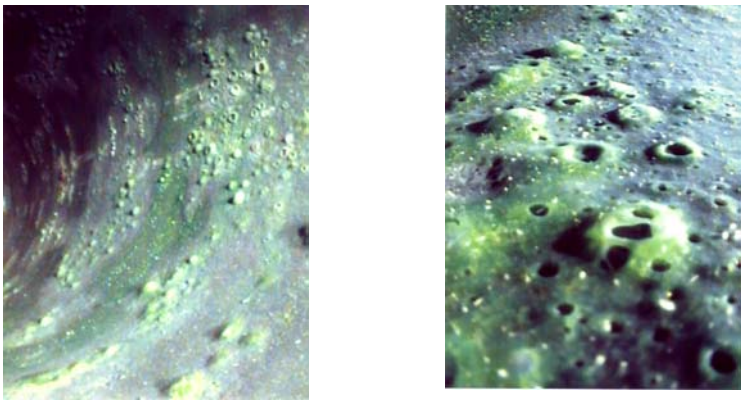

Figure 3.3-60 Glassy Phase Deposit on Inside Wall of Immersion Tube No. 8

Analyses conducted on immersion tube No. 8 was completed at Textron Systems. Tube No. 8 was shipped to Oak Ridge National Laboratory (ORNL) for mechanical and chemical evaluations. H.T. Lin of ORNL reported similar finding to that observed for immersion tube No. 6. These findings include the presence of radial cracks and the glassy phase silicon oxide deposited along the inside surface of the immersion tube. Chemical analyses of the glass indicate the presence of Na, K, Fe and Cr. It is hypothesized that the source of the Na and K is from the fused silica refractory core in which the electrical heating element is wound around. The source of the Cr and Fe is from the Kanthal heating element. These elements substantially decrease the viscosity of the glassy phase formed and may enhance the oxidation processes. This tube was sectioned for future mechanical stress evaluations.

Component Evaluation Immersion Tube No. 8

Microstructure: NB-SiC CFCC Electric Heated Immersion Tube No. 8

Analyses conducted on immersion tube No. 8 was completed at Textron Systems. Samples were taken from the immersed and non-immersed regions to evaluate oxidation levels throughout the wall thickness. Energy dispersive X-ray spectroscopy (EDS) analysis were performed on this tube's inside surface glassy phase deposit. This phase was found to be enriched with sodium and silicon oxides as was observed for immersion tube No. 6. Tube No. 8 was shipped to Oak Ridge National Laboratory for mechanical and chemical evaluations.

In addition to the circumferential cracking observed about the melt line region for Tube No. 8, evidence of radial cracking was also observed (Fig 3.3-61).

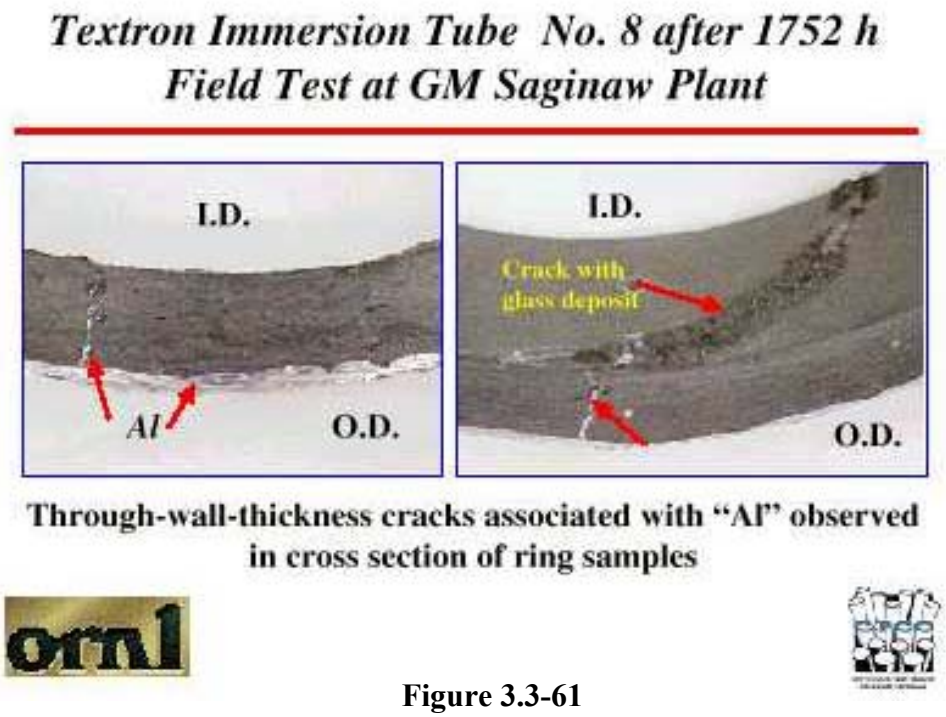

Figure 3.3-61

Analyses conducted on immersion tube No. 8 was completed at Textron Systems. Samples were taken from the immersed and non-immersed regions to evaluate oxidation levels throughout the wall thickness. Energy dispersive X-ray spectroscopy (EDS) analysis were performed on this tube's inside surface glassy phase deposit. This phase was found to be enriched with sodium and silicon oxides as was observed for immersion tube No. 6. Tube No. 8 was shipped to Oak Ridge National Laboratory for mechanical and chemical evaluations. ORNL reported the following information on their chemical analyses of this oxide film (Figures 3.3-62 through 3.3-68).

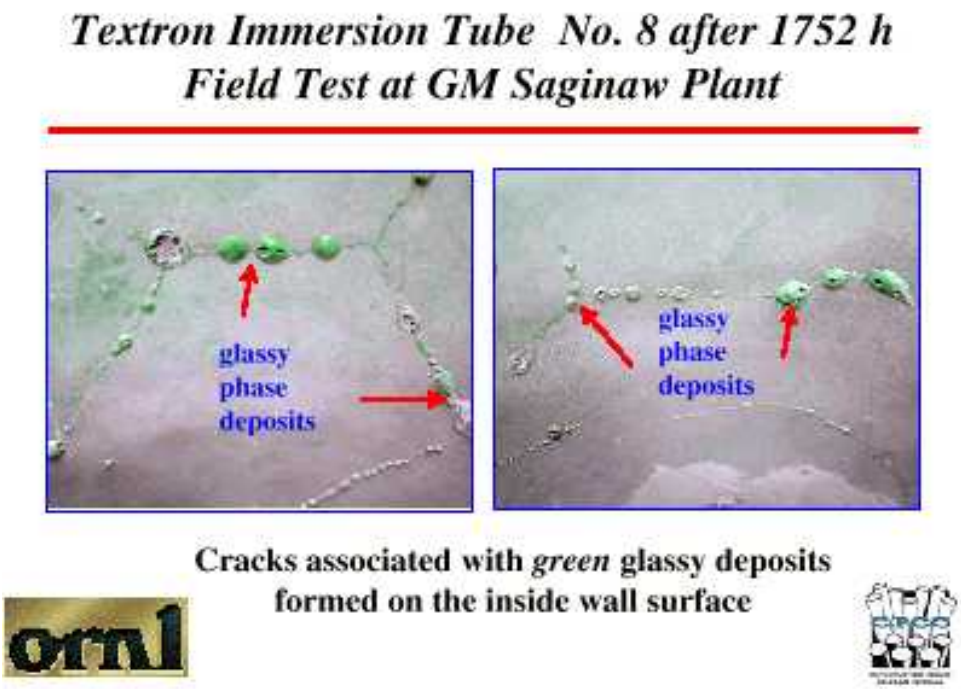

Figure 3.3-62

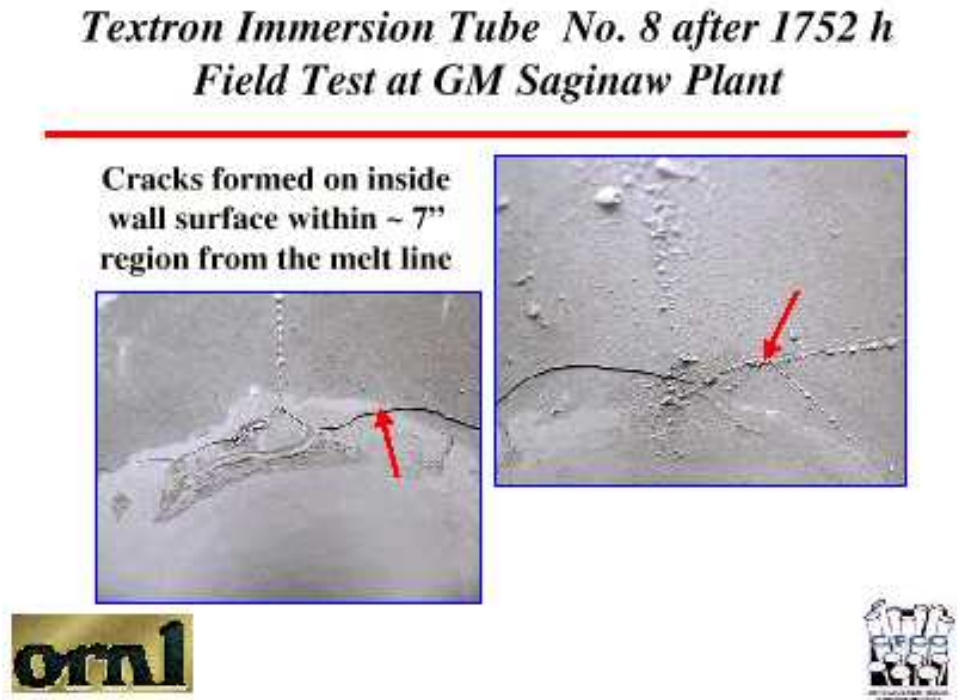

Figure 3.3-63

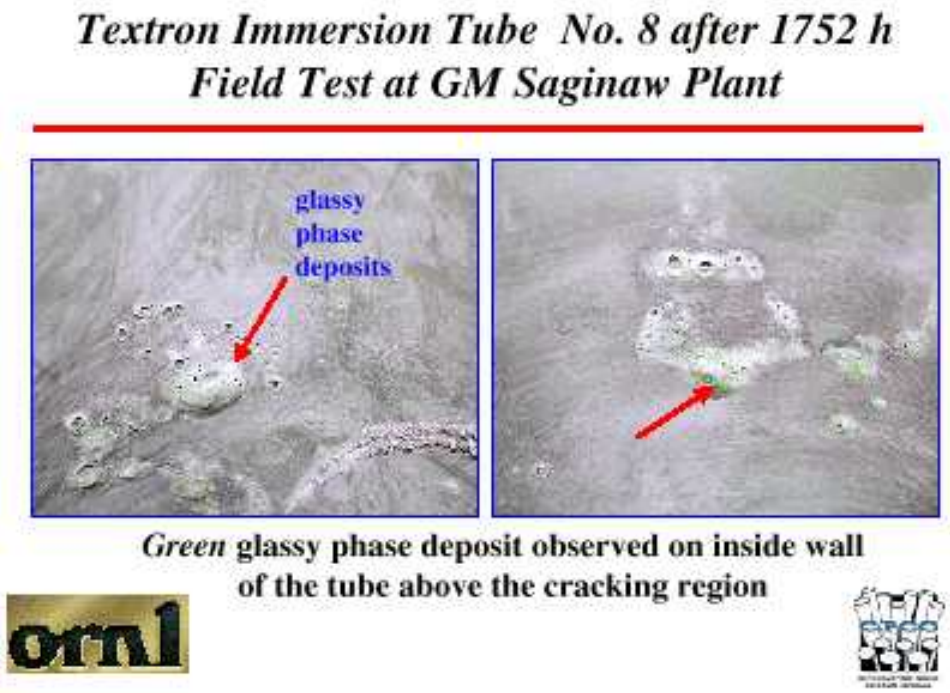

Figure 3.3-64

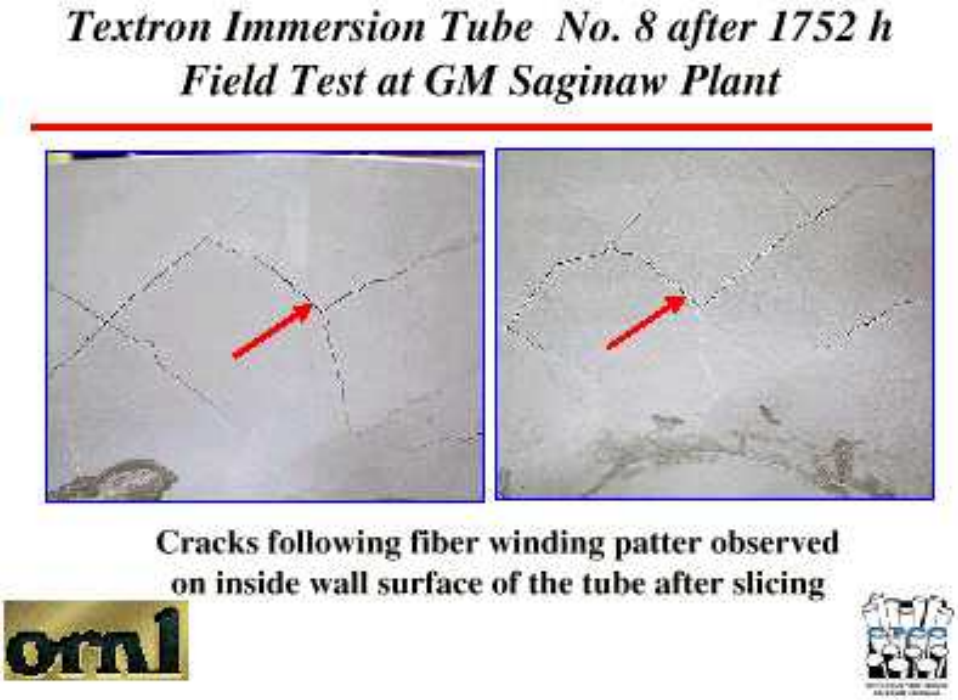

Figure 3.3-65

Textron Immersion Tube No. 8 after 1752 h Field Test at GM Saginaw Plant

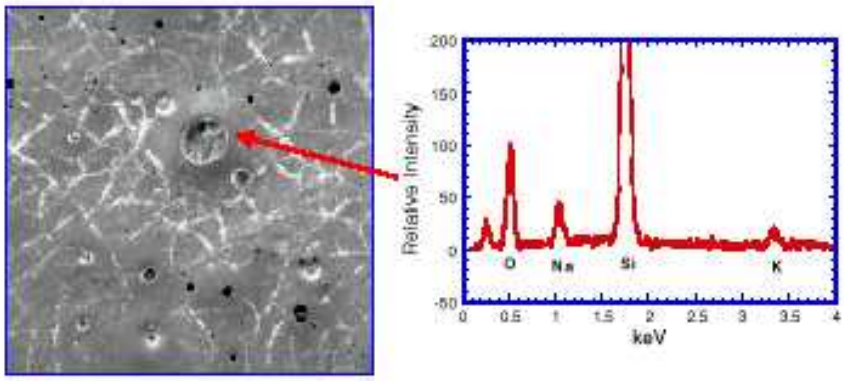

Glassy phase observed on I.D. wall surface reveals composition of "Na-K-Si-O"

Figure 3.3-66

Textron Immersion Tube No. 8 after 1752 h Field Test at GM Saginaw Plant

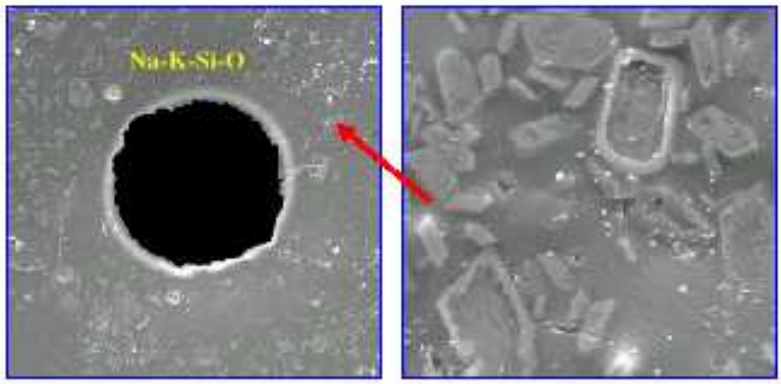

***Light Precipitates* observed within glassy phase (Na-K-Si-O) deposit**

Figure 3.3-67

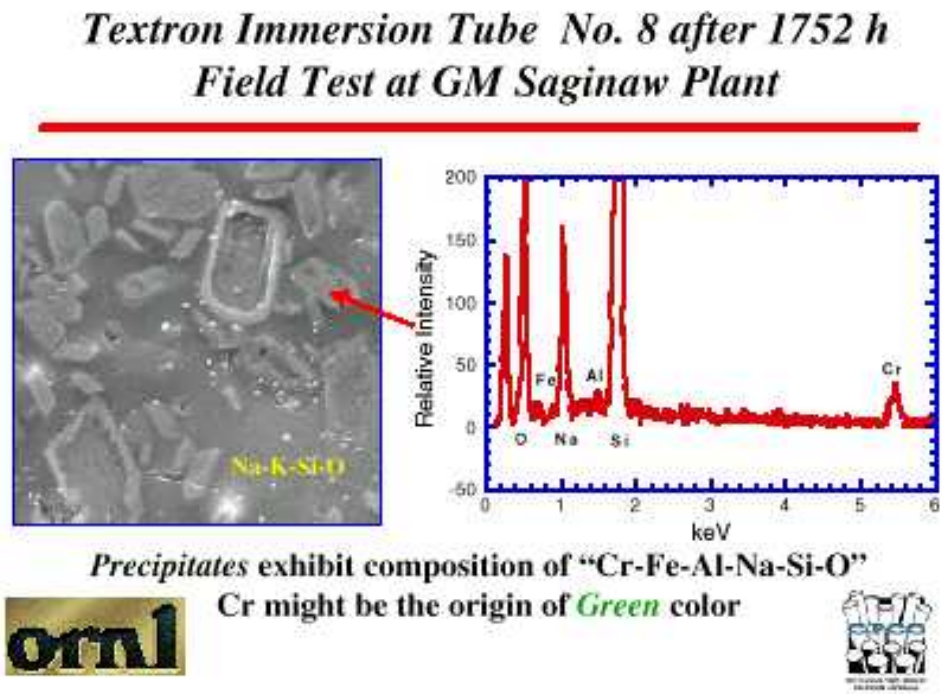

Figure 3.3-68

The presence of these elements can substantially decrease the viscosity of the glassy phase formed and may enhance the oxidation processes. We will review the heating environment and equipment used in the large-scale immersion tubes at GM's Bedford, IN facility. If the potential exists for Na and Fe enrichment we will devise a plan to accommodate this condition. We are optimistic that these foreign materials won't be present in GM's Bedford, IN facility and believe the immersion tubes will benefit and perform better for this reason.

Energy dispersive X-ray spectroscopy (EDS) analysis were performed to determine the degree of oxidation throughout the wall thickness for immersion tube No. 8. This method is not quantitative, but was used to qualitatively assess the oxygen level by sampling five spots in the radial direction for 100 seconds at each location. Samples 1 were taken just inside the outer radius of this tube for borings taken at the immersed heated zone and above the melt line. Samples 5 represent the inner most spots sampled for these two borings. From this analysis it is apparent that the degree of oxidation is more severe for the immersed region (Fig 3.3-69). This may be due to enhanced oxidation as a function of the glassy phase deposit, or it may be due to this region operating at higher temperatures from direct radiation off the heating element. Higher oxidation was also observed in this region for tube No. 6.

Fig. 3.3-69 Atomic Percent O for Immersed and Non-Immersed Tube No.8 Borings

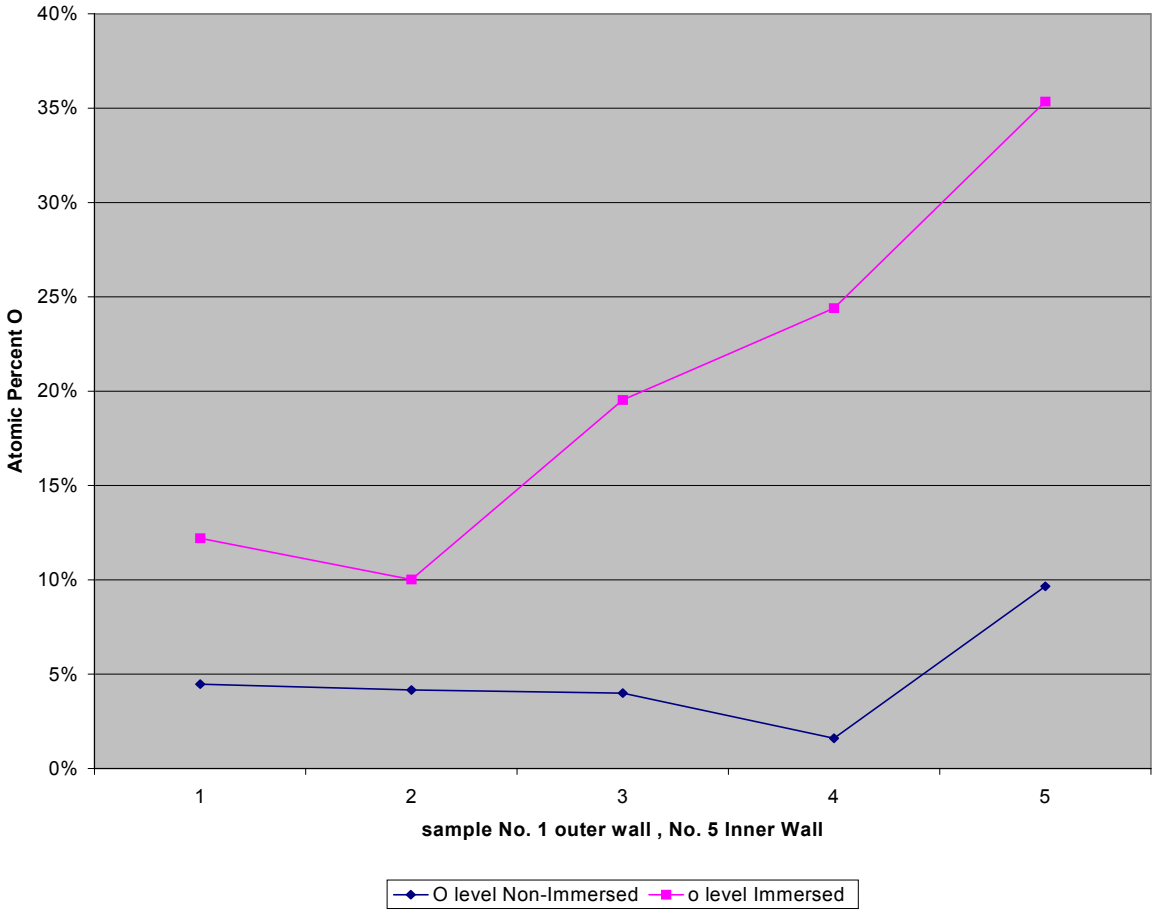

As we learn more from the planed field tests at GM's Bedford, IN facility, we may decide a protective coating is required to protect the inside wall of the immersion tube from oxidation. This protective coating may be applied post nitridation and fired in an oxygen environment. Another method may be to apply a different slip cast formulation for the inner wall region of the immersion tube. It would contain elements that will form a glassy phase oxide barrier in-situ, thus protecting the majority of the tube from oxidation by sealing off the inherent porosity of the NB SiC materials.

3.3.3 Representative Parts: NB-SiC CFCC Electric Heated Immersion Tube No. 9

End User Field Tests: NB-SiC CFCC Electric Heated Immersion Tube No. 9

General Motors in Saginaw, MI started using immersion tube No. 9 on February 11th, 1999. It was used in 57 heat cycles (a record for Textron Systems NB SiC/SCS-6 immersion tubes) and then taken out of service on April 14, after 1488 hours of service. Tube No. 9 cracked and dropped its lower section on the floor during a dross cleaning procedure. During this period tube No. 9 was subjected to the routine thermal stresses associated with removal and insertion into

molten aluminum. During the 52 heat cycle immersion tube No. 9 was run at above normal temperatures (1900°F) and at 100% power while the aluminum was superheated to 1644°F. All previous and subsequent heat cycles were run at lower temperatures.

Component Evaluation Immersion Tube No. 9

Immersion Tube No. 9 failed outside the crucible. It had been running relatively well and was close to achieving 1500 hours of operation. GM chose to accelerate the heat up of the aluminum by maximizing the heater output. This occurred five cycles prior to the failure. The control system was placed in manual with 100% power. GM said the aluminum was running at 1644°F and the heater was about 1880°F. Once the aluminum was up to temperature they placed the controller back into automatic. After this modified manual heat up, GM ran four more lower temperature cycles.

Prior to the last heat cycle, the crucible was shutdown for repairs. The immersion tube was maintained at 1260°F in air overnight. The immersion tube was placed inside the repaired crucible during this period to preheat the crucible. Molten aluminum was added to the crucible the following day. On the very last heat up they had added two ingots of aluminum and raised the immersion tube slightly so that the melt line was maintained at the same height on the immersion tube. GM adjusted the heater power to 100% under manual control to accelerate the aluminum warm up. While the ingots were melting the temperature rose from 1170 to 1270°F. The heater temperature was not recorded, but it ran at 100% power for 30 minutes. At the end of this cycle, the immersion tube was removed from the crucible. When they went to use it after pouring and recharging the crucible a large crack about the melt line region was observed. Upon further inspection outside the crucible, the lower section fell to the ground. The failed immersion tube was shipped to Textron Systems for analysis. The heating element, t/c, and refractory liner were also shipped to be inspected for evidence of erosion.

Microstructure: NB-SiC CFCC Electric Heated Immersion Tube No. 9

Immersion tube No. 9 with its heater element assembly was returned to Textron Systems for evaluation. Upon inspection this tube was found to be free of any foreign glassy phase deposits along the crack faces and internal tube wall surfaces (Fig 3.3-70). On previous field tested tubes, sodium based silicon oxides are formed and deposit a glassy phase coating in these regions. In addition, no ingress of aluminum could be found along the crack interfaces. Since this tube was found looking new inside one would suspect another mechanism caused this tube to fail. One possibility is this tube was broken by accidental impact on a hard object while it was removed from the crucible. GM had reported this tube failed when a technician had removed the tube from the crucible to remove dross from its outer surface.

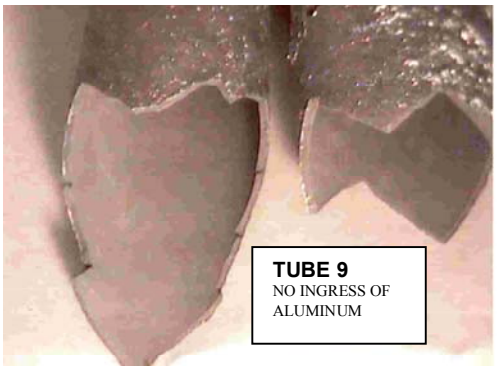

Figure 3.3-70

3.3.3 Representative Parts: NB-SiC CFCC Electric Heated Immersion Tube No. 10

End User Field Tests: NB-SiC CFCC Electric Heated Immersion Tube No. 10

Textron Systems first large-scale CFCC immersion tube was installed at GM Powertrain in Bedford, IN on Wednesday May 5th,1999. GM produces cast aluminum pistons, heads, transmission casings, rings, etc. These die castings are performed at multiple stations where each station contains three immersion tube heaters. Immersion Tube No. 10 was installed on a piston die cast furnace. Follow up on May 19th with GM showed this tube was still in service and performing well. On Friday, May 21st GM found the heating element shorted and was forced to remove this tube from service. The tube was removed in one piece and there was no evidence of catastrophic failure.

A failure analysis was performed for immersion tube No. 10, which failed prematurely during field testing at GM in Bedford, IN. A review of tube No. 10's manufacturing records and NDT evaluations along with field testing conditions identified a number of factors that may have had an affect on this tubes ability to perform well during its field test.

Field Test Summary: The first large-scale CFCC immersion tube (No. 10) was installed in a piston die casting furnace at General Motors Bedford, IN plant on May 5th. This tube was preheated in an insulated cabinet using its 20 kW heating element to provide the energy. The technician said they normally bring the immersion tube up to 1000°F slowly and hold it for many hours at this temperature. When an immersion tube needs to be replaced on a furnace they use one of these preheated assemblies. Textron Systems immersion tube No. 10 was not slowly heated up to 1000°F. Instead, the control system was turned on and 100% power was applied. Tube No. 10 heated to1000°F in 17 minutes.

After the initial warm up tube No. 10 was maintained at 1000°F for one hour. During it installation into the furnace the heating system was disconnected. It is estimated the tube had cooled down in the ambient to approximately 700°F. Once the immersion tube was aligned with the opening on the top of the furnace it was lowered quickly into the molten aluminum. The aluminum temperature was close to 1400°F.

A large steel flange was added to the flange end of the immersion tube to combat the buoyancy effect of our much lighter tube. This steel flange weighed 114 pounds and was used to hold the immersion tube vertical when immersed in the aluminum. The heating element assembly rested on top of the immersion tube flange.

Once the immersion tube was installed the electrical power was applied to the heating element and casting operations resumed after a 30 minute warm up period. The aluminum temperature is maintained at 1425°F. When heat is required the power to the heating element is applied at a 100% level. The control system is on/off control, therefore the immersion tube is exposed to peak heat fluxes when power is applied.

The heating element was positioned inside the immersion tube such that it allowed approximately a 3" region of the tube to be directly exposed to heating element radiation without the benefit of having the aluminum heat sink on the outside wall. This occurred at the melt line region of the tube. During the fourteen day period when Textron Systems tube was in operation the aluminum level would vary inside the furnace. The melt line can be as much as 10 inches lower that the initial height before the furnace is recharged with molten aluminum. At this condition the heater element is partially immersed and can be severely overheating in this region. The resulting thermal gradients about the tube can generate axial and hoop stresses in excess of 8 ksi as shown in previous thermal models reported on tube No.6's section.

On May 19th this tube was inspected first hand and the dross accumulation did not appear to be as severe as that found on the neighboring tubes. The dross is cleaned off on a daily to weekly basis depending on necessity. During the dross cleaning operation the combined mechanical and thermal stresses about the melt line region are compounded and could cause the tube to fail.

On May 21st the heating element shorted and the technicians removed tube No. 10 from the furnace. During this operation they removed the heating element and found much aluminum inside the tube. They turned the tube on its side and tried to pour some of the aluminum back into the furnace. Once the aluminum solidified it left a large pool of metal inside the immersion tube. The tube was observed to have no breaks at this point and was crated and shipped back to Textron Systems for failure analysis.

Component Evaluation Immersion Tube No. 10

The first large scale immersion tube was nitrided and X-rayed to look for porosity. The following pictures show the nitrided tube and its radiographs (Figures 3.3-71,72). There was no visible porosity and the tube was accepted for use. Thermal diffusivity testing will be performed at Argonne National Laboratory prior to field testing at GM.

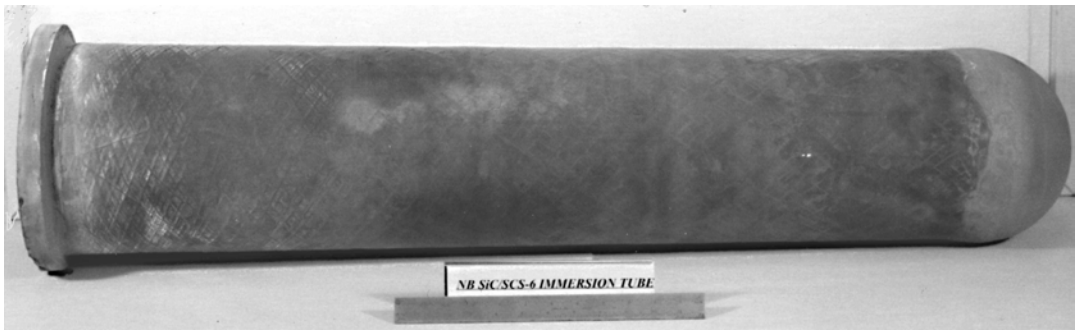

Figure 3.3-71 Large-scale Immersion Tube 8.5" I.D. x 43"

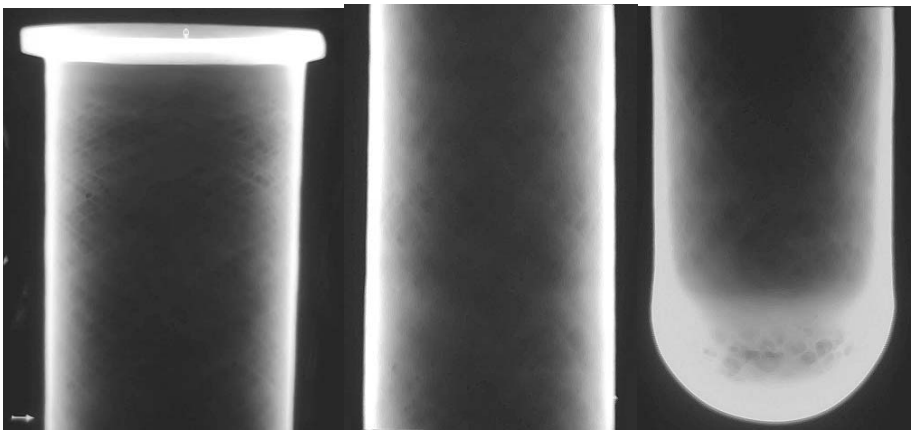

Figure 3.3-72 Tube No. 10 – Radiographs of top, middle, and dome sections

JG Sun at Argonne National Laboratory reported NDE data for immersion tube #10. Thermal diffusivity and air-coupled ultrasound transmission (UT) imaging tests were performed. A general discussion of this data and its correlation to fabrication conditions and immersion tube construction is given below.

The compiled thermal diffusivity and UT images show flaws (indicated as low diffusivity or low transmission) in tube No. 10 These flaws are either voids (or gross porosity) or delaminations. Judging from the flaw size and the correlation between thermal and UT data, it seems that the larger areas of flaws are delaminations. Most of the flaws are near the open end, while a few isolated small flaws are near the closed end of the tube. The lower diffusivity at the closed end of Tube #10 is likely due to a thicker wall construction.

The following picture shows the low thermal diffusivity regions found in tube No. 10 as compared to their axial position (Fig 3.3-73 thru 75).

Fig. 3.3-73
Setup of Thermal Imaging Test for Textron Immersion Tubes #10

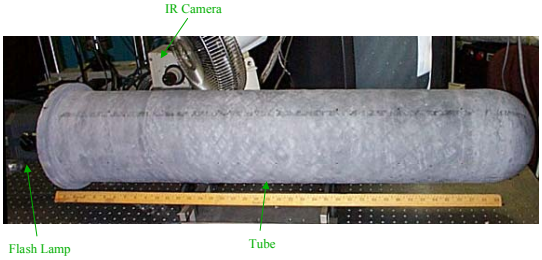

4/99

Fig. 3.3-74
Thermal Diffusivity Image of Textron Immersion Tube #10

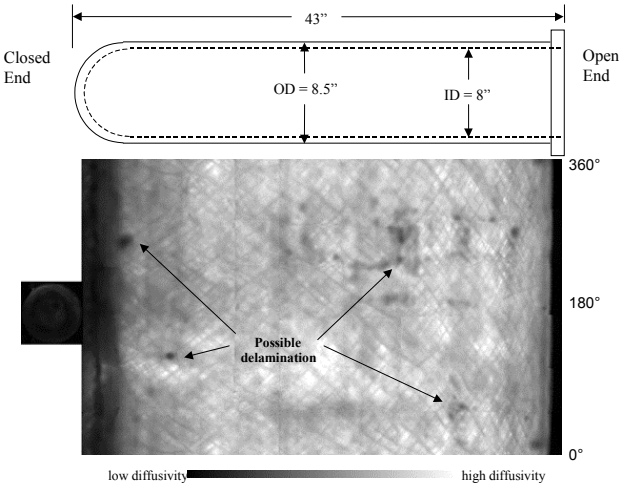

4/99

Fig. 3.3-75
Air-Coupled UT Image of Textron Immersion Tube #10

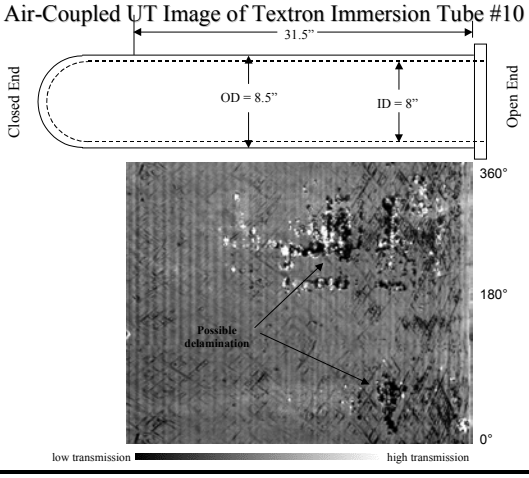

4/99

Tube No. 10 showed the presence of delaminations. The distinction between gross porosity and delamination is difficult to detect using thermal diffusivity and air-coupled UT imaging. Gross porosity is more detectable using radiography CT images.

Clearly in scaling up to these larger tubes Textron Systems must lean slurry application techniques that eliminates gross porosity and delamination within the tube structure.

When we learned about the premature failure of tube No. 10 one of the questions raised was whether the scaled-up tube required a different wall thickness or continuous fiber content to achieve similar performance characteristics as that found during the field tests conducted at GM in Saginaw, MI. The following question was submitted to H.T. Lin and Mr. Tom Cassin of MSC: "*Now that I and going to scale up these tubes to an 8.5" I.D. will the larger diameter CFCC tube, having the same wall thickness and volume fraction SCS-6 fiber as the smaller diameter tube, exhibit the same thermal stress capability as found for the smaller diameter tube?* The response from MSC indicated the present wall thickness and volume fraction of SiC_f is consistent with that used for the smaller tubes. Tom's response was as follows*: "The hoop stresses due to the radial delta T are proportional to (1+t/r) on the inside and (1-t/r) on the outside, and the axial stresses are similar. So, increasing the tube radius will reduce ID stresss. To examine the axial gradient, we did a quick check with one of the old FEM's...all the peak stresses went down when increasing the radius and keeping wall thickness the* same."

Failure Analysis for Immersion Tube No. 10 field tested at GM Powertrain in Bedford, IN:

Background: The first scaled-up prototype immersion tube No. 10 was field tested at GM Powertrain in Bedford, IN from May 5th to May 21st , 1999. This tube was preheated to 1000°F in seventeen minutes and then held at temperature for one hour prior to installation on a piston die casting furnace. This tube contained a 20kW heater which cycled on or off at 100 or 0% power as heat was needed. On Friday, May 21st this tube was taken out of service due to ingress of aluminum into the tube and shorting of the electrical heating element. Upon removal from the furnace there were no indications of catastrophic failure and the tube appeared to be in one piece. The heating element was removed and molten aluminum was poured out the flange end of the tube back into the furnace. This tube was shipped back to Textron Systems with a large amount of solid aluminum inside of it. Upon arrival it was uncrated and found to be fractured into many pieces. The body of aluminum came loose inside the immersion tube and hammered it during shipment. Much of this tube was reconstructed and crack interfaces were looked at for evidence of aluminum wetting.

Failure Anaylsis Summary: The CFCC immersion tube tested at GM Powertrain was the first scaled-up version for this type of tube previously tested very successfully at GM's Advanced Development Laboratory in Saginaw, MI. This tube was non-destructively tested (NDE) by X-ray, thermal diffusivity, and ultrasonic evaluations prior to its use at GM Powertrain in Bedford, IN. These results did show potential gross porosity and delamination flaws, but due to the location or nature of these flaws it was believed they would not severely impact the performance of the tube. This tube was shipped to many facilities to perform these analyses, and then finally delivered to Bedford, IN for field testing. It is possible other critical flaws may have developed during the handling of this tube. Textron Systems recognizes there is some learning to be

accomplished in the manufacture of these larger tubes. Ideally, future large scale immersion tubes will be manufactured free of gross porosity or delaminations.

The X-rays showed areas in the dome end where micro-cracks were present. These cracks were a result of surface drying of the slip cast formulation and did not penetrate into the wall thickness of the tube. Thermal imaging did show regions of gross porosity or delamination, but these areas were not considered significant because they were primarily above the melt line region or were seen about the dome end where heavier coatings of slip cast are applied. Ultrasonic evaluation did point to a similar region in the upper portion of this tube where delaminations may have been present. This weak area within the immersion tube wall may have contributed to its early failure during field testing at GM Powertrain.

The failure analyses performed on the tube after its field test did show sections where the tube had cracked. These cracks was found in the same areas that the NDE results had shown as potential flaws. In addition, these cracks were located at regions along the tube wall where the thermal stress would be at it highest levels. These regions were near the melt line and at the base of the heating element assembly.

Tube no. 10 was not filament wound with alternating layers of dome and helix winding patterns as was typically done on the smaller tubes successfully tested at GM in Saginaw, MI. Instead, Many more dome winding and less helix windings circuits were performed. The net result was a more uniformed green body appearance slip cast over the dome end of the tube, but the amount of helix reinforcement was effectively reduced by 25%. This may have been another reason why this tube failed prematurely.

Normally GM preheats the monolithic immersion tubes at 1000°F and holds for many hours at this temperature. The tubes are slowly heated from room temperature to 1000°F over the course of one hour. Textron Systems immersion tube no. 10 was not slowly warmed up to this temperature and was only held for one hour prior to it being placed in service. This abrupt heating could have impressed enough thermal stress about the heating element region that cracks or flaws were initiated prior to this tube being placed into service. This may have been another reason why this tube failed prematurely.

Microstructure: NB-SiC CFCC Electric Heated Immersion Tube No. 10

Failure Anaylsis: No failures were found in the dome end of this tube. Along the sides of the tube there were many cracks. Many of these cracks were secondary and the result of shipment. Two primary cracks were significantly wetted with aluminum. One crack was located approximately 4” above the dome region of the tube, near the base of the heating element assembly. The other crack was located approximately 3” below the melt line. These cracks were close to where the thermal stresses on the tube are their highest. This being the regions just above and below the heater element, where the temperature gradient along the tube wall will vary the most. These critical cracks were also found in regions of the tube where preliminary NDE indicated potential flaws.

The aluminum inside this immersion tube solidified and cast an impression of the tube wall to the outer surface of this aluminum body. The critical cracks, found to be wetted with aluminum, also had islands of aluminum shaped around the cracks. These same islands were observed on the body of aluminum removed from the immersion tube. The upper region of the tube near the melt line showed a change in the appearance of the aluminum body cast inside the immersion tube. This is believed to be one of the major leak areas that developed (Figures 3.3-76 thru 78).

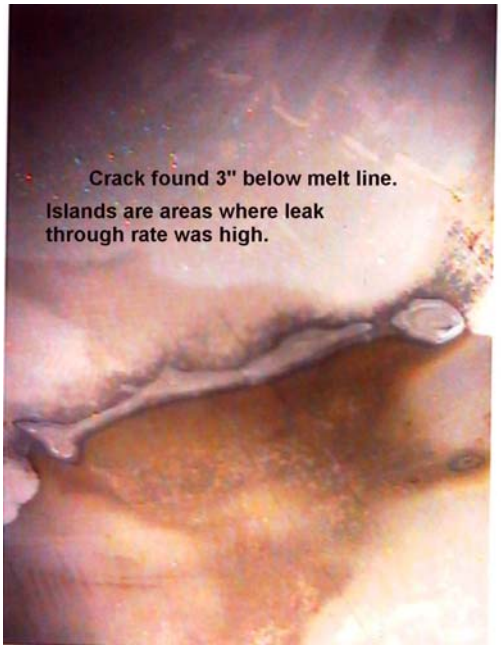

Figure 3.3-76

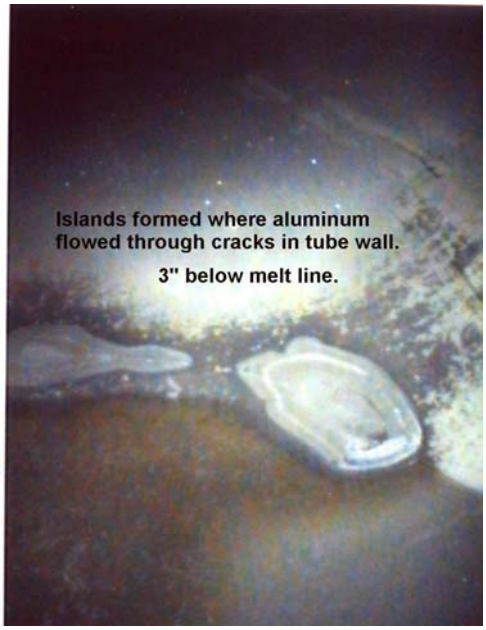

Figure 3.3-77

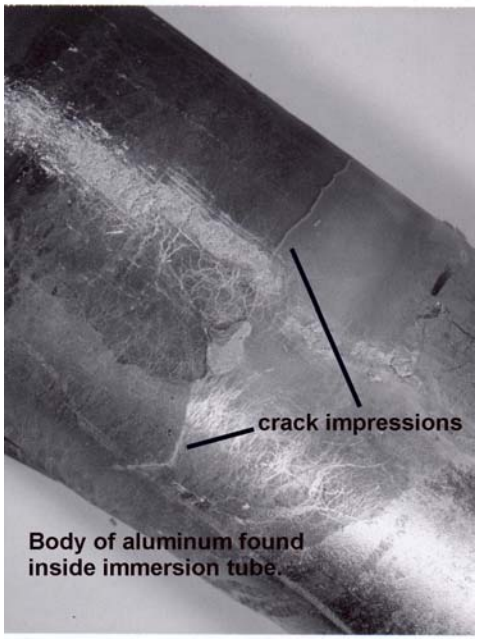

Figure 3.3-78

Another major crack was found approximately 4" above the dome section of the immersion tube. This crack also appeared to be wetted with aluminum and had pooling of the aluminum (Figures 3.3-79 thru 82).

Figure 3.3-79 This crack near the dome end of the tube is wetted with aluminum throughout the wall thickness.

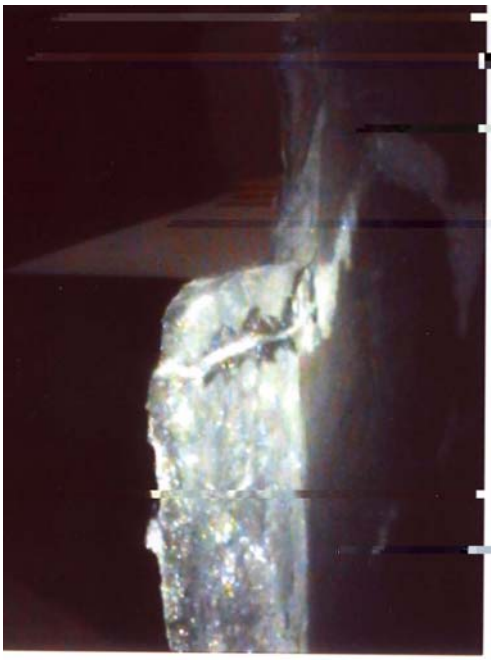

Figure 3.3-80

Figure 3.3-81 Picture of crack from outside of the tube near the dome end.

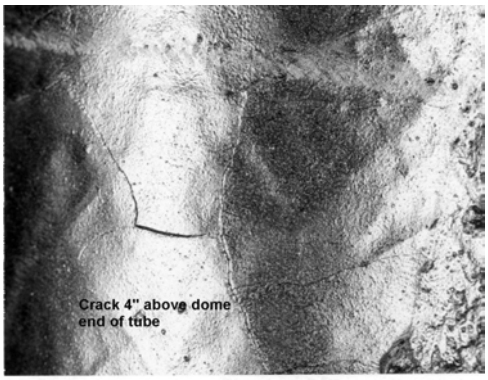

Figure 3.3-82

3.3.3 Representative Parts: Alcoa Immersion Tube

Textron and ALCOA had participated in discussions on the evaluation of CFCC tubes in an aluminum degassing furnace at the ALCOA facility in Alcoa, Tennessee. Textron would provide immersion tubes at subsidized cost to ALCOA, while ALCOA would provide in-service evaluation of tube performance.

The tubes in question are approximately 48" in length with an average diameter of 5" and a wall thickness of 0.33". Plaster mandrels were fabricated for use on the 5-axis filament winder. The winding pattern was similar to that which evolved out of the effort to fabricate the GM immersion tubes. The three winding segments were a) a helical wrap which covered all of the tube except for the dome end; b) a dome wrap which covered most of the tube including a geodesic wrap over the dome; and c) a short (12") helical segment positioned at the melt line of the tube. The final winding pattern alternated 7 dome wrap patterns, 7 full helix patterns and six melt-line helix patterns.

Two tubes were fabricated and nitrided according to the usual cycle. X-ray examination of the first tube showed a crack approximately 2" long across the dome end and extending through the thickness of the tube. During the winding of the second tube, short lengths (4") of additional fibers were added to the dome end, held in place by the geodesic dome winding. This second tube showed no evidence of visible flaws in the X-ray examination. Comparison with X-ray examination of earlier tubes showed this tube to be superior in the absence of both voids and cracks.

Completion of arrangements for field testing within the time scheduled for ALCOA's plant start up were made difficult by personnel changes at both Textron and ALCOA. The tube was not shipped for evaluation.

Task 3.4 Physical Properties (Chemical, Mechanical, Thermal)

100% Si_3N_4 (NBSN/SCS-6) Tensile Specimens

Textron Systems performed coupon-scale tensile tests on a series of ten specimens of SCS-6 reinforced CFCC with 100% silicon nitride matrices. Tensile specimens were sectioned from uniaxially-reinforced CFCC's that contained 20-22 vol. % SCS-6 monofilaments. Samples were slip cast Si metal slurries onto plaster molds which contained 6-8 plies of drum wrapped monofilaments. Peak nitridation temperatures were held at 1380°C for two hours. Tensile tests were also performed on individual filaments that were extracted from fully-nitrided composites.

Ultimate Tensile strengths of up to 100 ksi (680 MPa), with first matrix microcracking stresses of 35-50 ksi (240-340 MPa), with an elastic modulus of 29-30 Msi (200-210 GPa) and with a total strain to failure of up to one percent were recorded. Less than ten percent variation was noted in first matrix microcracking stress for this series of NBSN CFCC specimens.

A total of twenty filaments extracted from the fully nitrided NBSN/SCS-6 CFCC were tensile tested at one inch gage length. Monofilament tensile properties ranged from 350 to 600 ksi (2.4 – 4 GPa), which indicated SCS-6 tensile properties were not affected by nitridation cycle conditions in a silicon nitride matrix.

NB Si_3N_4 Atomic Structure Characterization

Textron Systems conducted analytical electron microscopy (AEM) and x-ray diffraction examinations of both the monolithic and SCS-6 reinforced NBSN CFCC's. Both techniques indicated that matrix phase purity was very good and that residual silicon levels were below instrument detection limits as determined by AEM energy dispersive x-ray analysis, x-ray diffraction analysis, and AEM diffraction, phase and lattice imaging methods. Most of the silicon nitride characterized was a hexagonal alpha crystallographic variant equiaxed and very well bonded. There was no gross SiO_2 present, although Si_2ON_2 was observed lining the interior of large pores. Overall matrix pore size was extremely fine and homogeneous. High resolution TEM lattice imaging also indicated grain boundaries were free of inclusion phases (such as iron silicides) as well as impurity segregation effects. These evaluations conducted during the onset of Phase II of the CFCC program supported current processing techniques and nitridation cycle development efforts.

NB SiC Atomic Structure Characterization

Textron Systems conducted x-ray diffraction analyses on monolithic and SCS-6 reinforced NB SiC sample coupons that were nitrided for up to four hours at temperatures between 1380 – 1400°C. Complete conversion of the silicon to silicon nitride was found in the bond phase on the NB SiC matrix. Alpha to beta phase ratios for the silicon nitride ranged from 1.5 to 2.2 , which was very encouraging from an oxidation and mechanical property (creep resistance) standpoint. Matrix phase purity showed no residual silica or silicon oxynitride.

NB SiC Oxidation Study

Static oxidation tests were conducted on a series of monolithic and NB SiC/SCS-6 specimens. All samples formed a protective silica film with no weight loss indicating a stable passive oxidation occurred. Weight gains after six weeks ranged from 8-12%.

Room Temperature Burst Test on NB SiC/SCS-6

University of Dayton Research Institute (UDRI) completed room temperature burst tests on NB SiC/SCS-6 tubular sections. The CFCC was constructed with ~ 3 vol.% SCS-6 fiber wound at a +/- 0° / 45° lay-up geometry. A prototype CMC tube was provided by Textron Systems for room temperature hoop strength evaluation and failure analysis. The nominal dimensions were 90 mm (3.6 in) inside diameter by 76 mm (3.0 in) length by 2.9 mm (0.12 in) wall thickness. The tube was hot waxed mounted and sawn by a diamond wheel with a water based coolant to create two tubular ring specimens having the final nominal length of 36 mm (1.4 in).

The two specimens were loaded to failure by internally pressurizing the tubes. The first tube failed at a questionably high stress (≈213 MPa or 30.8 ksi) due to an unwanted back pressure that developed in the test fixture feed ports. After fixture modifications to reduced the back pressure, the second tube failed at a hoop tensile stress of 96.9 MPa (14.0 ksi). Fractographic analysis indicates fiber pullout of both 0 and ±45° aligned fibers from the matrix, however, it is primarily dominated by pullout of 0° aligned fibers. Some fibr pullout lengths exceeded 5 mm.

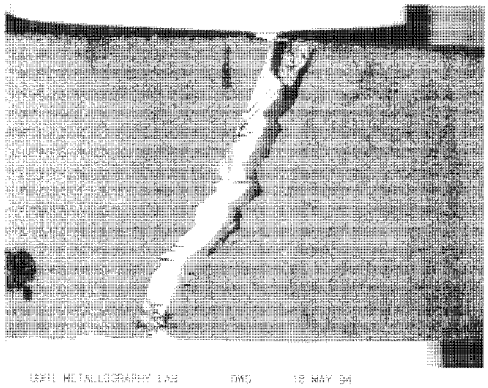

Figure 3. 4.1 Optical fractograph of specimen 1074-1 at a 45^{o} initiate fracture plane. Fiber pullout is predominately the 0° aligned fibers. The tube length (vertical axis) is nominally 36 mm.

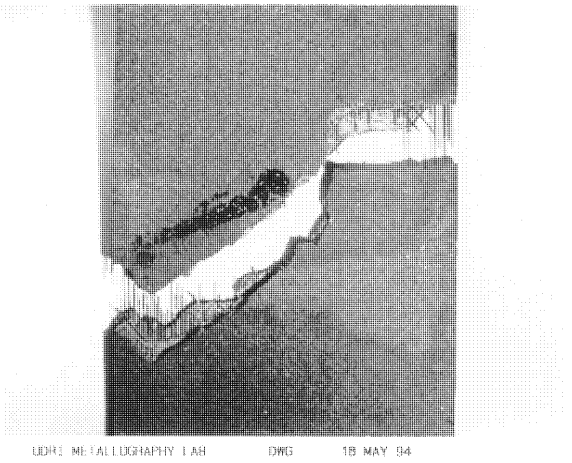

Figure 3.4.2
Optical fractograph of specimen 1074-2 at a 45° fracture plane. Fiber pull-out is dominated by the pull out of the 0° aligned fibers. The tube nominal tube length (horizontal axis) is 36 mm.

Carborundum Alpha SiC Fiber Evaluations

Textron Systems completed evaluation experiments utilizing the Carborundum alpha SiC fiber as a reinforcement in a nitride bonded silicon nitride matrix. Approximately three meters of alpha SiC fiber tow (100 ends/tow) was assessed for handling and mechanical characteristics. Initial indications as to handling characteristics were not favorable. This tow could not be brought to less than a one cm bend radius without breakage and was sensitive to slight surface damage. This behavior rendered this material unsuitable for filament winding operations.

Slurry impregnation and nitridation trials showed a PVA-based sizing was easy to remove with a butane torch or hot water and that the fiber tow accepted aqueous (submicron size) Si metal slurry quite readily. Nitridation at 1400°C for a few hours revealed that the fiber matrix interface was well bonded and tows were uniformly impregnated.

Coupon-type Samples for Material Characterization and/or Joining of CFCC's

Textron Systems supplied flat panel coupon-type samples of CFCC's for various characterizations and testing activities performed at DoE laboratories. These activities involved basic materials characterization and/or joining of CFCC materials. Monolithic and CFCC samples of compositions described in Table 3.4.1 were sent to DoE laboratories under the auspices of the Task 2 portion of the CFCC program and as part of the DoE/BES collaborative activities on CFCC joining. All samples fabricated were made by direct slip casting of monolithic and CFCC materials onto plaster molds.

Table 3.4.1 Coupon-type Samples for Material Characterization and/or Joining of CFCCs

Specimen Composition	**ORNL** (Keiser) (HiPHES steam-methane reformer corrosion tests)	Battelle PNL (Henager) (High temp crack bridging studies)	ORNL (Dinwiddie) (Thermal property measurements)	INEL (Rabin) (Reaction bonding joining studies)
SCS-9/NB SiC (25/75 Si_3N_4/SiC)[1]	flex bars and flat coupon sections			
SCS-6/NB SiC (50/50 Si_3N_4/SiC)		coupons and flex bars	small coupons	
SCS-6/NB SiC (25/75 Si_3N_4/SiC)	flex bars	coupons and flex bars		disks and flat coupons
Monolithic NBSiC (50/50 Si_3N_4/SiC)		coupons and flex bars	disks and flat coupons	disks and flat coupons
Monolithic NBSN[2]	flex bars	small coupons	small coupons	
SCS-6/NBSN	flex bars	flex bars	small coupons	

[1] "(25/75 Si_3N_4/SiC)" refers to CFCC or monolithic ceramic matrix phase composition.

[2] "NBSN" refers to 100% nitride bonded silicon nitride matrix phase composition.

Thermal diffusivity values obtained at ORNL on silicon carbide fiber (SCS-6) reinforced nitride-bonded silicon nitride (NBSN) and nitride-bonded silicon carbide (NBSiC) by R. Dinwiddie were as follows:

- SCS-6/NBSN in-plane; along fibers - 0.26 cm^2/sec (unidirectional)
- SCS-6/NBSiC in-plane; along fibers - 0.13 cm^2/sec (cross-ply)
- Monolithic NBSiC - 0.15 cm^2/sec
- Monolithic NBSN - 0.085-0.14 cm^2/sec

Dr. Chuck Henager and Dr. Charles Lewisohn of Battelle/PNNL reported on the first results of a collaborative study between Textron and PNNL that was intended to characterize the high temperature mechanical properties of Textron's monolithic and CFCC materials. This study was conducted under the terms of the DOE/BES collaborative research agreement which was initiated by Jill Jonkouski of the DOE Chicago Operations Office. Battelle reported as follows:

- Battelle's first report on the ambient and elevated temperature crack growth and fast fracture behavior revealed findings which were somewhat in opposition to what Textron and other laboratories have measured on their materials in two main areas:

- Battelle measured matrix porosity levels on SCS-6 reinforced materials which were in the vicinity of 30 to 50%. These measurements are not physically reasonable. Textron and Battelle both measured the geometrical densities of individual flexural specimens sent to PNNL and found them to be in the vicinity of 2.72 to 2.75 g/cc. When corrected for monofilament volume fraction, the calculated matrix density is anywhere from 82 to 86% of

theoretical. Since the geometrical density measurements are accurate and reliable, it is likely that the anomalously high matrix densities measured by PNNL are due to some image-processing related artifact in the quantitative image analysis software that PNNL used to estimate matrix porosity levels. This issue can be satisfactorily resolved, however, as we have made extensive use of an automated image analysis program at Textron called OPTIMAS and have found that this program can produce excellent estimates of matrix porosity levels in NBSN and NBSiC-based materials if appropriate care is taken to assign proper gray scales to relevant image features like grains or pores.

- Battelle observed relatively low strengths and toughness' in SCS-6 reinforced NBSN CFCC materials at both ambient and elevated temperatures. However, closer examination of the fracture surfaces showed that the SiC monofilament reinforcements were "bunched" into a small region of the flex specimens, and therefore, during flexural loading a matrix crack was initiated in a thick region of monolithic material and must have propagated essentially unimpeded through the fiber plies. Textron has observed this sort of phenomenon before in CFCC samples which have grossly anisotropic fiber distributions in which localized regions of the samples contain high volume fractions of fiber and other regions are reinforcement-free. Due to the nature of loading conditions during flexural testing, this type of sample will show pseudo-brittle behavior.

  Fortunately, a later batch of SCS-6/NBSN CFCC samples (ref. Table 3.4.2) with more uniform fiber distributions was shipped to PNNL and these samples showed graceful failure behavior and exhibited strengths comparable to what we have measured for such materials during prior tensile testing trials.

- One additional encouraging observation from the Battelle report was that the fast fracture strengths of Textron's monolithic and CFCC materials were nearly the same at temperatures of 1200 and 1400 degrees C as they were at room temperature.

Additional Flat panel coupon-type samples were fabricated for ORNL and Battelle Pacific Northwest Laboratories for testing and characterization activities in support of the DoE-funded CFCC and HiPHES programs.

Monolithic and CFCC samples with compositions as described in the table 3.4.3 were sent to ORNL and Battelle Labs under the auspices of the Task 2 portion of the CFCC Program and as part of the DoE/BES collaborative activities on CFCC joining. All samples were made by slip casting or pressure-assisted slip casting and were then machined to their final dimensions with #320 finish resinoid diamond wheels.

Table 3.4.2 Coupon-type Samples for Material Characterization and/or Joining of CFCCs

Specimen Composition	**ORNL (Keiser)** (HiPHES steam-methane reformer corrosion tests)	**Battelle PNL (Henager)** (High temp crack bridging studies)
Monolithic NBSiC (50/50 Si_3N_4/SiC)	flex bars and flat coupon sections	coupons and flex bars
Monolithic NBSN[2]		small coupons
SCS-6/NBSN	flex bars	flex bars

[1] "(50/50 Si_3N_4/SiC)" refers to CFCC or monolithic ceramic matrix phase composition.

[2] "NBSN" refers to 100% nitride-bonded silicon nitride matrix phase composition.

Samples supplied to ORNL were the second batch of materials to be supplied for steam/methane exposure testing in their simulated reformer rig. Technical feedback received from ORNL to date (via J.Kaiser and J.Jonkouski) indicates that 50/50 blends of nitride bonded silicon nitride/silicon carbide and 100% NBSN perform best, whether in monolithic or reinforced form, seem to perform better than Textron's other matrix compositions in steam-containing environments. The data are preliminary, however, and only reflect weight gain measurements performed on exposed specimens.

Additional samples were fabricated and shipped to ORNL and Battelle/PNNL for elevated temperature steam testing in their simulated reformer rig and for high temperature crack bridging measurement at PNNL

Table 3.4.3 Coupon-type Samples for Material Characterization and/or Joining of CFCC's

Specimen Composition	**ORNL (Keiser)** (HiPHES steam-methane reformer corrosion tests)	**Battelle PNNL (Henager)** (high temp crack bridging studies)
SCS-6/NBSiC[1]	flex bars	coupons and flex bars
SCS-6/NBSN[2]	flex bars	flex bars
Hi Nicalon^{TM}/NBSN[3]	flex bars	flex bars

[1] Matrix phase composition approximately 20% silicon nitride/80% silicon carbide.
[2] "NBSN" refers to 100% nitride-bonded silicon nitride matrix phase composition.
[3] Fabricated with uncoated Hi-Nicalon^{TM} ceramic tows in uniaxial lay-up.

Samples supplied to ORNL were the third batch of materials to be supplied for steam/methane exposure testing in their simulated reformer rig. Data received (via J.Kaiser and J.Jonkouski) on corrosion weight gain and strength retention of monolithic and monofilament reinforced flexural specimens received from ORNL show 100% NBSN matrix materials perform better that other matrix compositions in steam-containing environments.

Examination of data generated in this third series of HiPHES tests indicated that (uncoated) nitride-bonded silicon nitride, whether monolithic or reinforced with SCS-6, appeared to show promising strength retention characteristics and weight gain behavior after simulated steam/methane reformer exposure. NBSiC-based monolithic and SCS-6 reinforced CFCC's made by Textron appear to show poorer strength retention and oxidative weight gain behavior in the same steam/methane environment, indicating that protective glazing of the exterior surfaces is advisable, therefore Textron Systems made arrangements with team member Nova Industrial Ceramics to begin investigating the use of their glaze formulations on Textron's CFCC materials. Nova's aluminosilicate glazes have thus far been found to have a substantially beneficial effect on the oxidative weight gain behavior of monolithic NBSiC.

Additional Monolithic and CFCC samples with compositions as described in table 3.4.4 were sent to ORNL and Battelle Labs under the auspices of the Task 2 portion of the CFCC Program and as part of the DoE/BES collaborative activities on CFCC joining.

Table 3.4.4 Coupon-type Samples for Material Characterization and/or Joining of CFCCs

Specimen Composition	**ORNL (Keiser)** (HiPHES steam-methane reformer corrosion tests)	**Battelle PNL (Henager)** (High temp crack bridging studies)
Monolithic NBSiC (50/50 Si_3N_4/SiC)[1]	flex bars and flat coupon sections	coupons and flex bars
Hi Nicalon (uncoated)/NBSN[2]		small coupons
SCS-6/NBSN	flex bars	flex bars

1 "(50/50 Si_3N_4/SiC)" refers to CFCC or monolithic ceramic matrix phase composition.

2 Fine particle-sized Si slip with uncoated Hi Nicalon fiber; peak nitridation temp approx. 1390 C

All samples were made by slip casting or pressure-assisted slip casting and were then machined to their final dimensions with #320 finish resinoid diamond wheels.

Samples fabricated for ORNL to be tested in the HiPHES reformer rig were sent to teammate Nova Industrial Ceramics for protective glazing with their proprietary, cordierite-type, glaze formulation. This glaze has been found to work well on Nova's monolithic nitride-bonded SiC materials in steam-containing environments it may serve as an inexpensive and effective protective coating for Textron's NBSiC and NBSN-based CFCC materials. SCS-6/NBSN, SCS-6/NBSiC and uncoated Hi-Nicalon NBSN CFCC flexural samples were impregnated with a water-based glaze and fired at 1350 C in air.

Textron received test data on both glazed and unglazed samples which were supplied to Oak Ridge. Nova's glaze appears to be rather effective at reducing corrosion rates for a wide range of Textron monolithic and CFCC materials. Note also that this test series marked the first time in which Textron supplied Hi Nicalon/NBSN CFCC samples for reformer testing. Though the Hi

Nicalon fibers were uncoated and would thus not effectively toughen or strengthen our NBSN matrix, the corrosion performance of these composites is not all that bad. Further testing is therefore warranted on Hi Nicalon tows which have been CVD coated so as to optimize fiber/matrix debonding behavior.

Samples sent to Battelle were not glazed as the primary intent of the cooperative research effort between Textron and Battelle was to characterize the high temperature fracture behavior of various categories of yarn and monofilament-reinforced CFCC materials made by Textron. The work at Battelle dealt with oxidation behavior of CFCC's at elevated temperatures only to the extent that oxidation effects interact with crack opening behavior. Elevated temperature crack bridging measurements at Battelle were carried out in inert as well as oxidizing environments in order to be able to separate out pure thermal vs. thermal plus environmentally-assisted strength retention characteristics in our CFCC materials.

Dr. C. Henager of Battelle indicated that both monolithic and SCS-6 reinforced NBSN materials are showing predictable slow crack growth behavior and minimal strength loss at test temperatures of 1200 °C.

Hi Nicalon Ceramic Yarn Fiber Evaluations

Textron Systems purchased and received one kilogram of Hi Nicalon ceramic yarn during this reporting period. We initiated our first compositing trials with this fiber, using the following procedure to prepare small (approximately 50 mm width by 100 mm length by 6 mm thickness) coupons that will be used for nitridation trials, and possibly mechanical testing:

1. The Hi Nicalon fiber was (quite efficiently) de-sized by passing the tows through a small tube furnace at a temperature of 450^{o}C for a period of about one minute;

2. Unsized Nicalon tows were hand impregnated with micron-sized silicon metal slurry to infiltrate the fiber bundles. The unsized fibers seemed to readily be wet and impregnated with water-based slurries. This was an encouraging observation;

3. Slurry impregnated tows were then hand laid up into rectangular plaster molds; small green bodies were formed by pressure-assisted slip casting. The green bodies were air dried in an oven, yielding macroscopically crack-free (and binder-free) coupons;

4. Uniaxially-reinforced Hi-Nicalon^{TM} CFCC's green bodies were nitrided without restraint tooling or fixturing to a peak temperature of about 1390°C for four hours, machined into test bars and subjected to metallographic examination.

The fully nitrided Hi-Nicalon^{TM} CFCC's showed acceptable nitridation weight gains and appeared to be much more physically robust that earlier generations of Nicalon^{TM} – based CFCC's made with standard or "CG" grade Nicalon^{TM} – grade tows. Metallographic examination show no evidence of gross physical damage to the fiber or signs of extensive reaction between the uncoated Hi-Nicalon^{TM} fiber and the NBSN ceramic matrix.

Since it was unlikely that the interfacial bond characteristics of uncoated Hi-Nicalon^{TM} reinforced NBSN are optimized, a protective/debond coating of Hi-Nicalon^{TM} CFCC's would be required to establish acceptable levels of strengthening or toughening in NBSN or NBSiC matrix-based CFCC materials.

Thermal Shock Behavior of CFCC's

ABSTRACT

The thermal shock behaviors of a monolithic silicon carbide and two types of SCS-6 fiber reinforced silicon carbide matrix composites (1-D and 2-D), all fabricated by Textron Systems, were studied using the water quench technique to induce thermal shock. Thermal shock induced damage was characterized by a destructive technique of four-point flexure and nondestructive techniques of Young's modulus measurement by the dynamic resonance method and thermal diffusivity imaging techniques. In addition, these samples were exposed to repeated thermal shock tests to characterize damage evolution because of the cyclic thermal shock. As compared with monolithic silicon carbide, the continuous fiber-reinforced ceramic composites were capable of preventing catastrophic failure caused by thermal shock. Both the thermal diffusivity and dynamic resonance non-destructive techniques showed evidence of the progressive damage because of the thermal shock and indicated that these methods can be used to characterize progression of damage because of the thermal shock. Consequently, the feasibility of using the non-destructive techniques in detecting thermal shock damage of Textron materials was also demonstrated. Microstructural examinations of selected samples after thermal shock revealed damage via matrix cracking and fiber fracture which appeared to be responsible for decreased strength, modulus, and thermal diffusivity after thermal shock.

INTRODUCTION

Continuous fiber-reinforced ceramic composites (CFCCs) are being developed to improve the reliability of ceramics and meet the demands of high temperature applications. In most of these applications, fiber-reinforced ceramic composites are subjected to transient thermal conditions under which thermal stresses are generated that can induce damage by fracture. Such thermal shock damage degrades the load-carrying capability and oxidation resistance of composites in service. Thus, it is important to study the thermal shock behavior of fiber-reinforced ceramic composites, understand the mechanisms of thermal shock failure, and improve their resistance to thermal shock damage.

The thermal shock resistance of monolithic ceramics has been extensively studied and reported [1-3]. Theoretical analyses have been successfully applied to explain experimental observations and predict thermal shock behavior of monolithic ceramics [2-5]. However, similar studies of the thermal shock resistance of ceramic composites, especially continuous fiber-reinforced composites, are limited, in spite of the recent rapid advancements in ceramic composites and their improved properties [6]. As compared with monolithic ceramics, continuous fiber-reinforced ceramic composites are expected to display a much more complex behavior under thermal transient conditions. For example, the fiber reinforcement can change the crack initiation

and propagation behavior in fiber-reinforced composites under thermal shock, the expansion mismatch between fibers and matrices can introduce additional thermal stresses during thermal transients, and changes in interfacial properties can play an important role in influencing the thermal shock behavior of CFCCs. Many factors, such as the type of fiber/matrix materials, fiber architecture, interfacial characteristics, and matrix forming processes can also affect thermal shock behavior of continuous fiber-reinforced ceramic composites.

A methodology for inducing thermal shock damage and characterizing the damage has been developed in support of the CFCC Program [1, 7-16]. It consisted of water quench test for inducing thermal shock damage and characterization of the thermal shock-induced damage by destructive and non-destructive techniques [7-16]. The destructive technique of mechanical property measurements was used to characterize changes in mechanical response because of the thermal shock damage. The nature of thermal shock damage was characterized by optical microscopy. Non-destructive techniques of Grindosonic, Resonant Ultrasound Spectroscopy (RUS), Ultrasound, and thermal diffusivity imaging were successfully applied to detect damage in CFCCs because of the changes in the elastic modulus and thermal conductivity as a result of the thermal shock. In addition, CFCCs damaged by thermal shock were shown to be more susceptible to further degradation by fatigue and environmental effects [17]. Therefore, a comprehensive experimental study combined with non-destructive analyses were developed to assess the behavior of CFCCs in thermal transients [7-16].

This methodology was applied in this investigation on Textron composites for assessing the response of a monolithic SiC, and SiC $(SCS\text{-}6)_f$-SiC matrix CFCCs exposed to thermal transients including the thermal shock damage. Influence of testing conditions on the thermal shock damage was experimentally studied using destructive and non-destructive techniques. The results from these studies will be used by Textron to design and manufacture composites and to assess their performance in prototypic and/or unplanned thermal transients such as those present in radiant tubes for production casting of aluminum parts for automobiles.

More specifically, the objective of the proposed activity was to apply this methodology for characterizing thermal shock damage of the monolithic SiC, and uniaxial (1-D) and 0/90 (2-D) SiC $(SCS\text{-}6)_f$-SiC matrix CFCCs manufactured by Textron Systems.

APPROACH

The thermal shock tests were performed using water quench technique and the damage was characterized by destructive and non-destructive techniques. Destructive technique utilized strength measurements and optical microscopy before and after the thermal shock tests. The non-destructive techniques, such as Grindosonic and thermal diffusivity measurements, were used to assess damage as a function of the temperature difference during thermal shock tests and the number of thermal shock/transients. The thermal shock tests, strength measurements, optical microscopy, and Grindosonic tests were done at the University of Cincinnati, and the thermal diffusivity/thermal imaging measurements were performed at the Argonne National Laboratory. The test matrix for the monolithic SiC and each of the composites, (1-D) and (2-D), are shown in Table 3.4.5. Samples were prepared from rectangular bars supplied by Textron.

At least one sample in each condition of the mechanical test was polished before the test for microstructural characterization of the thermal shock damage. The ΔT's were chosen between 300°C to 1000°C but were not specifically listed here because the Grindosonic and microstructural characterization techniques were used to obtain incremental information to best determine the ΔT for the next test. It was particularly important to obtain this information prior to conducting too many destructive strength tests that may have consumed a considerable amount of the samples.

Table 3.4.5 Test Conditions for the Thermal Shock Study

Condition	Testing Technique		
	Mechanical Test 4 point bending	NDE thermal diffusivity	Microstructure
	----------# of Specimen----------		
as received	5	1	1
8 ΔT's*	16	8	8
cyclic, 2 ΔT's**	5	-	2
Total Samples	26	9	11
Spec. Geometry	45 x 7.6 x 2 mm	7.6 x 7.6 x 2 mm	45 x 7.6 x 2 mm

* Samples were quenched from 8 different temperatures between 300-1000° C into water bath maintained at 25° C

** Samples were repeatedly quenched from 2 different temperatures (500 and 800° C) to assess damage because of the cyclic thermal shock.

EXPERIMENTAL PROCEDURES

Three types of samples were supplied by Textron and used in this study. (1) monolithic nitride bonded SiC (NBSiC), (2) 1-D SiC$_f$/SiC (1D NBSiC/SCS-6), and (3) 2-D SiC$_f$/SiC (2D NBSiC/SCS-6) composites. The monolithic sample and composites were fabricated by similar methods by Textron using well-established techniques of preform processing by slip casting and hot-pressing. The 1-D composite had uniaxially aligned SCS-6 SiC fibers whereas the 2-D composites had alternating layers of 0 and 90 degrees fiber orientation. Each of these types of samples had some porosity after final consolidation.

Optical microscopy was used on polished samples of each type to determine the microstructures in the as-fabricated state. Specimens for the thermal shock study were fabricated from as-received specimens of the monolithic NBSiC, 1-D, and 2-D SiC$_f$/NBSiC composites by cutting into bend bars ($2.0 \times 7.5 \times 45$ mm^3 for NBSiC and $2.5 \times 7.5 \times 45$ mm^3 for composites) and two surfaces of each sample were polished to 0.3 μm surface finish for observation of damage after thermal shock tests. These sample dimensions were chosen because of the limited supply of samples, but the minimum dimension for each composite was larger than the critical size required to assure that the results were not dependent on sample size.

A water quench technique was employed to induce damage and study the thermal shock behavior of the monolithic and fiber-reinforced composites [3]. The experimental set-up for the water-quench thermal shock test is shown in Fig. 3.4.3. Specimens were held in the furnace at specific temperatures for 10 minutes to achieve a uniform temperature. The specimens were then dropped by free fall into a quench bath containing 4 liters of distilled water at room temperature. The distance from the specimen holder to the surface of water was about 0.3 m and the water bath was 0.23 m deep.

Damage to composites induced by thermal shock was assessed using both destructive and nondestructive techniques. The destructive technique involved subjecting the composite specimens to a 4-point flexure test and recording the load-displacement data from which the change in composite's ultimate strength, matrix cracking stress, work of fracture, and modulus of elasticity were determined. The flexure tests were conducted using a universal testing machine (Model 4206, Instron Corp., Canton, MA) with the loading and supporting spans of 20 and 40 mm, respectively. The crosshead speed was 0.5 mm/min. Due to the limitation on sample quantity, the baseline data were collected with three to five unquenched specimens, and the properties after thermal shock were measured with two specimens for each data point.

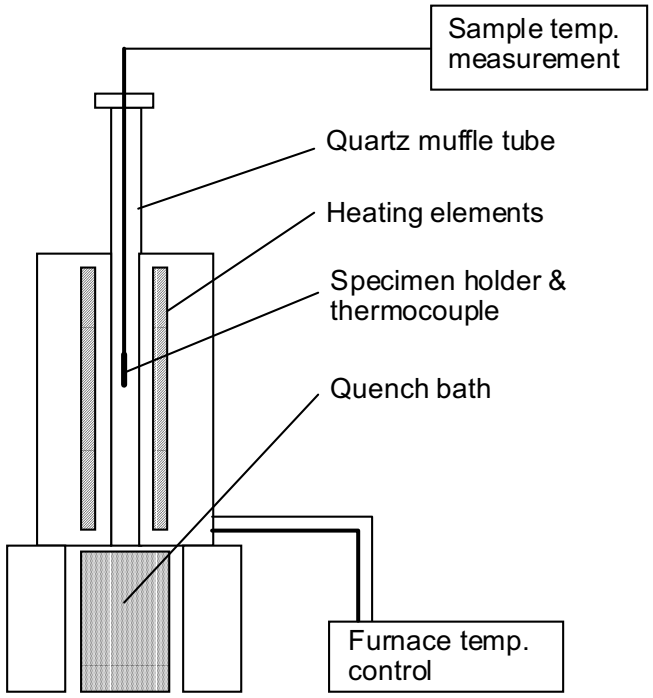

Figure. 3.4.3 Apparatus for the thermal shock study by water quench technique

One of the nondestructive techniques used in the present program consisted of measuring the Young's modulus before and after the water quench using a dynamic mechanical resonance technique (DRR) (Grindosonic MK5, J. W. Lemmens Co., St. Louis, MO). This NDE technique of monitoring the change in Young's modulus has been applied to all the samples in this study. Bar

specimens used for the strength test were also used for the Young's modulus measurement. The fundamental resonant frequency f_r (Hz) was detected and the Young's modulus E (Pa) was calculated according to the following equation [18, 19]:

$$E = A\frac{\rho l^4 f_r^2}{t^2} T \qquad (1)$$

where A = 0.94642, ρ is the density of the specimen (kg/m^3), l is the length (m), t is the thickness (m), and T is an accepted correction factor [19]. The effect of thermal shock on the Young's modulus was examined as a function of both quench temperature difference and number of quench cycles (cyclic thermal shock).

Another nondestructive technique of thermal imaging was also used to characterize thermal shock damage. This technique utilized specimens with 7.6 mm X 7.6mm X 3mm dimensions. An infrared thermal imaging system was used for full-field through-thickness measurement of thermal diffusivity distributions [20] based on the theoretical model of 1-D conductive heat transfer solution proposed by Parker [21]. In this technique, the front surface of a sample is heated instantaneously and the temperature rise of the back surface is measured as a function of time. Thermal diffusivity (α) is then calculated from the "half-rise-time" ($t_{1/2}$) and sample thickness (L) as,

$$\alpha = 1.37\, L^2/\pi^2\, t_{1/2}\,. \qquad (2)$$

The thermal imaging system is fully automated and included an IR camera with focal plane array of 256X256 InSb detectors, a PC equipped with digital frame grabber, and a flash lamp system for thermal impulse. Specimens of the monolithic and composites were scanned before the thermal shock tests. These identical samples were then scanned after the thermal shock tests at different ΔT's in order to determine changes in thermal diffusivity because of the thermal shock damage. Thermal images were also obtained of these samples before and after the thermal shock tests.

The thermal shock damage can occur in the form of changes in elastic modulus, matrix cracking and ultimate strengths, and interfacial properties, as well as fiber failure and oxidation of fibers or interfacial regions. Thus, characterization of these damage processes are not trivial in fiber-reinforced composites. A detailed microstructural examination of thermally shocked samples was also done to identify the nature of damage and to relate it to changes in mechanical properties because of the thermal shock.

Results and Discussion

The as-received specimens (monolithic NBSiC, 1-D, and 2-D SiC$_f$ /NBSiC composites) were characterized before and after the thermal shock tests using destructive and non-destructive techniques. The DMR (dynamic mechanical resonance) was used to measure the modulus of materials before their thermal shock tests. After the DMR measurements, three to four specimens were tested for mechanical properties using 4 point bend technique to establish the baseline mechanical properties before thermal shock. Samples were then given thermal shock from different ΔT's and their mechanical properties were determined after the shock tests.

Destructive Techniques:

Typical load-displacement curves of samples tested in the as-received state are shown in Fig.3.4.4. It shows that the monolithic NBSiC exhibits brittle behavior whereas composites clearly show the nonlinear deformation typical of composites. The matrix cracking stresses of the composites are statistically close to the ultimate strength of the monolithic NBSiC. In contrast, the ultimate strengths of composites are about three and two times higher than the monolithic NBSiC for 1-D and 2-D SiC$_f$ /NBSiC composites, respectively. It is also found that, to prevent the shear failure in composites during bend test, the specimen thickness needs to be smaller than 2.5 mm (a ratio of outer span to thickness of 16).

A summary of the matrix cracking stress, ultimate strength, and modulus of the monolithic and composites are given in Table 3.4.6. The modulus values of NBSiC measured from DMR and 4 point bend tests are similar. However, for composites, the modulus values measured from 4 point bend tests are smaller than those from DMR. Nevertheless, the results of DMR are consistent with the modulus data provided by Textron, namely, 124 to 152 GPa and these values were used as the baseline moduli of the as-received samples for comparison with values after the thermal shock.

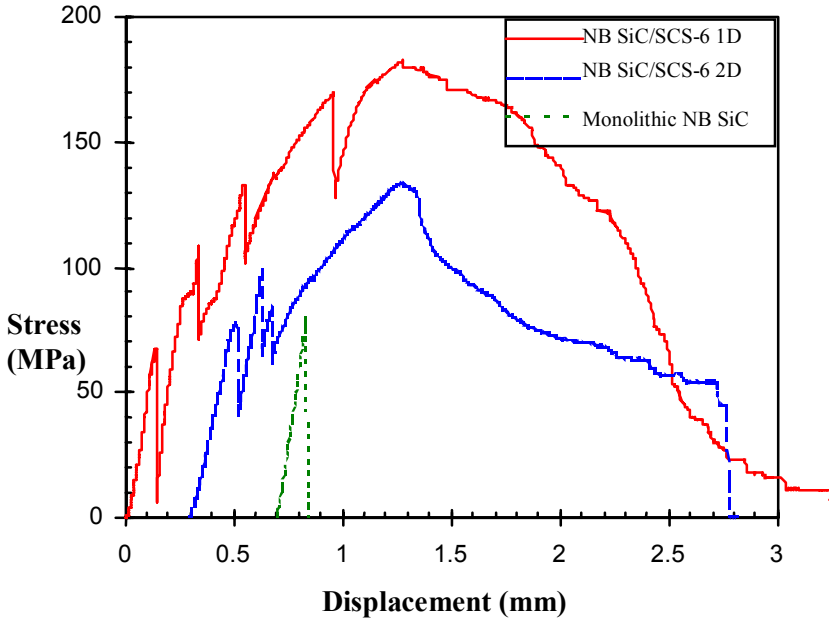

Figure 3.4.4 Typical load-displacement curves of the monolithic NBSiC, 1-D (NBSiC/SCS-6), and 2-D (NBSiC/SCS-6) SiC_f/SiC composites. The curves have been displaced horizontally for clarity.

Table 3.4.6 A summary of the mechanical properties obtained from the dynamic mechanical resonance and 4 point bend tests

Materials	DMR	4 Point Bend Test		
	Modulus (GPa)	Modulus (GPa)	Matrix Cracking Stress (MPa)	Strength (MPa)
NBSiC	124.1 ± 13.9	117.0 ± 21.3	—	58.4 ± 19.6
1-D SiC_f/SiC	153.5 ± 9.0	127.0 ± 5.7	83.5 ± 15.2	172.1 ± 13.8
2-D SiC_f/SiC	137.7 ± 7.0	107.9 ± 8.3	65.2 ± 17.4	137.5 ± 5.9

Thermal shock tests were performed by heating samples to different temperatures, holding them at the temperature for 15 minutes, and then inducing thermal shock by water quenching technique. The temperature difference between the furnace and water bath, ΔT, was varied from 300 to 1000°C. The tests were conducted on bend bars (2.0 × 7.5 × 45 mm^3 for NBSiC and 2.5 × 7.5 × 45 mm^3 for composites). After thermal shock tests, flexure tests using four point bend technique were conducted using a MTS mechanical testing machine using outer and inner spans of 40 and 20 mm, respectively. The loading rate of the test is 0.5 mm/min.

Figure 3.4.5 shows the flexure strength after thermal shock as a function of the quench temperature difference (ΔT). A degradation of flexure strength is evident at ΔT as low as 400°C for all materials. But, there appears to be more degradation to the monolithic NBSiC than to composites. In fact, the monolithic samples had strength of only about 30 MPa after ΔT of 400° C whereas composites displayed a gradual loss in strength with increasing severity of the thermal shock and all composites showed superior flexure strength than the monolithic. At ΔT > 700°C, the

flexure strength of 1-D composite was much higher than that of the 2-D composite. This may be related to the fiber orientation but more work is needed to understand this difference.

Figure 3.4.6 shows the influence of thermal shock (ΔT) on the first matrix cracking stress. The strength of the monolithic NBSiC is also plotted for comparison. An initial drop of the matrix cracking stress is observed at ΔT of 400°C. At ΔT < 600°C, the matrix cracking stress of composites is higher than the matrix strength, showing a strengthening effect of the fibers. However, at ΔT > 700°C, the matrix cracking stress of composites approached the matrix strength, indicating little contributions from fibers.

The dependence of the elastic modulus obtained from flexure test as a function of ΔT is shown in Fig. 3.4.7. The monolithic NBSiC shows degradation in modulus at ΔT of 400°C. In contrast, the modulus of composites does not degrade until ΔT > 700°C. This trend is consistent with the results measured by the dynamic mechanical resonance, DMR, technique, which was reported previously.

It should be noted that all materials used in this study contain 20 to 25% porosity. Consequently, the results of the mechanical tests may display a large variation in property from sample to sample because of the sampling. Unless more tests are conducted to obtain a statistical distribution, these results may not represent an actual value but only offer a general trend in the thermal shock damage.

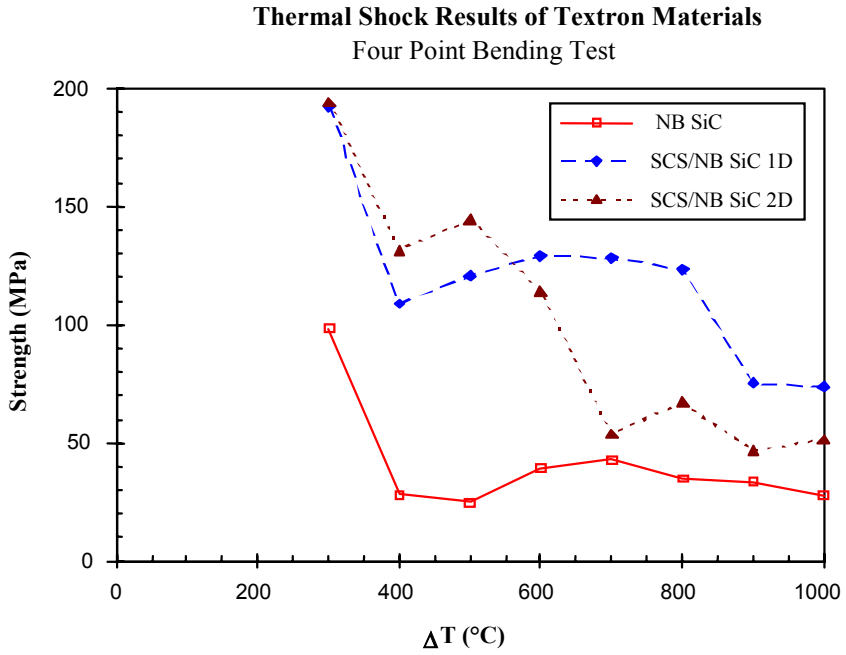

Figure 3.4.5 The flexure strength after thermal shock testing versus quench temperature difference for Textron monolithic NBSiC, 1-D (NBSiC/SCS-6), and 2-D (NBSiC/SCS-6) SiC$_f$/SiC composites.

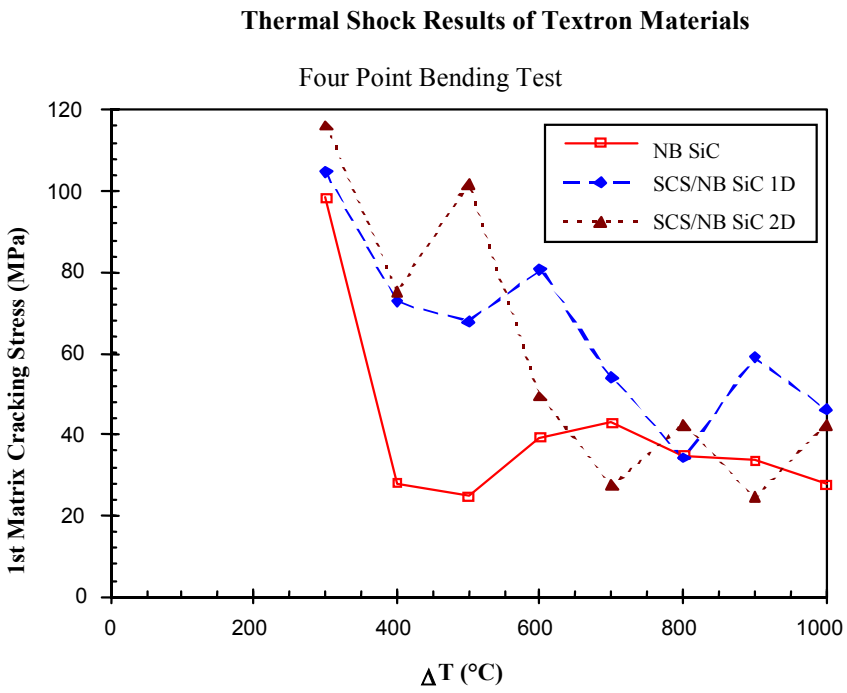

Figure 3.4.6 The first matrix cracking stress versus quench temperature difference for Textron 1-D, and 2-D SiC$_f$/NBSiC composites. Flexure strength of the monolithic NBSiC is also plotted for comparison.

After thermal shock tests, samples were examined under optical microscope. Figures 3.4.8 and 3.4.9, for examples, show evidence of the thermal shock damages in 2-D composites at ΔT of 1000°C. The matrix cracks evident in this figure are created upon thermal shock and propagated through several silicon carbide grains, as seen in Fig. 3.4.8. Figure 3.4.9 shows the fiber damage to the exposed fibers due to thermal shock at ΔT of 1000°C. These cracks are expected to be responsible for the loss of modulus and strength upon thermal shock of the monolithic and composites of this study.

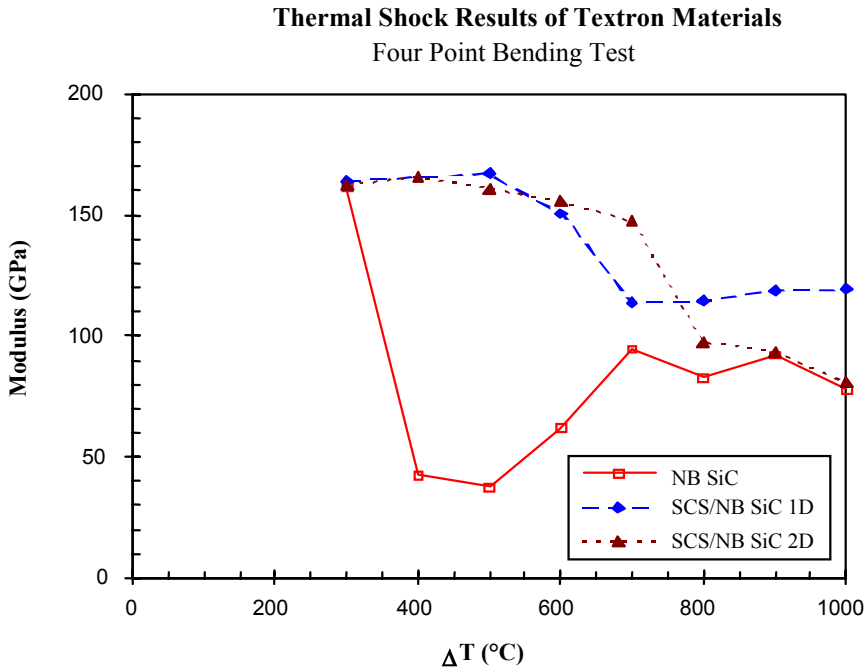

Figure 3.4.7 The modulus of flexure versus quench temperature difference for Textron monolithic NBSiC, 1-D, and 2-D SiC$_f$/NBSiC composites

Non-Destructive Techniques:

Dynamic Mechanical Resonance (DMR) and Thermal Imaging non-destructive techniques were also used in this program to characterize damage by thermal shock. These results are described below.

Figure 3.4.8 Matrix cracking was observed in 2-D composite after thermal shock test at ΔT of 1000°C.

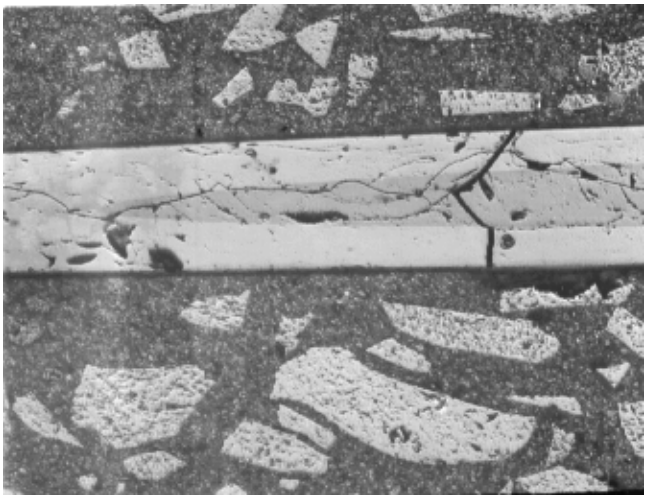

Fig**ure 3.4.9** Damage to fibers due to the thermal shock at ΔT of 1000°C of a 2-D composite.

(a) DMR Technique

The advantage of dynamic mechanical resonance (DMR) technique (grindosonic) in monitoring changes to elastic modulus because of the thermal shock damage resides in the fact that it can be performed on the same sample before and after the thermal shock to avoid problems of sample to sample variability. Thermal shock tests were performed by heating samples to different temperatures, holding the temperature for 15 minutes, and then inducing thermal shock by a water quenching technique. The temperature difference between the furnace and water bath, ΔT, was varied from 300 to 1000°C with 100°C increment. In addition, two temperatures, 500°C and 800°C were selected for the cyclic thermal shock testing. The cyclic test was stopped when no evident degradation in modulus was detected. All tests were conducted on bend bars specimen ($2.0 \times 7.5 \times 45$ mm^3 for NBSiC and $2.5 \times 7.5 \times 45$ mm^3 for composites). The data of thermal shock tests were reported with the percentage of the retained modulus versus ΔT, where the retained values were calculated by comparing data before and after thermal shock tests.

Figure 3.4.10 shows data of the retained Young's modulus as a function of the quench temperature difference (ΔT). The results show that the retained modulus of the monolithic NBSiC drops from 92% at ΔT of 400°C to 75% at ΔT of 1000°C. An additional drop of the retained modulus is observed at ΔT of 500°C. For composites, the retained modulus is better than the monolithic samples at all temperatures. At ΔT < 600°C the average retained modulus is about 94% and dropped to 87% and 83% for 1-D and 2-D composites, respectively, at ΔT > 700°C. It is noted that all materials exhibited drop in modulus at a specific temperature. This occurs at 500°C for the monolithic NBSiC and over a range between 700 and 800°C for the composites. Consequently, the better thermal shock resistance of composites than the monolithic is shown by not only higher retained modulus values but also a higher ΔT for a more severe thermal shock

damage. Furthermore, the 1-D composites generally exhibit a better thermal shock resistance than the 2-D composites, especially at $\Delta T > 700°C$.

Figure 3.4.11 shows results of the cyclic thermal shock tests. The retained modulus (%) is plotted as a function of the number of thermal shock tests at ΔT of 500°C and 800°C. These results show that most of the thermal shock degradation occurs in the early stages of the test and saturates by the third thermal shock cycle. This indicates a very good cyclic thermal shock resistance for these three Textron materials. Figure 3.4.11 also shows that 1-D composites have the best thermal shock resistance than the other two materials at ΔT of 500°C and 800°C. For 2-D composites, better thermal shock resistance than the monolithic NBSiC is found at ΔT of 500°C and first cycle at ΔT of 800°C, but the retained modulus (%) falls below that of the silicon carbide after the second cycle at ΔT of 800°C. Nevertheless, it should be noted that the modulus value of the 2-D composite (112 GPa) is still higher than that of the monolithic (95 GPa) at ΔT of 800°C, as shown in Table 3.4.7.

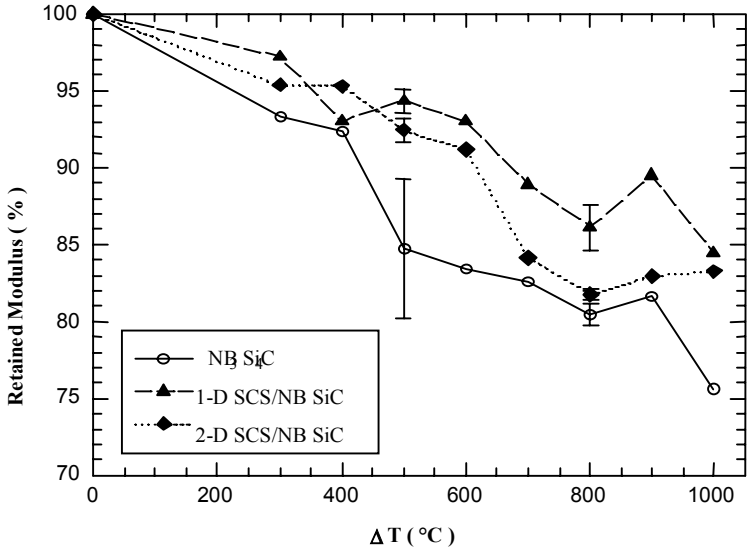

Figure 3.4.10 The retained modulus after thermal shock test versus quench temperature difference for Textron monolithic NBSiC, 1-D, and 2-D SiC_f/NBSiC composites.

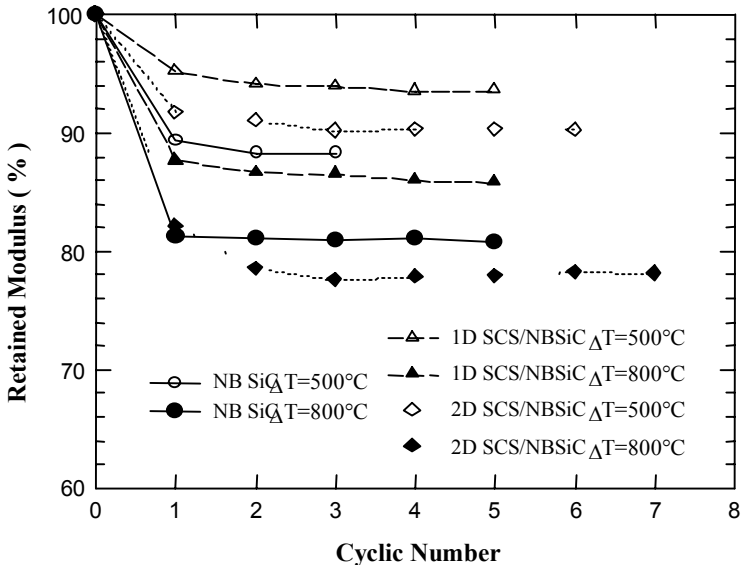

Figure 3.4.11 The retained modulus of Textron monolithic NBSiC, 1-D, and 2-D SCS /NBSiC composites after cyclic thermal shock tests at □T=500° and ΔT=800°C.

Table 3.4.7 Data of cyclic thermal shock tests for Textron monolithic NBSiC, 1-D, and 2-D SiC*f* /NBSiC composites. The number in the left column (#) indicates the number of the thermal shock tests.

	NBSiC				**1-D Composite**				**2-D Composite**			
	ΔT=500°C		ΔT=800°C		ΔT=500°C		ΔT=800°C		ΔT=500°C		ΔT=800°C	
#	GPa	%	GPa	%	GPa	%	GPa	%	GPa	%	GPa	%
0	125.8	100	118.1	100	140.7	100	152.8	100	145.7	100	144.1	100
1	112.3	86.0	95.9	77.2	133.9	93.1	133.9	85.8	133.6	90.3	118.4	79.1
2	111.1	85.0	95.7	77.0	132.4	92.1	132.3	84.8	132.5	89.6	113.2	75.6
3	111.1	85.0	95.6	77.0	132.1	91.9	132.1	84.7	131.3	88.7	111.7	74.7
4			95.8	77.1	131.6	91.5	131.3	84.2	131.5	88.9	112.1	74.9
5			95.4	76.8	131.6	91.5	131.0	84.0	131.5	88.8	112.2	75.0
6									131.4	88.8	112.7	75.3
7											112.5	75.2

(b) Thermal Imaging

Thermal diffusivity images of 7.6 mm X 7.6 mm X 3mm Textron monolithic silicon carbide (NBSiC), and 1-D (NBSiC/SCS-6), 2-D (NBSiC/SCS-6) composites were measured on 8 different samples before and after thermal shock at 300°, 400°, 500°, 600°, 700°, 800°, 900°, and 1000° C. The quenched and unquenched images are shown in Fig. 3.4.12 for the monolithic NBSiC. There is an evidence of general darkening (lower diffusivity) after ΔT of 400° C and then an evidence of increased diffusivity after ΔT of 700° C although the quenched samples always show thermal diffusivity lower than the corresponding unquenched samples. No attempts were made to scale these images of different samples. Thermal diffusivity images from 1-D and 2-D composites are shown in Figs. 3.4.13 and 3.4.14 which also show evidence of reduced diffusivity with increasing quench temperature. The thermal diffusivity of a few samples were scaled for comparison in the unquenched and quenched states. These images are shown in Figs. 3.4.15 and 3.4.16 and show a change in topology of thermal diffusivity after thermal shock indicating damage. For example sample #4 of 1-D NBSiC/SCS-6 quenched at 700° C show an evidence of crack-like feature after thermal shock. Since no surface cracks were apparent on this sample, these could be internal cracks. But, this needs to be verified by microstructural examination.

Besides thermal imaging, the average thermal diffusivity of these samples were also measured and changes to average diffusivity are plotted as a function of ΔT in Fig. 3.4.17. In addition, Table 3.4.8 gives a summary of the same data. There is a general decrease in thermal diffusivity with ΔT for all samples. The monolithic (NBSiC) sample display a 20% drop, 2-D composites show a 15% drop, and 1-D samples show 25% drop because of the thermal shock. These results have clearly shown that thermal imaging can be used to assess damage to composites because of the thermal shock.

Table 3.4.8 Mean Thermal Diffusivity (mm^2/s) of the Monolithic and Composites from Textron Systems

Monolithic-NBSiC				Composite-1D				Composite-2D			
#	ΔT-°C	U*	Q**	#	ΔT-°C	U*	Q**	#	ΔT-°C	U*	Q**
1	300	9.7	10.1	13	300	7.3	7.7	1	300	10.2	10.3
2	400	9.7	9.9	11	400	7.9	9.0	2	400	10.1	10.0
3	500	7.8	7.3	10	500	10.3	11.2	3	500	9.7	9.2
4	600	8.2	6.8	9	600	8.8	9.0	4	600	11.3	9.8
5	700	9.8	8.4	4	700	10.0	9.4	5	700	10.3	8.8
6	800	10.0	8.5	3	800	11.1	9.7	6	800	10.0	8.0
7	900	10.1	8.8	2	900	11.1	8.1	7	900	11.4	9.8
8	1000	9.3	8.6	1	1000	11.2	8.8	8	1000	12.7	11.0

* U-Unquenched ** Q-Quenched

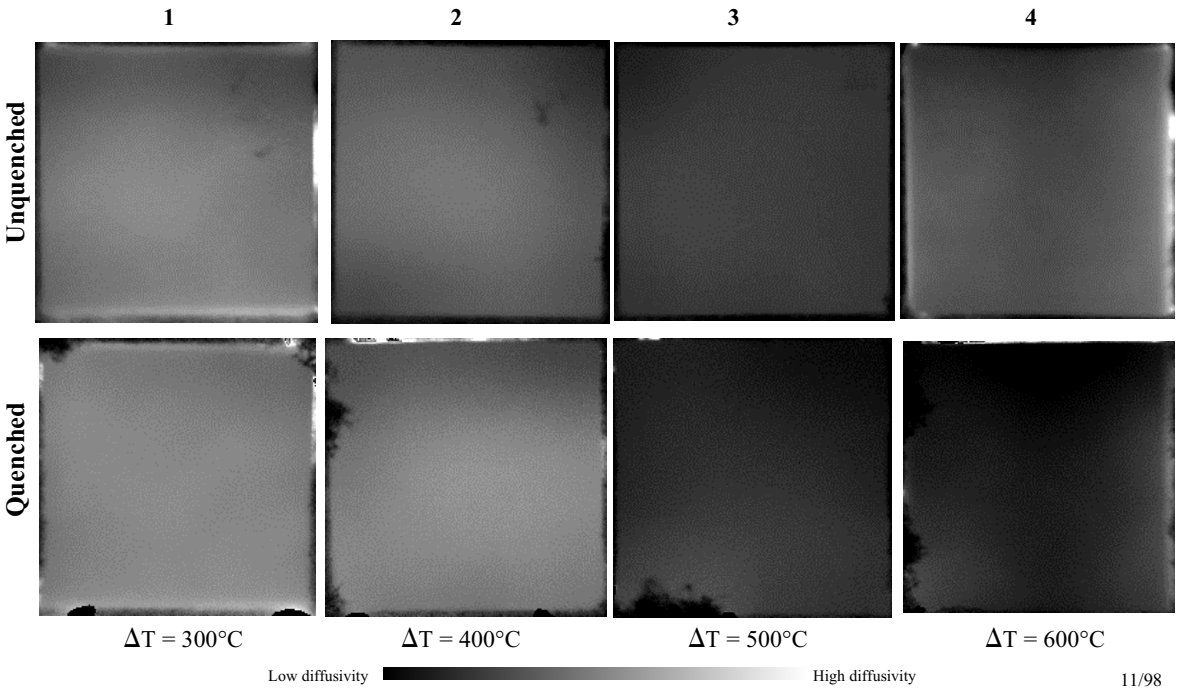

Figure 3.4.12a Thermal Diffusivity Images of Textron Monolithic Silicon Nitride (NBSiC) Samples from University of Cincinnati

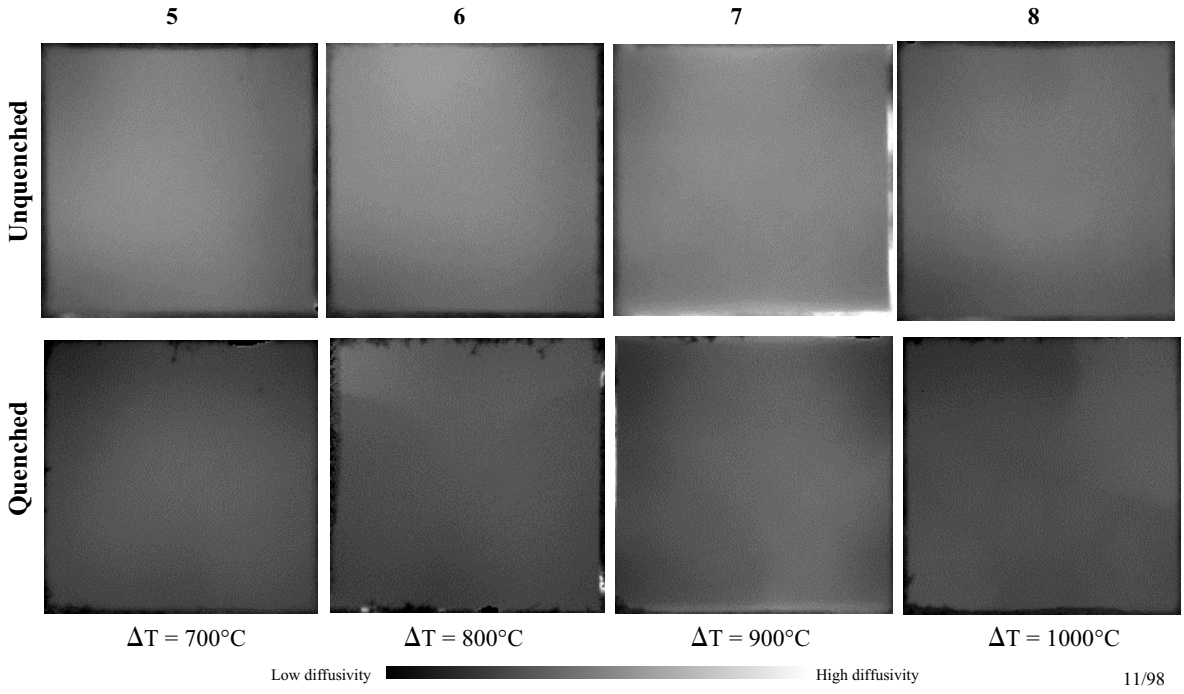

Figure 3.4.12b Thermal Diffusivity Images of Textron Monolithic Silicon Nitride (NBSiC) Samples from University of Cincinnati

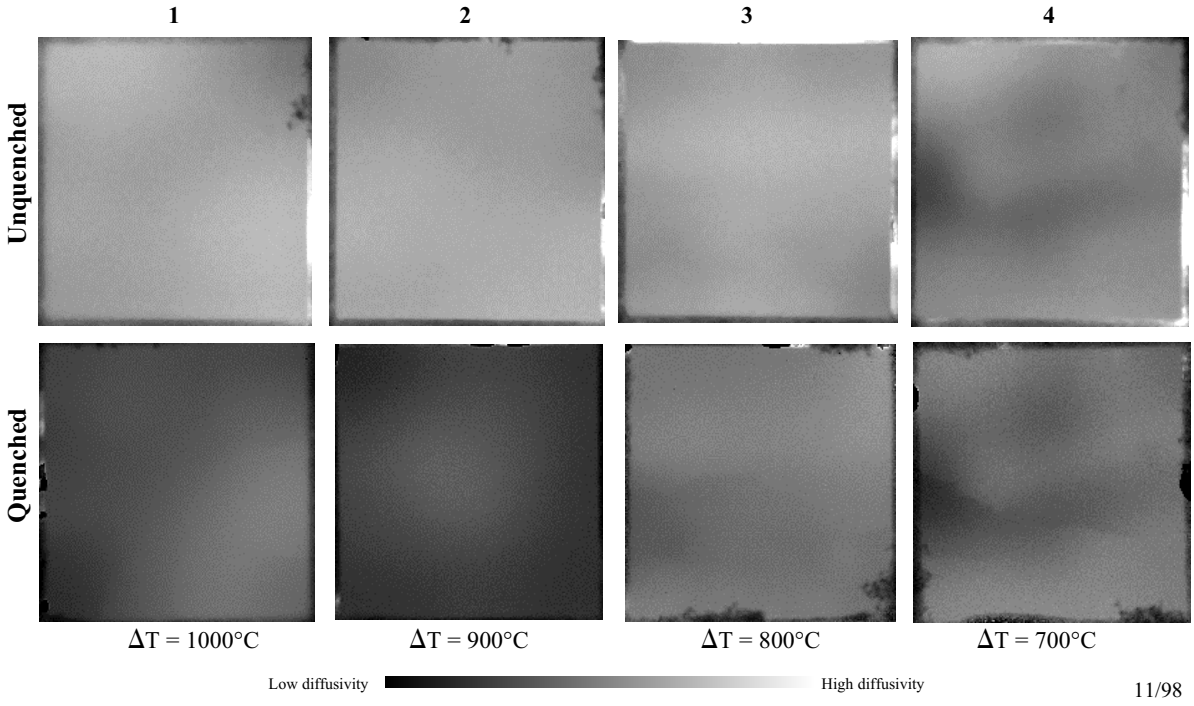

Figure 3.4.13a Thermal Diffusivity Images of Textron 1-D SCS Fiber Reinforced Silicon Carbide (1D NBSiC/SCS-6) Samples from University of Cincinnati

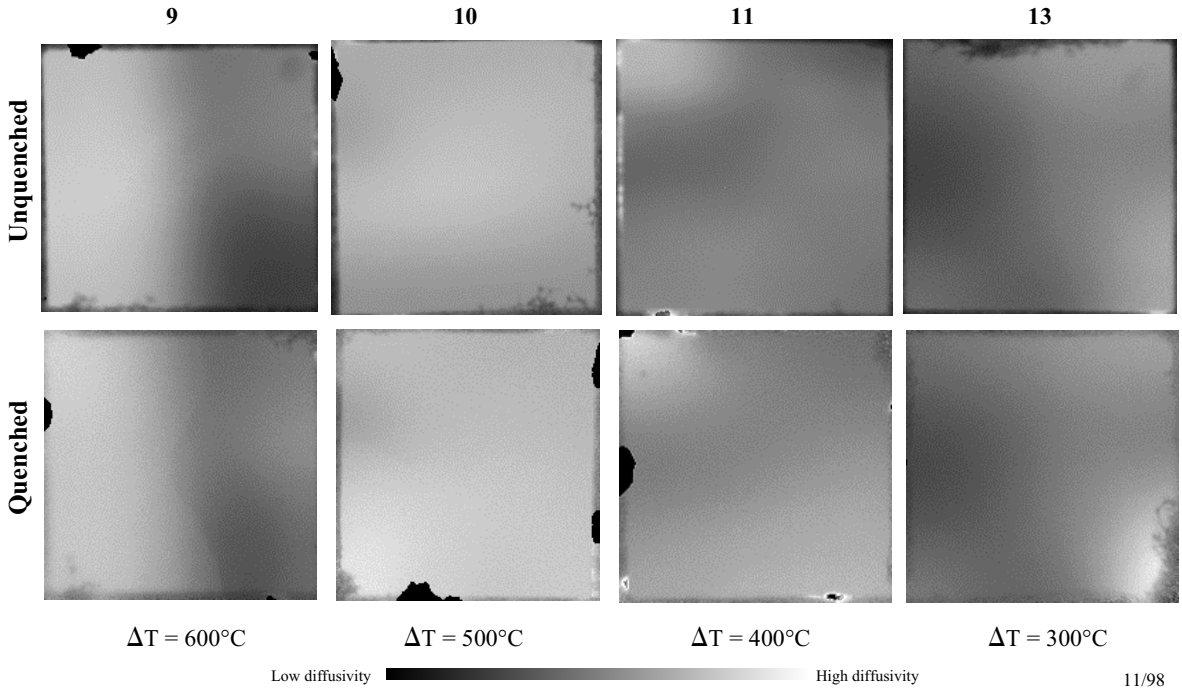

Figure 3.4.13b Thermal Diffusivity Images of Textron 1-D SCS Fiber Reinforced Silicon Carbide (1D NBSiC/SCS-6) Samples from University of Cincinnati

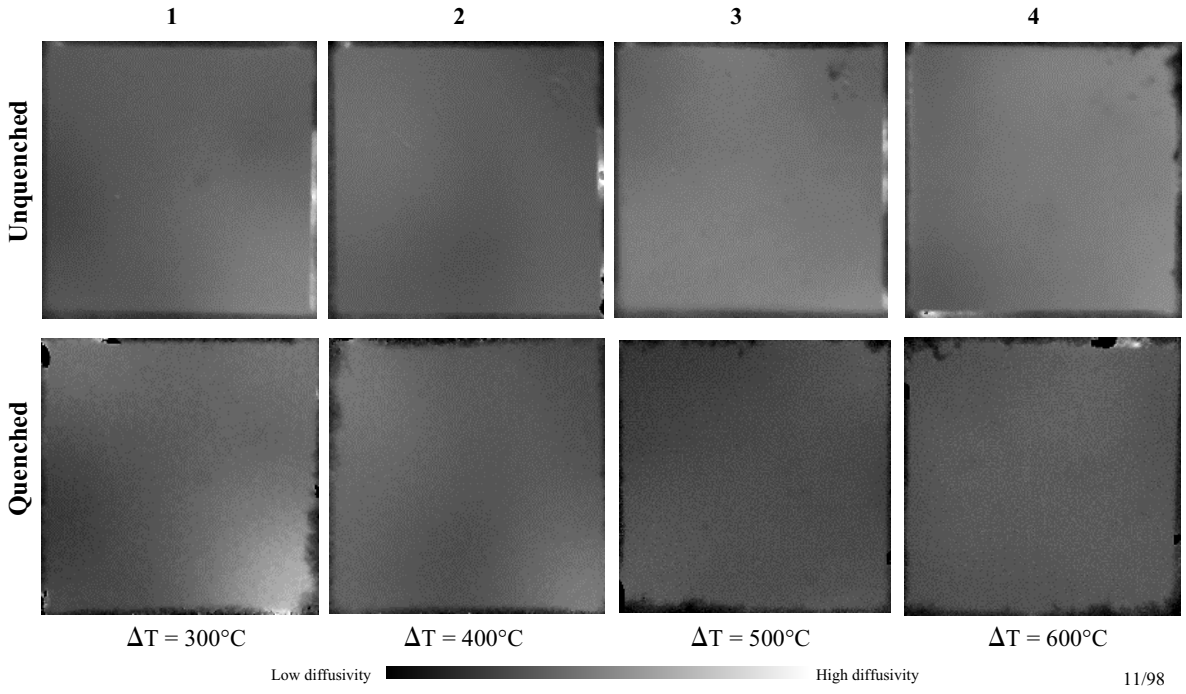

Figure 3.4.14a Thermal Diffusivity Images of Textron 2-D SCS Fiber Reinforced Silicon Carbide (2D NBSiC/SCS-6) Samples from University of Cincinnati

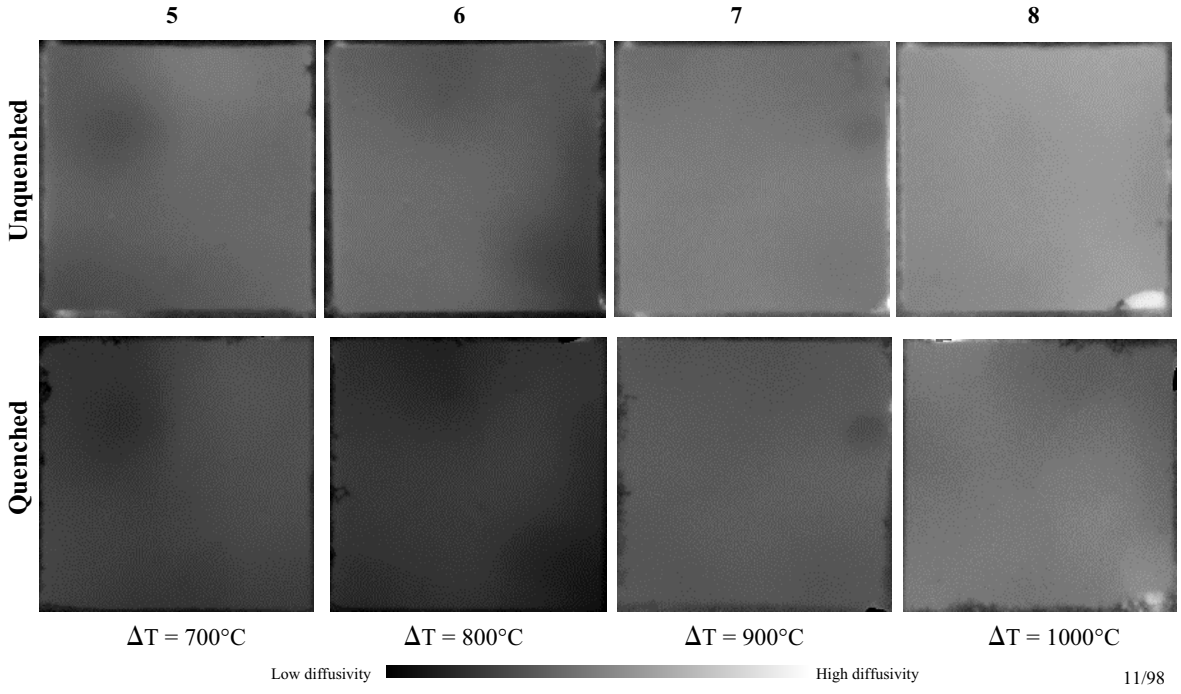

Figure 3.4.14b Thermal Diffusivity Images of Textron 2-D SCS Fiber Reinforced Silicon Carbide (2D NBSiC/SCS-6) Samples from University of Cincinnati

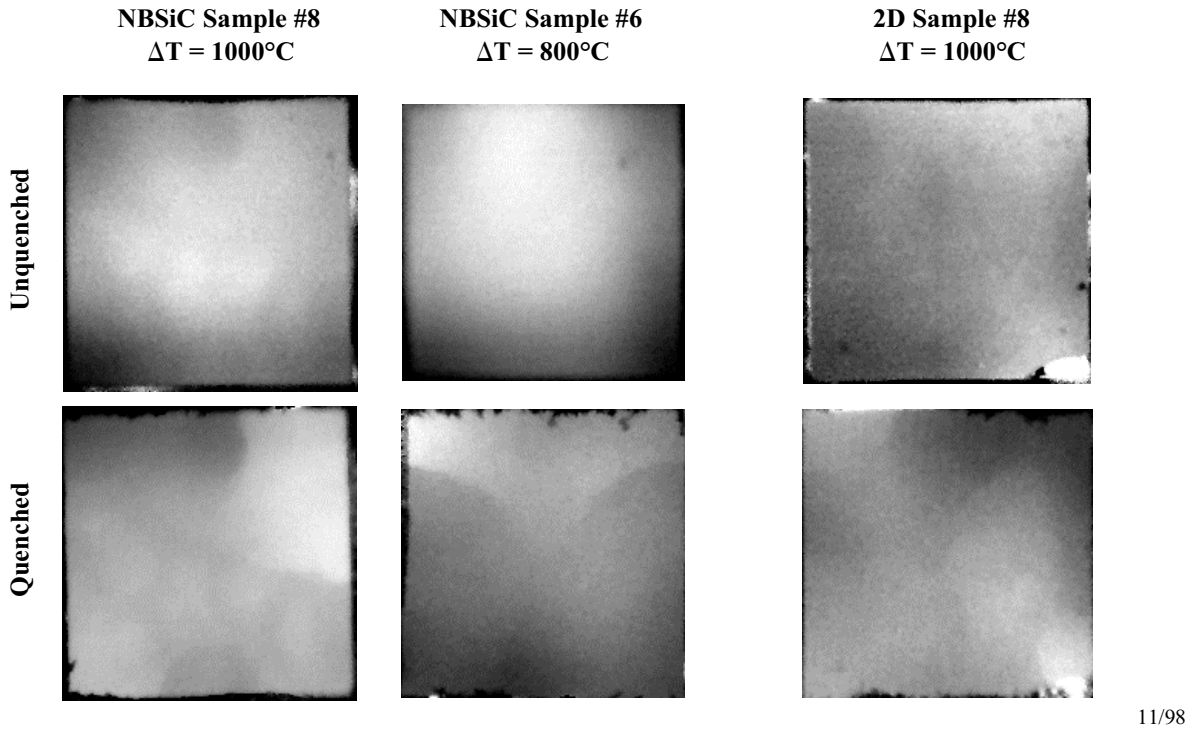

Figure 3.4.15 Comparison of Thermal Diffusivity Images

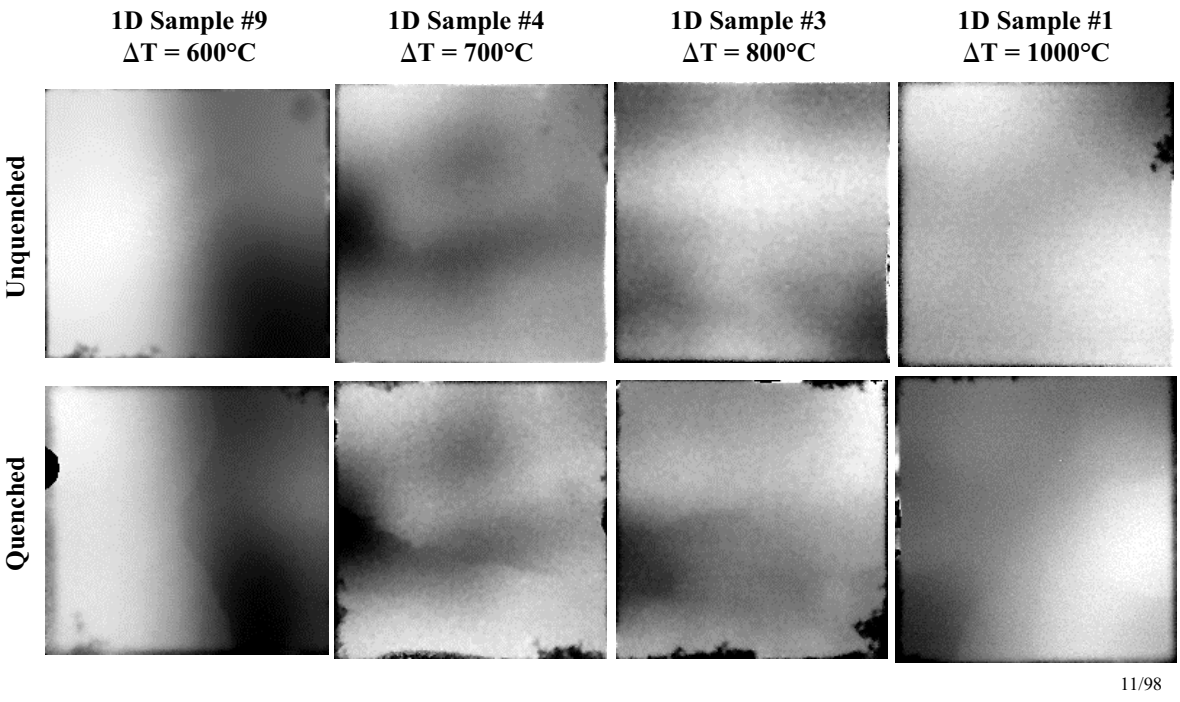

Figure 3.4.16 Comparison of Thermal Diffusivity Images

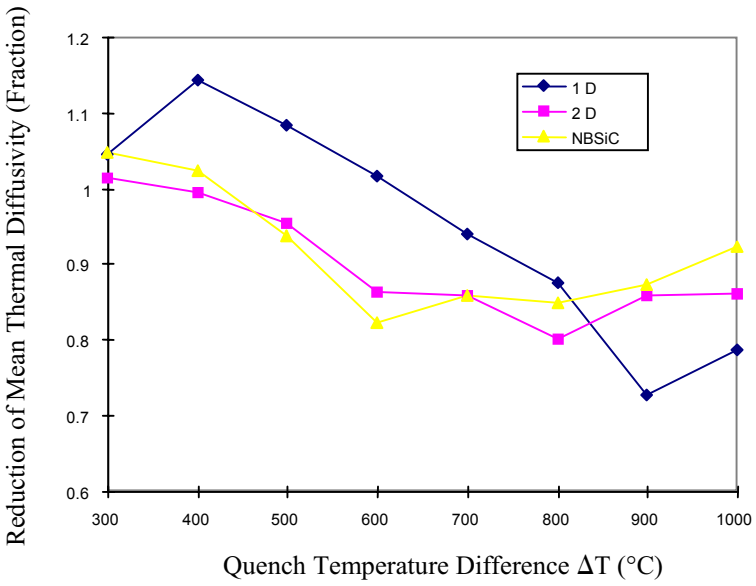

Figure 3.4.17 Reduction of Mean Thermal Diffusivity Due to Thermal Shock

ACKNOWLEDGMENTS

We thank Dr. Yu-Lin Wang for performing the thermal shock study at the University of Cincinnati, Drs. J. Sun and W. Ellingson, and C. Deemer of the Argonne National Laboratory for performing the thermal diffusivity experiments. The encouragement, interest, and support of Bill Darden of Textron Systems and Jill Jonkouski of the DOE-Chicago operations are very much appreciated. This work was performed through a subcontract from Textron as a part of their DOE-CFCC program.

REFERENCES

1. H. Wang and R. N. Singh, "Thermal Shock Behavior of Ceramics and Ceramic Composites," *Int. Mater. Reviews*, 39[6], 228-244 (1994).
2. D. P. H. Hasselman, "Unified Theory of Thermal Shock Fracture Initiation and Crack Propagation in Brittle Ceramics," *J. Am. Ceram. Soc.*, 52 [11] 600-604 (1969).
3. A. G. Evans and E. A. Charles, "Structural Integrity in Severe Thermal Environments," *J. Am. Ceram. Soc.*, 60 [1-2] 22-28 (1977).
4. H.-A. Bahr and H.-J. Weiss, "Heuristic Approach to Thermal Shock Damage Due to Single and Multiple Crack Growth," *Theor. Appl. Fract. Mech.*, 6, 57-62 (1986).
5. M. V. Swain, "R-Curve Behavior and Thermal Shock Resistance of Ceramics," *J. Am. Ceram. Soc.*, 73 [3] 621-28 (1990).
6. A.G. Evans, "The Mechanical Performance of Fiber Reinforced Ceramic Composites," *Mater. Sci. and Eng*. A107, 227-239 (1989).
7. H. Wang, R.N. Singh and R. A. Lowden, " Thermal Shock Behavior of Continuous Fiber Ceramic Composites (CFCC's)," Ceram. Eng. Sci. Proc., 15[4], 292-302 (1994).
8. R.N. Singh and H. Wang, " Thermal Shock Behavior of Fiber-Reinforced Ceramic Matrix Composites," Proc. MRS Symp, 365, 441-447 (1995).
9. R.N. Singh and H. Wang, " Thermal Shock Behavior of Fiber-Reinforced Ceramic Matrix Composites, " Composites Engineering, 5[10-11], 1287-1297 (1995).
10. H. Wang, R.N. Singh and R.A. Lowden," Thermal Shock Behavior of 2-D Woven Fiber-Reinforced Ceramic Composites," J. Am. Ceram. Soc., 79[7], 1783 (1996).
11. R.N. Singh and H. Wang, " Mechanisms of Thermal Shock Damage in Fiber-Reinforced Ceramic Matrix Composites," Ceram. Eng. Sci. Proc., 16(5), 699-707 (1995).
12. H. Wang and R.N. Singh, " Thermal Shock Behavior of Unidirectional, 0/90, and 2-D Woven Fiber-Reinforced CVI SiC Matrix Composites," J. Mater. Sci. (1997) in press.
13. H. Wang, R.N. Singh, S.B. Beecher, and R.W. Dinwiddie " Thermal Shock Behavior of Fiber Reinforced Composites," Ceramic Transactions, 46, 673-683 (1994).
14. J.E. Webb, R.N. Singh, and R.A. Lowden, " Thermal Shock Damage in a 2-D Woven Fiber-Reinforced CVI SiC Matrix Composite," J. Am. Ceram. Soc., 79[7], 1783 (1996).
15. J.E. Webb, R.N. Singh, and R.A. Lowden, " Damage Evolution Due to Thermal Shock in a 2-D Woven Fiber-Reinforced CVI SiC Composite," Ceram. Eng. Sci. Proc., 17[4], 203 (1996).
16. J.E. Webb, R.N. Singh, and R.A. Lowden, " Shear Strength and Non-Destructive Evaluation of Thermally Shocked CFCC's," Ceram. Eng. Sci. Proc., v. 18 (1997).
17. P. F. Tortorelli, C. A. Wijayawardhana, L. Riester, and R. A. Lowden, "Oxidation Effects on Nextel™-Reinforced SiC," *Ceram. Eng. Sci. Proc*., **15** [4] 262-71 (1994).
18. G. Pickett, "Equations for Computing Elastic Constants from Flexural and Torsional Resonant Frequencies of Vibration of Prisms and Cylinders," *Proceedings, Am. Soc. Testing Mater.*, **45**, 846-65 (1945).
19. S. Spinner and W. E. Tefft, "A Method for Determining Mechanical Resonance Frequencies and for Calculating Elastic Moduli from These Frequencies." *Proceedings ASTM*, **61**, 1229-43 (1961).
20. J. Stuckey, J.G. Sun, and W.A. Ellingson, " Rapid Infrared Characterization of Thermal Diffusivity in Continuous Fiber Ceramic Composite Components," Presented at 8th Int. Symp. on Nondestructive Characterization of Materials, Boulder, CO, June 15-20, (1997).
21. W. J. Parker, R.J. Jenkins, C.P. Butler, and G.L. Abbott, " Flash Method of Determining Thermal Diffusivity, Heat Capacity, and Thermal Conductivity," J. Appl. Phys., 32, 1679- 1684 (1961).

Stress (MPa), Strength (MPa), **Matrix Cracking Stress (MPa)**, **Modulus (GPa)**, **Modulus (%)**, **Retained Modulus (%)**

Thermal and Mechanical Characterization of SCS-6 Reinforced Immersion Tube

ABSTRACT

Textron Systems provided Southern Research Institute (SoRI) with a CFCC immersion tube reinforced with ~ 2.5 vol. % SCS-6 fiber for destructive testing. The test effort included evaluations to determine the axial, circumferential, and hoop mechanical properties, the fracture durability, and the thermal expansion characteristics of the composite tubes. The test methods, results, and raw experimental data obtained are as follows:

TEST MATRIX AND CUTTING PLANS

The test matrix shown in Table 3.4-8 identifies the test type, orientation, and test temperature performed for this effort. All of the specimens were machined by Chand Associates, Worcester, MA, from tube sections provided by Textron. The samples were subsequently shipped to Southern for evaluation.

Table 3.4-8 Test Matrix for the SCS8 Reinforced SiC Tubes

Test	Orientation	70°F	1600°F
Ring Tension	Hoop	7	
Flexure	Axial	20	5
Charpy	Axial	20	
CTE	Axial	2 →	→
CTE	Circumfrential	2 →	→

SPECIMEN IDENTIFICATION SYSTEM

An important part of the specimen preparation was individual specimen identification. Each specimen was assigned a unique designation. The specimen identification system employed in this investigation was as shown below:

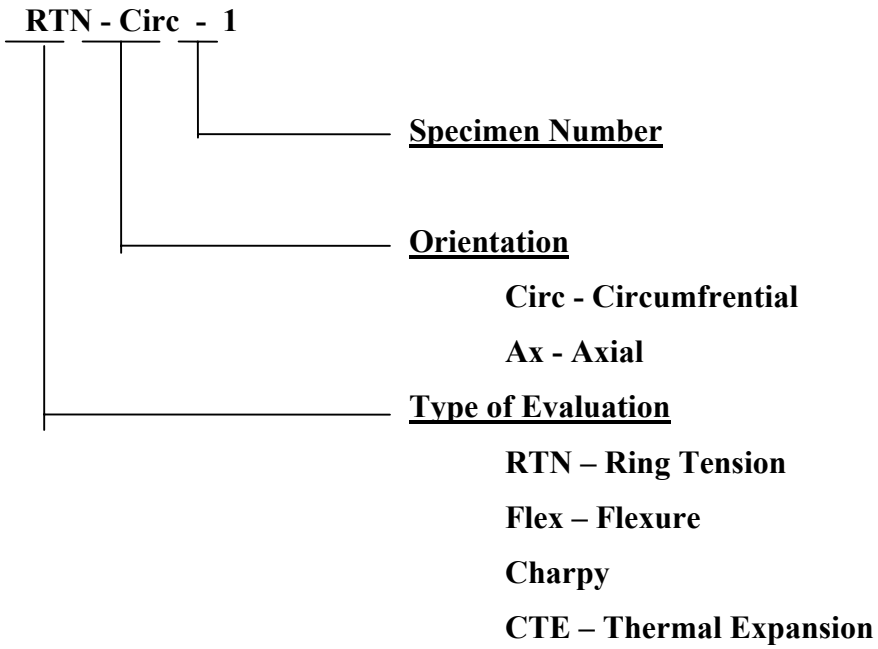

TEST PROCEDURES

NONDESTRUCTIVE CHARACTERIZATION (NDC) TESTS

Nondestructive characterization of the specimens included measurement of dimensions and weights for calculation of bulk density. In addition sonic velocity measurements were obtained in the direction of test for each finished specimen. The following paragraphs discuss the techniques utilized.

Visual Inspection Test

The surfaces of the parts were inspected for cracks, voids, discoloration, inclusions, weave geometry irregularities and surface porosity. Areas that appeared to contain such anomalies were appropriately documented.

Bulk Density

Specimen blanks were weighed on an analytical balance. Specimen blank dimensions were measured using micrometer calipers. Bulk density was calculated by dividing the weight by the volume.

Ultrasonic Measurements

Ultrasonic velocities of the specimen blanks were measured using a pulsed through-transmission technique. The basic apparatuses used for the ultrasonic measurement of velocity and attenuation was a Metrotek pulser and Tektronix 2430 Oscilloscope.

TEST CONDITIONS

The mechanical evaluations were conducted with a load rate of 10 Ksi/min. The rate was monitored throughout each test by recording the output of the clip-on extensometers against time. The thermal expansion was conducted at a standard heating rate of 10°F/sec.

RING TENSION

Description of Test

The apparatus, shown schematically in Figure 3.4.18, utilized for the hoop tensile evaluations was the Southern room temperature hydraulic ring facility. A hydraulic pressurized bladder provided the hydrostatic loading. A pressure transducer located in the rubber bladder chamber area monitored the hydrostatic pressure.

The strain measurement system consisted of a ribbon wrapped around the circumference of the cylindrical specimen and attached to a differential transducer at each end. The displacement of this ribbon, and hence, the growth of the specimens circumference was measured by two differential transducers located at each end of the ribbon.

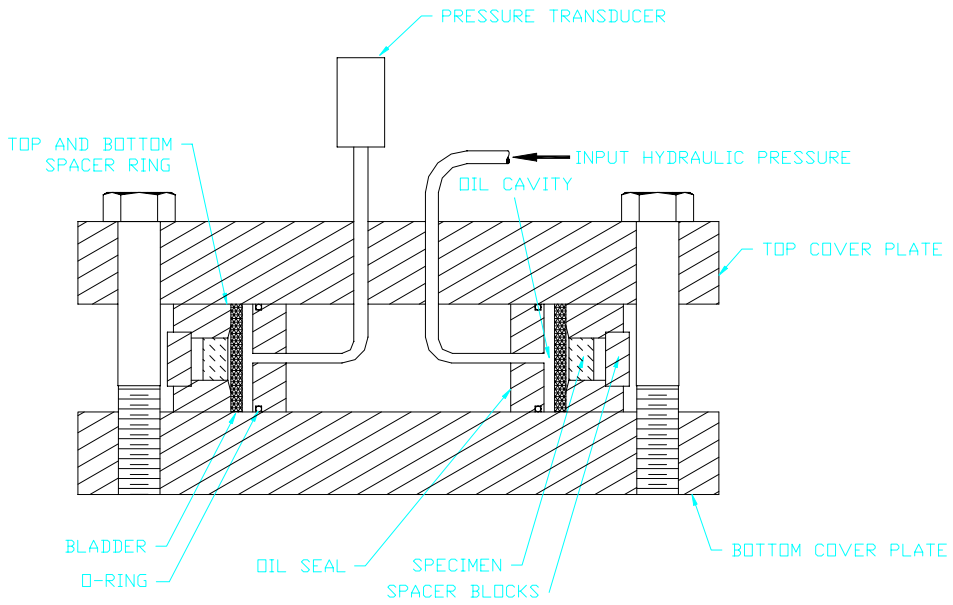

Figure 3.4.18 Schematic of Hydrostatic Ring Facility

Interpretation of Results

The output of the ring tensile evaluations was applied internal pressure versus circumferential displacement curve for each ring. These were then digitized to provide an outside diameter stress-strain curve. The stresses at the outside diameter (OD) and inside diameter (ID) of the rings were calculated using the solution for a thick-walled pressure vessel.

$$\sigma_t = \frac{r_1^2(r_2^2 + \rho^2)}{(r_2^2 - r_1^2)\,\rho^2} P_i$$

That is:

where σ_t = tangential stress, psi
r_i = inside radius, in.
r_2 = outside radius, in.
P_i = applied internal pressure, psia
ρ = radius at any point in the ring, in.

Examination of the equation indicates that the greatest tangential stress is located at the ring's ID. Hence, the strength is the ultimate stress at the ID.

Specimen Configuration

The specimen sizes were nominally 5.10" ID x 5.53" OD x 0.375" high. The individual specimen configurations can be found in the ring tension results table.

Calibration

The pressure transducer that monitored the hydraulic pressure was calibrated using a dead weight calibration fixture. System calibrations were made against a standard graphite ring.

Precision and Accuracy

The pressure transducer was accurate to 1%. The strain measurement system uncertainty was less than 5%.

FLEXURE

Description of Test

A schematic of the facility used to test flexural specimens is provided in Figure 3.4.19. The apparatus consists of three main components: a loading frame, a furnace and a system to measure the deflection at the mid length of the specimen.

Both four point and three point flexure tests are performed in this facility. A four point set-up is shown in the figure. The only alteration required for a three point test is to change the upper load block. The alignment of the load train is maintained by carefully machining each component and by the three spherical contacts. At the top of the load train is a load cell to measure the load applied to the specimen. The load cell is calibrated with either calibrated weights or in a calibrated testing machine. A shunt calibration is determined during this operation. This shunt

calibration is checked prior to each run to ensure that the calibration does not change over the duration of the program. The specimen is loaded by raising the screw jack. Since the screw is driven by a variable speed motor, either the loading rate or the deformation rate can be controlled during the test.

The deformation is measured with an LVDT. The LVDT coil is mounted within the tubular support rod. Centered in this tubular structure is a slender graphite rod. One end of the rod contacts the lower surface of the specimen. The other end is fastened to the core of the LVDT. The relative motion between the core and the coil produces an electrical output that is directly related to the deflection of the specimen. The electrical output of the LVDT is calibrated against displacement in a fixture that holds the coil and moves the core in increments determined by a supermicrometer.

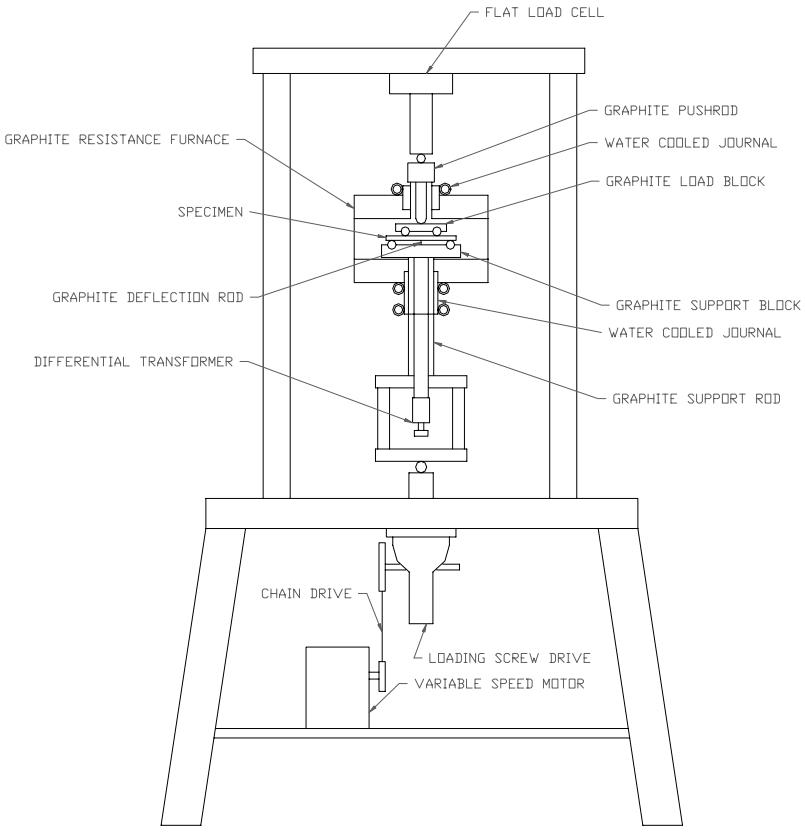

Figure 3.4.19 Schematic of the Flexural Evaluation Facility

A furnace with a graphite resistance heater is used for the tests at elevated temperatures. During these tests, the furnace is continuously purged with inert gas to prevent oxidation of the specimen. A small sight port is provided in the side of the furnace to view the specimen through an optical pyrometer; this instrument is used to determine the temperature at the mid- length of the specimen.

The test is conducted according to the following general procedures. The specimen is centered between the support and loading blocks in the furnace. (The furnace is an integral part of the load train; therefore even the room temperature tests are conducted in the furnace.) The graphite deflection rod is brought into contact with the bottom of the specimen. If the test is at elevated temperature, power is supplied to the heating element and the temperature of the specimen is monitored. When the prescribed temperature has been reached, the specimen is loaded at the designated rate. An XY-plotter is used to record the response of the specimen. The load signal from the load cell is plotted as the ordinate, the deformation signal from the LVDT is plotted as the abscissa.

The usual result determined from this test is the flexural modulus. For three point flexure, the equation used to calculate the modulus is:

$$E = \frac{PL^3}{48\delta I}$$

where P = applied load
L = support span
I = second moment of area for the cross section
and δ = mid point deflection.

For four point flexure, the equation for the modulus is:

$$E = \frac{Pd(3L^2 - 4d^2)}{24\delta I}$$

where 2P = total applied load
L = support span
d = (L - load span) / 2
I = second moment of area for the cross section
and δ = mid point deflection.

The flexural stress at failure can be calculated with the equation:

$$\sigma_f = \frac{M\,c}{I}$$

where M = bending moment
c = half height of beam
and I = second moment of area for the cross section.

The shear stress at failure, for a beam with a rectangular cross section, can be calculated with the equation:

$$\tau = \frac{3\,V}{2\,A}$$

where V = maximum shear load
A = area of cross section.

Due to the combined stress state and the nonuniform stress distribution in this specimen, the calculated moduli and strengths are usually not appropriate estimates of the material properties.

CHARPY IMPACT

Description of Test

The Charpy impact evaluations were conducted in a standard pendulum type impact machine equipped with a four-pound hammer. All impact readings were corrected for friction and windage using the standard calibration procedure for the impact machine. A modified Charpy

specimen was utilized due to the limited specimen length available. The specimen size was nominally 4.00” x 0.50” x 0.20”. The testing was to simulate major impacts to the heater tubes during installation and removal. Therefore, the outside diameter side of the specimen was the striking surface.

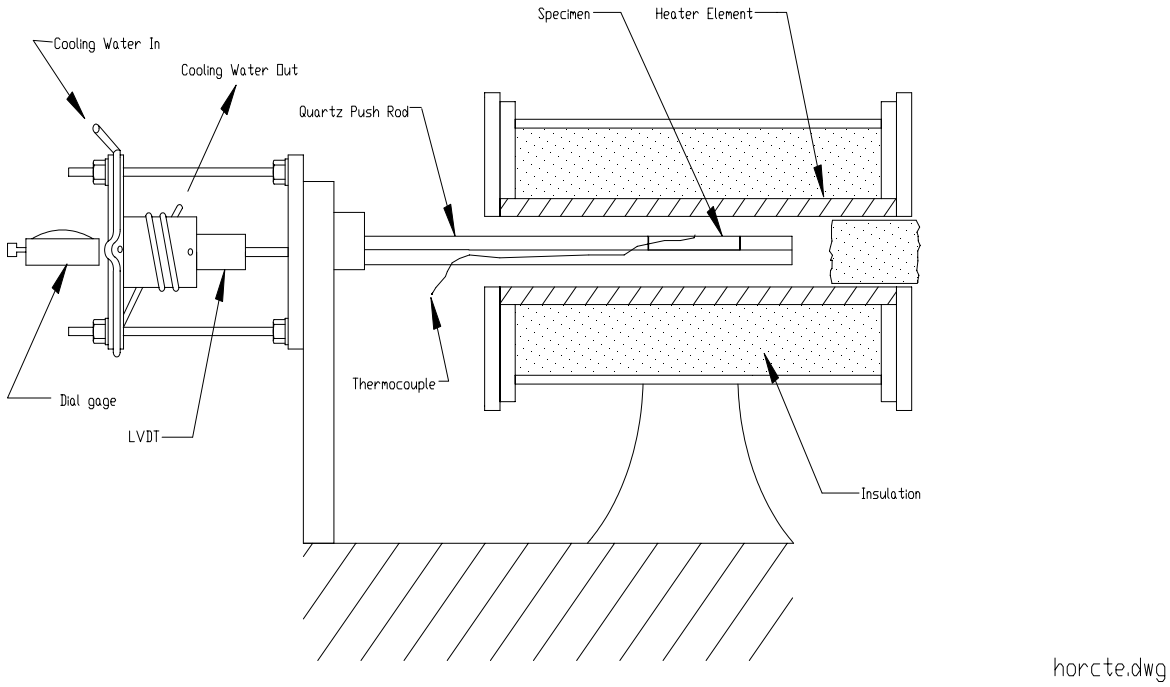

Figure 3.4.20 Schematic of the Horizontal Quartz Rod Dilatometer Apparatus

THERMAL EXPANSION (TE)

Description of Test

Free thermal expansion evaluations from room temperature (RT) to 1800°F were made using the quartz dilatometer test facility. An LVDT was used to dynamically measure the change in length of the specimen as a function of temperature. A dial gage also provided expansion data and was used as a check of the LVDT readout. Thermocouples were mounted on the centerline of each specimen and the output voltage recorded continuously as the test progressed.

Interpretation of Results

The expansion at any temperature as measured is known to be the current length minus the initial length divided by the initial length. The recorded data were reported as a plot and a table of expansion versus temperature.

Specimen Configuration

The thermal expansion specimens used for this effort were coupons measuring nominally 2.50” x 0.375” x 0.20” for the axial samples and 1.50” x 0.375” x 0.20” for the circumferential samples.

Calibration
To calibrate the quartz dilatometers SRI employs a primary standard of fused silica purchased from NIST and designated as SRM 739. A secondary standard of fused silica developed in-house is also used.

Precision and Accuracy
For the quartz dilatometer, the standard deviation is no greater than 0.025×10^{-3} in./in. at 1300 °F.

RESULTS

NON-DESTRUCTIVE EVALUATIONS

Gravimetric (Bulk) Density

The dimensions and weights were determined on the fully machined specimens in order to obtain bulk densities. The bulk density of each test specimen is included in appropriate results tables. An average value obtained from the measured densities of all of the room temperature flexure specimens showed the material to have an average bulk density of 2.5332 gm/cm³.

Sonic Velocity
The break and peak ultrasonic velocities were determined on the mechanical specimens in the representative test orientation. The sonic velocities are reported in appropriate results tables. Average values obtained from the measured velocities of the room temperature flexure specimens showed the material to have an average break and peak velocity of 0.3110 in./μsec and 0.2766 in./μsec respectively.

MECHANICAL PROPERTY EVALUATIONS

Ring Tension

Ring tensile evaluations were conducted at room temperature (RT) with a stress rate of 10 Ksi/min. Figure 3.4.21 displays a post-test section of the SCS6 reinforced material. Figure 3.4.22 shows the stress-strain curves for each run. Table 3.4.10 summarizes the results. The large data scatter is primarily attributed to varying surface conditions of the group of specimens. During the machining process, a portion of the ID and the OD is removed therefore leaving some of the reinforcing fibers exposed on the finished surface. These exposed fiber areas act as stress concentrations and failures usually occur at these locations as can be seen in Figure 3.4.21. Each specimen had a varying degree of exposed fibers and therefore had a varying degree of stress concentrations leading to significant scatter in the stress-strain responses.

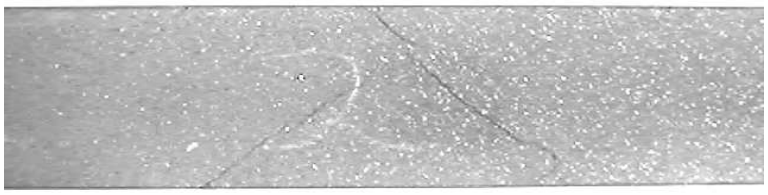

Figure 3.4.21 Photograph of a Post-Test Section of the SCS6 Reinforced

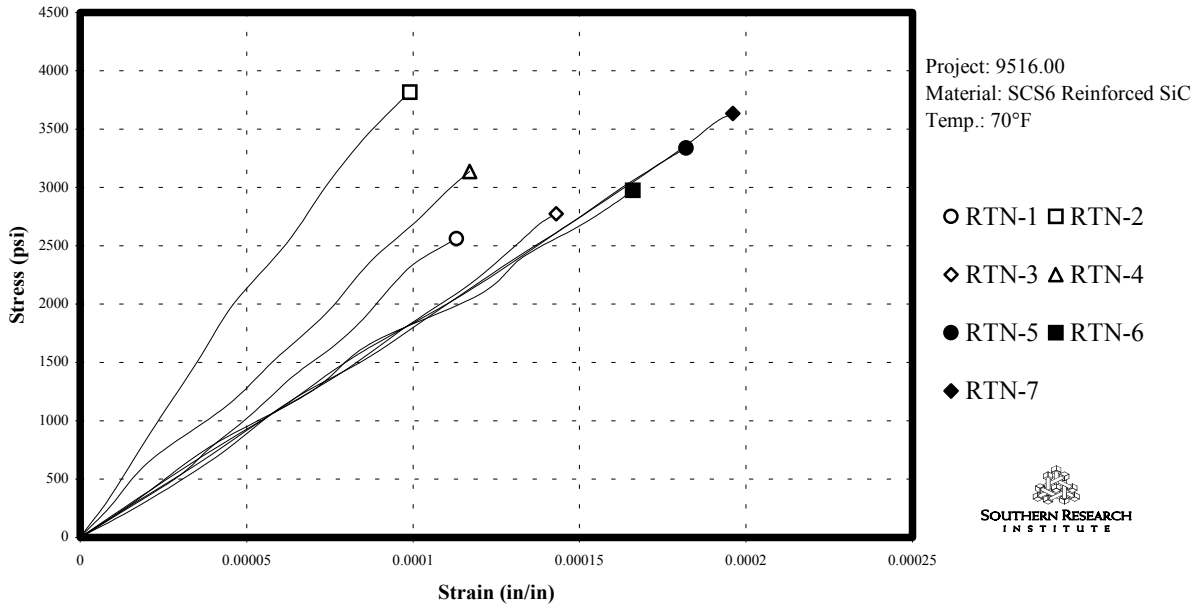

Figure 3.4.22 Hoop Tensile Stress-Strain Response of SCS6 Reinforced SiC at Room Temperature

Table 3.4.10 Hoop (Ring) Tensile Evaluations of SCS6 Reinforced SiC at 70ºF

MATERIAL	SPECIMEN NUMBER	SPECIMEN GAGE (inch)	STRESS RATE (Ksi/min)	TEMP. (°F)	DENSITY (g/cm³)	ULTIMATE STRESS (I.D.) (psi)	ULTIMATE STRESS (O.D.) (psi)	STRAIN TO FAILURE (O.D.) (in/in)	INI. ELASTIC MODULUS (O.D.) (Msi)	REMARKS
Silicon Carbide	RTN-1	5.104 id x 5.530 od x .375	10	70	2.5238	2551	2347	0.0001	20.41	
Silicon Carbide	RTN-2	5.104 id x 5.530 od x .375	10	70	2.6886	3827	3521	0.0001	35.80	
Silicon Carbide	RTN-3	5.104 id x 5.530 od x .375	10	70	2.3665	2764	2543	0.0001	17.84	
Silicon Carbide	RTN-4	5.104 id x 5.530 od x .375	10	70	2.5139	3157	2905	0.0001	30.37	
Silicon Carbide	RTN-5	5.104 id x 5.530 od x .375	10	70	2.5717	3359	3090	0.0002	18.90	
Silicon Carbide	RTN-6	5.104 id x 5.530 od x .375	10	70	2.5221	2966	2729	0.0002	17.00	
Silicon Carbide	RTN-7	5.104 id x 5.530 od x .375	10	70	2.5294	3614	3325	0.0002	17.01	
	NUMBER OF VALUES				7	7	7	7	7	
	AVERAGE				**2.5309**	**3177**	**2923**	**0.0001**	**22.48**	
	STANDARD DEVIATION				**0.0878**	**423**	**389**	**0.0001**	**6.95**	
	COEFFICIENT OF VARIATION (%)				**3.47**	**13.32**	**13.32**	**35.94**	**30.93**	

Flexure

Flexural evaluations were conducted on axially oriented specimens at room temperature (RT) and 1600°F with a stress rate of 10 Ksi/min. Figure 3.4.23 shows the room temperature flexural response for each run. Figure 3.4.24 shows the 1600°F responses. Table 3.4.11 summarizes the flexural results. Data scatter was also attributed to surface irregularities.

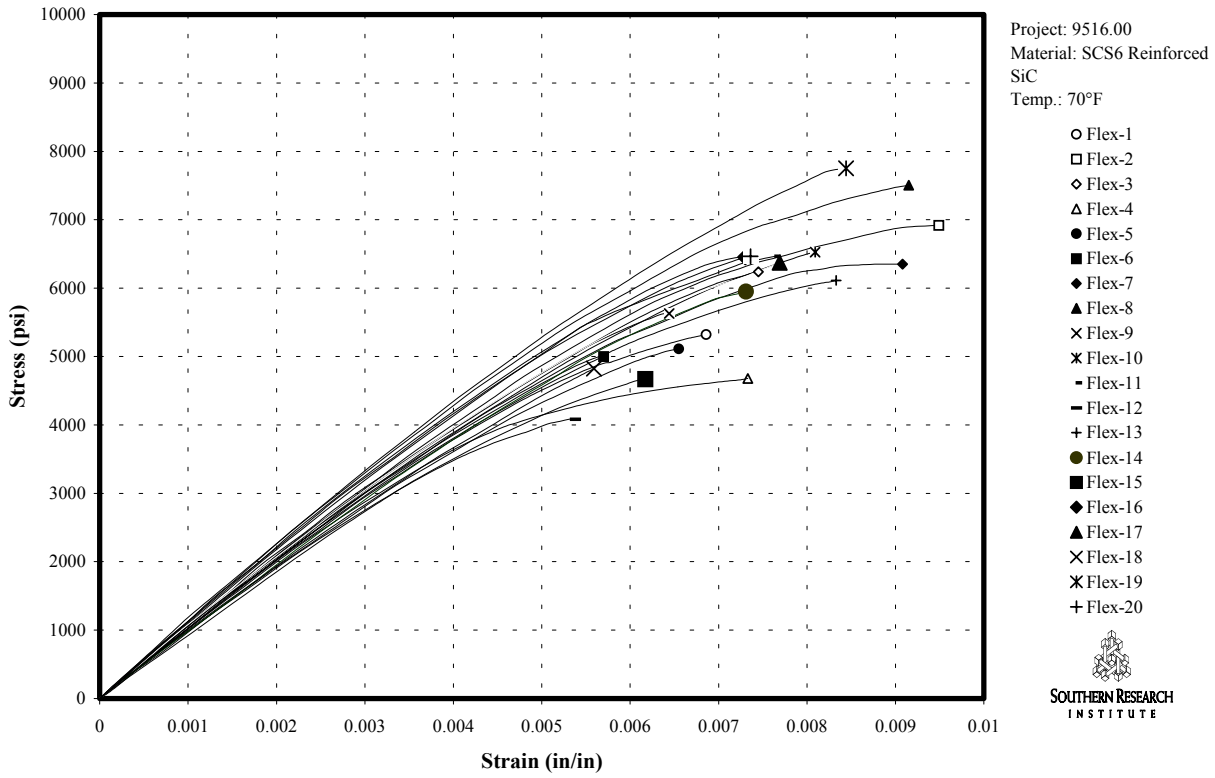

Figure 3.4.23 Flexural Stress-Strain Response of SCS6 Reinforced SiC Material at 70ºF

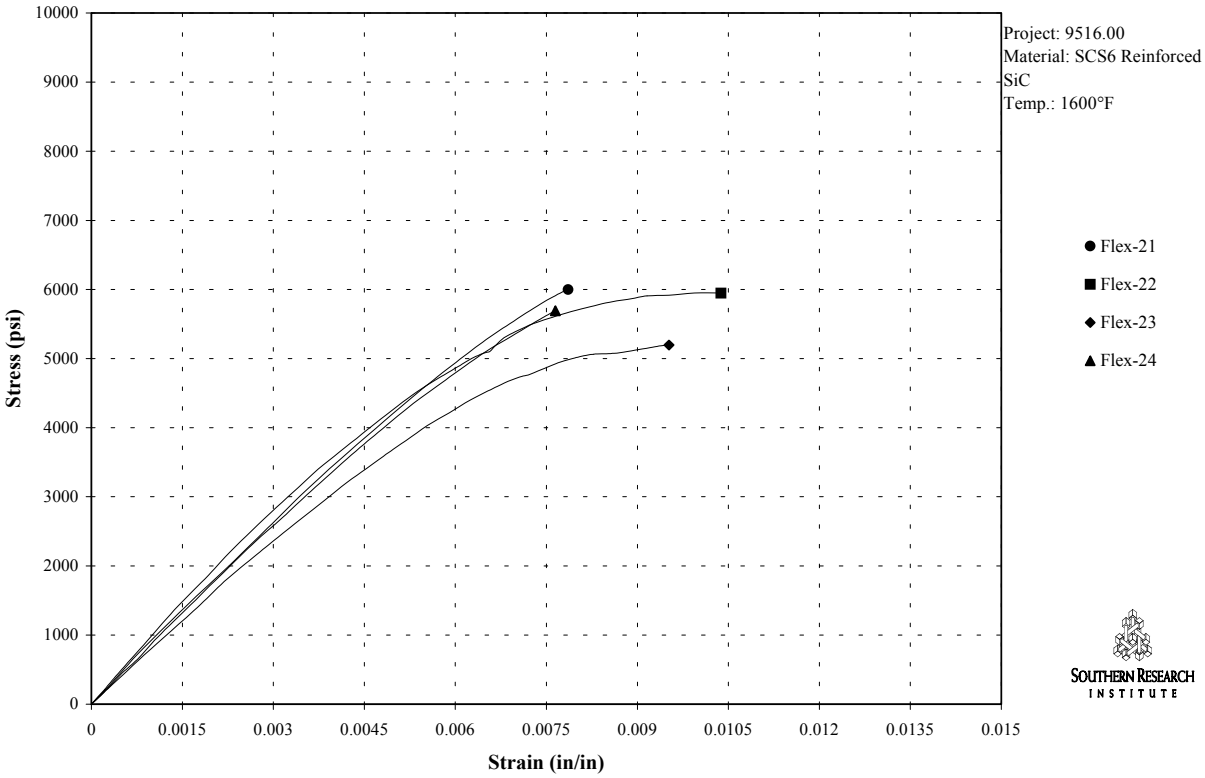

Figure 3.4.24 Flexural Stress-Strain Response of SCS6 Reinforced SiC at 1600°F

Table 3.4.11 4-Point Flexure Evaluations of SCS6 Reinforced SiC at 70°F and 1600°F

MATERIAL	SPECIMEN NUMBER	SPECIMEN GAGE (inch)	TEMP. (°F)	DENSITY (g/cm^3)	BREAK VELOCITY (in/µsec)	PEAK VELOCITY (in/µsec)	FLEXURAL MODULUS (Msi)	STRAIN TO FAILURE (in/in)	ULTIMATE STRESS (psi)
Silicon Carbide	FLX-1	.2001 x .4996	70	2.5365	0.3077	0.2730	14.69	0.0070	5361
Silicon Carbide	FLX-2	.2003 x .4997	70	2.5203	0.3106	0.2771	14.80	0.0095	6907
Silicon Carbide	FLX-3	.2001 x .4996	70	2.5549	0.3082	0.2779	14.89	0.0074	6217
Silicon Carbide	FLX-4	.2000 x .5001	70	2.5568	0.3067	0.2729	14.44	0.0074	4660
Silicon Carbide	FLX-5	.2003 x .5000	70	2.5421	0.3108	0.2760	13.93	0.0066	5134
Silicon Carbide	FLX-6	.2002 x .5002	70	2.5447	0.3159	0.2783	14.89	0.0057	4959
Silicon Carbide	FLX-7	.2001 x .5001	70	2.5202	0.3119	0.2782	14.65	0.0091	6320
Silicon Carbide	FLX-8	.2002 x .5001	70	2.5230	0.3151	0.2824	16.53	0.0092	7475
Silicon Carbide	FLX-9	.2001 x .5002	70	2.5533	0.3097	0.2780	15.22	0.0063	5578
Silicon Carbide	FLX-10	.2002 x .5003	70	2.5213	0.3117	0.2765	14.91	0.0081	6516
Silicon Carbide	FLX-11	.2002 x .5001	70	2.5550	0.3129	0.2786	16.08	0.0077	6444
Silicon Carbide	FLX-12	.2000 x .5002	70	2.5062	0.3098	0.2745	13.79	0.0054	4062
Silicon Carbide	FLX-13	.2003 x .5000	70	2.5204	0.3065	0.2771	15.02	0.0083	6093
Silicon Carbide	FLX-14	.1994 x .5003	70	2.5168	0.3066	0.2727	13.93	0.0073	5928
Silicon Carbide	FLX-15	.2003 x .5003	70	2.5224	0.3122	0.2749	13.25	0.0061	4650
Silicon Carbide	FLX-16	.1995 x .5002	70	2.5286	0.3128	0.2783	15.91	0.0073	6423
Silicon Carbide	FLX-17	.2000 x .4997	70	2.5403	0.3115	0.2779	14.76	0.0077	6361
Silicon Carbide	FLX-18	.2000 x .5003	70	2.5149	0.3110	0.2745	14.11	0.0056	4794
Silicon Carbide	FLX-19	.2004 x .5000	70	2.5266	0.3148	0.2780	16.02	0.0085	7712
Silicon Carbide	FLX-20	.2000 x .5002	70	2.5593	0.3134	0.2760	15.68	0.0073	6454
	NUMBER OF VALUES			**20**	**20**	**20**	**20**	**20**	**20**
	AVERAGE			**2.5332**	**0.3110**	**0.2766**	**15.12**	**0.0074**	**5902**
	STANDARD DEVIATION			**0.0164**	**0.0028**	**0.0024**	**0.85**	**0.0012**	**977**
	COEFFICIENT OF VARIATION (%			**0.65**	**0.91**	**0.86**	**5.65**	**16.19**	**16.55**
Silicon Carbide	FLX-21	.2000 x .5000	1600	2.5321	0.3095	0.2782	12.93	0.0079	5980
Silicon Carbide	FLX-22	.1995 x .5004	1600	2.5411	0.3114	0.2774	14.04	0.0104	5928
Silicon Carbide	FLX-23	.2000 x .5001	1600	2.5460	0.3089	0.2738	11.54	0.0096	5165
Silicon Carbide	FLX-24	.2002 x .5002	1600	2.5458	0.3064	0.2742	12.38	0.0077	5588
Silicon Carbide	FLX-25	.2000 x .5001	1600	2.5652	0.3081	0.2767	12.77	0.0090	5969
	NUMBER OF VALUES			**5**	**5**	**5**	**5**	**5**	**5**
	AVERAGE			**2.5460**	**0.3089**	**0.2761**	**12.73**	**0.0089**	**5726**
	STANDARD DEVIATION			**0.0121**	**0.0018**	**0.0020**	**0.91**	**0.0011**	**353**
	COEFFICIENT OF VARIATION (%			**0.48**	**0.59**	**0.71**	**7.13**	**12.77**	**6.16**

Charpy Impact

Charpy impact evaluations were conducted on axially oriented specimens at room temperature (RT) with a four-pound impact hammer on the SCS6 reinforced SiC tube material. Additional impact evaluations were conducted on a monolithic SiC for comparison purposes. Figure 3.4.25 shows the fracture energy comparison of the two materials. Tables 3.4.12 and 3.4.13 summarize the results. The Reinforced SiC exhibited approximately 20% higher fracture energy than the monolithic as was expected.

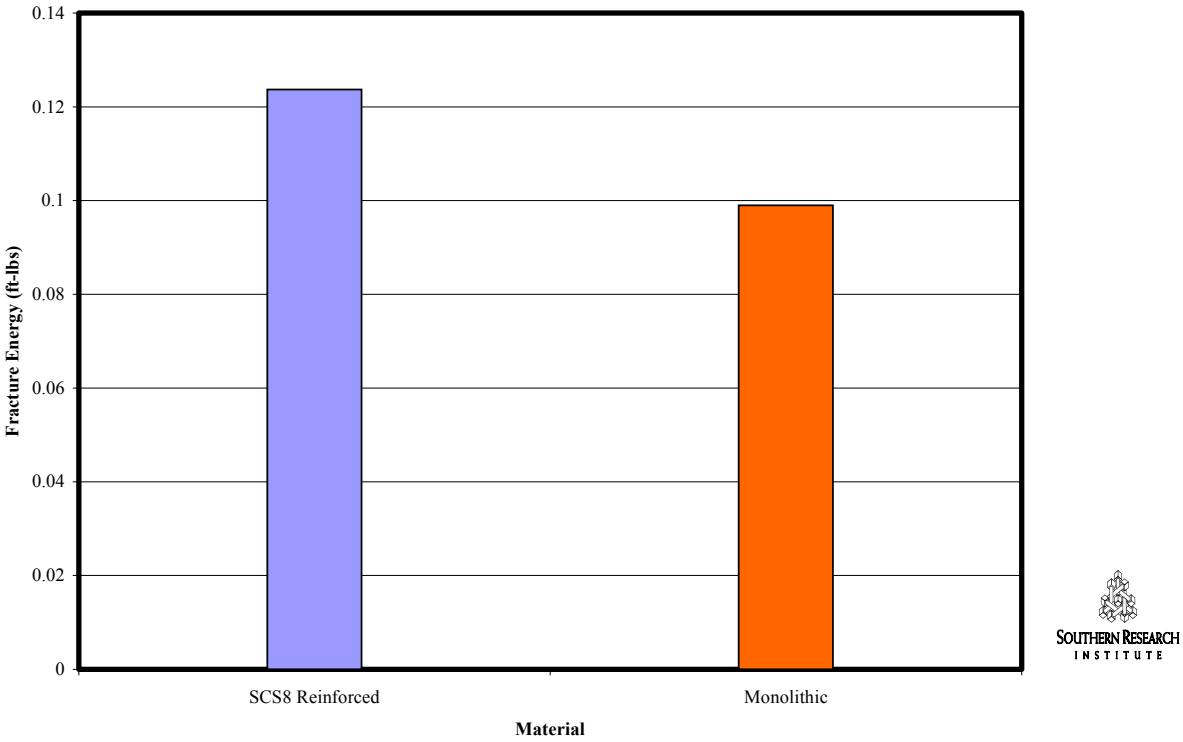

Figure 3.4.25 Comparison of SiC Materials - Fracture Energy

Table 3.4.12 Modified Charpy Results - SCS6 Reinforced Composite Tubes

Specimen Number	Reading (ft-lbs)	Wind/Friction Correction (ft-lbs)	Corrected Reading (ft-lbs)	Final 4 lb Hammer Fracture Energy (ft-lbs)	Comments
1	0.091	0.026	0.065	0.130	Calibration
2	0.099	0.026	0.073	0.146	
3	0.096	0.026	0.070	0.140	
4	0.086	0.026	0.060	0.120	
5	0.085	0.026	0.059	0.118	
6	0.089	0.026	0.063	0.126	
7	0.081	0.026	0.055	0.110	
8	0.082	0.026	0.056	0.112	
9	0.099	0.026	0.073	0.146	
10	0.086	0.026	0.060	0.120	
11	0.086	0.026	0.060	0.120	Calibration
12	0.082	0.026	0.056	0.112	
13	0.083	0.026	0.057	0.114	
14	0.088	0.026	0.062	0.124	
15	0.081	0.026	0.055	0.110	
16	0.079	0.026	0.053	0.106	
17	0.099	0.026	0.073	0.146	
18	0.089	0.026	0.063	0.126	
19	0.101	0.026	0.075	0.150	
20	0.075	0.026	0.049	0.098	
Averages	0.088	0.026	0.062	0.124	

Table 3.4.13 Modified Charpy Results - Monolithis Si/C Plate

Specimen Number	Reading (ft-lbs)	Wind/Friction Correction (ft-lbs)	Corrected Reading (ft-lbs)	Final 4 lb Hammer Fracture Energy (ft-lbs)	Comments
1	0.069	0.022	0.047	0.094	Calibration
2	0.095	0.022	0.073	0.146	
3	0.076	0.022	0.054	0.108	
4	0.066	0.022	0.044	0.088	
5	0.061	0.022	0.039	0.078	
6	0.062	0.022	0.040	0.080	
Averages	0.072	0.022	0.050	0.099	

Thermal Expansion

Measurement of the materials free thermal expansion as a result of isothermal heating was performed in the circumferential and axial orientations at 10°F/sec. Figure 3.4.26 displays the circumferential thermal expansion results up to 1800°F as measured in the quartz dilatometer. Table 3.4.14 summarizes the circumferential results. Figure 3.4.27 displays the axial thermal expansion results in the quartz dilatometer. Table 3.4.15 summarizes the axial results. The two orientations exhibited nearly identical thermal expansion characteristics.

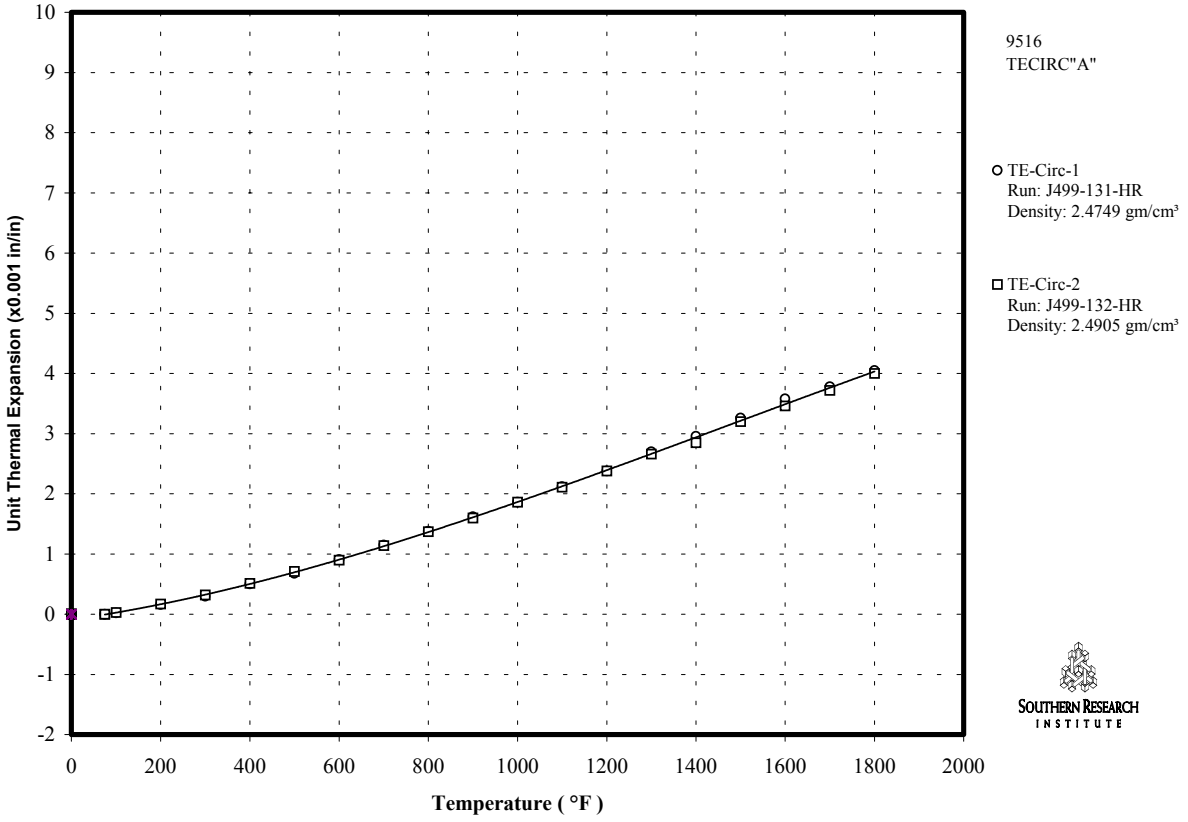

Figure 3.4.26 Circumferential Thermal Expansion of SCS6 Reinforced SiC

Table 3.4.14 Circumferential Thermal Expansion of SCS6 Reinforced SiC

Temperature (°F)	Unit Thermal Expansion (x 0.001 in/in)		Temperature (°F)	Unit Thermal Expansion (x 0.001 in/in)	
75	0.00	Specimen: TE-Circ-1	75	0.00	Specimen: TE-Circ-2
100	0.02	Run: J499-131-HR	100	0.03	Run: J499-132-HR
200	0.16	Density (g/cc): 2.4749	200	0.17	Density (g/cc): 2.4905
300	0.30	Initial Length (in.): 1.4937	300	0.32	Initial Length (in.): 1.4995
400	0.50	Final Length (in.): 1.4937	500	0.51	Final Length (in.): 1.4995
500	0.68	Initial Width (in.): 0.3746	300	0.71	Initial Width (in.): 0.3747
600	0.91	Final Width (in.): 0.3747	500	0.90	Final Width (in.): 0.3748
700	1.15	Initial Thickness (in.): 0.2003	700	1.14	Initial Thickness (in.): 0.2004
800	1.38	Final Thickness (in.): 0.2002	800	1.37	Final Thickness (in.): 0.2004
900	1.62	Initial Weight (gm.): 4.5454	900	1.60	Initial Weight (gm.): 4.5953
1000	1.86	Final Weight (gm.): 4.5374	1000	1.86	Final Weight (gm.): 4.5879
1100	2.12		1100	2.11	
1200	2.38		1200	2.38	
1300	2.70		1300	2.66	
1400	2.96		1400	2.85	
1500	3.26		1500	3.20	
1600	3.58		1600	3.46	
1700	3.78		1700	3.72	
1800	4.05		1800	4.00	
75	0.00		75	0.00	

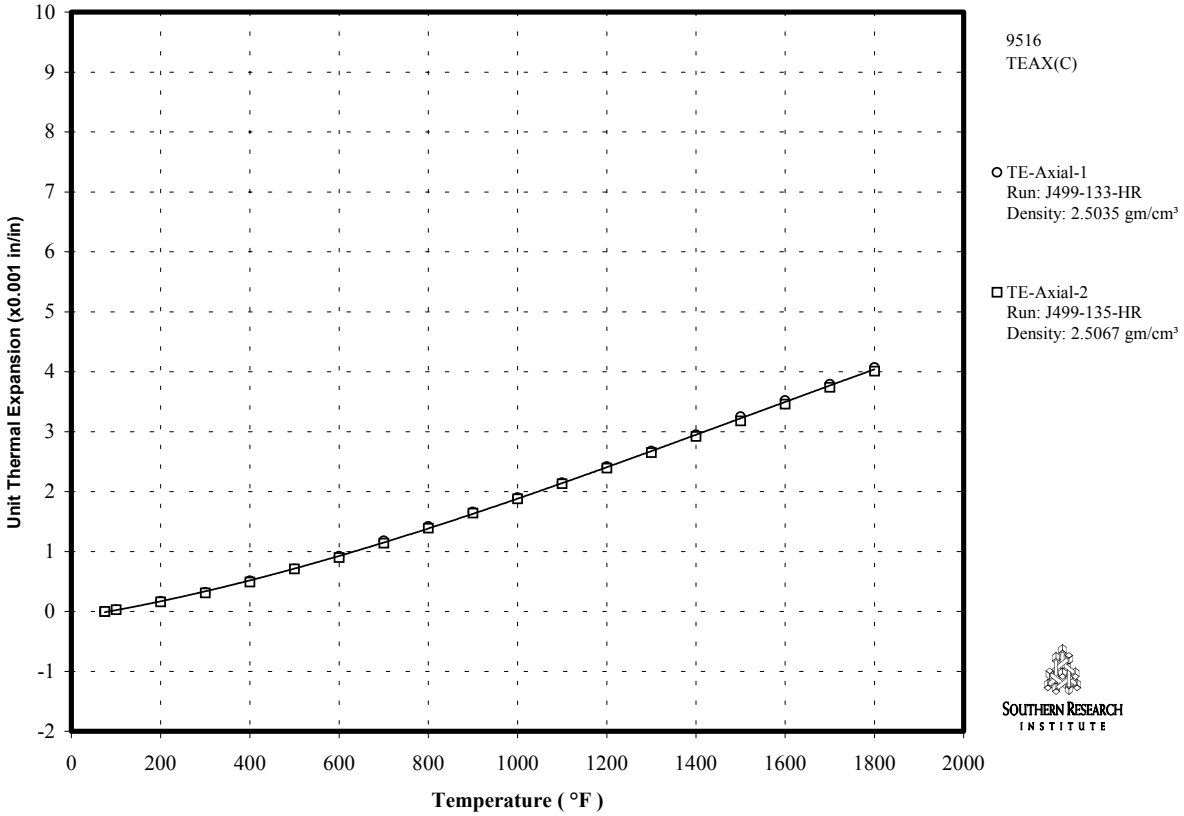

Figure 3.4.27 Axial Thermal Expansion of SCS6 Reinforced SiC

Table 3.4.15 Axial Thermal Expansion of SCS6 Reinforced SiC

Temperature (°F)	Unit Thermal Expansion (x 0.001 in/in)		Temperature (°F)	Unit Thermal Expansion (x 0.001 in/in)	
75	0.00	Specimen: TE-Axial-1	75	0.00	Specimen: TE-Axial-2
100	0.03	Run: J499-133-HR	100	0.03	Run: J499-135-HR
200	0.17	Density (g/cc): 2.5035	200	0.16	Density (g/cc): 2.5067
300	0.32	Initial Length (in.): 2.9963	300	0.31	Initial Length (in.): 2.9962
400	0.51	Final Length (in.): 2.9963	500	0.49	Final Length (in.): 2.9962
500	0.71	Initial Width (in.): 0.3749	300	0.71	Initial Width (in.): 0.3752
600	0.92	Final Width (in.): 0.3750	500	0.90	Final Width (in.): 0.3751
700	1.18	Initial Thickness (in.): 0.2000	700	1.14	Initial Thickness (in.): 0.2005
800	1.42	Final Thickness (in.): 0.1997	800	1.39	Final Thickness (in.): 0.2005
900	1.66	Initial Weight (gm.): 9.2168	900	1.64	Initial Weight (gm.): 9.2588
1000	1.90	Final Weight (gm.): 9.1976	1000	1.88	Final Weight (gm.): 9.2351
1100	2.15		1100	2.13	
1200	2.42		1200	2.39	
1300	2.68		1300	2.65	
1400	2.95		1400	2.92	
1500	3.25		1500	3.18	
1600	3.52		1600	3.46	
1700	3.79		1700	3.74	
1800	4.07		1800	4.01	
75	0.00		75	0.00	

SUMMARY/CONCLUSIONS

The mechanical data for this evaluation was dominated for the most part by the surface condition of the specimens. As was seen in Figure 3.4.21, the failure locations were primarily along the lines of fiber exposure to the specimen surface. The reinforcing fibers did significantly improve the impact strength over the monolithic material as was expected. The thermal expansion results showed the two orientations to have nearly identical behavior.

Interfacial Properties:

Samples of NB SiC/SCS-6 and /SCS-9A were submitted for fiber pushout testing at the University of Southern California; Testing at temperatures from 25ºC to 1000ºC were performed under the direction of Professor Stephen Nutt.

A new 7 micron indentor was successfully used for high-temperature pushout tests on nitride bonded SiC-SCS-6 at 700°C. Values of interfacial shear (bond) strength of approximately 93± 44 MPa were recorded. The interfacial shear (bond) strength is calculated from the peak load record, the fiber diameter, and the thickness of the specimen. Interfacial shear strength is defined as the peak load as the fiber debonds and slides out of the matrix. Data following this debond are a record of frictional loads as the fiber slides out of the matrix. This is indicated by a region shown as A in the graph presented below. A shear to axial balances of forces equation is used to calculate the bond strength assuming a uniform shear strength along the length of the fiber/matrix interface.

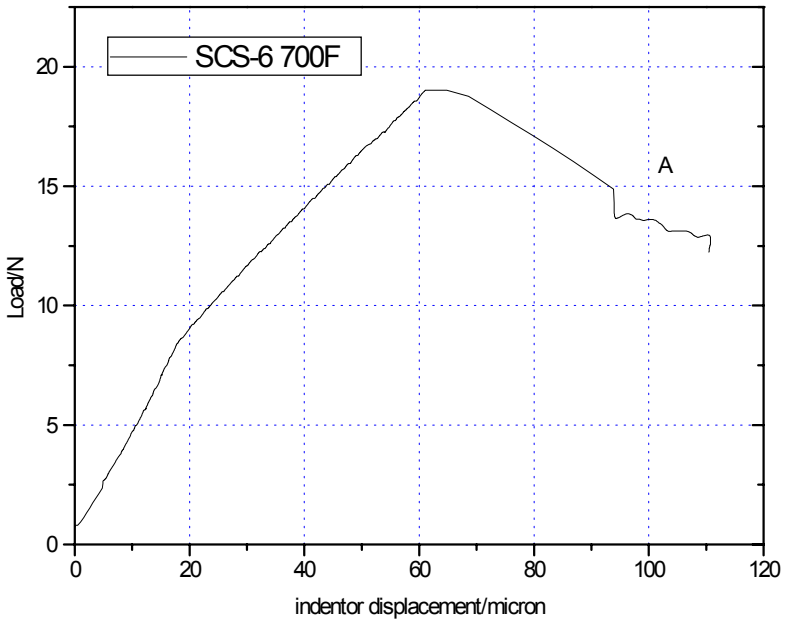

USC Executive Summary:

High-Temperature Interfacial Properties in Ceramic Composites: summary of results for Textron material tested under DOE CFCCs Program, grant DE–FG02–07CH10901.

A scanning electron microscope (SEM) has been equipped with an instrumented indenter and heating stage to measure the temperature dependence of interface properties in current CMC materials. Two ceramic matrix composite materials studied at 27°C, 700°C and 1000°C. The

materials were (a) nitride–bonded SiC/SCS–6 panel and (b) nitride–bonded SiC/SCS–9A panel. The load-displacement curves typically showed a steady increase to a peak load, followed by a load drop coincident with debonding, and a load plateau corresponding to frictional sliding resistance. The response of all materials was strongly temperature-dependent. At 27°C, debonding resulted in a sharp load drop, implying "brittle" failure of the interface. However, at high temperatures, the load drop after peak was gradual, implying progressive interface crack growth. Furthermore, the interfacial bond strength increased substantially (100% for the SCS-6 and 105% for the SCS-9A fibers) with increasing test temperature for all materials. The reason for this is not well understood at present. It is expected that a CTE mismatch between fibers and matrix is such that at high temperatures, the fibers are expected to experience an increased 'clamping' force in the radial direction. However, reliable CTE data is not available for all materials tested, and it's unlikely that this explanation is entirely sufficient, given that the CTE mismatch in other CMC material tested is probably negligible. A second possibility under consideration is that the interfaces are less brittle and thus more flaw-tolerant at higher temperatures, allowing debonding to occur by progressive crack growth. Certainly the matrix is more compliant at the higher test temperatures, as evidenced by the degree of sample flexure observed. Also, the mode of interface crack growth appears to be substantially different at higher test temperatures. Additional CMC materials are currently being studied to develop a clearer understanding of the temperature dependence of interface properties that will ultimately support the design of interfaces with improved performance characteristics.

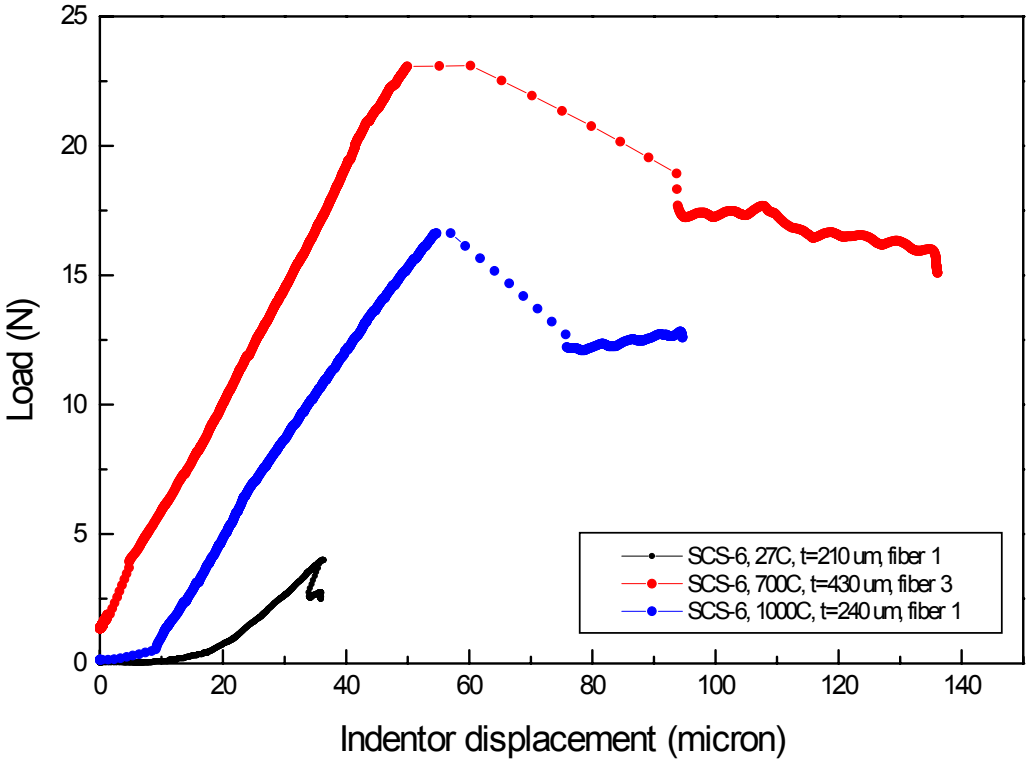

Figure 3.4.28 The load-displacement curves for the bonded SiC/SCS–6 panel

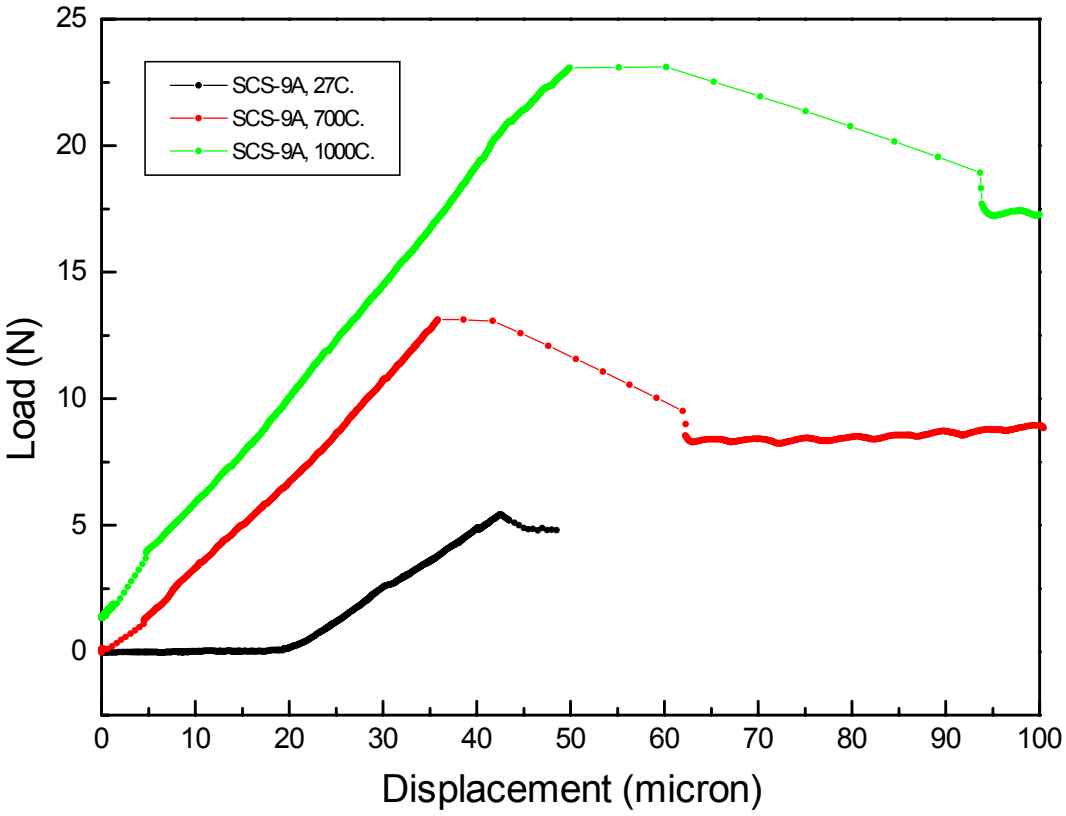

Figure 3.4.29 The load-displacement curves for the Nitride–bonded SiC/SCS–9A panel

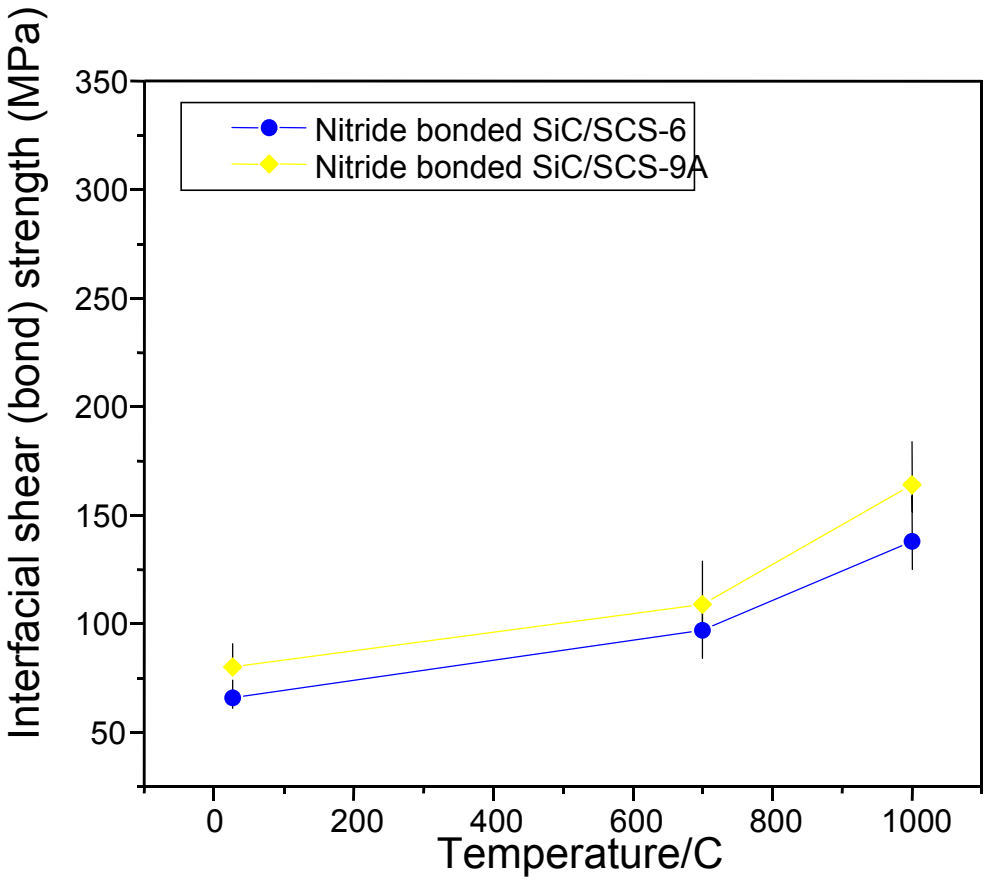

Figure 3.4.30 Interfacial shear (bond) strength vs. Temperature

In support of the first hypothesis, CTE mismatch between fibers and matrix, the following graph was provided to USC for their review. This graph shows the CTE for the NB SiC matrix and the SCS-6 fibers within the temperature range the testing was performed (Figure 3.4.31). It shows that the CTE for the SCS-6 fiber is approximately twice that of the matrix, so at elevated temperatures the fiber does experience an increased clamping force in the radial direction. This data represents the axial CTE for the SCS-6 fiber, however it is hypothesized that the radial CTE for the SCS-6 fiber is also much greater than that for the NB SiC matrix.

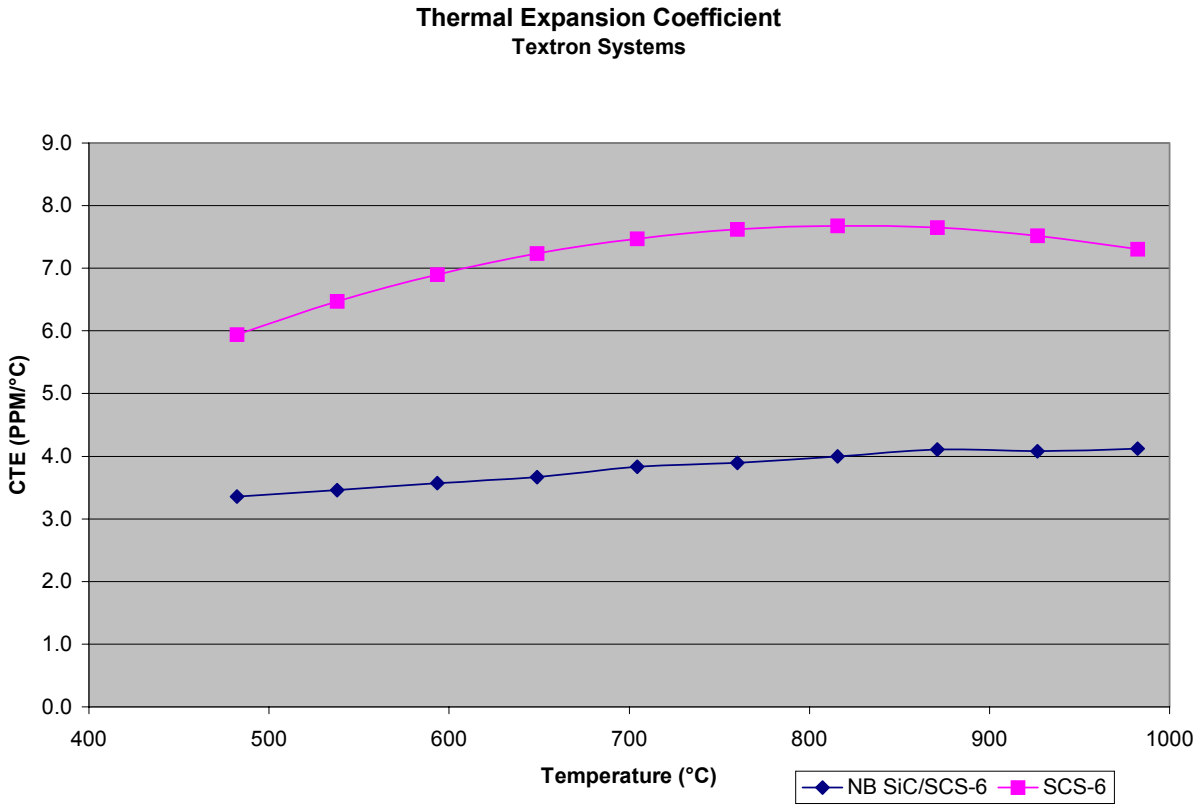

Figure 3.4.31 Thermal Expansion Coefficient for SCS-6 monofilament and NB SiC matrix

Material Property Evaluation: NB SiC CFCC Combustor Can

Test Specimen Configuration

Tensile, stress rupture and stress oxidation testing utilized flat, edge loaded tensile specimens as in Figure 3.4-32. Laser machining was attempted to cut the test specimens from the panels. This effort was unsuccessful due to cracking of the specimen near the laser cut edges along the fiber direction.

Diamond machining was used to cut the specimens from the test panels. Bomas Machine Specialties was the vendor used to machine the test specimens. Test specimens were machined from both the unidirectional and ±45° fiber orientation test panels.

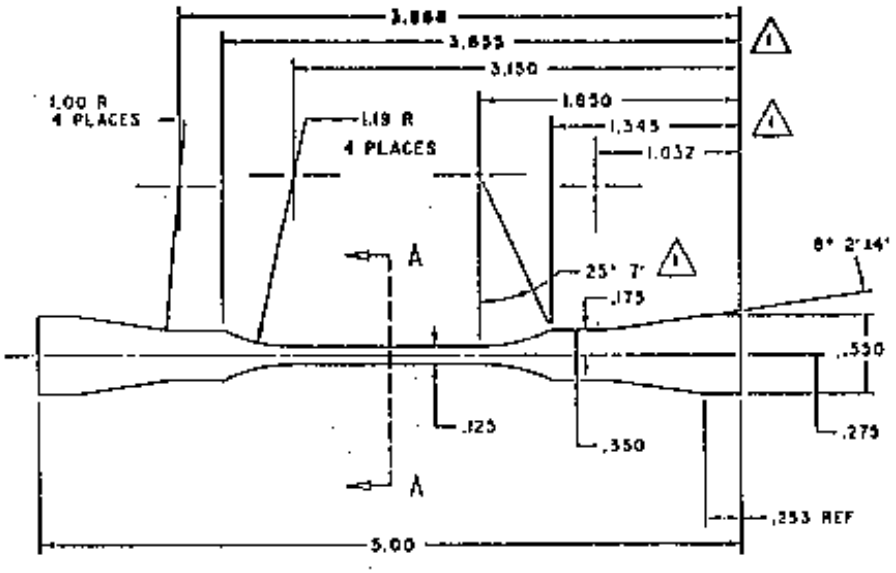

Figure 3.4-32 Test Specimen Configuration

Tensile Testing

Mechanical property testing was conducted by Composite Testing and Analysis, Inc. (CTA) by Dr. John Holmes. All of the tensile testing was conducted in air using flat edge loaded tensile specimens. Monotonic tensile testing was conducted from room temperature to 2500°F. Tensile strength, modulus and elongation was measured during each of the tests.

Tensile Test Data

Monotonic tensile testing was conducted at 70°F, 1500°F, 2000°F, 2200°F, 2400°F and 2500°F. The loading rate for all testing was 3.6 KSI/S. All of the testing was conducted in air. None of the test specimens were heat treated prior to testing.

Table 3.4-16 Tensile Test Data Unidirectional Orientation

Specimen ID	Fiber Orientation	Temperature °F	Tensile Strength KSI	Tensile Modulus MSI	Strain %
MT1	ZERO	70	23.1	24	0.44
MT2	ZERO	70	22.5	23	0.58
MT3	ZERO	70	20.6	22	0.69
MT7	ZERO	1500	13.5	23	0.05
MT8	ZERO	1500	19.1	24	0.07
MT9	ZERO	1500	15.7	22	0.06
MT13	ZERO	2000	18.1	21	0.08
MT14	ZERO	2000	16.0	21	0.07
MT15	ZERO	2000	15.5	22	0.07
MT19	ZERO	2200	13.5	19	0.07
MT20	ZERO	2200	17.6	18	0.10
MT21	ZERO	2200	16.2	18	0.09
MT25	ZERO	2400	11.0	18	0.06
MT26	ZERO	2400	13.9	19	0.07
MT27	ZERO	2400	10.2	17	0.06
MT31	ZERO	2500	12.4	19	0.06
MT32	ZERO	2500	16.5	19	0.08
MT33	ZERO	2500	9.9	18	0.05

Table 3.4-17 Tensile Test Data ±45° Fiber Orientation

Specimen ID	Fiber Orientation	Temperature °F	Tensile Strength KSI	Tensile Modulus MSI	Strain %
MT4	±45	70	15.4	23	0.21
MT5	±45	70	15.5	20	0.36
MT6	±45	70	14.1	23	0.35
MT10	±45	1500	12.5	19	0.06
MT11	±45	1500	12.8	20	0.06
MT12	±45	1500	11.6	19	0.06
MT16	±45	2000	14.2	22	0.06
MT17	±45	2000	11.6	23	0.05
MT18	±45	2000	13.6	20	0.06
MT22	±45	2200	11.6	18	0.06
MT23	±45	2200	15.8	19	0.08
MT24	±45	2200	13.2	18	0.07
MT28	±45	2400	13.3	19	0.07
MT29	±45	2400	10.4	16	0.07
MT30	±45	2400	11.1	17	0.07
MT34	±45	2500	9.0	19	0.05
MT35	±45	2500	11.3	18	0.06
MT36	±45	2500	10.4	19	0.05

The tensile test data indicates that the material is very stable from room temperature through 2200°F for both the ±45° and 0° reinforced materials.

For unidirectional reinforced material at room temperature the tensile strength is about 22 KSI, see Table 3.4-16. The material maintains about 16 KSI tensile strength when the test temperature is increased to 1500°F, 2000°F and 2200°F. At 2400°F the tensile strength decreases to 11.7 KSI. At 2500°F the tensile strength increases slightly to approximately 12.93 KSI. The increase in tensile strength may be due to residual stresses being relieved as seen in the stress rupture testing.

Material with the ±45° reinforcement has a lower tensile strength when compared to the unidirectional reinforced material as expected, see Table . The fibers are at a 45° angle to the loading and are shortened due to the narrow test specimen configuration. Taking into account the fibers are at an angle the load carrying ability of the fiber should be about 70.7% of the unidirectional fibers, assuming full fiber load up on the shortened fibers.

At room temperature the tensile strength of the ±45° material is 15 KSI which is slightly less than 70.7% of the strength of the unidirectional material. The fiber loading is low at 10% and may not account for all of the change. Similar to the 0° material the ±45° material is stable with a tensile strength of approximately 13 KSI at 1500°F, 2000°F and 2200°F. At 2400°F the tensile strength drops to 11.6 KSI and at 2500° the tensile strength is 10.23 KSI.

The strain data indicates a change in the material elongation from room temperature to elevated temperature. At room temperature the strain to failure of the 0° material is approximately 0.57%. When the temperature is increased to 1500°F through 2500°F the strain to failure drops to approximately 0.07%. This conditions is also apparent in the ±45° material. The room temperature strain to failure of the ±45° material is approximately 0.31%. The difference between the 0° and ±45° material suggests that it may be related to the fiber orientation.

Stress Rupture Testing

CTA conducted the stress rupture testing. This testing was conducted in air using the same specimens geometry as the tensile test. Initially two temperatures were evaluated, 2200°F and 2500°F with two different fiber orientations, ±45° and unidirectional. The first specimen tested at each temperature and fiber orientation was tested in a step loaded fashion. Several test specimens had voids, the best test specimens were used for stress rupture and tensile testing. The remaining specimens were used for stressed oxidation testing at Williams International.

The first specimen at each test condition was tested at approximately 50% of the ultimate tensile strength. The load was maintained for 25 hours then increased by 2 KSI load increments with holds of 25 hours between the increases until the specimens broke. Based on this data subsequent stress levels were chosen for the remaining tests. The addition of the 2400°F temperature testing was decided upon after reviewing the results of the stress rupture data at 2500°F. Based upon the data and creep rates at the 2500°F test temperature it was apparent that there were changes in the material at this temperature. A summary of the stress rupture testing can be found in Table 3.4-18.

Table 3.4-18 Summary of Tensile Stress Rupture Data

Spec. ID	Fiber Orientation	Temp. °F	Stress KSI	Time Hrs	Notes
38	0°	2200	8, 10, 12	50	Failed upon loading to 12 KSI
41	±45°	2200	4, 6, 8	50	Failed upon loading to 8 KSI
40	±45°	2200	6	-	Failed upon loading
42	±45°	2200	6	>200	Held at 2500°F/25 h prior to testing
15-1	0°	2400	8, 10, 12	50-	Failed upon loading to 12 KSI
11-4	0°	2400	8	-	Failed upon loading
14-2	0°	2400	10	-	Failed upon loading
15-3	0°	2400	10	>200	Held at 2400°F/25 h prior to testing
43	0°	2500	4, 6, 8, 10	75	Failed upon loading to 10 KSI
44	0°	2500	8	-	Failed upon loading
46	±45°	2500	4, 6, 8	50	Failed upon loading to 8 KSI
47	±45°	2500	6	-	Failed upon loading
48	±45°	2500	6	-	Failed upon loading

2200°F Stress Rupture Testing With 0° Specimens

The first step loaded specimen started with a stress level of 8 KSI which was held for 25 hours. The creep rate during this phase of the testing was approximately zero. The loading was increased to 10 KSI and held for 25 hours with no failure. The specimen creeped by approximately 0.005% during the exposure at the 10 KSI level for 25 hours. The specimen broke when the stress level was increased to 12 KSI. Figure 3.4-32 is a plot of strain versus time of the step loaded test specimen. In this strain versus time plot the composite started to strain before the specimen fractured. At the lower stress levels the material appears to be stable with low creep rates.

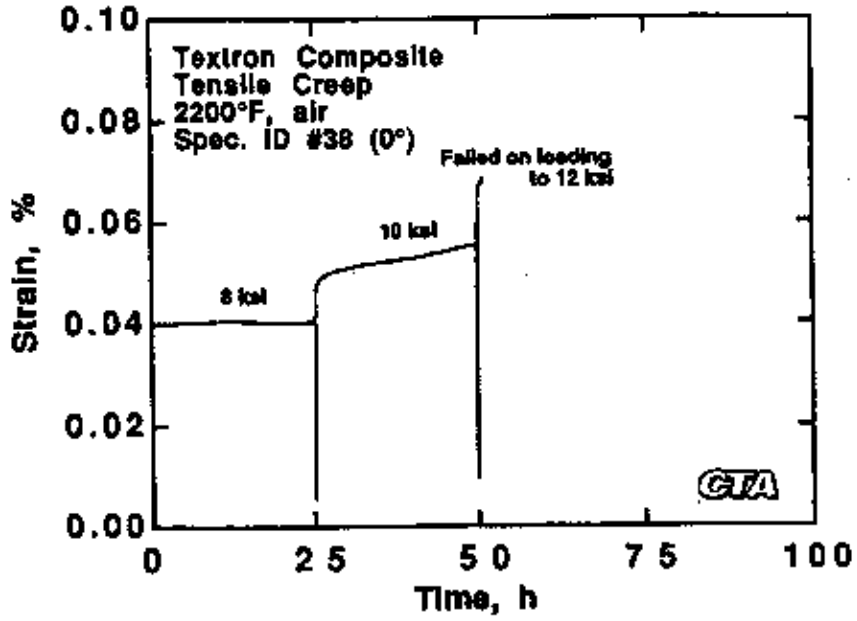

Figure 3.4-32 2200ºF Tensile Creep With 0º

2200°F Stress Rupture Testing With ±45° Specimens

Step loading of the ±45° test specimens was started at 4 KSI at 2200°F and held under these conditions for 25 hours. The creep rate during this time period was approximately zero. The total strain was about 0.025%. The loading was increased to 6 KSI and the specimens survived another 25 hours. The strain increased to about 0.04% and no creep was measured during this time interval. Failure of the specimen occurred upon loading of the specimen to 8 KSI. A plot of this test data can be seen in Figure 3.4-33.

The next specimen was tested at a stress level of 6 KSI and failed upon loading.

Another test specimen was setup and heat treated for 25 hours at 2500°F before testing. This was based upon previous test results. This specimen was tested at 2200°F and a stress level of 6 KSI, see Figure 3.4-34. The strain was slightly less than 0.06% and the specimen survived 200 hours of testing at this condition. There was no measurable creep during the testing of this specimen.

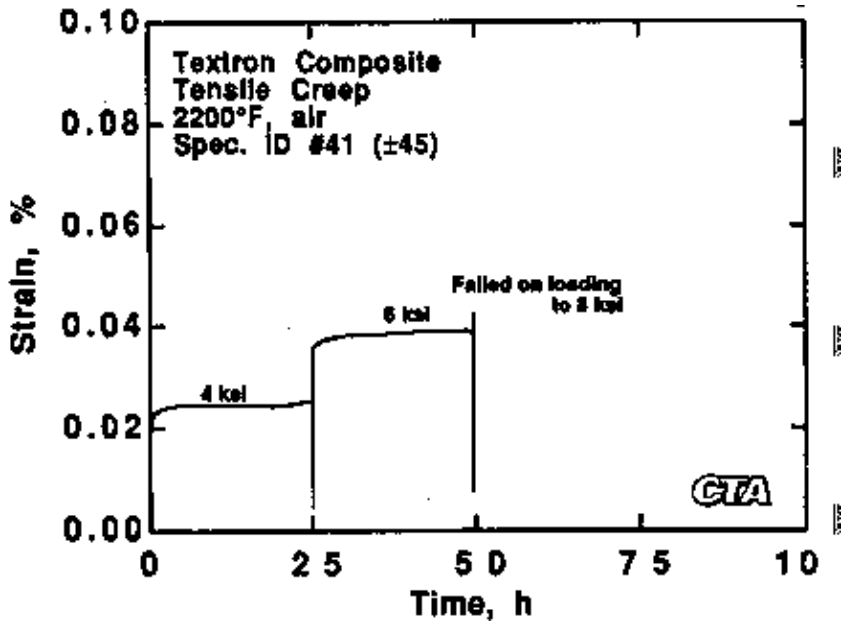

Figure 3.4-33 2200°F Step Loaded Creep With ±45° Specimen

2500°F Stress Rupture Testing With 0°F Specimens

Testing at 2500°F produced some unexpected results. The first step loaded specimen started testing at 4 KSI which was held for 25 hours. The strain of the specimen started out at about +0.03% then decreased to about -0.01%. The load was increased to 6 KSI and held for approximately 34 hours. The strain was increasing linearly from about 0% to 0.02% during this test segment. The next stress increase was to 8 KSI and the strain was increasing linearly during this segment of the test. The specimen broke upon loading to 10 KSI.

Based upon the above data the next specimen was tested at 8 KSI and broke upon loading. This was unexpected since the step loaded specimen maintained this load for 25 hours without fracturing.

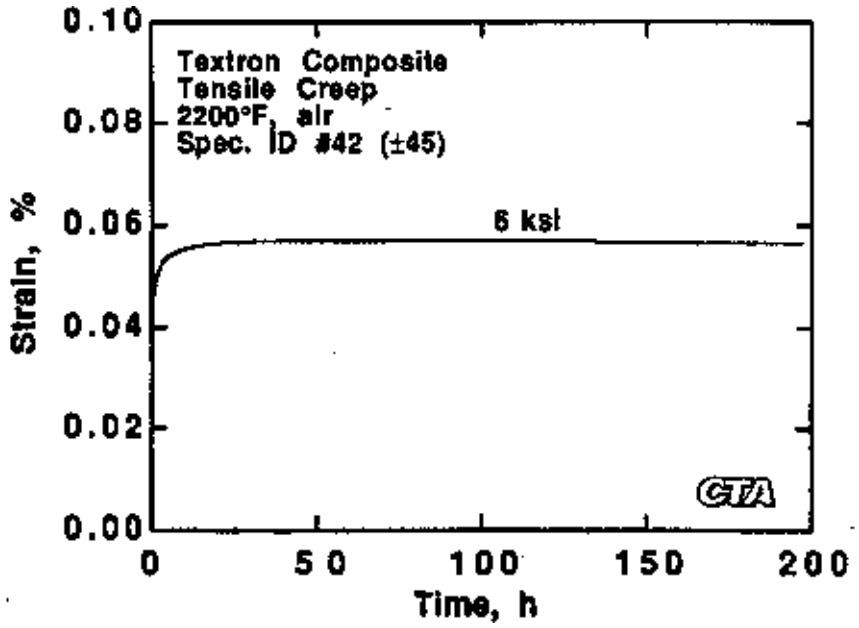

Figure 3.4-34 2200°F Tensile Creep after 2500°F Heat Treatment With ±45° Specimen

2500°F Stress Rupture Testing With ±45° Specimens

The first ±45° specimen was step loaded starting at 4 KSI as seen in Figure . On loading to 4 KSI the specimen strained to approximately 0.02% then contracted to approximately -0.07% over the 25 hour test period. The next stress level was 6 KSI and the strain jumped up to about -0.05% then slowly contracted back to about -0.07%. Upon loading to 8 KSI the specimen survived another 25 hours of exposure with similar strain results as the 6 KSI condition. The test specimen failed upon loading to 10 KSI (Fig 3.4-35).

Based on the 0° and ±45° test data it may be assumed that there are some residual stresses in the material that are being relieved at the 2500°F test temperature. Mr. Darden of Textron indicated that the processing temperature was 2552°F (1400°C) which is very close to the test temperature. It was decided in a telecon with Mr. Darden, Mr. Holmes of CTA and WI that the test temperature should be reduced to 2400°F.

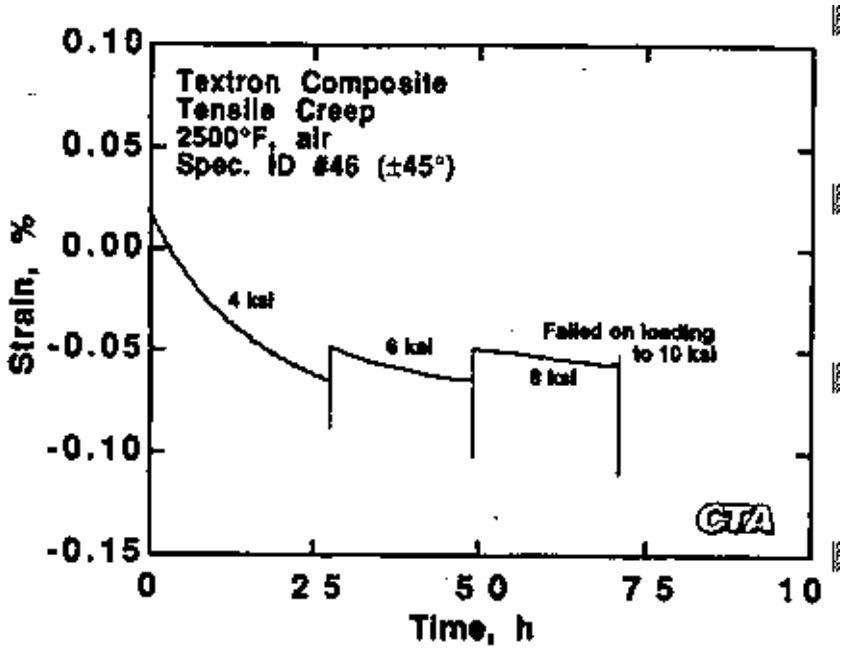

Figure 3.4-35 2500°F Step Loaded Tensile Creep With ±45° Specimen

2400°F Stress Rupture Testing With 0°F Specimens

Step loading of the first sample started at a stress level of 6 KSI at a temperature of 2400°F and held for 25 hours. The strain level started at about 0.03% then contracted to approximately zero. The specimen survived and the stress was increased to 8 KSI and no creep was measured during this 25 hour test segment. With the load increased to 10 KSI the strain held constant at approximately 0.03% for the duration of the 25 hours test segment. Upon loading to 12 KSI the specimen fractured. Stain versus time plot of this test can be found in Figure 3.4-36.

This data indicates that heat treating the material may reduce residual stresses or reduce the creep rate of the material at this test temperature.

The next specimen was setup and broke upon loading at 10 KSI. The step loaded test specimen survived 25 hours at this condition after lower levels of loading at temperature.

Based upon the earlier results the specimen was heat treated for 25 hours in air at 2400°F. This specimen was loaded at 10 KSI and the initial strain was 0.075% and at the end of 200 hour exposure at these conditions the strain was just slightly above 0.08%. There was very little creep of the material at 2400°F with a 10 KSI load.

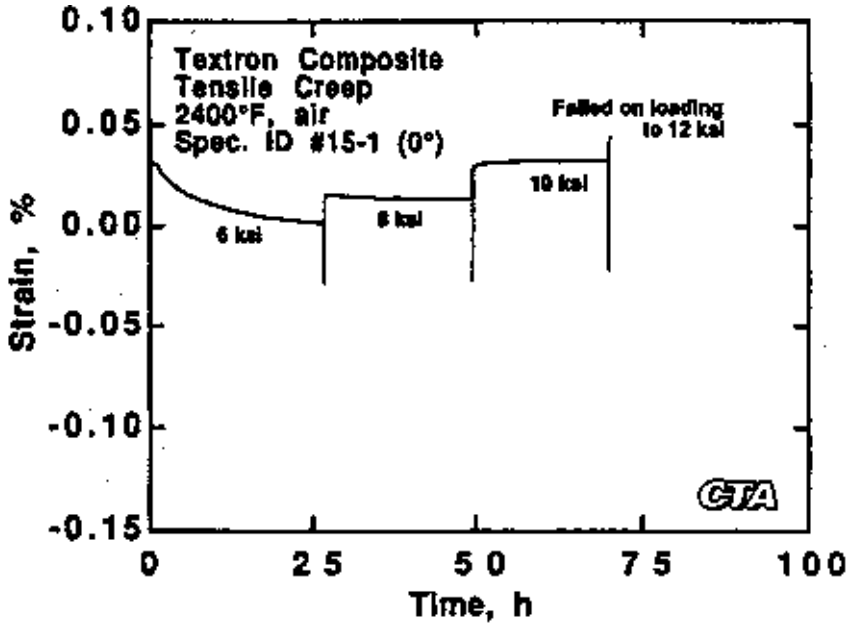

Figure 3.4-36 2400°F Step Loaded Tensile Creep With 0° Specimen

Stress Rupture Testing Summary

It was noted that the maximum stress level that could be applied at elevated temperatures was influenced by heat treating the specimens in air. This was first noticed when the specimens subjected to stepped stressed rupture could be successfully tested at higher stress levels than specimens loaded at a higher starting stress level. This was demonstrated with two test specimens 14-2 and 15-3 as seen in Table 3.4-18. The heat treated test specimen was successfully tested for 200 hours while the non heat treated specimen failed upon loading.

Dr. John Holmes of CTA suggested several possible mechanisms that may be responsible: (1) initially very high residual stresses are reduced by high temperature exposure, (2) a change in interfacial bonding during high temperature exposure and (3) a sintering effect that reduces the stress-concentration near the pores.

Based on the processing temperature of 2552°F (1400°C), it is possible that there are sintering effects in the material at 2500°F test temperature. The 2500°F test temperature was very aggressive and was above the use temperature of this material. Elevated heat treatment seems to stabilize the material and improve the high temperature properties of this system.

Stressed Oxidation Testing

The Williams International stressed oxidation rig was used to evaluate the Textron material. The rig stresses the tensile specimen in tension while exposing the material to a high velocity high temperature combustion environment.

The stress oxidation rig, Figure 3.4-37, is an adaptation of the burner rig used to evaluate the ceramic burner fabricated by Textron. The fuel was JP5 for most of the tests, the last few specimens were tested with JET A fuel.

Load is applied to the stress oxidation test specimen with an air cylinder attached to a load cell. The test specimens were loaded into the stressed oxidation rig which used edge loaded grips. Ceramic felt was used as a compliant layer between the ceramic test specimens and the metal grips.

Burner rig startup and shut down procedures are described in Appendix A. The procedure was to first bring the test specimen up to temperature then apply the appropriate stress to the test specimen. Upon shut down of the test rig the load was first removed from the test specimen followed by shut down of the combustor.

Testing was conducted at two temperatures, 2200°F and 2400°F with two different fiber orientations, 0° and ±45°. Three specimens were tested at each test condition. The first specimen tested with each orientation and test temperature was step loaded with three hour holds at each stress level. If the specimen survived the first stress level the load was increased such that the stress increased in 2 KSI increments. Step loading was continued until the specimen broke or the maximum capability of the load frame was reached.

A summary of the test specimen geometry and description can be found in Table 3.4-19. The flat panel specimens had many small defects such as voids. Most of the voids appear to have formed next to the first layer of fibers. The material has a matrix rich region which contained most of the voids that extended to the first fiber layers. The fiber content was 10% by volume and consisted of four layers.

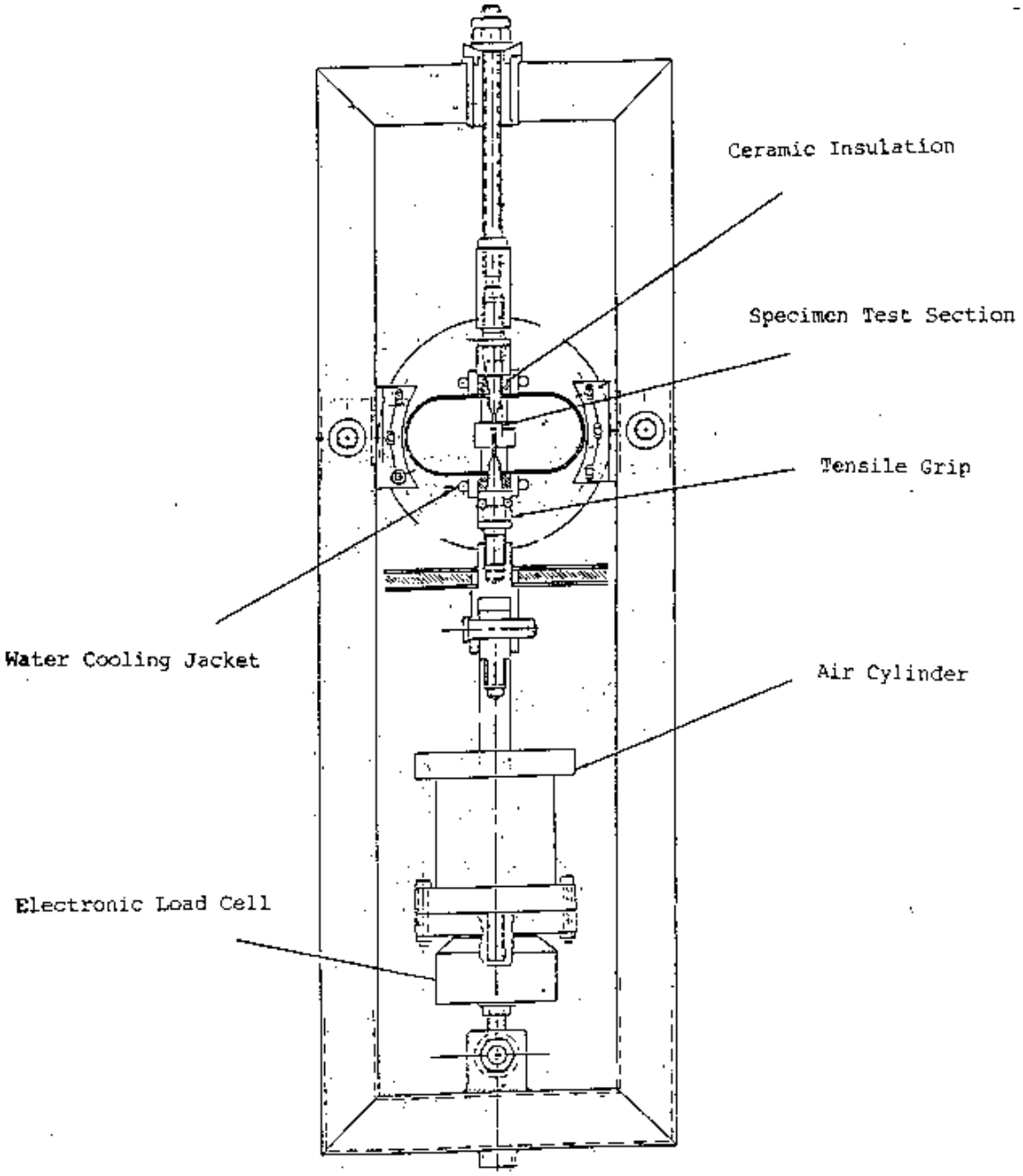

Figure 3.4-37 Stressed Oxidation Burner Rig

Table 3.4.19 Stressed Oxidation Test Specimen Description

Spec. ID	Width In.	Thick In.	Area $In.^2$	Orient. 0°/±45°	Test Temp. °F	Weight Grams	Comments
1-1	0.2485	0.1460	0.0363	0°	2200°	9.4704	0.020" hole in gage
1-2	0.2490	0.1460	0.0365	0°	2200°	9.5263	OK
1-3	0.2485	0.1460	0.0363	0°	2200°	9.4553	Crack in middle
3-1	0.2490	0.1470	0.0366	0°	2200°	9.6616	Small hole in grip
3-3	0.2500	0.1470	0.0368	0°	2200°	9.6743	Small hole in grip
3-4	0.2500	0.1480	0.0370	0°	2200°	9.6584	0.020" hole in gage
5-1	0.2495	0.1430	0.0357	0°	2200°	9.1490	0.010" hole in gage
10-1	0.2455	0.1270	0.0312	±45°	2400°	7.6997	Holes in gage
10-2	0.2460	0.1270	0.0312	±45°	2400°	7.80402	Holes in gage
10-3	0.2455	0.1265	0.0311	±45°	2400°	7.8722	Hole in gage
11-2	0.2480	0.1440	0.0357	±45°	2400°	9.0714	Hole in gage
12-1	0.2485	0.1260	0.0313	±45°	2400°	8.0977	OK
12-3	0.2480	0.1260	0.0312	±45°	2400°	7.7906	Hole in gage
12-4	0.2480	0.1260	0.0312	±45°	2400°	7.7326	Holes in gage > 0.010"
13-2	0.2470	0.1260	0.0311	±45°	2400°	8.1897	Holes in gage 0.100"

2200°F Stress Oxidation Testing With 0° Specimens

Testing was initiated at 2200°F with the 0° reinforced test specimens. The first specimen, number 1-1, was tested in a step loaded fashion starting at 4 KSI stress level. This stress level was held for 3 hours. The test rig was restarted with an increase in stress level to 6 KSI. The rig was shut down after 3 hours at 6 KSI. The rig was restarted with the stress level increased to 8 KSI and the load and temperature was maintained for 3 hours. Stress level was increased to 10 KSI and run for 3 hours. At the end of the 10 KSI segment the burner rig was stopped. The rig was restarted and the stress level was increased to 12 KSI and survived the 3 hours exposure. The rig was shut down after the 12 KSI segment. Upon loading for the next 14 KSI segment the specimen broke on loading at 10.2 KSI.

The fracture was in the grip with extensive fiber pullout, see Figure 3.4-38. Although one grip section of the specimen failed completely the other end of the specimen was cracked which the fibers bridged.

While the tensile load is on the specimen the Inconel 718 grips heat up and expand. Upon cool down the grips shrink onto the test specimen loading it into compression. This may be a factor in this grip fracture in the test specimen.

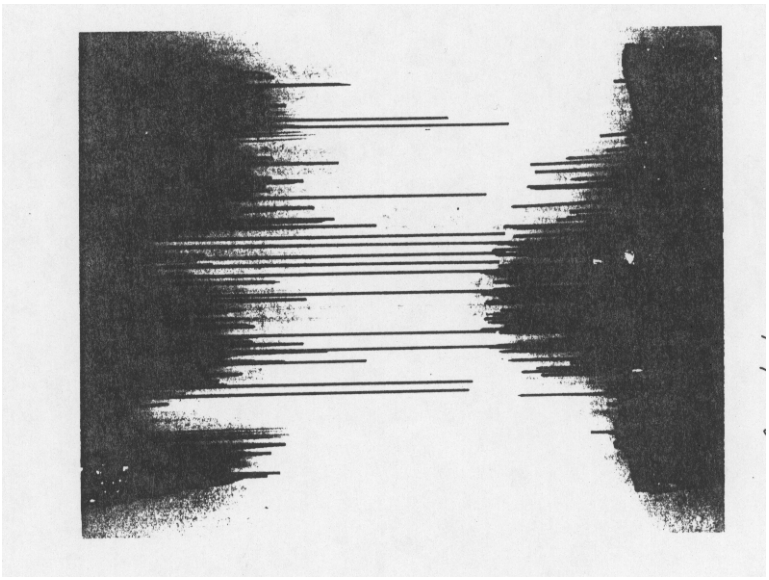

Figure 3.4-38 2200°F Stepped Stressed Oxidation With 0° Specimen 1-1

2200°F Stress Oxidation Testing With ±45° Specimens

The first two specimens loaded into the test rig broke upon loading to 4 KSI at a temperature of 2200°F. The fractures were at defect sites in both test specimens.
Figure 3.4-39 shows test specimen 10-1 fracture surface with a void.
The next specimen was step loaded starting at 4 KSI. The first segment of testing lasted 3 hour then the rig was shut down. The rig was restarted and a 6 KSI load was applied to the specimen and held for 3 hours. The specimen survived until the stress level was increased to 8 KSI. The specimen broke upon loading to the 8 KSI stress level.
A new specimen was loaded into the test rig and testing was started at 4 KSI. The specimen was run continuously for 10 hours without fracturing.
The last specimen tested was run at 6 KSI and was also run continuously for 10 hours without breaking.

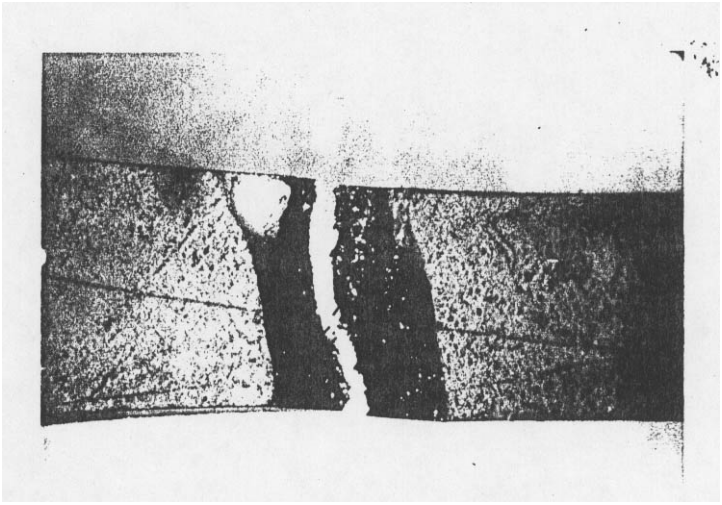

Figure 3.4-39 2400°F Stress Oxidation Fracture Surface With ±45° Specimen 10-1

2400°F Stress Oxidation Testing With 0° Specimens

Testing was initiated with a unidirectionally reinforced test specimen with step loading starting at 6 KSI at a temperature of 2400°F. The specimen survived 3 hours at 6 KSI then the loading was increased to stress the specimen at 8 KSI and the load was held for 3 hours. The load on the specimen was then increased to 10 KSI, 12 KSI and 14 KSI and each time the test conditions were maintained for 3 hours. The air cylinder was only capable of applying the 14 KSI stress level and the testing was terminated without fracturing the test specimen.

Based on the results of the first step loaded specimen the next test was run with a loading of 12 KSI and held for 10 hours. This test was run continuously for 10 hours without shutting the rig down.

The last test specimen was loaded at 14 KSI. The specimen fractured after approximately 2 minutes of run time while the load was being stabilized.

2400°F Stress Oxidation Testing With ±45° Specimens

The first step loaded specimen was initially loaded at 4 KSI stress level at a temperature of 2400°F. 1 hour into this test the fuel pump failed and forced a shut down of the test rig. The fuel pump was not immediately repairable so the fuel system was switched from JP5 to JET A fuel for the remainder of the testing. Testing was resumed using the JET A fuel and the remaining 3 hours were successfully completed. The stress level was increased to 6 KSI and the specimen fractured upon loading.

The next specimen was loaded into the rig and run at 4 KSI stress level for 4 hours and 40 minutes then the rig was shut down. The rig was restarted with a stress level of 4 KSI. Testing was run continuously until the completion of the 10 hours. The specimen survived 10 hours of exposure with 4 KSI and a total of 10 hours.

The last specimen tested was run at 6 KSI and broke upon loading. The fracture occurred at a defect in the gage section of the test specimen.

Summary of Stressed Oxidation Testing

A summary of all of the stressed oxidation testing is included in Table 3.4-20. The temperature, fiber orientation, stress levels, time and brief comments are presented. Based on the summary of the data there seems to be some correlation between panel number and strength of the materials. As an example, panel 10 seems to have had more defects and more specimens breaking on loading or with defects in the gage section. Overall the ±45° reinforced material had more voids and defects that the unidirectional material.

Included in Table 3.4-20 is the residual tensile strength data from specimens that survived the stressed oxidation testing. Tensile testing was conducted at room temperature with a cross head speed of 0.10 inches per minute. Specimen number 5-1 broke in the grip area during the residual tensile test. The remaining samples all broke in the gage section. All of the fracture surfaces and extensive fiber pull out. Fiber pull out on some specimens was approximately 0.8 inches. Test

specimens that were tested at CTA in the as fabricated condition had very little fiber pull out. This may indicate that the fiber matrix interface changed during the stressed oxidation test.

The composite combustors appeared to have fewer voids that the panels. The panels used the same materials as the combustors, however a different process was used to fabricate flat as opposed to tubular shapes. It would be anticipated that with a little more development the flat panel porosity could have been reduced.

Table 3.4-20

Summary of Stress Oxidation Testing at Williams International

Specimen	Temp. °F	Orient. 0°/±45°	Stress Level KSI	Time Hr:Min	Residual Ten Str KSI	Comments
1-1	2200	0°	4, 6, 8, 10, 12	13:45		Broke in grips on start up Fibrous fracture
3-1	2200	0°	8	10:00	5.194	Survived
1-2	2200	0°	10	10:00	4.909	Survived
10-1	2200	±45°	4	0:00		Broke on loading Defect in gage section
10-3	2200	±45°	4	0:00		Broke on loading Defect in gage section
12-1	2200	±45°	4, 6, 8	6:00		Broke on loading to 8 KSI Broke at grip
12-4	2200	±45°	4	10:03	3.261	Survived
13-2	2200	±45°	6	10:00		Survived Broke upon removal
3-4	2400	0°	6, 8, 10, 12, 14	14:45	8.000	Survived
3-3	2400	0°	12	10:00	5.031	Survived
1-3	2400	0°	14	0:02		Broke after loading Broke in gage section
12-3	2400	±45°	4, 6	3:00		Broke on loading to 8 KSI Broke at grip
11-2	2400	±45°	4	10:00	2.981	Survived
10-2	2400	±45°	6	0:00		Broke on loading Defect in gage section
				87:35		Total run time

3.5 Joining

Textron supplied NBSN material for evaluation to Sandia National Laboratory for evaluation using their refractory oxide joining compositions or brazing alloys. Sandia proposed two types of testing: screening for wetting, reactivity, and bonding between the CFCC material and the joining composition and four-point bend specimens to measure bond strength.

Initial wetting adhesion experiments run at Sandia on Textron-supplied CFCC test coupons was successful. Refractory glass was heated on top of and between some of the test coupons and they did stick together; sectioning and polishing of the samples indicate that the wetting angle is higher than expected but the adhesion to the Textron material was good.

Sandia National Laboratories continued their failure analysis evaluations of the four-point bend specimens used to evaluate CFCC joining methods. Based on their findings, Textron's material performed equal to or better than the other supplied materials.

Panel material (two 6" x 6" panels: one NBSiC/SCS-6 and one NBSiC/SCS-9A) was shipped to Ames Laboratory at Iowa State University for a joining study involving asymmetric four point bending tests. This study evaluated joining by using asymmetric four point bending tests. Ames reported results that indicated that very high bond strengths were observed in the joints made using Textron supplied material, although crack formation at the joint regions due to the fine powder particles used was also seen.

Prepared samples were butt-joined using Ames' preceramic oligomeric polymer (SiC9H8) and a joining paste with high Si-content metal powder (50 at.% Si - 50 at.% Al). Mechanical tests were conducted at room temperature and 1000 °C using a four-point flexure fixture. The room temperature strength was about 55 MPa and at 1000°C was about 40 MPa. These values are lower than the samples joined with CERASET polymer which were about 90 MPa at 1000 °C. The lower strength in the former samples could be attributed to higher pore density observed at the joint region. The decrease with temperature was believed to be due to the presence of a small amount of untransformed Al-Si alloy at the joint.

4.0 CFCC COST & MARKET CONSIDERATIONS

Perhaps one of the best attributes of the CFCC Program is its goal of aligning contractors with industrial partners to find appropriate applications for these CMC's. This forces the technology to be end-user driven, and focuses us to solve specific technical problems to meet the customer needs. Ultimately, this can result in driving us to develop a business, which in turn benefits the contractor, the customer, and the Department of Energy.

Textron originally worked with Hauck Burner Manufacturing to evaluate potential industrial applications for our CMC immersion tubes. Limited testing of tubes occurred in an aluminum furnace through partnering with F. W. Schaefer and Doehler-Jarvis. For various reasons, including financial insolvency of one of the partners, Textron began to look for other partners. Initial contact with General Motors was made at the North American Die Caster's Association Trade Show at the DOE's OIT Metal Casting booth. This led to the evaluations at GM's Advanced Development Laboratory in Saginaw, MI, and to eventual trials at GM's Powertrain production facility in Bedford, IN.

Additional partners have been discovered by other means. Textron's website generated the interest of an engineer at a Texaco gasification plant in Kansas. After some discussion, a small piece of a William's combustor was sent to him for evaluation, and the part did extremely well in very limited testing. While the ongoing negotiations to develop a full partnership with Texaco have hit some snags, we are currently very close to adding them as a partner for a very aggressive application where our tubes could be used as thermocouple sheaths.

A similar application was discovered as a result of having a booth at the OIT Energy Efficiency Symposium in Washington, D.C. in February of this year. Energy Research Company has an OIT-funded program to help develop a laser-induced spectrographic analyzer for real-time melt constituents. Our tube could be eventually used as a sensor sheath. Still another application has developed through our contact with GM, and one of their distributors, Refractory Engineers of Indianapolis, IN. Amcast manufactures aluminum alloy wheels, and consumes 300 immersion tubes per year. The conditions are similar to GM Saginaw, where our tubes have been successful.

We are continuing to look for new partners by various means. Our goal is to search for applications where some variation of our immersion tubes can be readily made. While we recognize that there may be applications for which we are not yet aware, we nevertheless have developed a general strategy for our immersion tubes. Specifically, our target market is CMC immersion tubes and radiant burners for light metal casting (Al, Mg, Zn) with primary emphasis on immersion tubes for aluminum.

We perceive the customer needs of this market to be:

- -Increased heat transfer efficiency
- -Lower energy consumption
- -Longer life, with less down time for maintenance and changing of tubes
- -Faster heat up, and elimination of tube pre-heats

Growth in this market is promising, led primarily by the automotive manufacturers. This industry has relied upon steel as its main material constituent. They have been forced to increase their use of plastics where they can, and are beginning to use aluminum in structural applications previously limited to steel. Factors accelerating this trend include lower emission standards, and higher miles per gallon averages in their fleet, even as the marketplace cries out for more gas guzzling SUV's. These trends led to a recent $10 B multi-year agreement between GM and Alcan Aluminum to increase use of aluminum in autos.

We believe there are minimal barriers to entry to this marketplace, particularly when compared to the typical applications for CMC's, such as turbine engine parts. Potential customers are willing to evaluate tubes without extensive databases on the parts. This allows a much faster qualification process. There is low risk to the customer, because even a failed tube will not ruin the aluminum bath. Basically, if the tubes last a long time and are cost effective, the end user will buy them. The primary negatives to this market are the higher initial costs of CMC tubes, and the larger market share held by radiant burner tubes.

In attempting to arrive at a potential macro-market, we assessed the die casting market. The average annual production of aluminum by die casting is approximately two billion pounds per year, and the average holding tank is 2,000 lbs. On average, then, there are 3,100 die casting furnaces in the U.S. Assuming most die casters use radiant burner tubes, one could assess the immersion tube market at 40%. Reducing that to a more likely achievable market share of 20% yields 620 furnaces, and assuming 10 immersion tubes per furnace results in a market of 6,200 immersion tubes per year.

Taking that one step further, we looked specifically at GM's Bedford plant where we are currently evaluating our immersion tubes. There are 60 die casting furnaces, and 30 permanent mold, gravity pour furnaces, and they are running all the time. Each furnace has three heaters, and each immersion tube lasts an average of 45 days. With the current monolithic tubes, this results in 700 to 800 tubes per year, at a current price of $700 per tube. A similar analysis for the Texaco coke gasification application results in a potential for 30,000 tubes per year.

Summarizing these two applications results in the following:

-Potential for Immersion Tubes
Annual production: 400 (GM) to 3,000 (Total Market)
Existing tubes last 45 days @ $700 per tube
2 X Life @ higher efficiency = ~ $0.5M to $4.5M annual market

-Potential for Coke Gasification Tubes
Annual production: 1,500 (10% market share)
Existing tubes last 14-20 days at $1200 each
2 X Life = ~ $2.5M annual market

In order to make sure that we could reach the cost targets that these applications will require, we had Ibis Associates develop a cost model for our projected production facility to manufacture tubes. This cost model assumes a new plant, and addresses all cost issues. As we anticipated, the cost of the fiber in our tubes is a large portion of the total production cost. We will continue to use this model to project production costs of immersion tubes of varying configurations and sizes as we complete this Phase 2 effort. We are continuing to look for new applications for the fiber that will lead to lower fiber for all applications. The model also told us that a relatively low number of immersion tubes (~800 annually) is needed to achieve optimal per part costs. As the market develops, Textron is fully prepared to license the technology to other manufacturers who may have the capability to achieve even lower production costs, which will further expand CFCC utilization.

5.0 Summary

In the course of this cooperative agreement, Textron has developed a mature process for the fabrication of continuous fiber ceramic composite (CFCC) tubes for application in the aluminum processing and casting industry**.** The major milestones in this project are described below.

System Composition On the basis of chemical and thermal compatibility with processing and application conditions, the composite system chosen for full development activity was SCS-6 silicon carbide monofilament reinforcing nitride-bonded silicon carbide (NBSiC). Unlike commercially available small diameter ceramic yarns, the SCS-6 fiber does not suffer thermal degradation or adverse chemical interaction either during fabrication or use. Thr RBSN matrix shows a high degree of stability towards both high temperature oxidation and contact with molten aluminum.

Matrix Formulation The "green" matrix primarily consists of a mixture of silicon carbide and elemental silicon particulates; the latter are converted to silicon nitride by reaction with nitrogen during a firing step. The green matrix in the form of a slurry is cast around the fibers to form a green body for firing. The slurry formulation developed during the program has the following characteristics: a) high solids loading. Weight percent solids above 80% minimize shrinkage and cracking and permit the fabrication of net-shape parts. b) stability against sedimentation. Stabilizing additives and proper particle size distribution assure interparticle repulsion that produces a stable suspension. c) low viscosity. Water-based suspensions have viscosities in the 150-1000 centipoise range; these are castable and provide infiltration around fibers without residual macroscopic voids. The aqueous base eliminates the need to deal with flammable materials during drying and firing. d) green body porosity. The particle size distribution assures that the green body has a network of open connected porosity for the later gas phase nitridation. The silicon to silicon carbide ratio assures that the volume change upon nitridation fills the porosity, allowing net shape fabrication, and also provides silicon carbide diluent to the exothermic nitridation step, preventing composite damage due to exotherms.

Preform Fabrication Tooling and winding algorithms were developed for the direct filament winding of closed-end tubes on a 5-axis filament winder. Slurry was added to the mandrel while the fibers were wound dry. Patterns of alternating dome, helical and melt-line band wraps produced uniform wall thickness and fiber dispersion.

Nitridation A 48 hour nitridation cycle was developed to convert the green slurry to RBSN matrix. Experimental cycles as short as 36 hours were demonstrated.

Material Characterization An extensive database of physical, thermal and microstructural properties of the SCS-6 RBSN system at both room and elevated temperatures was developed.

Component Evaluation Testing of sub-scale and representative components in simulated and actual in-service conditions was performed at Doehler-Jarvis, Williams International and General Motors. Gas-fired reheater burner tubes were evaluated at Doehler-Jarvis, combuster cans for stationary gas turbine generators at Williams International, and electrically heated immersion tubes for aluminum casting at General Motors. Performance data was used to further refine the pre-production scale manufacture of components.